University of Lille1
Science and Technology
Doctoral School of Science of Matter,
Radiation and Environment (SMRE)
Field: Optics and lasers, physical chemistry, atmosphere

University of Szeged
Faculty of Science and Informatics
Doctoral School of Chemistry

Atmospheric kinetics and photochemistry of oxygenated volatile organic compounds

PhD Thesis

Emese Szabó

Thesis Supervisors: Sándor Dóbé, DSc – Chemical Research Center,
Hungarian Academy of Sciences
Christa Fittschen, HDR – PC2A, University of Lille 1

LILLE, SZEGED
2011

To Jérémy

Tables of Contents

Chapter 1: Introduction

The Earth's atmosphere is characterized by variation of temperature and pressure with height. In fact, the variation of the average temperature profile with altitude is the basis for distinguishing the different levels of the atmosphere. From the point of view of atmospheric chemistry, two parts of atmosphere - the troposphere and stratosphere - are the most important regions.

In the troposphere, the temperature falls with increasing altitude. This is due to the strong heating effect at the Earth's surface which absorbs and converts the radiation from the Sun to heat. The chemical species from biogenic and anthropogenic sources have the most significant effect in this region. As the hot air rises there is a strong vertical mixing so that species emitted at the Earth's surface can reach the tropopause in a few days or even shorter time, depending on the meteorological conditions.

The tropopause separates the troposphere from the stratosphere. However, at the tropopause the temperature profile changes, increasing with altitude throughout the stratosphere. One of the reasons for the temperature increase is that different photochemical reactions occur that are followed by exothermal chemical reactions [Finlayson-Pitts and Pitts 2000].

In the stratosphere, the ozone production is the most characteristic and most important processes. 90 % of atmospheric ozone can be found in this region [Mészáros 1997], and it absorbs the UV radiation which is harmful for ecological systems including human life. The lower, about 10 - 15 km high region of the atmosphere is the troposphere.

Figure 1.1 displays all the mechanisms of emissions, transformations and depositions occurring the troposphere. The sources of atmospheric minor constituents are located mainly on the Earth's surface. There are natural sources, such as the emission of the vegetation and volcanic eruptions, and anthropogenic sources, all of which lead to the emission of a high variety of gases and particles. After emission, the different constituents are transported and mixed by horizontal and vertical motion of air masses and are transformed, initiated by solar radiation either in the gas phase (homogeneous chemistry), in the liquid phase, or on the surface of aerosols or the surface of solid particles (heterogeneous chemistry).

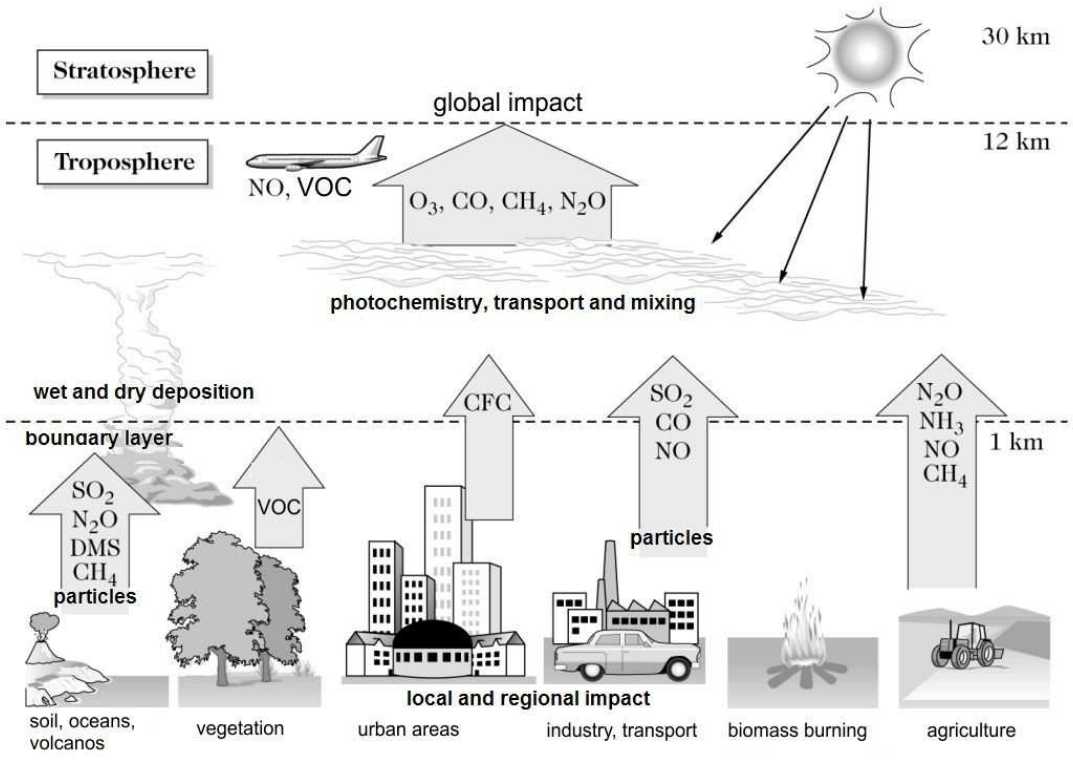

Figure 1.1: Schematic representation of key processes of atmospheric chemistry.

1.1. Impact of volatile organic compounds (VOCs) on the environment and human health

Volatile organic compounds can cause direct and indirect effects on the environment and human health:

1. Direct effects: there are several VOCs that are themselves toxic on the human health. Inhalation of VOCs in strongly polluted areas was shown to be associated with the increase of symptoms of respiratory diseases, headache and irritation of eyes [Bernard 2001]. Carbonyl and aromatic compounds are known to be carcinogenic and mutagenic compounds [IARC 2010]. The toxicity of VOCs on the human health depends on two factors: concentration during the exposure and the time of exposure.

2. Indirect effects: VOCs emitted in the atmosphere will participate in chemical reactions leading to the formation of secondary photochemical pollutants such as ozone and other harmful photooxidants. That is, VOCs act indirectly on biological system through forming carbon-monoxide (CO), ozone (O_3) and PAN (peroxyacetyl nitrate).

Ozone and PAN are highly toxic components of urban smog which are formed by the photochemical oxidation of VOCs in the presence of NO_x (NO and NO_2) arising mainly from exhaust of automobiles. Ozone reacts with several materials causing a rapid degradation of objects made of plastic or rubber; aggravates forest decline and diminishes agriculture productivity.

1.2. Degradation of VOCs in the troposphere

In the troposphere, all the chemical reactions in the gas phase are initiated by the solar radiation, directly or indirectly, and proceed to a radical mechanism, involving reactions with hydroxyl (OH) radical, NO_3 radical, or O_3. The degradation by Cl atoms can also be important. The photolysis mechanism of VOCs will be presented through the carbonyls.

1.2.1. The solar spectrum

Figure 1.2 from [Finlayson-Pitts and Pitts 2000] shows the solar flux as a function of wavelength outside the atmosphere and at sea level. The radiation that the Earth receives from the Sun at the top of the atmosphere can be cover the infrared, visible and near UV region. The solar flux approaches the 6000 K blackbody radiation outside the atmosphere. On the sea level the Earth receives only a fraction of this solar radiation. The region of the spectrum lower than ~ 170 nm is absorbed by the first layer of the atmosphere (above about 100 km altitude). The radiation between 190 and 290 nm could penetrate deeper but it is absorbed by the stratospheric ozone at 50 - 20 km altitude. Apart from a weak absorption of ozone at 600 nm, the atmosphere is transparent in the visible and near UV region, that is, this irradiation can reach the ground level.

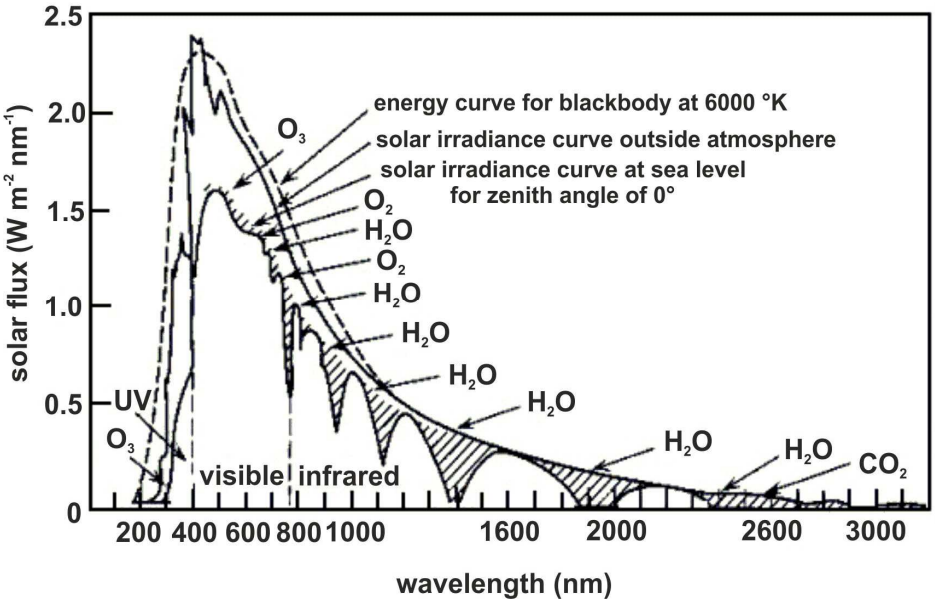

Figure 1.2: Solar flux outside the atmosphere and at sea level. The emission of a blackbody at 6000 K is also shown for comparison. The species responsible for light absorption in the various regions are also shown [Finlayson-Pitts and Pitts 2000].

Light scattering phenomena by atmospheric constituents also modify the spectral distribution. These are the scatter by molecules (Rayleigh scatter) in the near UV region and that by suspended particles (Mie scatter) in the whole spectral region. The 290 - 800 nm region corresponds to the wavelength range of photochemical interest in the troposphere; the infrared radiation does not have sufficient energy to lead to photochemical reactions. H_2O and CO_2 absorb strongly in the infrared region, mostly they are responsible for the greenhouse effect.

1.2.2. Degradation of carbonyl compounds by photolysis

Carbonyl compounds absorb light in the near UV region and can undergo different types of photochemical and photophysical changes:

- Dissociation by bond cleavage to free radicals or formation of stable molecules by a more complex mechanism;
- emission of radiation (fluorescence, phosphorescence) and
- photo-isomerisation.

Some photochemical processes are presented below by examples of aliphatic aldehydes and ketones.

The formaldehyde molecule can photolyse either to radicals or to stable molecules [Finlayson-Pitts and Pitts 2000]:

$$HCHO + h\nu \rightarrow H + HCO$$
$$\rightarrow H_2 + CO$$

In the atmosphere, the H and HCO radicals react with oxygen giving HO_2 which is a source of OH in the presence of NO:

$$H + O_2 (+M) \rightarrow HO_2 (+M)$$
$$HCO + O_2 \rightarrow HO_2 + CO$$
$$HO_2 + NO \rightarrow OH + NO_2$$

In the case of acetaldehyde, three different photolysis ways are possible thermochemically [Moortgat 2010]:

$$CH_3CHO + h\nu \rightarrow CH_3 + HCO \qquad (\lambda \leq 337 \text{ nm})$$
$$\rightarrow CH_4 + CO \qquad (\text{all } \lambda)$$
$$\rightarrow CH_3CO + H \qquad (\lambda \leq 320 \text{ nm})$$

The CH_3, HCO and H radicals will be transformed again to HO_2 and then to OH. The CH_3 radical is converted to HCHO and HO_2 through the reactions with O_2 and NO. Finally, the CH_3CO radical can form peroxyacetyl nitrate (PAN) in the reaction with O_2 and then with NO_2 or is transformed to CH_3 and CO_2:

$$CH_3CO + O_2 (+M) \rightarrow CH_3C(O)O_2 (+M)$$
$$CH_3C(O)O_2 + NO_2 \rightarrow CH_3C(O)O_2NO_2 \qquad (PAN)$$
$$CH_3C(O)O_2 + NO \rightarrow CH_3C(O)O + NO_2$$
$$CH_3C(O)O (+M) \rightarrow CH_3 + CO_2 (+M)$$
$$CH_3 + O_2 (+M) \rightarrow CH_3O_2 (+M)$$
$$CH_3O_2 + NO \rightarrow CH_3O + NO_2$$
$$CH_3O + O_2 \rightarrow HCHO + HO_2$$

In the case of acetone, three photolysis ways are possible which depend on the wavelength of the photolysis, similarly to CH_3CHO [Nádasdi 2007]:

$$CH_3C(O)CH_3 + h\nu \rightarrow CH_3CO + CH_3 \qquad \lambda \leq 338 \text{ nm}$$
$$\rightarrow 2\ CH_3 + CO \qquad \lambda \leq 299 \text{ nm}$$
$$\rightarrow CH_3C(O)CH_2 + H \qquad \lambda \leq 295 \text{ nm}$$

The CH_3CO radical reacts with oxygen and then with NO_2 giving PAN, or it can decompose to CH_3 radical and CO. The CH_3 radical reacts with oxygen and gives

formaldehyde and HO_2 as it was shown above with acetaldehyde. At low NO_X concentrations, such as at remote areas, the peroxyl + peroxyl radical reactions also play role giving aldehydes and alcohols, as degradation intermediates.

1.2.3. Oxydising transient species in the troposphere

The OH radical

As noted in the previous Section, the hydroxyl radical is the key reactive species in the troposphere, undergoing reactions with almost all organic compounds. In the troposphere, the main source of OH radicals is the reaction of $O(^1D)$ atoms with water vapour. The $O(^1D)$ atoms come from the photolysis of ozone. A small fraction of $O(^1D)$ atoms reacts with the water molecule, most of them are deactivated to ground-state $O(^3P)$ atom [Atkinson 2000].

$$O_3 + h\nu \rightarrow O_2 + O(^1D) \qquad (\lambda \leq 335 \text{ nm})$$

$$O(^1D) + M \rightarrow O(^3P) + M \qquad (M = N_2, O_2)$$

$$O(^1D) + H_2O \rightarrow 2\ OH$$

An average 0.2 OH radicals are produced per each $O(^1D)$ atom formed at 298 K and atmospheric pressure [Atkinson 2000].

The OH radicals can be formed also by the photolysis of HONO:

$$HONO + h\nu \rightarrow OH + NO \qquad (\lambda < 400 \text{ nm})$$

Formation of HONO has been observed in urban areas during night time [Lammel and Cape 1996]. The rapid photolysis of HONO after sunrise leads to an early high level of OH concentration and acts in this way as an initiator to urban photochemistry [Harris 1982] in the morning hours.

The OH radicals are products of the reaction of HO_2 with ozone and with NO. The HO_2 radicals originate from the oxidation of VOCs and actually from all reactions which produce H and HCO in the troposphere (see in Section 1.2.2).

$$HO_2 + O_3 \rightarrow OH + 2\ O_2$$

$$HO_2 + NO \rightarrow OH + NO$$

The atmospheric photooxidation of VOCs is a chemical chain reaction in which the OH radicals are the chain carrier species. OH initiates the degradation of the organic molecules, but usually several OH radicals are formed when one VOC molecule completely degrades to CO_2 and H_2O.

Hydrogen peroxide generates also OH radicals by photolysis in the atmosphere:

$$H_2O_2 + h\nu \rightarrow 2\ OH \qquad (\lambda \leq 360\ nm)$$

The hydroxyl radical can be consumed in the reaction with NO_2 and HO_2, and indirectly by the recombination of HO_2 in this way terminating the chain oxidation processes:

$$OH + NO_2 \rightarrow HNO_3$$

$$OH + HO_2 \rightarrow H_2O + O_2$$

$$HO_2 + HO_2 \rightarrow H_2O_2 + O_2$$

The diurnally and annually averaged global tropospheric OH radical concentration has been estimated to be ~ 1.0×10^6 molecule cm^{-3} [Atkinson 2000].

Tropospheric ozone

Ozone in the troposphere originates mostly from photooxidation process and the rest comes from the stratospheric transport. The ozone is generated by two successive reactions. The NO_2 photolysis in air gives an oxygen atom, $O(^3P)$, which reacts with oxygen molecule to form ozone:

$$NO_2 + h\nu \rightarrow NO + O(^3P) \qquad (\lambda \leq 400\ nm)$$

$$O(^3P) + O_2 + M \rightarrow O_3 + M \qquad (M = air)$$

The nitrogen monoxide can react with ozone providing nitrogen dioxide.

The result of the above reactions is a photoequilibrium, between NO, NO_2 and O_3, with no net formation or loss of ozone, see Figure 1.3 [Atkinson 2000]:

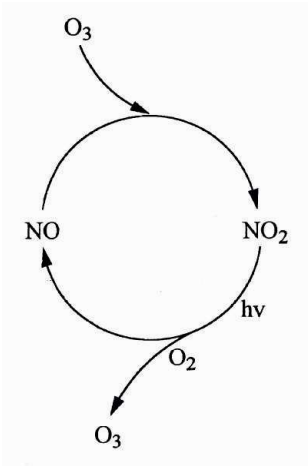

Figure 1.3: NO-NO_2-O_3 reaction cycle in the absence of VOCs.

However, in the presence of VOCs, - including methane and non-methane organics of biogenic and anthropogenic origin - the degradation reactions lead to the formation of intermediate alkyl-peroxy (RO_2) and HO_2 radicals. These RO_2 and HO_2 radicals react with NO, converting NO to NO_2, which then can photolyse to form ozone. This NO-NO_2-O_3 system in the presence of VOCs gives a net ozone production, see Figure 1.4 [Atkinson 2000]:

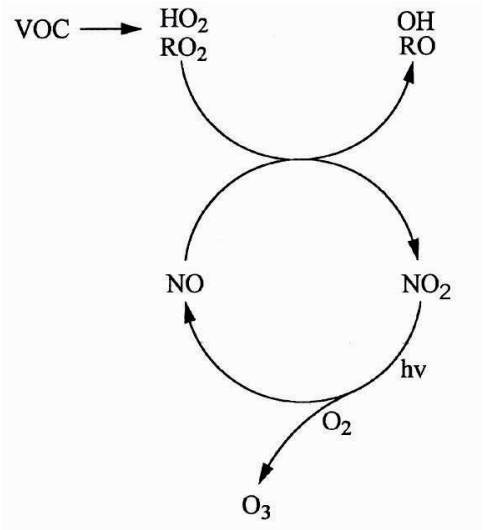

Figure 1.4: NO-NO_2-O_3 system in the presence of VOCs.

The NO_3 radical

The nitrate (NO_3) radical is formed from the reaction of NO_2 with ozone:

$$NO_2 + O_3 \rightarrow NO_3 + O_2$$

This NO_3 radical photolyses rapidly during daylight hours, its lifetime is ~ 5 seconds.

$$NO_3 + h\nu \rightarrow NO + O_2 \qquad (\sim 10\%, \lambda < 700 \text{ nm})$$

$NO_3 + h\nu \rightarrow NO_2 + O(^3P)$ (~ 90%, $\lambda < 580$ nm)

The NO_3 radical concentrations remain low during daylight hours but can increase during night-time.

The nitrate radical can react with NO:

$NO_3 + NO \rightarrow 2\ NO_2$,

and also with NO_2 to form dinitrogen pentoxide (N_2O_5, the anhydride of nitric acid) in a reversible process:

$NO_3 + NO_2\ (+M) \leftrightarrow N_2O_5\ (+M)$

NO_3 reacts only slowly with saturated VOCs, but its reaction is fast with alkenes which process is a typical night-time atmospheric reaction.

Cl atoms

Cl is a very reactive species; the rate coefficient of its reaction with VOCs is significantly faster than even that of the OH radicals. Nevertheless, the chlorine initiated oxidation of organics is only of minor importance because of the low Cl concentration in the troposphere. Cl atoms play a more important role in the marine environment where they are formed via heterogeneous processes and subsequent photolysis [Finlayson-Pitts and Pitts 2000]:

$N_2O_5(s) + NaCl(s) \rightarrow ClNO_2(g) + NaNO_3(s)$

$ClNO_2 + h\nu \rightarrow Cl + NO_2$

1.2.4. Degradation of volatile organic compounds by oxidation

The degradation reactions of VOCs which occur in the troposphere are presented in Figure 1.5 with a general reaction scheme [Atkinson 2000]. The oxidation of VOCs by different radicals (OH, NO_3) or Cl atoms can proceed by different mechanisms, namely H atom abstraction or addition to the double bond. The next step is the reaction between the carbon-centred radicals formed in the initiation steps and the oxygen molecule giving peroxy radicals. Figure 1.5 shows a few important intermediate radicals such as alkyl radicals (R), alkyl-peroxy radicals (RO_2) and alkoxy radicals (RO) [Atkinson 2000].

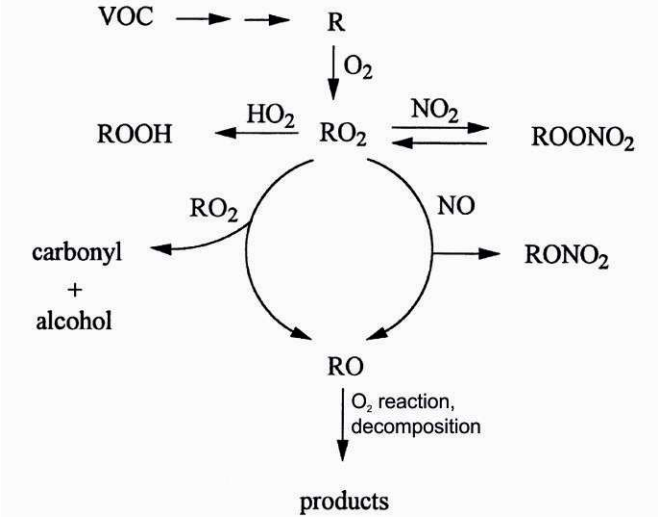

Figure 1.5: Degradation of VOCs in the troposphere.

The alkyl-peroxy radicals can react by different reaction pathways. In the presence of NO, alkyl-peroxy radical gives alkoxy radicals (RO) and alkyl-nitrates ($RONO_2$). The presence of NO_2 leads to the formation of peroxy-nitrates ($ROONO_2$) which are not stable species and they can be decomposed to RO_2 and NO_2.

The alkyl-peroxy radicals can react with HO_2 to form hydroperoxides (ROOH).

The relatively stable intermediates in the oxidation scheme are carbonyls and alcohols. As presented in the previous section, the degradation of VOCs is closely linked to the tropospheric budget of OH radicals and O_3.

1.2.5. Degradation of carbonyl compounds by oxidation

The degradation of the intermediate carbonyl compounds occurs by similar mechanisms to their parent molecules but the photolysis also takes place which is often the most important initiation step (see Section 1.2.2).

The OH radical reacts with saturated carbonyl compounds by hydrogen atom abstraction. In the case of aldehydes, the aldehyde H atom is abstracted giving rise to acyl radical (RCO). This radical reacts then with oxygen to form peroxyacyl radical ($RC(O)O_2$), which, in turn, reacts with NO or NO_2.

$$RCHO + OH \rightarrow RCO + H_2O$$

$$RCO + O_2 (+M) \rightarrow RC(O)O_2 (+M)$$

$$RC(O)O_2 + NO \rightarrow RC(O)O + NO_2$$

$RC(O)O\ (+M) \rightarrow R + CO_2\ (+M)$

$RC(O)O_2 + NO_2\ (+M) \leftrightarrow RC(O)OONO_2\ (+M)$

The reaction of peroxyacyl radical with NO_2 leads to the formation of PAN-type molecules, namely peroxy-acyl-nitrates. The peroxy-acyl-nitrates are relatively stable, but decompose to NO_2 and $RC(O)O_2$ when they are transported away from the emission sources thus allowing a redistribution of NO_2 to even remote areas.

1.3. Objectives

As presented in the previous sections volatile organic compounds are important actors in the chemistry of the atmosphere. They are emitted into the air from anthropogenic and biogenic sources and are also formed as products of atmospheric transformations of other VOCs [Atkinson and Arey 2003]. During their degradation, different radicals are formed which contribute to the oxidative capacity of the atmosphere and affect the concentration of OH radicals, ozone and NO_X (NO and NO_2). The most important classes of VOCs include alkanes, alkenes, aromatic hydrocarbons, and oxygenated compounds [Atkinson and Arey 2003]. Oxygenated volatile organic compounds (OVOCs) are emitted directly from vegetation (natural and agricultural sources) [König 1995], [Baraldi 1999]. They can be formed in situ in the atmosphere from hydrocarbons as a result of chemical and photochemical reactions. They are found in high concentration in the polluted urban air [Atkinson and Arey 2003]. Among the OVOCs carbonyl compounds, aliphatic alcohols and carboxylic acids are particularly important in atmospheric chemistry. Carbonyls absorb light in the 290 - 400 nm region and generate free radicals. The increasing use of alcohols and biofuels has led to an increasing interest in their atmospheric fate. Carboxylic acids are known to contribute very significantly to the total acid charging and acid deposition in the atmosphere [Finlayson-Pitts and Pitts 2000]. OVOCs contribute also to the formation of secondary organic aerosols (SOA), the predicted global production of SOA is 11.2 Tg yr^{-1} [Chung 2002].

One of the major goals of a laboratory basic research in atmospheric chemistry is to provide kinetic and photochemical data for computer modelling and to deduce atmospheric transformation mechanisms in the case of some important chemicals such as those proposed as new solvents, alternative fuels etc.

The aim of this work is to contribute to the understanding of the atmospheric behaviour of a few oxygenated volatile organic compounds by measuring their kinetic and photochemical parameters. The following compounds were investigated: acetic acid (d_0-AA) and its deuterated isotopes (($CH_3C(O)OD$ (d_1-AA), $CD_3C(O)OH$ (d_3-AA), $CD_3C(O)OD$ (d_4-AA)), methyl-ethyl-ketone (MEK), 2,3-pentanedione (2,3PD), and glycolaldehyde (GA).

The photochemical and kinetic studies of oxygenated volatile organic compounds were carried out in two laboratories: in France, at Ecole des Mines de Douai (EMD) and in Hungary, in Budapest at the Chemical Research Center (CRC).

The following reactions were studied:

OH + $CH_3C(O)OH$ (d_0-AA) → product	k_1	(1)
OH + $CH_3C(O)OD$ (d_1-AA) → product	k_2	(2)
OH + $CD_3C(O)OH$ (d_3-AA)→ product	k_3	(3)
OH + $CD_3C(O)OD$ (d_4-AA) → product	k_4	(4)
OH + $CH_3C(O)CH_2CH_3$ (MEK) → products	k_5	(5)
$CH_3C(O)C(O)CH_2CH_3$ (2,3PD)+ $h\nu$ → products	$\sigma_{2,3PD}$, $J_{2,3PD}$, $\Phi_{2,3PD}$	(6)
OH + $CH_3C(O)C(O)CH_2CH_3$ (2,3PD)→ products	k_7	(7)
$HOCH_2CHO$ (GA)+ $h\nu$ → products	J_{GA}	(8)

Reactions (1-4) and, (6-8) were investigated in EMD and reactions (5-7) in CRC. The methyl-ethyl-ketone was chosen because a direct measurement with the discharge-flow technique has not been reported yet and also, because I wanted to use this reaction and the k_5 value determined from direct measurements in relative rate kinetics experiments as reference. I have selected 2,3PD for kinetic and photochemical studied because practically no information was available about the reactions and photochemistry of this interesting and important molecule. Comprehensive investigations were performed in the two laboratories using different experimental techniques. An other reason was, that I wanted to make comparison with the kinetic and photochemistry of other diketones. To my knowledge, only one single α-diketone, 2,3-butanedione ($CH_3C(O)C(O)CH_3$, biacetyl) has been a subject of OH-kinetic studies [Dagaut 1988b] and [Darnall 1979].

In my Thesis, the experimental methods will be described first, and it will be followed by the section of results and discussion. The experimental results will be presented and compared with the literature separately for each reaction. The reactivity of OH radicals with carbonyls, the atmospheric implications and the summary will be given in the last three chapters.

The pressure is given in *mbar*, the concentration in *molecule* cm^{-3}, the absorption cross section in cm^2 *molecule*$^{-1}$ and the rate constant in cm^3 *molecule*$^{-1}$ s^{-1} in my Thesis.

The given errors mean 1σ statistical uncertainties, usually returned from regression analysis if not otherwise stated. Parameter estimations have been made throughout the Thesis by applying the Origin (version 8) program package.

Chapter 2: Experimental methods

The direct kinetics measurements were carried out using the discharge flow-resonance fluorescence technique (reactions 5,7) at the Chemical Research Center (CRC) in Budapest. For the relative rate kinetics studies (reactions 1-4 and 7) and the photolysis studies (reactions 6,8) I used a Teflon-bag chamber at Ecole des Mines de Douai (EMD). A Pyrex reactor was employed to investigate reaction (7) at CRC. Pulsed laser photolysis studies (reaction 6) were also performed in Budapest. In the present chapter, the experimental setups and the associated analytical devices will be described.

2.1. Direct experimental technique of discharge flow-resonance fluorescence

Reactions (5) and (7) were investigated with the discharge flow - resonance fluorescence (DF-RF) apparatus. This is one of the "absolute" or "direct" techniques used in reaction kinetics investigations. Specific feature of the method is that the reactions occur in a fast inert gas flow and the reaction time is given by the reaction's length and the linear flow velocity of the carrier gas. The velocity of the gas flow can be varied between 1 - 50 m s^{-1}. This technique is suitable for the investigation of elementary gas phase reactions at the millisecond timescale. Reactions of atoms (e.g. H, O, N etc.), diatomic or even polyatomic radicals (e.g. OH, CH_3O, $CH_3C(O)CH_2$, etc.) can be studied with this technique.

The apparatus consist of two main parts: a flow reactor equipped with a moveable injector and a detection part, see Figure 2.1. A gas handling and vacuum system is also connected to the setup. The latter part of the system had multiple functions. It contains Pyrex bulbs to store the diluted gas mixture of reactants and radical sources. H atoms and NO_2 were used to produce the OH radicals: $H + NO_2 \rightarrow OH + NO$; H atoms were generated by dissociating H_2 / He in a microwave discharge (Figure 2.1). 5 % H_2 gas mixture and 1 % NO_2 were prepared in helium. The H_2 / He mixture contained ~10 % Ar to facilitate the dissociation of the molecular hydrogen.

The main carrier gas, high purity helium (99.996 %), was passed through liquid-nitrogen-cooled silicagel traps before entering the flow system to trap even minutes of water vapour. The gas flow of helium was regulated by electric mass flow controllers and the flows of the reactants by needle-valves, which were determined by measuring the pressure-rise in calibrated volumes. Gas mixtures of the reactants in helium were also prepared with the gas handling system.

The gas handling system could be evacuated using a two-stage rotary vacuum pump, which provides an end-vacuum of $p = 1.33 \times 10^{-2}$ mbar. Between the gas handling manifold and the vacuum pump a liquid-nitrogen-cooled trap is placed to trap the condensable gases and prevent back-diffusion of oil vapour to the system.

The flow reactor was made of Pyrex and had the dimension of 40.3 mm internal diameter and 600 mm length. It could be thermostated and its internal surface was coated with halocarbon wax to reduce the heterogeneous loss of OH radicals. The reactor contained a coaxially positioned moveable injector which was used to vary the reaction time. The sliding Pyrex double injector consisted of an outer tube of 16 mm o.d. surrounding a coaxial shorter tube of 6 mm o.d. A quartz discharge tube is attached to the moveable injector to produce H atoms. The H_2 molecules were passed through the discharge where they dissociated in ~15 %. Then the H atoms were reacted with NO_2 inside the injector. An excess NO_2 was used, $[NO_2] / [H_2] > 3$. All of the H atoms were converted to OH radicals before exiting the injector. As it is seen in Figure 2.1, formation of OH radicals occurs separately from the reactants flow. This arrangement reduces the significance of interfering secondary reactions in the studied reaction systems. The reactants were highly diluted in He and were introduced through a side arm of the reactor.

Direct detection of OH radicals was achieved by using the resonance fluorescence (RF) technique. Advantage of this method is that the OH RF lamp emits light exactly at those wavelengths where OH absorbs with high absorption cross sections. OH radicals in the reaction mixture absorb the RF photons and re-emit them. The emitted fluorescence light intensity is proportional to the concentration of the reacting OH radicals. The resonance radiation was induced by a microwave powered OH resonance lamp operated with flowing H_2O vapour / Ar gas mixture at low (~1 mbar) pressure. The emitted fluorescence photons were focused onto the cathode of a perpendicularly positioned photomultiplier ((PM), EMI 9781 QB) and spectral separation was achieved with a 307 nm interference filter placed in front of the

photomultiplier. A light trap was put in the light beam of the resonance lamp leaving the detector block. The analogue signal from the PM was amplified and then it was digitized before entering data acquisition PC board. The minimum detectable OH concentration was approximately 2×10^9 molecule cm^{-3}.

Two high-capacity single-stage pumps were used to produce the fast gas flow in the reactor. A large N_2(l)-cooled trap was placed between the rotary pumps and the end of the flow reactor. The reaction pressure was measured with a capacitance manometer (MKS Baratron).

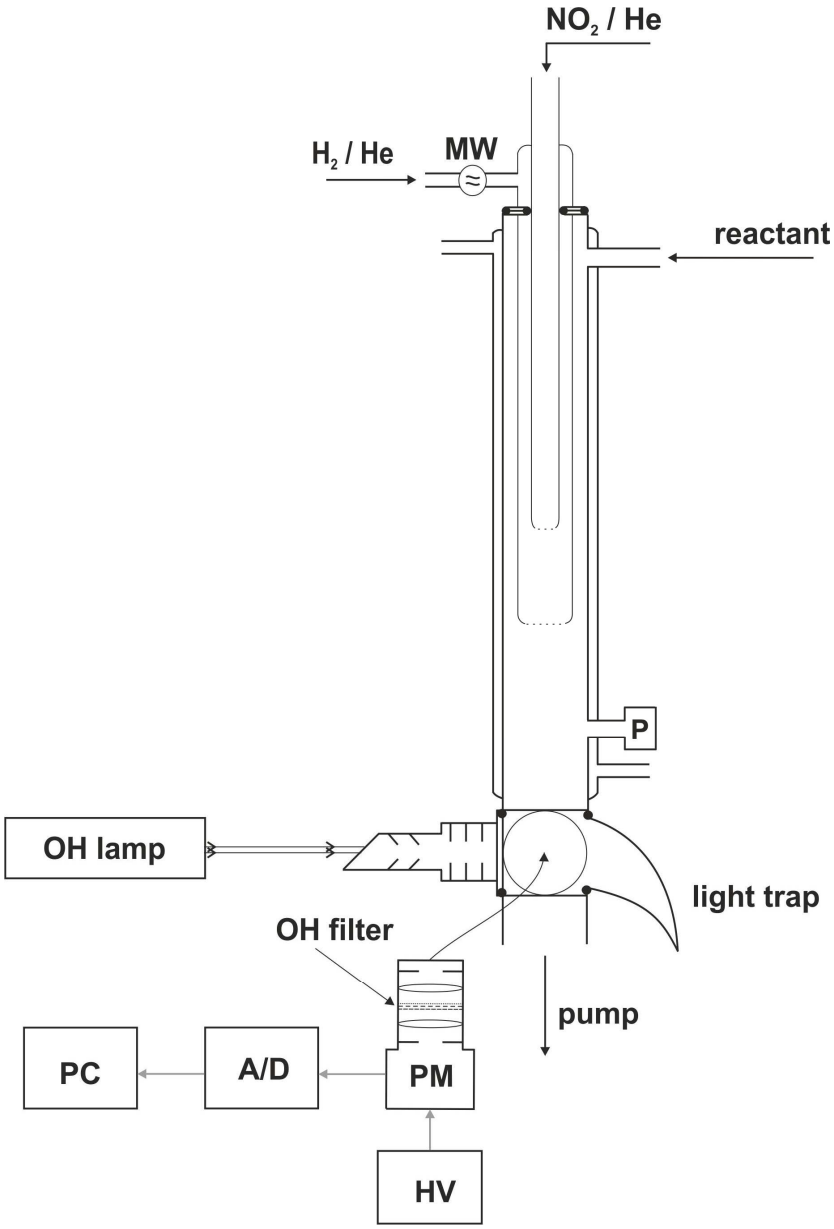

Figure 2.1: The discharge flow-resonance fluorescence (DF-RF) apparatus (Budapest).

2.2. Experimental techniques used in smog chamber type experiments

2.2.1. General description of smog chamber *

Environmental chambers have been widely used in atmospheric chemistry studies since the first research works on photochemical air pollution. Design criteria for these chambers are aimed at reproducing as realistically as possible the conditions in the "real" ambient air, excluding meteorology and the uncontrolled occurrence of pollutants. Thus, chambers can differ in many of the following characteristics:

1. size and shape,
2. surface materials to which the pollutants are exposed,
3. range of pressure and temperature which can be attained,
4. methods of the preparation of reactants,
5. conditions (i.e., static or dynamic mode),
6. analytical capabilities,
7. spectral characteristics of the light source.

The use of chambers involves by necessity the presence of surfaces in the form of the chamber walls, and this represents the largest uncertainty in using them as a surrogate for ambient air studies. Contributing to this uncertainty are the possible unknown heterogeneous reactions occurring on both fresh and conditioned chamber surfaces. Additionally, the outgassing of uncharacterized reactive vapours either those deposited on the walls during previous experiments or released from the plastic films used to construct the chambers can have pronounced effects on certain reaction systems, especially in case of kinetic studies of low-reactivity organics [Lonneman 1981]. Another problem is the reproduction of the actinic radiation to which pollutants are exposed in the real atmosphere.

*This literature survey is based mostly on the monography by Barbara J. Finlayson-Pitts and James N. Pitts, Jr. [Finlayson-Pitts and Pitts 2000]

A brief summary of the types and characteristics of the different smog chambers is presented below:

(A) Glass reactors

Many studies have been carried out in borosilicate (Pyrex) glass reactors similar to those used in typical laboratory studies of gas-phase reactions. They are usually relatively small, ranging from a few litres up to ~100 L. While glass reactors are convenient, inexpensive, and readily available, there are some problems associated with their use. For example, Pyrex glass starts to absorb light at wavelengths ≤ 350 nm and UV light < 300 nm is completely filtered out by the Pyrex walls. In addition, such small vessels have high surface-to-volume (S/V) ratios, which may increase the relative contributions of reactions that occur on the surface.

(B) Collapsible reaction chambers

As a result of these problems, larger smog chambers with surfaces thought to be relatively inert have gained increasing use. Thus, conditioned FEP Teflon films have been shown to have relatively low rates of surface destruction of a variety of reactive species. Collapsible smog chambers are easily constructed using flexible thin films. In addition to the low rates of destruction of reactive species and their transparency to actinic UV, they have the advantage that the size of the chamber can be easily varied.

(C) Rigid chambers

Ideally, one would like to be able to vary the pressure and temperature during environmental chamber runs and to establish the pressure and temperature dependencies of reactions. While glass reactors can be easily designed to include pressure and temperature control, they suffer from other limitations. In addition, the use of very large glass chambers at low pressures presents a potential safety problem. On the other hand, pressure and temperature are not easily controlled using collapsible reaction chambers. Rigid chambers satisfies most design criteria in that both pressure and temperature can be varied, the intensity and spectrum of the irradiation can be altered, and the surface can be coated with a relatively inert material to minimize heterogeneous reactions, pollutant adsorption and offgassing. In addition, ports for both in situ spectroscopic product analysis and sampling can be easily included. The disadvantage is that they are relatively expensive.

2.2.2. Teflon-bag chamber in Douai

The atmospheric simulation facility at the Ecole des Mines de Douai consisted of a wooden enclosure, a collapsible Teflon-bag reactor, one line for introduction of reactants, another line for sampling of the products and different UV fluorescent tubes (Figure 2.2). Reactions (1-4) and (6-8) were investigated in this setup.

The enclosure was a cube with dimensions of 1.20 × 1.20 × 1.00 m. One of its sides can be opened to put-in the Teflon reactor. On two of its side walls, a maximum of 12 fluorescent tubes could be housed. The following lamp models were available to carry out the irradiations:

- fluorescent tubes Philips TUV Tl-D 30 W SLV model, λ_{max} = 254 nm (Figure 2.3).
- fluorescent tubes Philips Tl-K 40 W/05 SLV or 20 W model, λ_{max} = 365 nm (Figure 2.4).
- fluorescent tubes Vilbert-Lourmat T-20M model, 20 W, λ_{max} = 312 nm (Figure 2.5).

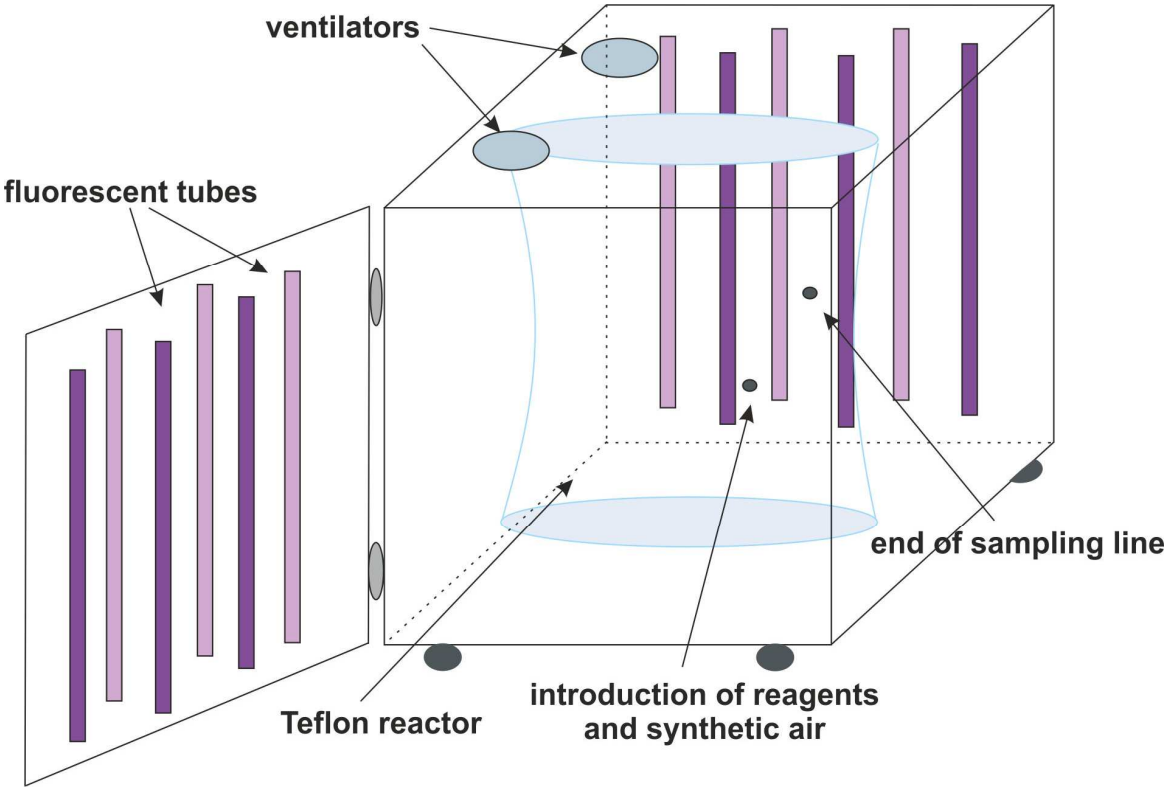

Figure 2.2: Teflon-bag chamber at Ecole des Mines de Douai.

Aluminium plates cover the interior faces of the chamber to allow a uniform distribution of the luminous flux emitted by the lamps.

Two electric fans with a 180 m^3 h^{-1} total capacity are fixed on the walls of the wooden cabinet. They have served to thermostate the chamber by removing extra heat which is released by the operation of the lamps.

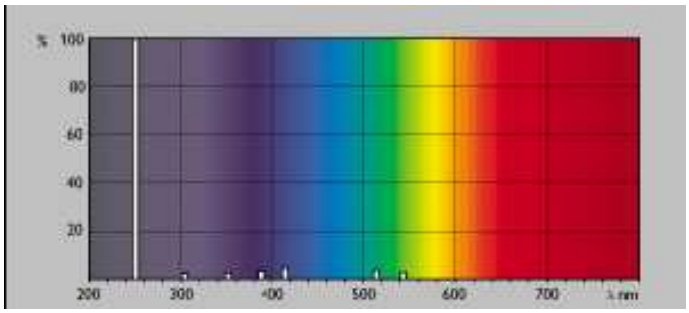

Figure 2.3: Spectra of fluorescent tubes, maximum emission at 254 nm (according to the technical data supplied by the manufacturer).

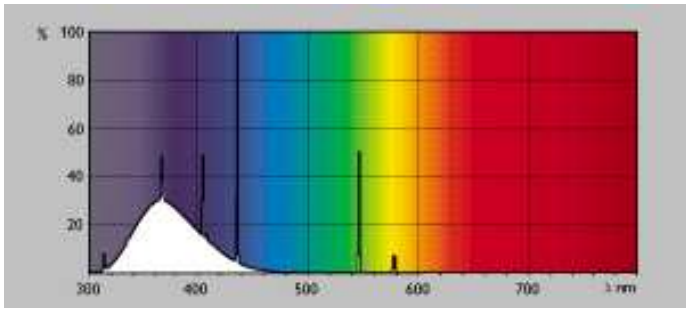

Figure 2.4: Spectra of the fluorescent tubes, maximum emission at 365 nm (according to the technical data supplied by the manufacturer).

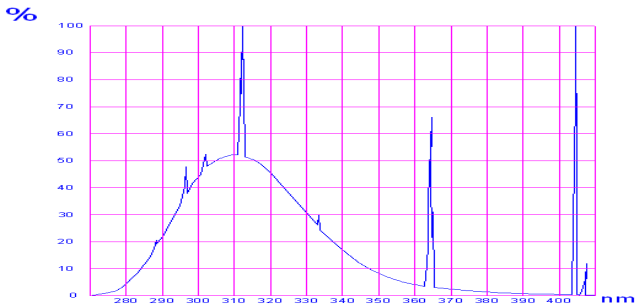

Figure 2.5: Spectra of the fluorescent tubes, maximum emission at 312 nm (according to the technical data supplied by the manufacturer).

The reaction bag is made of 50 µm thickness Teflon FEP film (Du Pont de Nemours). The bag was manufactured in the laboratory by thermal welding of two

rectangular foils of 1.22 m width. This measure of the folia resulted in a reactor a volume of ~250 litres.

Teflon material has been selected because it is more than 80 % transparent at 254 nm and more than 95 % for wavelengths longer than 365 nm [Kelly 1982]. Moreover, Teflon is an inert polymer, which reduces the significance of the heterogeneous reactions on the walls. Finally, Teflon is relatively cheap, which allows replacing of the Teflon reactor regularly thus reducing the risk of contamination by offgasing.

Introduction of the chemicals into the chamber can be carried out in several ways depending on the different physical states of the compounds.

Gases were injected in a synthetic air flow using a gas syringe. The synthetic air is prepared with an air generator (Claind, type AZ 2020), which provides clean air without hydrocarbon contamination (purity > 99 %).

Liquids were injected into a small evacuated glass vessel using a micro-syringe (Figure 2.6), and were allowed to vaporise. A light heating of the vessel could be applied to speed-up the vaporization of the liquid.

The solid reactants were either melted by heat or were solved in water or methanol and vaporized after that by employing the same procedure as for the liquid compounds.

The Teflon-bag reactor was connected to the analytical instrument with a stainless-steel tube with inert coating (Silcosteel) through a mass flow controller (MKS).

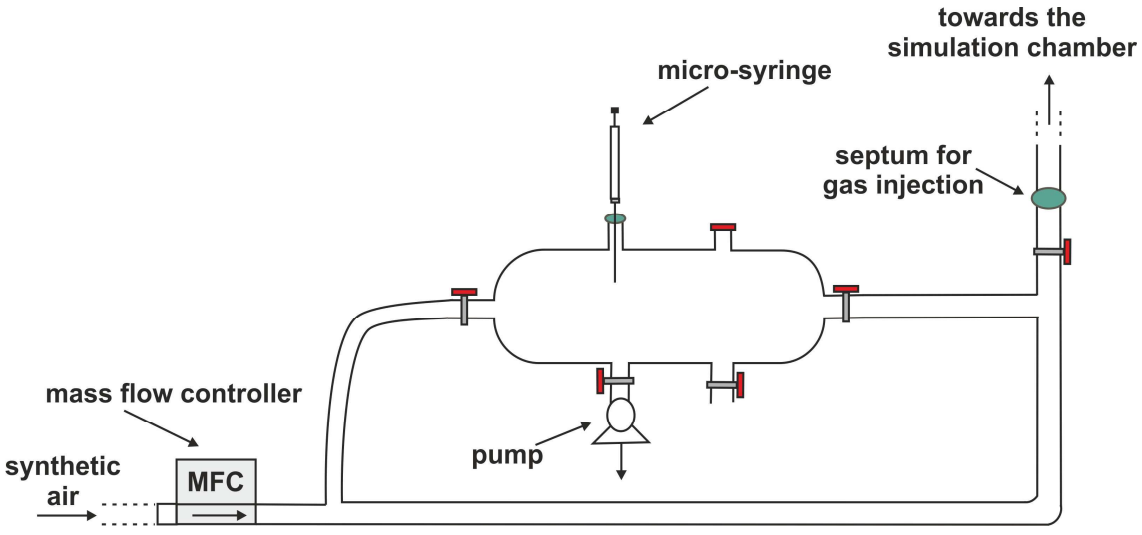

Figure 2.6: The glass chamber used for liquid or solid compounds introduction.

Analytical techniques used for the Teflon-bag chamber experiments

1. Gas chromatograph (GC):

Gas chromatography with flame-ionization detection (GC-FID), (Perkin Elmer, Clarus 500) permits the separation and sensitive detection of the organic compounds of the gas mixture that are sampled from the simulation chamber. The sampling could be carried out by using a gas sampling loop and a thermodesorption system (TCT, Thermal desorption and Cold Trap, Chrompack) which were attached to the GC on-line to provide quantitative analysis. A stainless-steel transfer line with inert coating ("Silcosteel") connected the simulation chamber to the injection system. The gas loop had an internal volume of 20 cm^3. It was connected to a 6-ways valve with manual switching (Valco). The sample was drawn to the loop by a constant flow (~60 ml min^{-1} regulated by a mass flow controller (MKS) and transferred to the TCT for pre-concentration and injection.

The TCT thermodesorption system operates in three successive stages (see Figure 2.7):

- 1: Filling the gas loop and cooling of the cryogenic trap by liquid nitrogen.
- 2: Injection of the gas sample of the loop towards the TCT. The upper part of the TCT is heated to at least 150 °C in order to avoid the deposition of compounds. The lower part is maintained at -190 °C in order to concentrate the sample.
- A very fast heating of the cold trap from -180 °C to 280 °C (60 °C s^{-1}) and in this way a flash injection of the compounds onto the capillary column.

Elution of the organic components is achieved by using a non-polar capillary column (CP SIL 5CB, 50 m length and 0.32 mm internal diameter).

The separated compounds are transported then by a helium gas flow towards the FID detector. The detection limit for oxygenated compounds was a few tens of ppb.

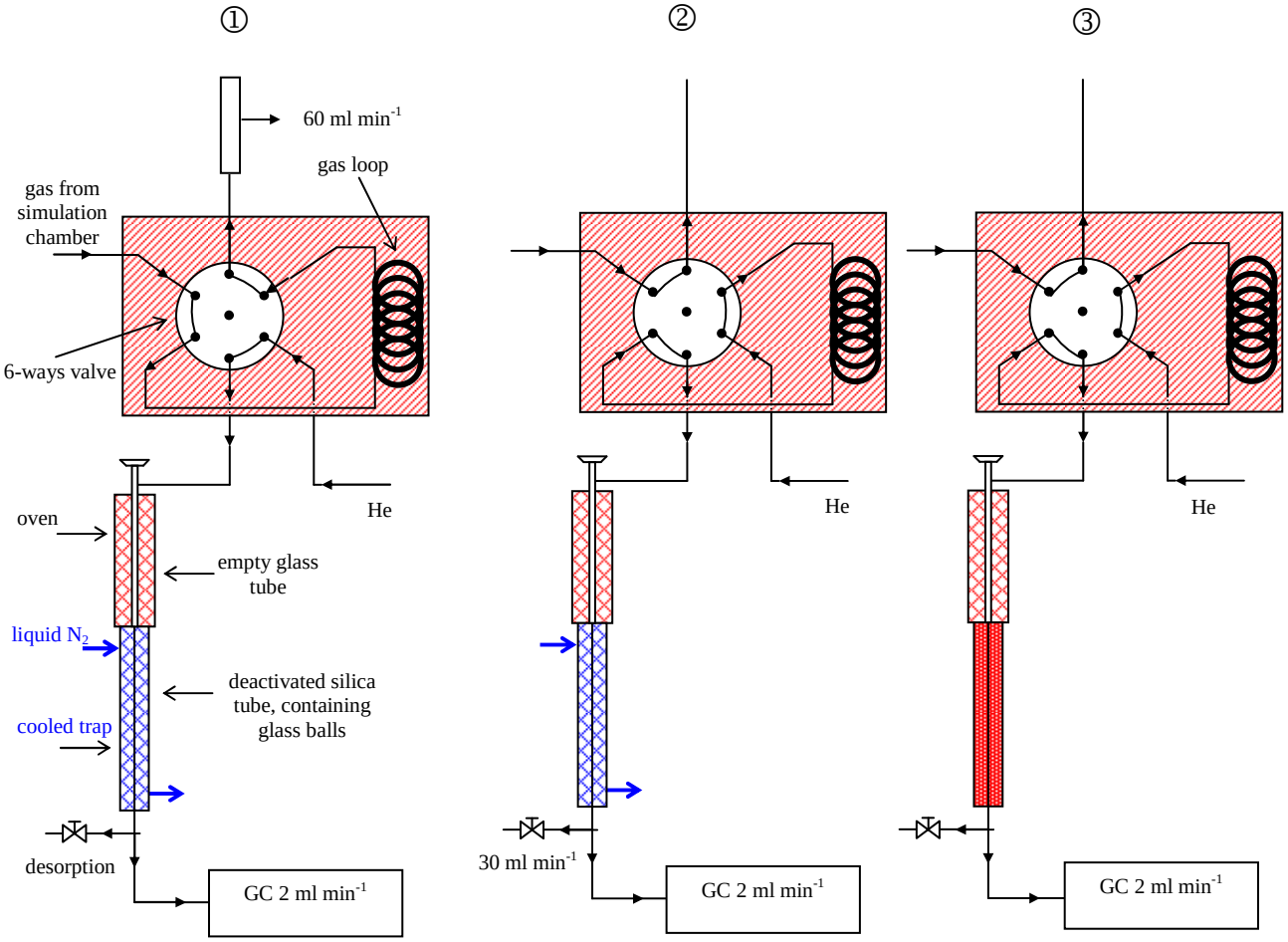

Figure 2.7: Diagram of TCT injection system.
heated zone: 100°C
cooled zone: -190°C
heated zone: 280°C

2. <u>High performance liquid chromatograph (HPLC):</u>

HPLC was used to measure glycolaldehyde concentration and to quantify the formed aldehydes during the photolysis of 2,3PD. Gas samples were taken from the simulation chamber using DNPH cartridges (di-nitro-phenyl-hydrazine) (XPOSURE from Waters) to derivatize carbonyl molecules to hydrazones for a sensitive and selective analysis, see Figure 2.8. The cartridge was connected to the simulation chamber with a Teflon line and the gas sample was transferred through it with a flow of 50 ml min^{-1}; 300 ml of the gas mixture was collected in the cartridge.

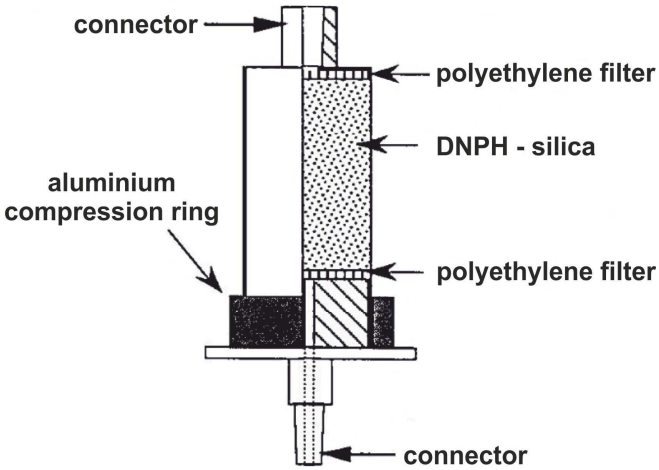

Figure 2.8: DNPH cartridge.

HPLC was used to separate compounds injecting liquid samples. The basic operating principle is to press the chemical compound to be analysed through a column filled with a proper stationary phase by means of a high pressure liquid flow of the mobile phase. I have used a Waters 2695 HPLC model to separate the compounds and detect them with a Waters 2487 UV detector. The detection wavelength was 365 nm.

An Ultra C18 column used which was supplied by Restek and had the following characteristics: length: 250 mm, diameter: 4.6 mm, particle size: 5µm.

The column temperature was maintained at 40 °C during the analyses. The composition of the mobile phase was: 20 % tetrahydrofuran, 30 % acetonitrile and 50 % water; the flow was 1.5 ml min^{-1}.

The DNPH cartridges were eluted with 3 ml acetonitrile, the solution was filtered and an aliquot of 20 µl was injected to the HPLC column. The analysis took 18 minutes.

2.2.3. Actinometry investigations in the Teflon-bag chamber

Basis of NO_2 photolysis for actinometric use

One of the practical problems in simulation chambers is that temperature, surface-to-volume ratio, and relative humidity may have a substantial effect on the results of the experiments. Among these factors, the most crucial parameters include the intensity and spectrum of the light sources used for irradiation. Knowledge of the

intensity and spectrum of the light sources are required for quantitative simulations of the chemistry in smog chambers.

The most widely used technique of measuring ultraviolet radiation intensity in photochemical smog studies is the NO_2 actinometry: it involves the irradiation of dilute NO_2 in a nitrogen atmosphere. This method has long been known in basic photochemistry and it has become generally accepted also in atmospheric research for the calibration of UV sources [Holmes 1973], [Tuesday 1961] [Finlayson-Pitts and Pitts 2000].

The fundamental photochemical process in smog formation is the photolysis of NO_2 and therefore it is also well suited as an actinometer for smog chamber studies:

$$NO_2 + h\nu \rightarrow NO + O(^3P) \qquad (\lambda \leq 420\ nm) \quad (9)$$

A basic feature of the method is to measure the photodepletion of NO_2 as a function of time to determine the photolysis rate constant, J_{NO2} :

$$-\frac{d \ln [NO_2]}{dt} = J_{NO2}, \qquad -\ln\left(\frac{[NO_2]_t}{[NO_2]_0}\right) = J_{NO2} \times t \qquad \text{(Eq. 1)}$$

A potential problem of using NO_2 photolysis in N_2 to determine J_{NO2} is that the photolysis is generally not a first-order process because a number of interfering reactions occur in competition with (9) [Bohn 2004].

In view of this potential problem, the right approach is to conduct NO_2 photolysis in N_2, but taking into account the complex chemistry by computer simulations or using the assumption of stationary states for the reactive intermediates [Holmes 1973].

The mechanism generally employed in interpreting the photolysis of NO_2 in N_2 is presented in Table 2.1.

Table 2.1: Reactions and rate constants for photolysis of NO_2 in N_2 buffer gas.

No	Mechanism: [Holmes 1973]	Rate constant: [Atkinson 2004]
9	$NO_2 + h\nu \rightarrow NO + O$	to be determined
10	$O + O_2 + M \rightarrow O_3 + M$	5.6×10^{-34} cm^6 molecule^{-2} s^{-1}
11	$O_3 + NO \rightarrow NO_2 + O_2$	1.8×10^{-14} cm^3 molecule^{-1} s^{-1}
12	$O + NO_2 \rightarrow NO + O_2$	1.0×10^{-11} cm^3 molecule^{-1} s^{-1}
13	$O + NO_2 + M \rightarrow NO_3 + M$	1.3×10^{-31} cm^6 molecule^{-2} s^{-1}
14	$NO_3 + NO \rightarrow 2\ NO_2$	2.6×10^{-11} cm^3 molecule^{-1} s^{-1}
15	$O + NO + M \rightarrow NO_2 + M$	1.0×10^{-31} cm^6 molecule^{-2} s^{-1}
16	$2\ NO + O_2 \rightarrow 2\ NO_2$	2.0×10^{-38} cm^6 molecule^{-2} s^{-1}
17	$NO_3 + NO_2 \rightarrow N_2O_5$	1.9×10^{-12} cm^3 molecule^{-1} s^{-1}
18	$N_2O_5 \rightarrow NO_3 + NO_2$	6.9×10^{-2} s^{-1}
19	$NO_2 + O_3 \rightarrow NO_3 + O_2$	3.5×10^{-17} cm^3 molecule^{-1} s^{-1}

The primary process (reaction (9)) is dependent on light intensity and the spectrum of the light source while most of the other reactions are related to the oxygen atoms that are formed in reaction (9).

In their paper on the measurement of light intensities in smog chambers, Holmes et al., [Holmes 1973] established the validity of the chemical mechanism presented in Table 2.1 and derived the following equation:

$$\frac{-2\ J_{NO2}}{\dfrac{\mathrm{d}\ln[NO_2]}{\mathrm{d}t}} = 1 + \frac{k_{13}[M]}{k_{12}} + \frac{k_{15}}{k_{12}}\frac{[M]\,[NO]}{[NO_2]} + \frac{k_{10}[M]\,[O_2]}{k_{12}[NO_2]} \qquad \text{(Eq. 2)}$$

where the *k*'s are the rate constants for the corresponding reactions in Table 2.1. According to equation (2) J_{NO2} can be obtained by measuring $[NO_2]$ as a function of the reaction time.

Experimental results for J_{NO2}

The experiments for the determination of J_{NO2} at 312 nm and 365 nm have been carried out in the atmospheric simulation chamber using a 5 % NO_2 gas filling diluted in nitrogen. In the first set of experiments, six lamps emitting at 365 nm were used and the initial concentrations of NO_2 varied between 0.99 and 1.95×10^{13} molecule cm^{-3}. In the

second set of experiments, eight lamps emitting at 312 nm were used and the initial concentrations changed between 2.34 and 8.12 × 10^{13} molecule cm^{-3}. The concentrations of NO_2 and NO were measured using a calibrated commercial NOx analyser (TEI 49 C). The sampling flow was 0.6 L min^{-1}.

Figure 2.9 shows the absorption cross section, σ_{NO2}, between 260 nm and 660 nm [JPL 2006]. σ_{NO2} is 2.16 × 10^{-19} and 5.49 × 10^{-19} cm^2 $molecule^{-1}$ at 312 nm and 365 nm, respectively.

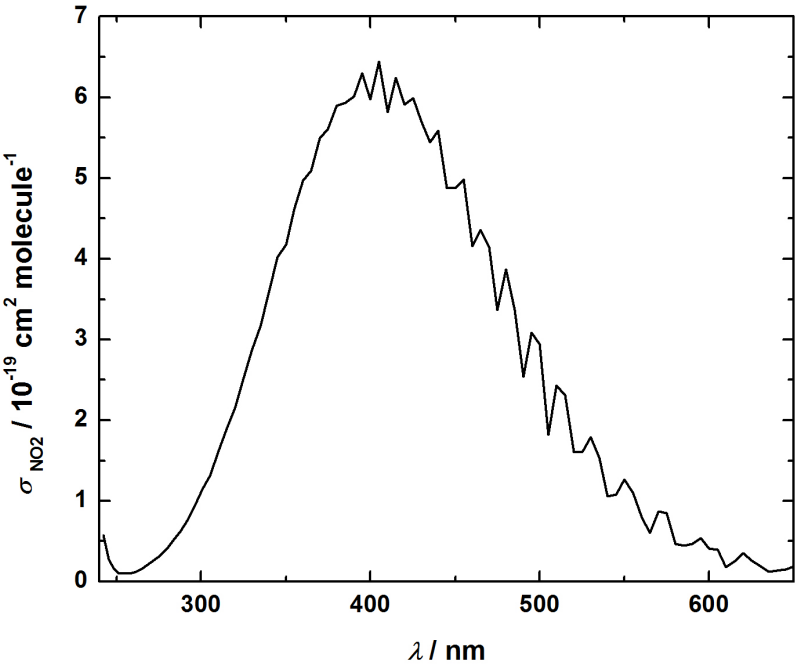

Figure 2.9: Absorption spectrum of NO_2 between 240 - 660 nm [JPL 2006].

In Figure 2.10 the concentration-time profiles of [NO_2], [NO] and [NOx] = [NO_2] + [NO] are presented at 312 nm. The total NOx concentration was found unchanged during the experiment (Fig. 2.10) indicating consistency between the analysis method and the reaction mechanism used.

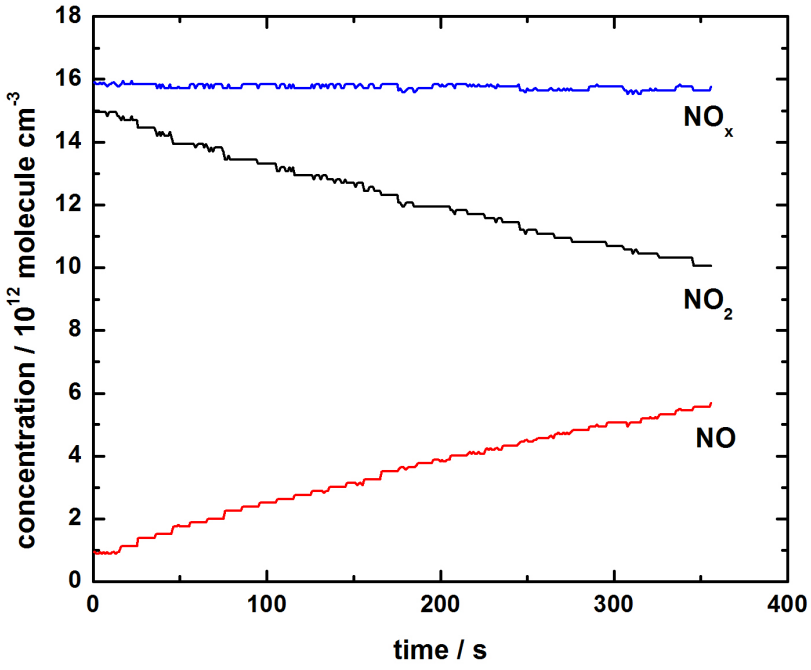

Figure 2.10: NO_2, NO and NOx concentrations versus reaction time during the NO_2 photolysis at 312 nm.

Figure 2.11 shows a plot of ln[NO_2] vs. the photolysis time. As seen, a straight line was obtained and the slope of which was used in Eq.2 to calculate the J_{NO2}.

Since d ln [NO_2] / dt has been found constant and so the same also at t = 0 photolysis time, when $[NO]_0$ and $[O_2]_0$ are zero, Eq.2 is simplified to:

$$\frac{-2\ J_{NO2}}{\dfrac{\mathrm{d}\ln[NO_2]}{\mathrm{d}t}} = 1 + \frac{k_{13}\ [M]}{k_{12}} \qquad \text{(Eq. 3)}$$

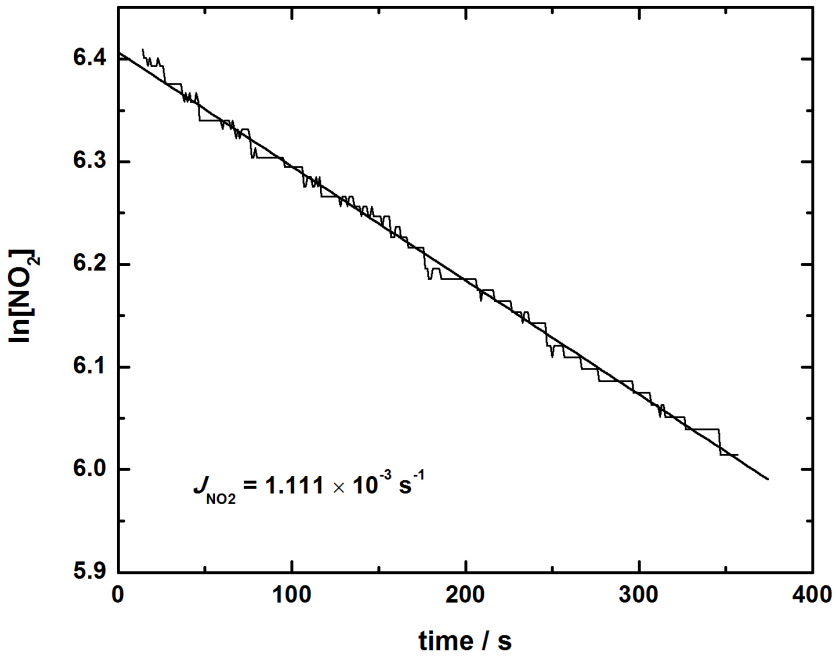

Figure 2.11: Plot of the consumption of NO_2 in a typical photolysis experiment at 312 nm.

The NO_2 photolysis rate constants measured at 312 nm and at 365 nm are summarized in Table 2.2, where the number of experiments and the number of lamps used for the photolyses are also listed.

Table 2.2: Rate constants for NO_2 photolysis.

λ / nm and N° of lamps	**N° of runs**	**$[NO_2]_0$ / 10^{13} molecule cm^{-3}**	**J_{NO2} / 10^{-3} s^{-1}**	**Average J_{NO2} / 10^{-3} s^{-1}**
312 nm and 8 lamps	3	8.01	1.055	1.041 ± 0.003
	3	5.49	1.023	
	3	2.36	1.046	
365 nm and 6 lamps	3	1.95	0.757	0.692 ± 0.040
	3	1.48	0.676	
	3	0.99	0.642	

I note that J_{NO2} values are typically in the range (0.3 – 1.0) × 10^{-2} s^{-1} in the troposphere [Finlayson-Pitts and Pitts 2000]. A globally avereged value of ~ 4 × 10^{-3} s^{-1} can be estimated by detailed modelling studies as reported by Wild and co-workers [Wild 2000] and similar values have been measured experimentally in the SAPHIR outdoor

smog chamber facility: J_{NO2} = 7 – 10 × 10^{-3} s^{-1} (clear sky conditions, noon, 28 July 2002) [Bohn 2004].

Actinometry using acetone photolysis

In this series of experiments, the photolysis rate constant of acetone, J_{Ac}, was measured in the Teflon-bag chamber in synthetic air at atmospheric pressure in order to determine the actinic flux at 254 nm where NO_2 absorbs only very weakly (Fig. 2.9). Six experiments were carried out; the initial concentration of acetone was varied between (5 – 10) × 10^{14} molecules cm^{-3}. Five lamps emitting at 254 nm were used for the irradiation.

At this wavelength, acetone is known to photodissociate into CO and CH_3 with a quantum yield of 1 [Atkinson 2006]:

$$CH_3C(O)CH_3 + h\nu \rightarrow 2\ CH_3CO + CH_3 \qquad (20)$$

$$CH_3CO + M \rightarrow CH_3 + CO + M \qquad (21)$$

The O_2 molecules of the synthetic air captured the CH_3 radicals as non-reactive CH_3O_2 radicals thus preventing the reformation of acetone via radical recombination reactions.

The photolysis rate can be expressed as

$$-\frac{\mathrm{d}[CH_3C(O)CH_3]}{\mathrm{d}t} = J_{Ac} \times [CH_3C(O)CH_3] \qquad \text{(Eq. 4)}$$

After integration of the equation and plotting $\ln([CH_3C(O)CH_3]_0 / [CH_3C(O)CH_3]_t)$ against time, the photolysis rate constant J_{Ac} has been obtained from the slope of the straight line. Figure 2.12 shows the plotted values determined in the photolysis of acetone at 254 nm. The photolysis rate constant obtained is J_{Ac}= (8.68 ± 0.07) × 10^{-5} s^{-1}.

The following equation was used to calculate the actinic flux $F(\lambda)$ (photons cm^{-2} s^{-1}) of the five lamps emitting at 254 nm:

$$F(\lambda) = \frac{J_{Ac}}{\Phi(\lambda)\ \sigma_{Ac}(\lambda)} \qquad \text{(Eq. 5)}$$

where J_{Ac} is the acetone photolysis rate coefficient (s^{-1}), $\Phi(\lambda)$ is the photodissociation quantum yield (molecules $photon^{-1}$) and $\sigma_{Ac}(\lambda)$ is the absorption cross section of acetone (cm^2 $molecule^{-1}$). From the literature, we got $\sigma_{Ac}(254\ nm) = 3.01 \times 10^{-20}$ cm^2 $molecule^{-1}$ and $\Phi_{Ac} = 1$ at $\lambda < 290$ nm [Atkinson 2006]. The actinic flux is then calculated to be $F(254\ nm) = 2.88 \times 10^{15}$ photons cm^{-2} s^{-1}.

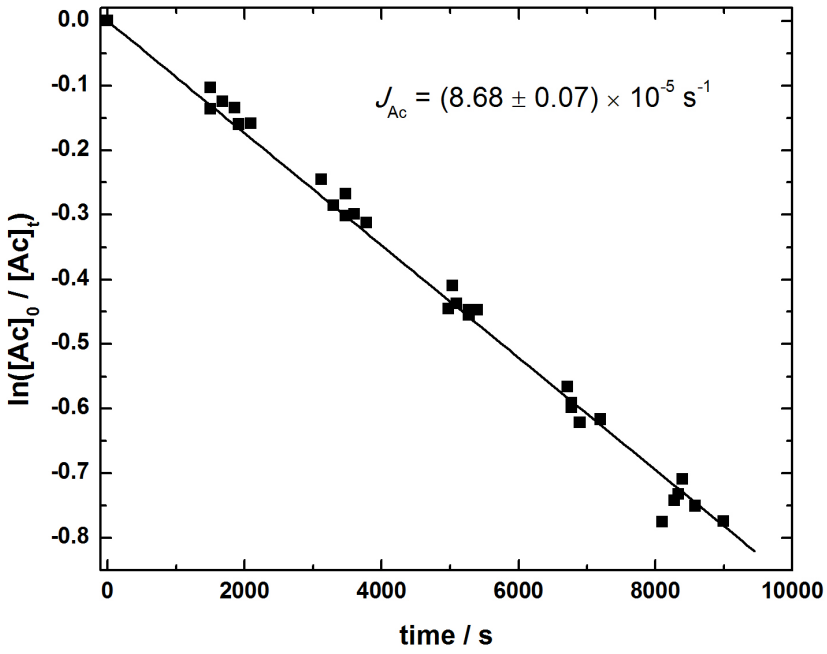

Figure 2.12: Plot to determine the photolysis rate of acetone at 254 nm in the smog chamber.

2.2.4. Pyrex reactor setup used for the relative rate kinetics measurements in Budapest

The relative rate (RR) kinetic measurements of reaction (6) were carried out in Budapest using the experimental set-up shown in Figure 2.13. For the production of OH radicals, we used a modified movie projector by photolysing CH_3ONO in synthetic air. The light source was a 3 kW Xe arc.

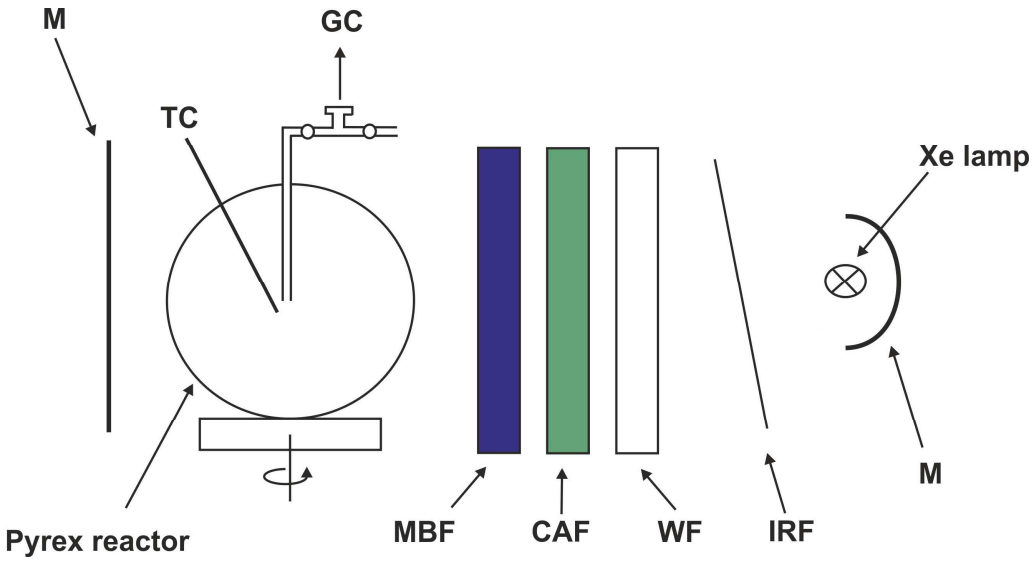

Figure 2.13: Set-up for relative rate kinetics measurements in Budapest.
M = mirror, IRF = infrared filter, WF = water filter, CAF= chrome alum filter, MBF = methylene blue filter, TC= retractable thermocouple.

A parabolic reflector collimated the light of the Xe arc to a parallel beam of about 30 cm diameter. The infrared part was removed from the irradiating light by means of a heat reflecting mirror in the lamp house and a water filter was placed in the light beam. Solution filters were used to isolate the wavelength around 360 nm. The filter combination reported Pearlyn and co-workers was applied [Pearlyn 1977]: a 7×10^{-3} mol dm^{-3} $Cr_2KO_8S_2$ x 12 H_2O (chrome alum) and a 3×10^{-5} mol dm^{-3} methylene blue hydrate aqueous solution were prepared. The water filter, chrome alum and methylene blue solution filters (12 cm optical path each) were placed between the light source and the Pyrex-bulb reactor. The light intensity transmitted through the water and solution filters was measured with the Merlin spectrophotometer, see Section 2.3. Figure 2.14 shows the spectrum of transmitted light. The maximum is at 362 nm and the FWHM (full width at half maximum) is 28 nm.

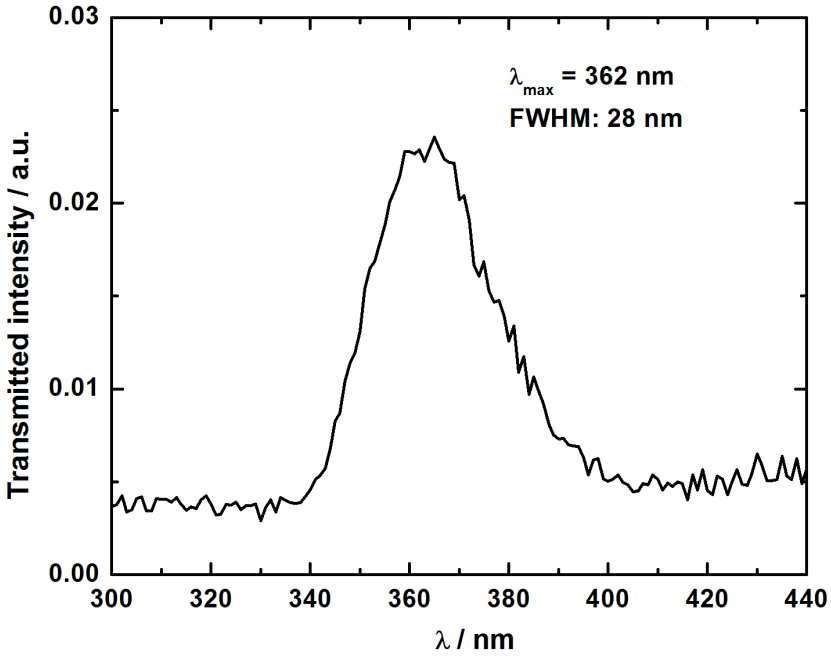

Figure 2.14: The spectrum of the transmitted light of the Xe lamp used for the RR experiments in Budapest.

To maintain uniform reaction conditions in the irradiated mixture, the Pyrex-bulb reactor was rotated with a speed of 16 rpm and a mirror was placed behind it. The reaction temperature was measured with a retractable thermocouple inside the reactor and was found constant in the whole reaction volume, $T = 302 \pm 4$ K. The Pyrex reactor was equipped with a thin glass tube which reached in the centre of the reactor and it was connected to a septum for gas chromatographic analysis. The dead volume of the sampling line was evacuated and flushed through with the reaction mixture at least 3 times before sampling.

A HP 5840A type gas chromatograph with flame ionization detector was used to follow the 2,3PD concentration depletion during the pulsed laser photolysis (PLP) and relative rate kinetic measurements in Budapest. For the injection of the gas sample, a 250 µl gas-microsyringe was used. To avoid the uncertainty arising from reproduction problems during injections, a chemically and photochemically inert internal gas chromatographic standard, perfluoro-cyclobutane (*c*-C_4F_8), was used premixed with the reaction mixture. This GC standard does not absorb at the wavelengths used for laser photolysis and the relative rate kinetic measurements. A DC 550 type column (length:

45 m, internal diameter: 0.5 mm) was used to separate the organic compounds at 80 °C, N_2 was the carrier gas.

2.3. Description of the Merlin spectrophotometer

The UV absorption cross section measurements of 2,3-pentanedione were carried out using a home-built single-path UV / Vis spectrophotometer (Figure 2.15). The central part of this apparatus is a digital control unit (Oriel, Merlin^{TM} control unit), hereinafter called “Merlin spectrophotometer”.

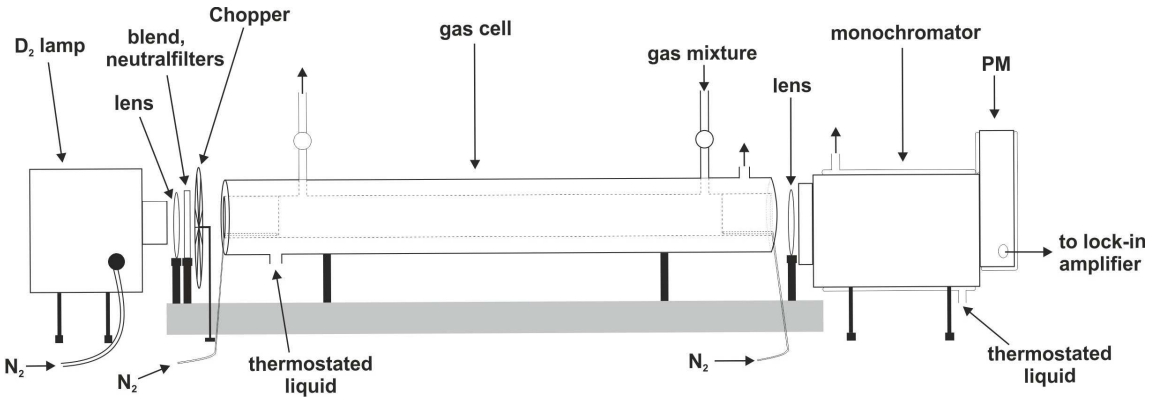

Figure 2.15: The Merlin spectrophotometer for determination of UV / Vis absorption cross sections in the gas phase.

The main parts of the equipment are:

– D_2 lamp (Hamamatsu L2196, HB type, SQ cathode): the emission of excited D_2 molecules gives a continuous spectrum in a wide UV range. To avoid ozone formation, which is toxic and absorbs UV light the lamp was purged with N_2.

– Gas cell: the light beam of D_2 lamp was passed through the gas cell using Surasil lenses, an iris blend and neutral filters. The absorption cell was 50.2 cm long, made of quartz, and could be thermostated.

– Monochromator (Oriel 77200): the light beam leaving the cell was focused onto the entrance slit of the monochromator. The monochromator was also thermostated since it was found to be very important in order to obtain accurate absorption cross sections in previous measurements [Nádasdi 2009].

– Photomultiplier ((PM), Thorn Emi 9781 B): the photomultiplier was attached to the exit slit of the monochromator. A highly stable power supply provided the 800 V high voltage to operate the PM. The electric current from the photomultiplier was passed through a 100 kΩ resistance to be converted to voltage which was fed to a digital control unit.

– Digital control unit (Oriel, Merlin^{TM} control unit): this part served as a wide-range lock-in amplifier and provided control and data acquisition functions for automatic recording of spectra using the Runes^{TM} II software.

2.4. Description of the pulsed laser photolysis technique

The pulsed laser photolysis (PLP) technique was employed to determine the photolysis quantum yield of 2,3-pentanedione at 351 nm using a XeF exciplex laser (Lambda Physik, LPX 100). Other parts of set-up were: a cylindrical quartz reactor, a gas handling system, a gas chromatograph (HP 5840) and a laser energy meter (Gentec, OE25SP-H-MB-DO).

The optical path length, internal diameter and the volume of the quartz cell were 11.6 cm, 3.6 cm and 120.6 cm^3, respectively. The reactor was equipped with a GC sampling port mounted with a septum joint to withdraw samples for analysis using a 250 µl gas syringe (Figure 2.16). The dead volume of the sampling line was evacuated and flushed through two times with the reaction mixture before sampling.

The laser energy was measured with a laser energy meter. The transient voltage signal of the energy meter was measured with an oscilloscope (HP, 54601A), and 64 laser pulses were averaged. The laser energy entering the photolysis cell was measured before and after the photolysis, their average was used for the quantum yield calculations, see Section 3.3.2. The energy was typically ~20 mJ pulse^{-1}.

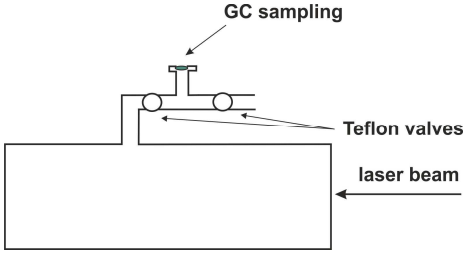

Figure 2.16: The cylindrical quartz cell used in the pulsed laser photolysis experiments (Budapest).

2.5. Materials

The different chemicals used in the experiments are summarized in Table 2.3. At EMD the carrier gases and reactants were used from the gas cylinders without further purifications. The liquid and solid compounds were also applied as provided by the suppliers.

At CRC Budapest, the carrier gas helium, used in the (DF-RF) experiments was passed through liquid-nitrogen-cooled silicagel traps before entering the flow system. The liquid compounds used were degassed by freeze-pump-thaw cycles to remove solved air before preparing a gas mixture. 2,3-pentanedione (Merck, 98%) used in the experiments in Budapest was purified by vacuum distillations (6 times), and the purity was checked by gas chromatographic analysis; the purity of the sample was > 99 %.

Methyl-nitrite (CH_3ONO) was synthesised following the classical procedure [Taylor 1980]. It was prepared in a three-neck flask by adding 50 % H_2SO_4 – H_2O (ion exchanged) to a saturated $NaNO_2$ solution of 50 % CH_3OH – H_2O. The tubing of the dropping funnel with H_2SO_4 / H_2O reached below the surface of the $NaNO_2$ solution. The flask was immersed in ice water bath and was slowly stirred. The methyl-nitrite product of the synthesis was carried away by a stream of N_2 gas of the flask by introducing N_2 through one of the side arms of the flask. The other side arm was equipped with a 20 cm long reflux condenser which was attached to a trap containing granulated $CaCl_2$. $CaCl_2$ served to remove the unreacted methanol and water traces. The effluent CH_3ONO / N_2 gas was led through a trap kept at – 80 °C – (– 90) °C by using an ethanol bath cooled to the desired temperature by adding liquid nitrogen. An absorbing tube filled with $CaCl_2$ granulates was attached to the cooled trap to avoid back diffusion of laboratory moisture. The methyl-nitrite product was obtained as a pale yellow liquid. The trap with the collected CH_3ONO was attached to a vacuum system. The methyl-nitrite was cooled to liquid N_2 temperature and was degassed by a multiple pump-freeze-thaw cycles. After that it was warmed up to room temperature and ~ 10 % of it was distilled as a prefraction and was pumped away. The middle fraction was collected at N_2(l) temperature and about 10 % residual was left. The middle fraction was put to -75 °C (EtOH – N_2(l)) bath and was subjected to bulb-to-bulb distillation by collecting again about 80 % middle fraction. This later procedure was repeated three more times. The purified CH_3ONO was stored protected from light at the deep freeze

temperature of a refrigerator in a vial equipped with Teflon valve. The purity of the synthesised CH_3ONO was checked by GC analysis on a DC550 column using FID detection. Only a small amount (< 0.15 %) of unidentified impurity was detected.

Table 2.3: Materials used in the experiments.

Materials	Supplier	Purity	Reaction	Application method
$CH_3C(O)OH$	Merck	96 %	1	reactant
$CH_3C(O)OD$	Acrôs Organics	98 % D	2	reactant
$CH_3D(O)OH$	CDN Isotopes	99.2 % D	3	reactant
$CH_3D(O)OD$	Euriso-top	99.1 % D	4	reactant
methanol [a]	Merck	99.9 %	1, 3	RR
CD_3OD [a]	Euriso-top	99.8 % D	2, 4	RR
methyl-ethyl-ketone [a]	Sigma-Aldrich	99.9 %	5, 7	reactant, RR
glycoladehyde	Fluka	≥ 98.0 %	8	reactant
2,3-pentanedione [c]	Sigma-Aldrich	97 %	6, 7	reactant
	Merck	≥ 98 %		
ethanol [a]	Merck	99.9 %	7	RR
NO_2 (5% in He) [b]	Linde			AE
acetone [b]	Merck	> 99.9 %		AE
HCHO solution in water and 15 % CH_3OH	ACS reagent	38 %	8	HCHO calibration
sodium-nitrite	Sigma-Aldrich	99.5 %	1-4, 7	CH_3ONO synth.
methanol	Riedel-de-Haën	> 99.7 %	1-4, 7	CH_3ONO synth.
sulphuric acid	Sigma-Aldrich	95-98 %	1-4, 7	CH_3ONO synth.
nitrogen	Messer	99.5 %	1-4, 7	CH_3ONO synth.
calcium chloride	Fluka	> 97.0 %	1-4, 7	CH_3ONO synth.
argon	Linde Gas	99.999 %	5, 7	DF-RF
helium	Messer-Griesheim	99.996 %	5-7	DF-RF and PLP
NO_2 [d]	Messer-Griesheim	98 %	5, 7	DF-RF
hydrogen	Linde Gas	99.998 %	5-7	DF-RF, GC
F_2 (5% in 99.996% He)	Messer		6	PLP
xenon	Messer	99.998 %	6	PLP

Table 2.3: (continued)

Materials	Fabricant	Purity	Reaction	Application method
perfluoro-cyclobutane (*c*-C_4F_8)	PCR Inc.	99 %	6, 7	GC standard
synthetic air	air generator [e]	> 99 %	1-4, 6-8	
	Messer	≥ 99.99 %	6, 7	
	Messer	technical purity		for the FID of GC
$Cr_2KO_8S_2$ x 12 H_2O (chrom alum)	Sigma-Aldrich	> 98 %	6	solution filter
methylene blue hydrate	Sigma-Aldrich	≥ 99.0 %	6	solution filter
water	ion changed			CH_3ONO synth
	Merck	99.9 %		HPLC analysis
acetonitrile	Merck	99.9 %		HPLC analysis
tetrahydrofuran	Merck	99.9 %		HPLC analysis
helium	Linde Gas	99.996 %		GC carrier gas
N_2	Messer	99.995 %		GC carrier gas
cyclohexane (*c*-C_6H_6)	Merck	99.5 %		OH-scavenger
1-pentene	Merck	99 %		OH-scavenger

[a] Reference compound in relative rate kinetic experiments (RR).
[b] Actinometry experiments (AE).
[c] 2,3PD from Sigma Aldrich was used in EMD, 2,3PD from Merck was used in CRC.
[d] NO_2 was put from the gas cylinder into a cooled vessel and was kept during 1 day under O_2 to eliminate lower oxidation nitrogen-oxides. After that, it was purified by vacuum distillation and kept in dark before use.
[e] Air generator used et EMD (from Claind, type AZ 2020).

Chapter 3: Results and discussions

3.1. Relative-rate kinetic study of the reactions of OH radicals with acetic acid and its deuterated isomers

Recently, the atmospheric chemistry of organic acids has become again the focus of interest since these organics contribute significantly to the acidity of the atmospheric precipitation. The monocarboxylic acids for example formic acid and acetic acid, are responsible mainly for the acidity observed in the remote regions [Andreae 1988].

Acetic acid is one of the most important oxygenated volatile organic compounds (OVOCs) in the atmosphere. It contributes significantly to the atmospheric HO_x and O_3 budget and the acidity of rain and cloudwater. In the troposphere, it is produced by the reactions of peroxy-acetyl radicals ($CH_3C(O)OO$) with HO_2 and CH_3O_2:

$$CH_3C(O)OO + HO_2 \rightarrow CH_3C(O)OH + O_3$$
$$CH_3C(O)OO + CH_3O_2 \rightarrow CH_3C(O)OH + CH_2O + O_2$$

$CH_3C(O)OH$ has got also direct sources: it is emitted directly from the vegetation, from the soil [Talbot 1990], [Enders 1992] and from snow packs [Dibb 2002] . The anthropogenic sources are also significant including biomass burning [Talbot 1995] and vehicle exhaust from transport [Kawamura 1985].

Reaction kinetics of the reaction between $CH_3C(O)OH$ and the OH radical have been investigated in substantial detail in the past few years and it has been discussed in a recent feature article [Carl 2007]. In contrast, literature data on the OH-initiated reactions of the deuterated acetic acids are very sparse [Crunaire 2006, Singleton 1989, Vimal 2006]. Kinetic data on the OH + deutero-acetic-acid reactions are useful for a better understanding of the mechanism of the OH reaction of $CH_3C(O)OH$ itself and in this way for assessing the impact of acetic acid on the chemistry of the atmosphere.

The following reactions were investigated [Szabó 2009]:

$$OH + CH_3C(O)OH \rightarrow \text{products} \quad (1)$$
$$OH + CH_3C(O)OD \rightarrow \text{products} \quad (2)$$
$$OH + CD_3C(O)OH \rightarrow \text{products} \quad (3)$$
$$OH + CD_3C(O)OD \rightarrow \text{products} \quad (4)$$

Henceforth, *AA* is used as a general abbreviation for all of the four acetic acid isomers studied, while d_0-*AA*, d_1-*AA*, d_3-*AA*, and d_4-*AA*, designate $CH_3C(O)OH$, $CH_3C(O)OD$, $CD_3C(O)OH$, and $CD_3C(O)OD$, respectively.

All experiments were carried out in the 250 L Teflon reactor at Douai. The rate constant of each reaction has been determined at T = (300 ± 2) K and atmospheric pressure in air buffer gas using the relative rate method (see Appendix 1). The OH radical precursor was methyl nitrite (CH_3ONO), it was synthesised following the classical procedure [Taylor 1980] and stored at -30 °C. The reference compounds, (*ref*), were methanol (CH_3OH) for the kinetic study of d_0-*AA*, d_3-*AA* and methanol-d_4 (CD_3OD) for d_1-*AA*, and d_4-*AA*. The concentrations of reactants were followed as a function of the reaction time by using a GC-FID; for details see Section 2.2.2. The GC analysis was started at 50 °C and the following programmed temperature heating was used: temperature was held at 50 °C for 2 minutes, and then increased from 50 °C to 250 °C with a rate of 15 °C min^{-1}.

The experimental conditions and results have been summarized in Table 3.1.

Table 3.1: Experimental conditions and results for the OH + *AA* reactions.

reactant (i)	**N° of exp.**	$[AA]_0$ [a]	$[ref]_0$ [a]	$(k_i / k_{ref}) \pm 1\sigma$	$(k_i \pm 1\sigma)$ [b]
$CH_3C(O)OH$ (1)	2	0.5 – 2	0.3 – 1.5	0.70 ± 0.10	6.3 ± 0.9
$CH_3C(O)OD$ (2)	3	0.5 – 2	0.5 – 2	0.46 ± 0.08	1.5 ± 0.3
$CD_3C(O)OH$ (3)	2	0.5 – 2	0.3 – 1.5	0.70 ± 0.10	6.3 ± 0.9
$CD_3C(O)OD$ (4)	4	0.5 – 2	0.5 – 2	0.28 ± 0.04	0.90 ± 0.1

[a] In 10^{15} molecule cm^{-3}, reference compound, *ref*, is CH_3OH for $CH_3C(O)OH$ and $CD_3C(O)OH$, and CD_3OD for $CH_3C(O)OD$ and $CD_3C(O)OD$.
[b] In 10^{-13} cm^3 $molecule^{-1}$ s^{-1}.

Representative plots of $\ln([AA]_0 / [AA]_t)$ versus $\ln([ref]_0 / [ref]_t)$ are shown in Figures 3.1 and 3.2. The straight lines correspond to a linear regression on the experimental data. The acetic acid isomers d_0-*AA* and d_3-*AA* present identical rate constant ratios: $k_1/k_{22} = 0.70 \pm 0.10$ and $k_3/k_{22} = 0.70 \pm 0.10$. Using the recommended rate constant of reaction OH + CH_3OH (22), $k_{22} = (9.00 \pm 0.08) \times 10^{-13}$ cm^3 $molecule^{-1}$ s^{-1} [Atkinson 2006], the respective rate constant ratios can be translated to the absolute values of $k_1 = (6.3 \pm 0.9) \times 10^{-13}$ cm^3 $molecule^{-1}$ s^{-1} and $k_3 = (6.3 \pm 0.9) \times 10^{-13}$ cm^3 $molecule^{-1}$ s^{-1}.

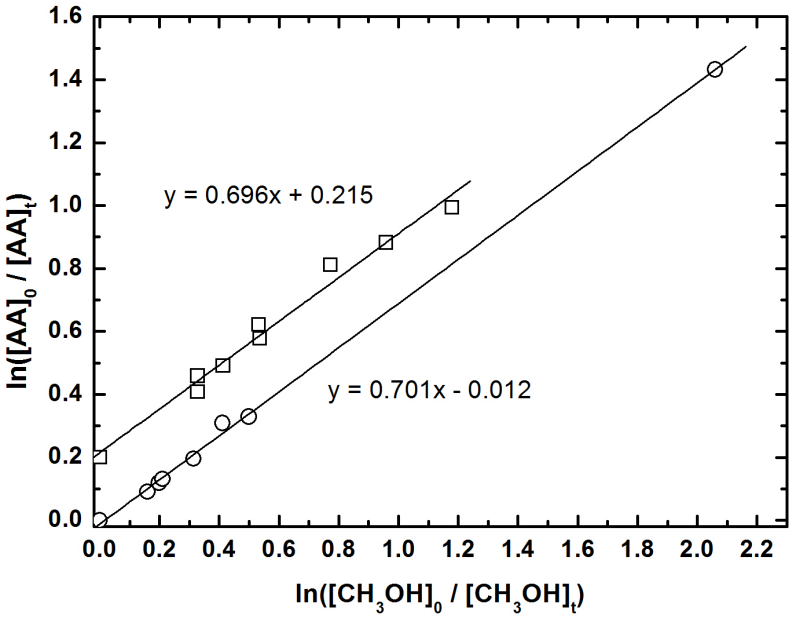

Figure 3.1: Typical plots of $\ln([AA]_0 / [AA]_t)$ vs $\ln([CH_3OH]_0 / [CH_3OH]_t)$ for *AA* = $CH_3C(O)OH$ (squares) and $CD_3C(O)OH$ (circles). The $\ln([AA]_0 / [AA]_t)$ data for $CH_3C(O)OH$ have been shifted by 0.2 for clarity.

The rate constant ratios for d_1-*AA* and d_4-*AA* differ by a factor of 1.6: $k_2/k_{23} = 0.46 \pm 0.08$ and $k_4/k_{23} = 0.28 \pm 0.04$. For the reaction of OH + CD_3OD (23), the rate constant value of Parker et al. was used: $k_{23} = (3.2 \pm 0.2) \times 10^{-13}$ cm^3 $molecule^{-1}$ s^{-1} [Parker 2009]. The resulting k_2 and k_4 values are: $k_2 = (1.5 \pm 0.3) \times 10^{-13}$ cm^3 $molecule^{-1}$ s^{-1}, and $k_4 = (0.90 \pm 0.1) \times 10^{-13}$ cm^3 $molecule^{-1}$ s^{-1}. Uncertainties do not include the uncertainties in the reference rate constants, which was re-estimated to be about 15% for the OH + CH_3OH [Atkinson 2006] and at least 30% for the OH + CD_3OD reaction [Szabó 2009].

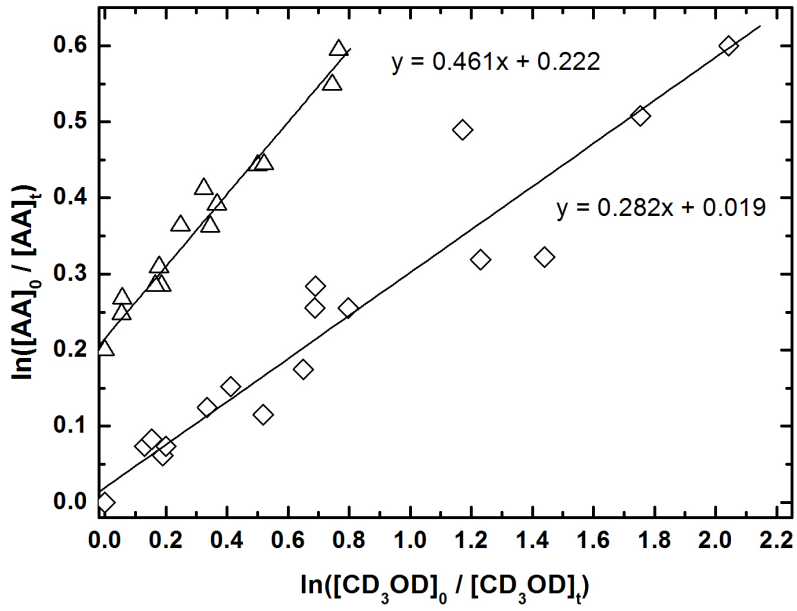

Figure 3.2: Typical plots of $\ln([AA]_0 / [AA]_t)$ vs $\ln([CD_3OD]_0 / [CD_3OD]_t)$ for *AA* = $CH_3C(O)OD$ (triangles) and $CD_3C(O)OD$ (rhombus). The $\ln([AA]_0 / [AA]_t)$ data for $CH_3C(O)OD$ have been shifted by 0.2 for clarity.

A comparison of all the rate constant values that have been reported for reactions (1-4) in previous works is presented in Table 3.2 ([Khamaganov 2006], [Butkovskaya 2004], [Crunaire 2006], [Singleton 1989], [Vimal 2006], [Zetzsch and Stuhl 1982], [Dagaut 1988a], [Huang 2009]).

Table 3.2: Comparison of room temperature rate constants for the reactions of OH radicals with acetic acid and deutero acetic acids. The errors given are those reported by the authors.

reaction (i)	k_i [a]	reference
OH + $CH_3C(O)OH$ (1)	5.99 ± 0.39	[Zetzsch and Stuhl 1982]]
	7.4 ± 0.3	[Dagaut 1988a]
	8.6 ± 0.3	[Singleton 1989]
	6.6 ± 0.4	[Butkovskaya 2004]
	6.5 ± 0.3	[Crunaire 2006]
	7.42 ± 0.06	[Vimal 2006]
	8.50 ± 0.45	[Khamaganov 2006]
	6.77 ± 0.14	[Huang 2009]
	6.3 ± 0.9	[Szabó 2009]
OH + $CH_3C(O)OD$ (2)	1.5 ± 0.3	[Szabó 2009]
OH + $CD_3C(O)OH$ (3)	8.1 ± 0.2	[Singleton 1989]
	7.79 ± 0.08	[Vimal 2006]
	6.3 ± 0.9	[Szabó 2009]
OH + $CD_3C(O)OD$ (4)	1.09 ± 0.09	[Vimal 2006]
	0.9 ± 0.1	[Szabó 2009]

[a] In10^{-13} cm^3 $molecule^{-1}$ s^{-1}.

The rate constant for the OH + d_0-*AA* reaction has been determined in several investigations. My result is in good agreement with those from previous studies, though it is in the lower range of the literature values. I note that my rate constant agrees very well with the very recent absolute determination of k_1 (295 K) = (6.77 ± 0.14) × 10^{-13} cm^3 $molecule^{-1}$ s^{-1} by Huang and co-workers [Huang 2009].

To the best of my knowledge, the rate constant measured for the OH + d_1-*AA* (2) reaction represents the first kinetic determination.

Rate constants for the OH + d_3-*AA* (3) reaction have been reported in two papers [Singleton 1989], [Vimal 2006], with which my result agrees reasonably well: it is on average about 25 % smaller. In view that Singleton et al. and Vimal and Stevens applied direct kinetic methods under very different experimental conditions, the agreement is satisfactory.

Concerning the OH + d_4-*AA* (4) reaction, the agreement with the only determination of k_4 available in the literature [Vimal 2006] is very good, despite the fact that the authors used much higher acetic acid concentrations (up to 4.5×10^{16} molecule cm^{-3}) than that was applied in the present study (2×10^{15} molecule cm^{-3}). It should be mentioned that the uncertainty is still significant (only three determinations). Application of CH_3OH as a reference for the OH + $CD_3C(O)OD$ (4) reaction was unsuccessful because of the occurrence of a significant isotope exchange reactions in the reaction system.

A few conclusions can be directly established by the kinetic data presented in Table 3.2. The rate constant of the OH + $CH_3C(O)OH$ (1) is about 6-times higher than that of the OH + $CD_3C(O)OD$ (4) indicating a significant primary kinetic isotope effect. The rate constant value of the OH + $CH_3C(O)OD$ (2) reaction is close to that of the OH + $CD_3C(O)OD$ (4) reaction while it is only about ¼-th of that of the OH + $CH_3C(O)OH$ (1) reaction. These findings are in accordance with the literature suggestions, e.g. [Butkovskaya 2004] and [Vimal 2006], that the acidic H-atom is abstracted preferentially in the reaction of OH with acetic acid. For further discussions of the reactivity properties of the studied VOCs with OH see Section 3.5.

3.2. Direct rate constant for the reaction of OH radicals with methyl-ethyl-ketone

Methyl-ethyl-ketone (MEK) or butanone ($CH_3C(O)CH_2CH_3$) has a significant concentration in the global troposphere [Singh 2004]. It originates both from direct anthropogenic and biogenic sources, but it is mostly produced from the photooxidation of *n*-butane and >C5 iso-alkanes in the atmosphere [Singh 2004] [Sommariva 2008]. MEK occurs in relatively high concentrations in air masses for example in urban plumes [Fehsenfeld 2006], coastal marine atmosphere [Galbally 2007] and rural mountain air [Khwaja 2008], occasionally amounting up to 13 – 17 % of the total carbon detected [Khwaja 2008]. MEK is removed from the atmosphere primarily by its reaction with OH-radicals [Szabó 2008] and to a lesser extent also by photolysis [Le Calvé 1998] [Nádasdi 2010].

$$OH + CH_3C(O)CH_2CH_3 \rightarrow \text{products} \qquad (5)$$

This reaction was investigated previously by several research groups, applying both direct [Carr 2008], [Jiménez 2005] and relative-rate methods [Edney 1986], [Cox 1981]. Prior to my work, among the absolute rate constant determinations there was no rate constant reported by the application of the thermal low-pressure discharge flow method (DF). I have applied the DF technique with resonance fluorescence (RF) detection of OH. The measured rate constant was used in the relative rate experiments of reaction OH + 2,3PD (7), see Section 3.3.5.

The experiments were performed at $T = 297 \pm 3$ K and $p = 3.17 \pm 0.08$ mbar pressure, helium was the carrier gas. In Table 3.3, the experimental parameters and kinetics results are given, where $\bar{v}$ is the linear flow velocity of the carrier gas, k'_5 is the pseudo-first-order rate constant and k_5 is the bimolecular rate constant for the reaction (5).

Table 3.3: Experimental conditions applied and kinetics results obtained for the reaction OH + MEK (5).

$\bar{v}$ / cm s^{-1}	[H_2] [a]	[NO_2] [a]	[MEK] [b]	k'_5 / s^{-1}	N° of runs	($k_5 \pm 1\sigma$) [c]
1040 - 1127	0.81 - 5.18	0.98 - 6.95	1.67 - 13.85	48.3 - 195.8	18	1.09 ± 0.09

[a] In 10^{12} molecule cm^{-3}, [b] in 10^{13} molecule cm^{-3}, [c] in 10^{-12} cm^3 molecule^{-1} s^{-1}.

The bimolecular rate constant, k_5, was determined under pseudo-first-order conditions with $[CH_3C(O)CH_2CH_3] >> [OH]_0 \approx 4 \times 10^{11}$ molecule cm^{-3}. The consumption of OH radicals was significant on the reactor surface, the heterogeneous loss of OH was found to obey also first-order kinetics. The experiments were carried out by using the so-called "reactant-on reactant-off" measurement technique, which directly corrects for the wall loss of OH radicals [Hoyermann 1975]. The wall-activity was observed to be not significantly different in the presence and absence of $CH_3C(O)CH_2CH_3$.

The following equations were used to evaluate the OH resonance fluorescence signals:

$$-\ln (S_{on}^{OH} / S_{off}^{OH}) = k_5^{'} (z / \bar{v}) \qquad \text{(Eq. 6)}$$

$$k_5^{'} = k_5 \, [CH_3C(O)CH_2CH_3] + const. \qquad \text{(Eq. 7)}$$

$$-\ln S_{off}^{OH} = k_w \, (z / \bar{v}) \qquad \text{(Eq. 8)}$$

where $\bar{v}$ is the linear flow velocity of the carrier gas, z is the reaction distance, S_{on}^{OH} and S_{off}^{OH} are the OH resonance fluorescence signal strengths with and without the reactant methyl-ethyl-ketone flow, and k_w is the"wall-rate constant".

In Figure 3.3 the semi-logarithmic decay plots are presented according to Eq. 6: as seen, reasonably good straight lines were obtained. The ln S_{off} data plotted vs. the reaction distance, (Eq. 8) displayed also straight lines, an example is shown in Figure 3.3.

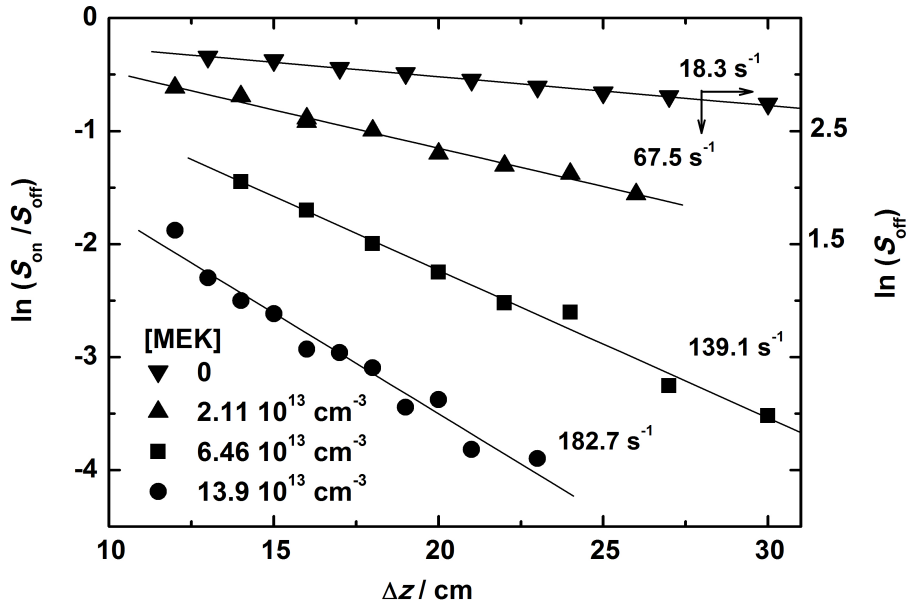

Figure 3.3: Typical experimental OH decays presented in semi-logarithmic plots.

The typical k_w values measured in previous experiments at Budapest were in the range of 3 - 20 s^{-1}, but in the current study the k_w has been found significantly larger in the range of 18 - 62 s^{-1}. It appears, however that the "on-off" technique has corrected for the wall effects even in this case as demonstrated by the linearity of the plots.

The slopes of the straight lines, such as those presented in Figure 3.3, give the pseudo-first-order rate constants. They have been plotted as a function of MEK concentration and are shown in Figure 3.4. The relatively large scatter of the data may indicate that some non-reproducible wall effect has occurred in the experiments. The bimolecular rate constant for the reaction OH + MEK is obtained as the slope of the straight line using linear least squares (LSQ) fitting procedure.

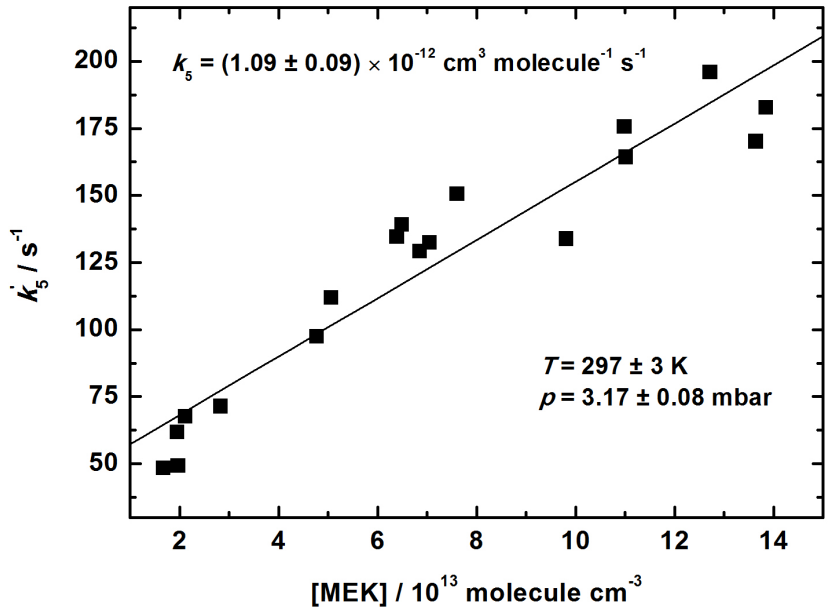

Figure 3.4: Plot of pseudo-first-order rate constant versus the MEK concentration.

The following rate constant value is proposed:

$$k_5 \text{ (297 K)} = (1.09 \pm 0.09) \times 10^{-12} \text{ cm}^3 \text{ molecule}^{-1} \text{ s}^{-1}$$

In a very recent IUPAC data evaluation [IUPAC 2009a], the rate constants reported for the reaction between OH radicals and methyl-ethyl-ketone have been critically evaluated. The analysis included 4 direct and 4 relative rate kinetic studies which applied pulsed photolysis and stationary photolysis methods for the production of OH radicals in the experiments. The rate constant value of k_5 (298 K) = 1.1 × 10^{-12} cm^3 molecule^{-1} s^{-1} has been recommended. The IUPAC recommendation agrees very well with our k_5 value. The agreement is excellent with a most recent study as well: k_5 (298 K) = (1.06 ± 0.06) × 10^{-12} cm^3 molecule^{-1} s^{-1} which has been reported by Carr and co-workers who used pulsed laser photolysis coupled with laser induced fluorescence (LIF) detection of OH [Carr 2008]. As noted above, all determinations in the literature were done by using photolysis technique for the production of OH radicals, while in my experiments the thermal H + NO_2 → OH + NO source was used. The good agreement of the reported data indicate that the rate constant of the OH + MEK (5) reaction has become well established, indeed.

3.3. Photolysis and OH reaction kinetics of 2,3-pentanedione

2,3-pentanedione (2,3PD, $CH_3C(O)C(O)CH_2CH_3$), also called acetyl-propionyl, is an α-diketone. It is a yellow liquid which is highly flammable. Diketones are well known as biodegradable solvents, inhibitors in many polymerization reactions and as substrates for the pharmaceutical industry [Burdock 2005]. 2,3PD is a polar solvent with high selectivity which can be due to the two bulky carbonyl groups substituted in a short carbon chain and also since it is an efficient electron donor molecule, and can form hydrogen bonds with alcohols.

The following reactions were studied:

$$CH_3C(O)C(O)CH_2CH_3 + h\nu \rightarrow \text{products} \quad (6)$$

$$OH + CH_3C(O)C(O)CH_2CH_3 \rightarrow \text{products} \quad (7)$$

3.3.1. The absorption spectrum of 2,3-pentanedione

The photochemical studies in Budapest were started with the measurement of the absorption spectrum of 2,3-pentandione. The spectrum was determined by using the home-built Merlin spectrophotometer, (see Section 2.3). A gas mixture of ~4 % was prepared from 2,3PD and He in a vacuum manifold using a high precision mechanical pressure gauge. This premixed gas mixture was kept in the dark. I have used gas mixtures that were stored for 1, 2 and 15 days to test the stability of the gas mixture. No changes were observed in the spectra. The measurements were performed under stationer and slow-flow conditions as well, but no differences were observed. Both the monochromator and the absorption cell were thermostated to 298 ± 1 K during the measurements. The intensity of the analytical light source, D_2 lamp was strongly reduced by using neutral filters to minimize the potential photolysis of the analyzed samples. The 2,3PD concentration was varied between 0.63 - 2.26 × 10^{17} molecule cm^{-3} and the total pressure was between 70 and 210 mbar. The absorption spectrum was determined over the wavelength range of λ = 210 – 450 nm. The wavelength-dependent

absorption cross sections, $\sigma_{2,3PD}(\lambda)$, were obtained from absorption measurements applying the Beer-Lambert law:

$$\ln\left(\frac{I_0}{I}\right) = \sigma_{2,3PD}(\lambda)\ l\ [2,3PD] \qquad \text{(Eq. 9)}$$

where l is the optical path length (50.2 cm), I_0 and I are the transmitted light intensities in the absence and presence of 2,3PD, respectively.

Figure 3.5 presents a typical Beer-Lambert plot at 351 nm, which was the wavelength used for the laser photolysis measurement in Budapest. The Beer-Lambert plots at all wavelengths used in the photolysis and kinetic experiments both at EMD and in CRC Budapest obeyed straight lines with intercepts close to zero (see Appendix 2).

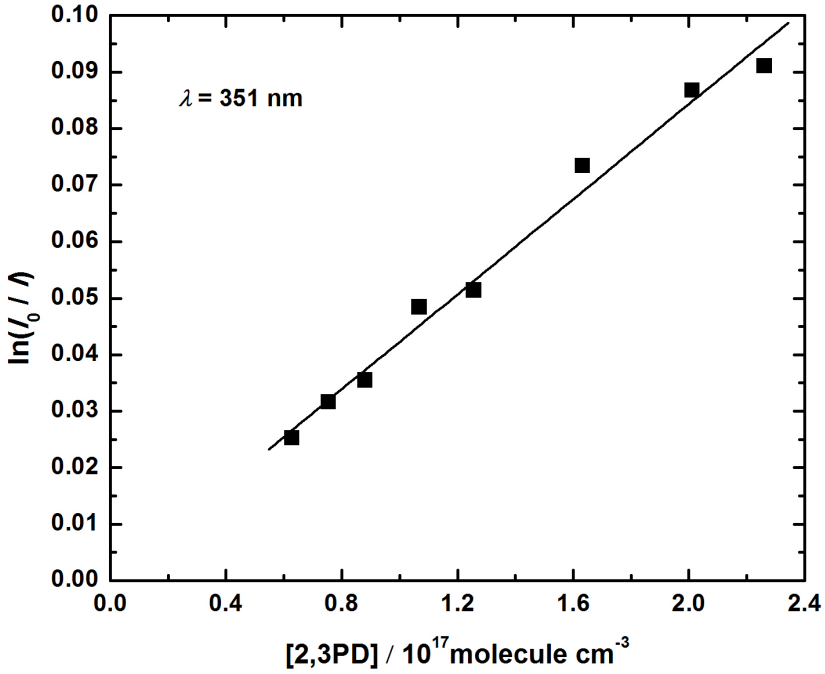

Figure 3.5: Beer-Lambert plot of 2,3-pentanedione at 351 nm.

Figure 3.6 presents the absorption cross section ($\sigma_{2,3PD}$) of 2,3-pentanedione at T = 298 ± 1 K. The absorption cross section values are tabulated in 1 nm intervals in Appendix 2. As seen in Figure 3.6, 2,3-pentanedione has two broad absorption bands in the spectral range above ~220 nm: one in the UV and the other one in the visible range. The maxima are at 270 nm and at 415 nm. There is some indication for a vibrational

structure of the second band, which may have been blurred, however, by the relatively low resolution (~0.4 nm) of the Merlin spectrophotometer. Absorption was observed extended to even longer wavelengths in the visible region, but was not presented in the spectrum above 450 nm because of the large scatter and significant intercept of the Beer-Lambert plots experienced at the analysis of the data. The absorption spectrum of 2,3PD is similar to that of biacetyl ($CH_3C(O)C(O)CH_3$), in terms of the band positions, absorption cross sections and band widths [Horowitz 2001].

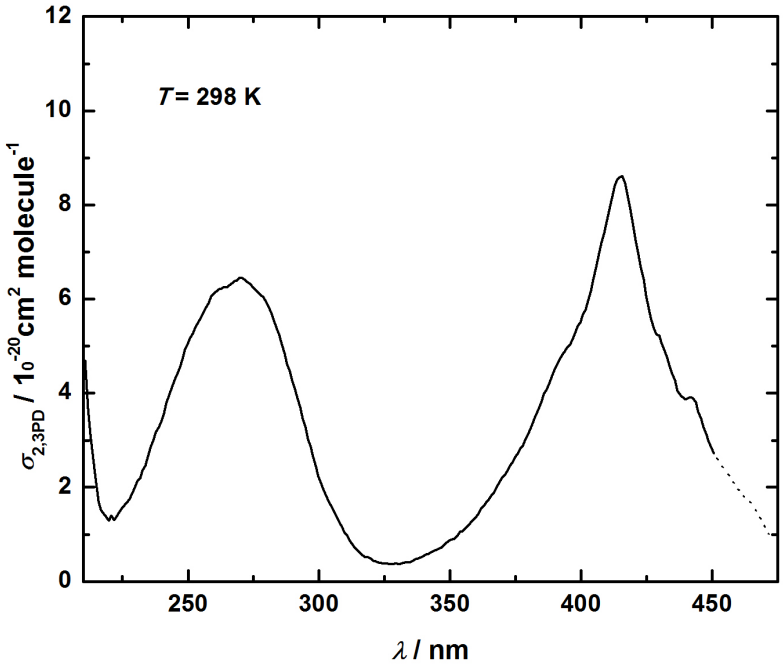

Figure 3.6: Absorption spectrum of 2,3PD at room temperature.

In the literature, only Jackson and Yarwood published the absorption spectrum of 2,3PD [Jackson and Yarwood 1972], also in the gas phase, see Figure 3.7. They purified the sample by gas-liquid chromatography [Jackson and Yarwood 1971], and reported the purity to be 99.98 %. In our case, the 2,3PD was purified by multiple vacuum distillations and the purity of the liquid phase was found better than 99 %. The purity of the 2,3PD / He gas mixtures used for taking the spectra were also analysed: they contained no measurable impurities. As seen in Figure 3.7, our spectrum is substantially different to that reported by Jackson and Yarwood [Jackson and Yarwood 1972]. The most characteristic difference is the very strong absorption band in the literature spectrum with maximum at 253 nm and a shoulder at 280 nm. I note that we

also observed this strong absorption band when the spectrum was recorded with non-purified 2,3PD, but this spectral feature disappeared after purification of the sample.

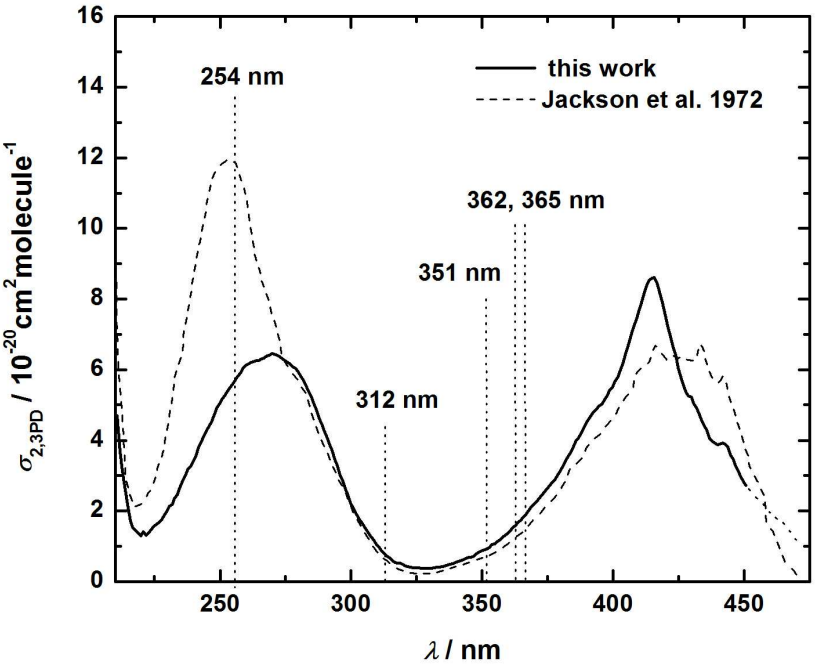

Figure 3.7: Absorption spectrum of 2,3PD in the gas phase. Designated are also the wavelengths at which the photolysis and kinetic experiments were carried out.

Table 3.4 presents the parameters of the light sources and the respective absorption cross sections that were utilised in the photolysis and kinetic experiments of 2,3PD. In the case of the absorption cross sections, the error limits are 2 standard deviations.

Table 3.4: The FWHM values and maxima of the emission of the applied light sources along with the respective absorption cross section of 2,3PD.

	λ / nm	**FWHM [a] / nm**	**$\sigma_{2,3PD}$ / 10^{-20} cm^2 molecule^{-1}**
Budapest	351	-	0.910 ± 0.160
	362	28	1.593 ± 0.212
Douai	254	-	5.585 ± 0.446
	312	11	0.788 ± 0.135
	365	34	1.817 ± 0.165

[a] FWHM: full width at half maximum.

3.3.2. Pulsed Laser Photolysis (PLP) study

The PLP measurements were carried out at 300 ± 2 K laboratory temperature to determine the photolysis quantum yield of 2,3-pentanedione at 351 nm using a XeF exciplex laser. A gas mixture containing 4 mbar perfluoro-cyclobutane (*c*-C_4F_8), and 17 mbar 2,3PD filled to 555 mbar with synthetic air was prepared and stored in dark in a 10 L bulb. Perfluoro-cyclobutane served as an internal gas chromatographic standard. From this premixed gas mixture, 85 mbar, containing 6.3×10^{16} molecule cm^{-3} 2,3PD and 1.5×10^{16} molecule cm^{-3} *c*-C_4F_8, was put into a cylindrical quartz reactor (Section 2.4.), the mixture was filled up with synthetic air to 1000 mbar and was allowed to mix at least for one hour before photolysis. The laser frequency was 5 Hz, the energy varied between 19 and 33 mJ per pulse.

The experimental data are presented in Figure 3.8. Each point is obtained from separate photolysis runs. The data are plotted vs. the pulsed laser energy *E*, (J $shot^{-1}$) multiplied by the number of laser shots *n*; the energy was measured in front of the entrance window of the photolysis cell. The plotted experimental data are the logarithm of the ratio of 2,3PD concentrations measured with the GC before and after *n* laser shots. The 2,3PD concentration was measured relative to that of the gas chromatographic standard. The reaction time was varied between 15 and 120 minutes and the conversion was between 6 - 37 % during the photolysis.

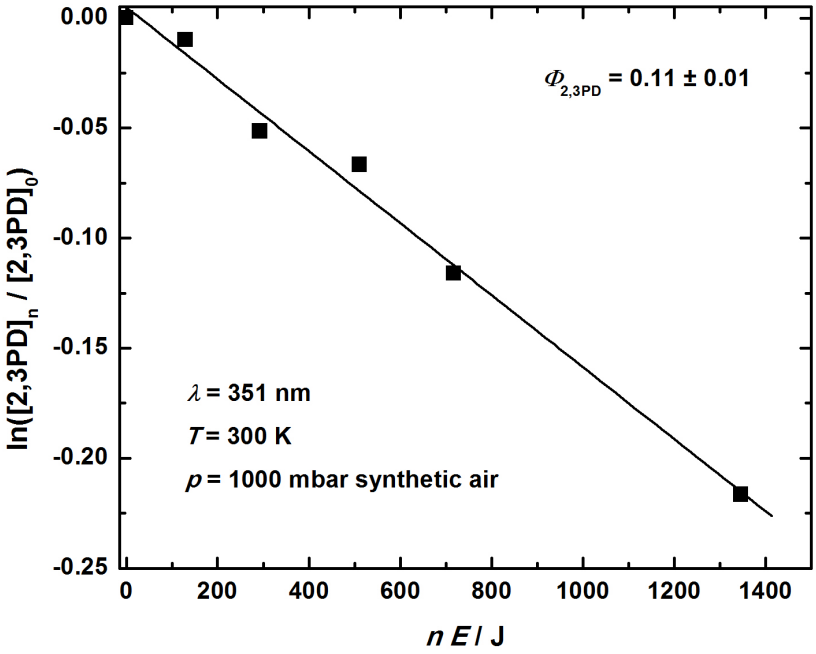

Figure 3.8: Depletion of 2,3PD concentration in pulsed laser photolysis experiments.

The plot of $\ln([2,3PD]_n / [2,3PD]_0)$ against ($n\ E$) has provided a straight line (Figure 3.8). The slope of the straight line multiplied by the second part of Eq. 10 gives the photolysis quantum yield:

$$\Phi_{2,3PD} = -\frac{\ln \frac{[2,3PD]_0}{[2,3PD]_n}}{n\ E_{laser}} \times \frac{V\ E_{photon}}{\sigma_{2,3PD}\ l\ f_{window}} \qquad \text{(Eq. 10)}$$

where,

$[2,3PD]_0$:	2,3PD concentration before photolysis,
$[2,3PD]_n$:	2,3PD concentration after photolysis,
n:	number of laser shots,
E_{laser}:	laser energy,
V:	volume of the quartz reactor,
E_{photon}:	energy of one photon at 351 nm,
$\sigma_{2,3PD}(T, \lambda)$:	absorption cross section of 2,3PD (λ =351 nm),
l:	length of quartz reactor,
f_{window}:	transmittance of the entrance window (f_{window}(351 nm) = 0.930).

The photon energy and the absorption cross section depend on the wavelength, λ; V, l and f_{window} are measurable parameters of the quartz reactor. Thus, at a given wavelength and at a given temperature using the same quartz cell for the photolysis experiments, the slope of the straight line is just multiplied by a constant to obtain the photolysis quantum yield. The method has been developed and Eq. 10 derived previously by the Budapest group [Nádasdi 2007], [Nádasdi 2010].

The determined photolysis quantum yield at 351 nm wavelength, 300 ± 2 K reaction temperature, in 1000 mbar synthetic air is the following:

$$\Phi_{2,3PD}\ (351\ nm) = 0.11 \pm 0.01$$

3.3.3. Photolysis study in the Teflon-bag chamber

The photolysis of 2,3-pentanedione has been investigated in the Teflon-bag chamber at Douai, using different types of fluorescent lamps for irradiation. 5 lamps with a maximum emission at 254 nm (30 W), 6 lamps emitting at 312 nm (20 W) and also 6 lamps emitting at 365 nm (40 W) were used. All measurements were carried out in synthetic air at atmospheric pressure at 300 ± 2 K. The initial concentrations of 2,3PD were between (2.5 - 6.5) × 10^{14} molecule cm^{-3}. In some of the experiments 1-pentene was added as OH-scavenger to capture the OH radicals potentially formed in the photooxidation systems. The initial concentration of 1-pentene was 9.1 × 10^{14} molecule cm^{-3}. The significance of "dark reaction" (e.g., loss of 2,3PD on the walls of the Teflon-bag chamber) was found negligible: there was no observable change in the composition (< 1 %) when the mixtures were allowed to stand in the dark for at least 3 hours. In the case of experiments at 254 nm, 3 - 3 runs were carried out, while at 312 nm and 365 nm 2 - 2 runs were performed, with and without the OH scavenger 1-pentene.

The photolysis rate constants ("photolysis frequencies"), $J_{2,3PD}$, were determined by monitoring the loss of 2,3PD via on-line GC analysis. Chromatographic separation was achieved using a CP SIL 5CB column. Figure 3.9 and Figure 3.10 present an example for the depletion of 2,3PD concentration at 365 nm with and without OH scavenger, respectively, where the $\ln([2,3PD]_t / [2,3PD]_0)$ date are plotted against the

reaction time. The decrease of 2,3PD concentration has been found to follow first-order kinetics at all three wavelengths used (see also in Appendix 3). $J_{2,3PD}$ values have been obtained by linear regression as slopes of the straight lines and are listed in Table 3.5.

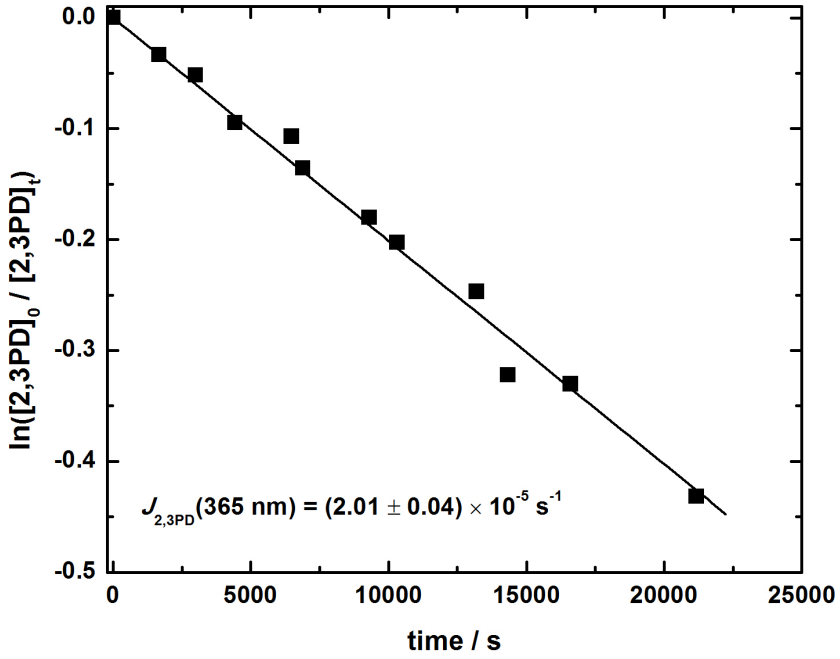

Figure 3.9: A semi-logarithmic plot used to determine the photolysis rate constant of 2,3PD at 365 nm in the presence of an OH scavenger.

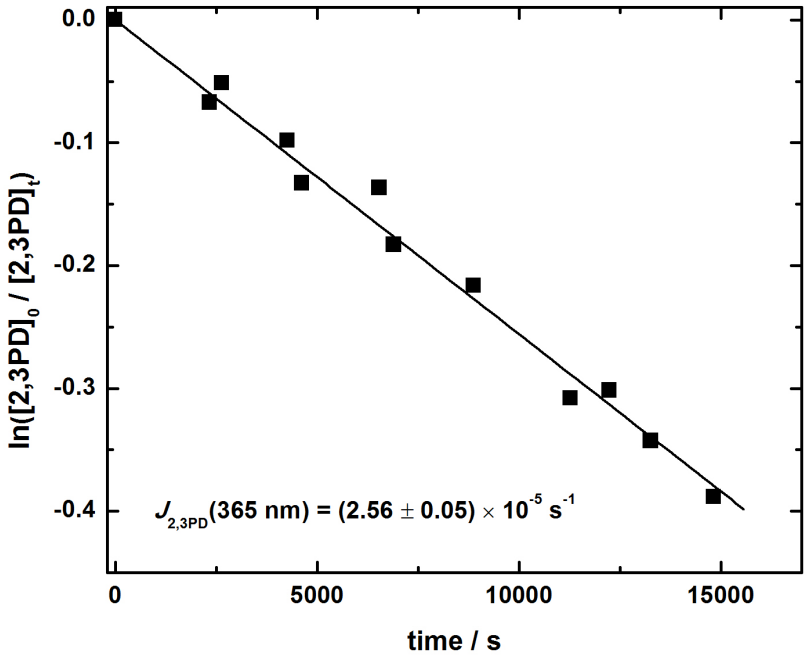

Figure 3.10: A semi-logarithmic plot used to determine the photolysis rate constant of 2,3PD at 365 nm without OH scavenger.

Table 3.5: Photolysis rate constants measured with and without OH-scavenger at 254 nm [a], 312 nm [a] and 365 nm [a].

	254 nm	**312 nm**	**365 nm**
$J_{2,3PD}$ / 10^{-5} s^{-1} without OH-scavenger	5.45 ± 0.03 (3)	1.92 ± 0.04 (2)	2.56 ± 0.05 (2)
$J_{2,3PD}$ / 10^{-5} s^{-1} with OH-scavenger [b]	4.60 ± 0.09 (3)	1.40 ± 0.03 (2)	2.01 ± 0.04 (2)

[a] The number of runs are given in the parentheses.
[b] OH-scavenger: $[1\text{-pentene}]_0 = 9.1 \times 10^{14}$ molecule^{-1} cm^3.

The photolysis rate constant obtained at 365 nm with OH-scavenger, $J_{2,3PD}(365\ nm) = 2.01 \times 10^{-5}\ s^{-1}$, was used to take into account the photolysis loss of 2,3PD in the RR kinetics study in the Teflon-bag chamber experiments at deriving the rate constant ratios (see Section 3.3.5.).

The photolysis rate constants determined for 2,3PD are higher by 15 % at 254 nm and by ~ 25 % at 312 and 365 nm wavelengths in the absence of OH-scavenger. The OH radicals that caused the additional consumption of 2,3PD were probably formed via secondary reactions involving peroxy-radical chemistry in the photooxidation systems.

The formation of OH by the primary photodissociation of 2,3PD can not be excluded either. Holloway and co-workers used the 248 nm photolysis of the parent molecule, 2,4-pentanedione (2,4PD) as a source of OH radicals for the pulsed laser photolysis-laser induced fluorescence (PLP-LIF) kinetic experiments of the OH + 2,4PD reaction [Holloway 2005]. In this case, OH was generated via primary photodissociation of 2,4PD, which is a well known photo-process for the enolic-form β-diketones [Upadhyaya 2003]. In contrast, the 2,3PD exists predominantly in the keto form that would require more complex rearrangement to produce OH radicals via a primary photochemical process.

The formation of products in the photooxidation of 2,3PD was studied using 254 nm irradiation. Two experiments were carried out: one in the absence of OH-scavenger and the other one by adding 9.1×10^{14} molecule cm^{-3} 1-pentene to trap the OH radicals potentially formed in the photoxidation system. The initial concentration of 2,3PD was 1.9 and 5.5×10^{14} molecule cm^{-3}. The analysis of reaction products was carried out using HPLC: 300 ml of reaction mixture was sampled with the DNPH cartridges, at regular intervals, at about every 30 - 40 minutes after the initiation of the reaction (see Section 2.2.2.). The results are presented in Figure 3.11 and Figure 3.12. Both figures show the consumption of 2,3PD with increasing irradiation time. The rate of consumption of 2,3PD is somewhat smaller in the presence of OH-scavenger indicating some extra consumption of 2,3PD beside the photolysis due to OH reaction.

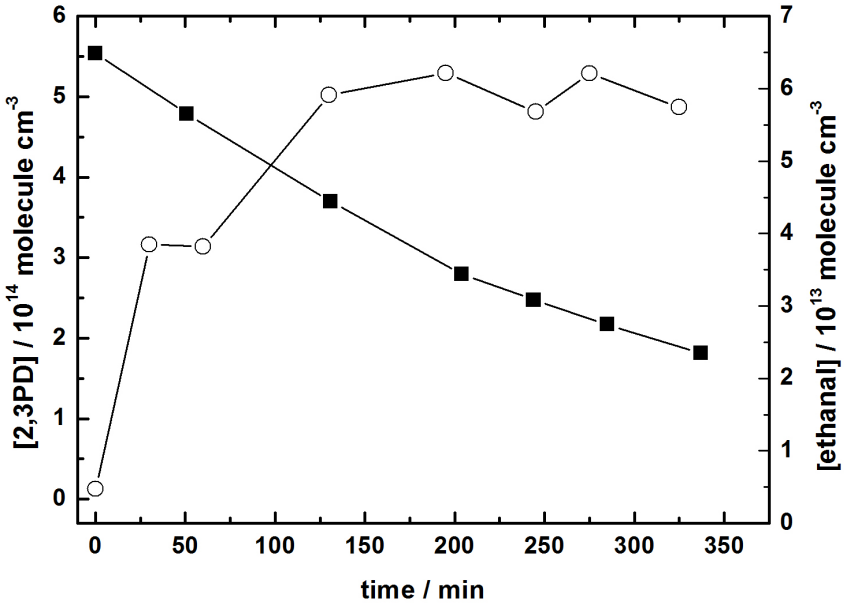

Figure 3.11: The photolysis products of 2,3PD at 254 nm without OH scavenger (square, 2,3PD; circle, ethanal).

Figure 3.11 shows to build up of the product ethanal (i.e. acetaldehyde) antiparallel to the consumption of 2,3PD. This behaviour is thought to indicate that CH_3CHO is indeed a product related to primary photochemical processes,(6a)-(6b) of 2,3PD (see also in the next section). The formation of ethanal can be explained by the following photooxidation processes that occur in the reaction system:

$$CH_3C(O)C(O)CH_2CH_3 + h\,v \rightarrow \quad (6)$$

$$\rightarrow CH_3CO + CH_3CH_2CO \quad (6a)$$

$$\rightarrow CH_3CO + CH_3CH_2 + CO \quad (6b)$$

$$\rightarrow CH_3C(O)C(O) + CH_3CH_2 \quad (6c)$$

The CH_3CH_2 radical undergoes the following reactions to form ethanal:

$$CH_3CH_2 + O_2 + M \rightarrow CH_3CH_2O_2 + M$$

$$CH_3CH_2O_2 + CH_3CH_2O_2 \rightarrow \underline{\mathbf{CH_3CHO}} + C_2H_5OH + O_2$$

$$\rightarrow 2\ CH_3CH_2O + O_2$$

$$CH_3CH_2O + O_2 \rightarrow \underline{\mathbf{CH_3CHO}} + HO_2$$

In this reaction scheme the reactions of CH_3CO, CH_3CH_2CO and $CH_3C(O)C(O)$ radicals are not considered because they probably decompose in fast reactions at the

applied low wavelength (254 nm) photolysis. Presumably, this was the reason that no characteristic products for this acyl radicals, e.g. $CH_3C(O)OH$, $CH_3CH_2C(O)OH$, were found among the reaction products. The formation of the product ethanal can be taken as evidence for the presence of CH_3CH_2 radicals in the reaction system (formed either directly in channels 6b, 6c or / and by decomposition of the CH_3CH_2CO radical).

Figure 3.12 displays the measured kinetic curves in the presence of the OH-scavenger, 1-pentene.

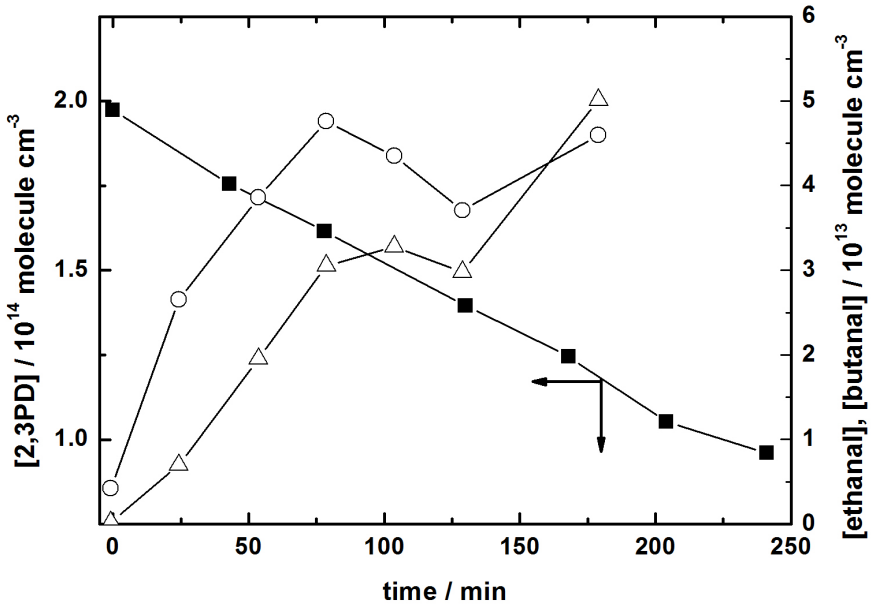

Figure 3.12: Photooxidation kinetic curves for 2,3PD at 254 nm in the presence of OH scavenger (square, 2,3PD; circle, ethanal; triangle, butanal).

As noted, the depletion rate of 2,3PD is somewhat slower than in the absence of the OH-scavenger. The build-up concentration of CH_3CHO is of similar magnitude than that without OH-scavenger. Surprisingly, the formation of a new significant product has been observed which was identified as *n*-butanal, *n*-C_3H_7CHO. The formation of this product is probably originated from the photoxidation of 1-pentene without any connection to the photolysis of 2,3PD itself. One possible explanation for the formation of *n*-butanal is the secondary reaction of 1-pentene with OH radicals potentially formed in the photooxidation system. OH adds to 1-pentene and the oxidation of the hydroxyl-alkyl radical involving peroxyl and alkoxyl radicals may give rise to the formation of *n*-C_3H_7CHO.

The formation of OH radicals in the reactions of acyl radicals has been studied in detail previously at CRC Budapest [Kovács 2007]. I have joined the recent studies to investigat OH formation in the $CH_3CH_2CO + O_2$ and $(CH_3)_3CC(O) + O_2$ reactions [Zügner 2010], [Szabó 2011b]. Significant OH yields were determined at the low pressures ($p \approx 1 – 10$ mbar of He) of the DF technique, but the yields decreased quickly with increasing pressure and likely become entirely negligible at atmospheric pressure [Zügner 2011]. Therefore, the acyl radicals formed in the primary reaction steps (6a)-(6c) could not be sources of OH radicals at the high pressure investigations carried out in the Teflon-bag reactor ($p \approx 1000$ mbar).

3.3.4. Photochemistry of 2,3-pentanedione

The photolysis frequencies determined for 2,3PD, $J_{2,3PD}$, at the 312 nm and 365 nm wavelengths have been normalized for the different photon fluxes by using NO_2 actinometry (note that the emission spectra of the fluorescent lamps and the absorption spectra of 2,3PD and NO_2 [JPL 2006] overlap in a substantial wavelength range).
The $J_{2,3PD}$ / $J_{actinom}$ values in Table 3.6 have been utilized to estimate an 'integral' or 'effective' quantum yield [Tadic 2001], [Raber 1995], $\Phi_{2,3PD}^{eff}$, for the photolysis of 2,3PD with the broad-band fluorescent lamps with λ_{max} = 312 nm and 365 nm peak emissions and w = 12 nm and 34 nm full widths at half maxima, respectively. The following expression was used:

$$\Phi_{2,3PD}^{eff} = \frac{J_{2,3PD}}{J_{NO2}} \times \left\{ \frac{\frac{1}{2}\sigma_{NO2}\left(\lambda_{max} - \frac{1}{2}w\right) + \sigma_{NO2}\ \lambda_{max} + \frac{1}{2}\sigma_{NO2}\left(\lambda_{max} + \frac{1}{2}w\right)}{\frac{1}{2}\sigma_{2,3PD}\left(\lambda_{max} - \frac{1}{2}w\right) + \sigma_{2,3PD}\ \lambda_{max} + \frac{1}{2}\sigma_{2,3PD}\left(\lambda_{max} + \frac{1}{2}w\right)} \right\} \times \Phi_{NO2} \qquad \text{(Eq. 11)}$$

In Eq. 11, Φ_{NO2} is the quantum yield for NO_2 photolysis, which was taken unity [JPL 2006], [Raber 1995] over the whole wavelength range studied; the absorption cross sections of NO_2, $\sigma_{NO2}(\lambda)$, were taken from [JPL 2006] for the calculations and the $\sigma_{2,3PD}(\lambda)$ values from my own measurements. The estimated effective quantum yields are $\Phi_{2,3PD}^{eff}$ = 0.41 ± 0.02 and 0.78 ± 0.05 for the fluorescent lamps with λ_{max} = 312 nm

and 365 nm peak emissions, respectively. Trial calculations have shown only small change in the effective quantum yields when more overlap between the emission spectra of the lamps and the absorption spectra of NO_2 and 2,3PD were taken into account.

In view of the fact that the fluorescent lamp used at 254 nm is practically monochromatic, a 'true quantum yield of $\Phi_{2,3PD}$' can be calculated by the results of the acetone actinometry using Eq. 12 (see Section 2.2.3.):

$$\frac{J_{2,3PD}}{J_{Ac}} = \frac{\Phi_{2,3PD} \times \sigma_{2,3PD}}{\Phi_{Ac} \times \sigma_{Ac}} \qquad \Phi_{2,3PD} = \frac{J_{2,3PD} \times \Phi_{Ac} \times \sigma_{Ac}}{J_{Ac} \times \sigma_{2,3PD}} \qquad \text{(Eq. 12)}$$

where, J_{Ac} is the acetone photolysis rate constant, $(8.68 \pm 0.07) \times 10^{-5}$ s^{-1} (see Section 2.2.3.). From the literature one obtains $\sigma_{Ac}(254\text{ nm}) = 3.01 \times 10^{-20}$ cm^2 $molecule^{-1}$ and $\Phi_{Ac} = 1$ at $\lambda < 290$ nm [Atkinson 2006]; $J_{2,3PD}$ and $\sigma_{2,3PD}$ have been measured in my present work. The photolysis rate constants and quantum yields are summarized in Table 3.6.

Table 3.6: Photolysis rate constants and quantum yields determined in the Teflon-bag reactor ($T = 300 \pm 2$ K, $p = 1000$ mbar).

λ (nm)	$J_{2,3PD}$ [a] (10^{-5} s^{-1})	$J_{actinom}$ [a] (10^{-3} s^{-1})	$100 \times (J_{2,3PD}/J_{actinom})$	$\Phi_{2,3PD}$
365 ± 34	2.56 ± 0.05 (2) without OH-scavenger 2.01 ± 0.04 (2) with OH-scavenger [b]	0.69 ± 0.040 (9)	2.90 ± 0.18 [c]	0.78 ± 0.05 [c, d]
312 ± 11	1.92 ± 0.04 (2) without OH-scavenger 1.40 ± 0.03 (2) with OH-scavenger [b]	0.78 ± 0.003 (9)	1.80 ± 0.04 [c]	0.41 ± 0.02 [c, d]
254 [e]	5.45 ± 0.03 (3) without OH-scavenger 4.60 ± 0.09 (3) with OH-scavenger [b]	0.0868 ± 0.0007 (6)	52.99 ± 1.12 [c]	0.29 ± 0.01 [c, f]

[a] The number of experiments are given in the parentheses; 6 × 20 W (at 312 nm) and 6 × 40 W (at 365 nm) lamps and 5 × 30 W (at 254 nm) were used in the experiments.
[b] OH-scavenger: $[1\text{-pentene}]_0 = 9.1 \times 10^{14}$ molecule cm^{-3}.
[c] Using $J_{2,3PD}$ values determined in the presence of OH-scavenger.
[d] Effective quantum yield for 312 and 365 nm, $\Phi_{2,3PD}^{eff}$ (see text).
[e] Practically monochromatic.
[f] Quantum yield for 254 nm.

At the lowest wavelength, the photolysis quantum yield of $\Phi_{2,3PD}(254\text{ nm}) = 0.29 \pm 0.01$ has been determined. This is a relatively small value compared e.g. with the

photodissociation quantum yield measured for monocarbonyls at 248 nm laser excitation [Nádasdi 2010], [Zhu and Zhu 2010]. It appears therefore that the photophysical quenching of the electronically excited 2,3PD plays important role in the photochemical mechanism at 254 nm.

Thermochemistry and the scarce information available from the literature suggest channels (6a)–(6d) to be primary photolysis channels for 2,3PD at the relatively low excitation energies of 312, 351 and 365 nm:

$CH_3C(O)C(O)CH_2CH_3 + h\nu$

$\rightarrow CH_3CO + CH_3CH_2CO$ (6a)

$\Delta_{6a}H°_{298}$ = 302 kJ mol^{-1} [JPL 2006], [Kercher 2005] $\lambda_{threshold}$ = 395 nm

$\rightarrow CH_3CO + CH_3CH_2 + CO$ (6b)

$\Delta_{6b}H°_{298}$ = 344 kJ mol^{-1}[JPL 2006], [Kercher 2005] $\lambda_{threshold}$ = 346 nm

$\rightarrow CH_3C(O)C(O) + CH_3CH_2$ (6c)

$\Delta_{6c}H°_{298}$ = 354 kJ mol^{-1} [JPL 2006], [Kercher 2005], [Jagiella and Zabel 2008]

$\lambda_{threshold}$ = 336 nm

→ 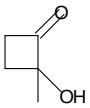 (6d)

$\Delta_{6d}H°_{298}$ < 274 kJ mol^{-1} $\lambda_{threshold}$ > 435 nm [Turro and Lee 1969]

The applied photolysis wavelengths of 312 nm, 351 nm and 365 nm correspond to the excitation energies of 382, 340 and 327 kJ mol^{-1}, respectively. Three different C–C photodissociation routes are energetically accessible at 312 nm excitation, channels (6a)–(6c), while at 365 nm, only the formation of $CH_3CO + CH_3CH_2CO$, channel (6a), is feasible at ambient temperatures. The free radical product $CH_3C(O)C(O)$ formed via channel (6c) may undergo decomposition depending on its excess energy [Baeza-Romero 2007], [Jagiella and Zabel 2008] to form CH_3CO and CO. The photoisomerisation reaction (6d) may take place at all three excitation wavelengths studied; this channel has been proposed by Turro and Lee in a classical liquid-phase photochemical study [Turro and Lee 1969] (see below). (The reaction enthalpies for the different photolysis channels have been obtained by taking the

recently published standard enthalpy of formation of $\Delta_f H°_{298}$ (2,3PD) = –343.7 ± 2.5 kJ mol^{-1} from [Kercher 2005], and the other enthalpy data from [JPL 2006], [Kercher 2005], [Jagiella and Zabel 2008].

Only little is known about the photochemistry of 2,3PD from the literature. Turro and Lee have studied the photochemistry of 2,3PD in solution at 435 nm [Turro and Lee 1969]. They have shown that photolysis of 2,3PD forms 1-hydroxy-1-methyl-2-cyclobutanone via an intramolecular photoreduction process, (6d), with a quantum yield of ~0.06. Jackson and Yarwood have investigated the fluorescence and phosphorescence of 2,3PD in the gas phase at 365-, 405 and 436 nm [Jackson and Yarwood 1971]. They have derived a rate constant expression by the temperature dependent quenching of the phosphorescence of 2,3PD [Jackson and Yarwood 1971] consistent with the (6d) photoisomerisation process [Turro and Lee 1969]. As presented in Figures 3.11 and 3.12, the build-up of ethanal was observed concomitant with the consumption of 2,3PD at 254 nm indicating the occurrence of the photodissociation channels (6a)–(6c).

3.3.5. Kinetic study of the reaction of OH radicals with 2,3-pentanedione

Direct (DF-RF) and relative-rate (RR) kinetic techniques were employed to determine rate constant for the reaction:

$$OH + CH_3C(O)C(O)CH_2CH_3 \rightarrow \text{products} \qquad (7)$$

Direct kinetics experiments were carried out in Budapest at T = 300 ± 3 K and relative-rate experiments were done both in Budapest and Douai at T = 302 ± 4 K and T = 300 ± 2 K, respectively.

Direct kinetic study (DF-RF), (Budapest)

The low-pressure discharge flow technique coupled with resonance fluorescence monitoring of OH (DF-RF) was applied to determine absolute rate constant for the OH + 2,3PD (6) reaction. The DF-RF apparatus has been described in detail in Chapter 2. Following were the experimental conditions: He buffer gas was used, p = 2.49 ± 0.03 mbar and the initial OH concentration was $[OH]_0 = 3 \times 10^{11}$ molecule cm^{-3}. A gas mixture containing 2 % 2,3PD was prepared in He gas and was stored in 10 L Pyrex bulb. This mixture was introduced through a side arm at the upper end of the discharge-flow reactor. The home-built spectrophotometer (Section 2.3.) was used to check the concentration and stability of the mixture by measuring its absorption spectrum which was compared with the 2,3-pentanedione spectrum that was obtained with fresh mixtures. The concentration of 2,3PD was also checked by GC. The mixture in the DF-RF study was useable for about a week or so, therefore new 2,3PD / He mixtures were prepared in every 3 – 4 days time.

The bimolecular rate constant for reaction (7) was determined the usual way under pseudo-first-order conditions, [2,3PD] >> $[OH]_0$. The experimental parameters and kinetic results have been summarized in Table 3.7, where $\bar{v}$ is the average linear flow velocity, k'_7 is the pseudo-first-order rate constant and k_7 is the bimolecular rate constant for the reaction (7).

Table 3.7: Experimental conditions applied and kinetics results obtained for the reaction OH + 2,3PD (7).

N° of runs	$\bar{v}$ **/ cm s^{-1}**	**[H$_2$]** [a]	**[NO$_2$]** [a]	**[2,3PD]** [a]	k'_7 **/ s^{-1}**	**($k_7 \pm 1\sigma$)** [b]
17	873 - 1055	0.9 - 5.2	0.9 - 5.0	4.8 - 46.9	84.1 - 185.1	2.25 ± 0.12

[a] In 10^{12} molecule cm^{-3}, [b] in 10^{-12} cm^3 molecule^{-1} s^{-1}.

The experiments were performed by recording the OH resonance signal strengths versus the varied reaction distance, z, with (S_{on}^{OH}) and without (S_{off}^{OH}), of the 2,3PD flow. Under the plug-flow condition of the low-pressure DF technique, the reaction time equals $z \times \bar{v}^{-1}$ [Howard 1979]. The bimolecular reaction between OH and 2,3PD was kinetically isolated from the interfering reactions in the homogeneous gas phase, but the consumption of OH was significant on the surface of the reactor which was found to obey first-order-kinetics with an effective "wall rate constant" of k_w:

OH + wall → products (w)

The equations which were used to evaluate the OH resonance fluorescence signals are presented in Section 3.2.

The measured hydroxyl decays, when plotted according to (Eq. 6), displayed straight lines, indicating the validity of first-order kinetics. The slopes provided the pseudo-first-order rate constant, k_7', by linear least square analysis (LSQ). Some typical semi-logarithmic decay plots of the OH radicals are presented in Figure 3.13. An example is shown for the S_{off}^{OH} data plotted versus the reaction distance, which is seen to give a straight line too providing k_w (see Eq. 8).

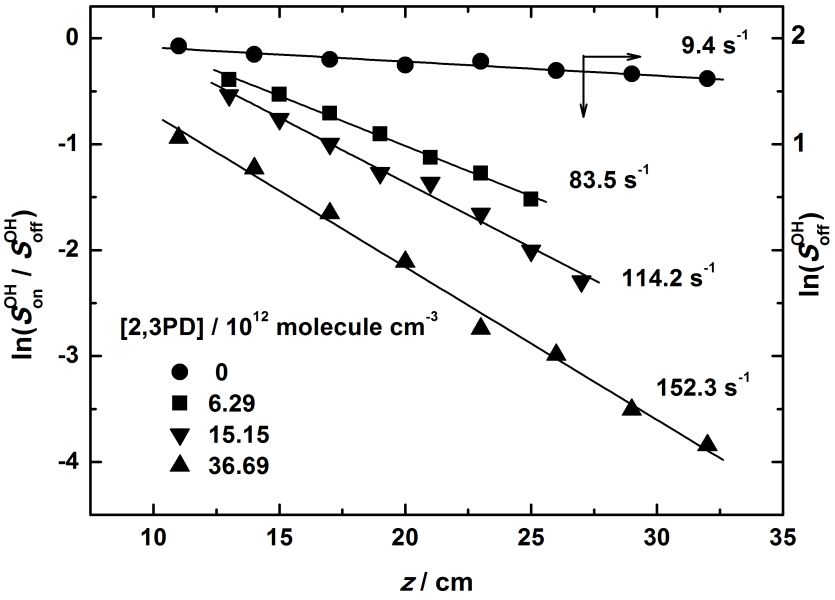

Figure 3.13: Experimental OH decays presented in semi-logarithmic plot.

The plot of pseudo-first-order rate constant versus [2,3PD] is shown in Figure 3.14. The slope of the straight line gives the bimolecular rate constant for the reaction OH + 2,3PD. The following value was obtained by the LSQ analysis:

$$k_7\ (300 \pm 3\ \text{K}) = (2.25 \pm 0.12) \times 10^{-12}\ \text{cm}^3\ \text{molecule}^{-1}\ \text{s}^{-1}$$

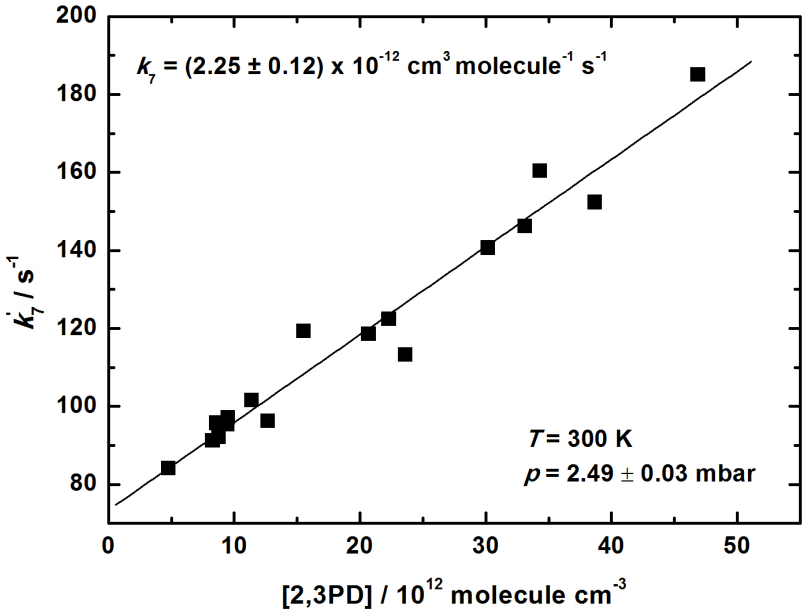

Figure 3.14: Plot of pseudo-first-order rate constant versus the 2,3-pentanedione concentration.

Large heterogeneous effects were observed in the first experiments portrayed by very high OH consumption on the surface of the reactor and a smaller than expected signal magnitudes in the experiments that were carried out in close succession to each other. Such effects are indications for the adsorption of 2,3PD on the walls of the reactor and an enhanced heterogeneous reaction with the OH radicals. Similar behavior was reported by Stevens and co-workers for discharge flow reactions of OH with different polar reactants including carbonyls (see, [Baasandorj 2009] and references therein). These authors have reported the heterogeneous effects to be minimized by the addition of O_2. However, this option was not feasible in my experiments since a substantial reformation of OH was observed when oxygen flow was added to the reaction system that might have caused an underestimation of the rate constants in the measurements. Long evacuation time and conditioning of the walls of the flow tube with OH radicals were used prior to each experiment. In this way, reasonable reproducibility was achieved, but the bimolecular rate constant plot showed a significant intercept (Figure 3.14), and the k_w = 7 – 47 s^{-1} values were somewhat larger than the usual wall consumption of OH (~3 – 20 s^{-1}) that were observed previously in DF experiments with inert wall coatings.

The measured rate constant was not corrected for viscous flow and axial diffusion. Instead, an 8 % contribution was included in the error margins to account for such effects and other potential systematic errors. Thus, the following rate constant is proposed by the DF-RF studies for the reaction OH + 2,3PD:

$$k_7\,(300 \pm 3\ \mathrm{K}) = (2.25 \pm 0.30) \times 10^{-12}\ \mathrm{cm^3\ molecule^{-1}\ s^{-1}}$$

Relative rate kinetic study (RR), (Budapest)

Experiments were performed in a 10 L Pyrex reactor at atmospheric pressure in synthetic air buffer gas. The photooxidation of CH_3ONO was used to produce OH radicals at 362 nm wavelength. The RR set-up and the light source transmission spectrum are presented in Section 2.2.4.

The relative rate method (Appendix 1) was used to determine the rate constant of reaction (6). The reference compound was methyl-ethyl-ketone; the rate constant for the reaction OH + MEK is $k_5 = (1.09 \pm 0.09) \times 10^{-12}$ cm^3 molecule^{-1} s^{-1} at 297 ± 3 K ([Szabó 2008] and Section 3.2.), which value agrees well with the IUPAC recommendation: k_5 (298 K) = 1.1×10^{-12} cm^3 molecule^{-1} s^{-1} with the error given as $\Delta \log k = \pm 0.10$ [IUPAC 2009a]. The Pyrex reactor was thoroughly evacuated before each experiment to clean the walls.

A gas mixture, containing perfluoro-cyclobutane (*c*-C_4F_8, gas chromatographic standard), methyl-ethyl-ketone (MEK), and 2,3PD was put in a Pyrex bulb container and filled with synthetic air to 1000 mbar; the concentrations were 0.2 %, 1 %, and 2 %, for *c*-C_4F_8, MEK and 2,3PD respectively. 1.5 - 2.3 mbar CH_3ONO and ~30 mbar from this premixed gas mixture were measured in the Pyrex reactor which finally was filled up to 1050 mbar with synthetic air. The gas mixtures were freshly prepared and were allowed to mix protected from light for at least 2 hours before irradiation. The reaction temperature was $T = 302 \pm 4$ K. Samples for GC analysis were withdrawn by a 250 µl gas-syringe through a septum connected to a thin glass tube which reached in the middle of the bulb (see Section 2.2.4.). The chromatographic separation was achieved under isothermal conditions at 80 °C. The photolysis time was varied between 10 and 40 minutes, and the conversion for the reactants was in the range 8 - 30 %. In a test

experiment, the reaction mixture was allowed to stand for 20 hours in the dark in the Pyrex photoreactor: there was no observable loss of the reactants.

In Table 3.8 are presented the experimental conditions along with the kinetic results.

Table 3.8: Experimental conditions in the Pyrex reactor and kinetic results for the reaction OH + 2,3PD (7).

N° of exp.	**$[2,3PD]_0$ [a]**	**$[MEK]_0$ [a]**	**$(k_7 / k_5) \pm 1\sigma$**	**$(k_7 \pm 1\sigma)$ [b]**
3	5.64 – 6.01	7.90 - 8.49	1.89 ± 0.03	2.06 ± 0.17

[a] In 10^{15} molecule cm^{-3}, [b] in 10^{-12} cm^3 $molecule^{-1}$ s^{-1}.

Figure 3.11 presents the plot used to determine the rate constant ratio from measurements with MEK as reference compound according to Equation 13:

$$\ln\left\{\frac{[2,3PD]_0}{[2,3PD]_t}\right\} - J_{2,3PD} \times t = \frac{k_7}{k_5} \times \ln\left\{\frac{[MEK]_0}{[MEK]_t}\right\} \qquad \text{(Eq. 13)}$$

The photolysis of 2,3PD also took place to a smaller extent at the 362 nm wavelength that was taken into account in (Eq. 13). In order to determine $J_{2,3PD}$, separate experiments were carried out by irradiating 2,3PD / air mixture in the absence of MEK and CH_3ONO. Single exponential decay was observed providing $J_{2,3PD} = 1.99 \times 10^{-5}$ s^{-1} as the decay constant. This value was used in (Eq. 13) to correct for the loss caused only by the OH reaction: the correction was less than 9 %. Linear least squares analysis of the data plotted in Figure 3.15 have supplied the rate constant ratio $k_7 / k_5 = 1.89 \pm 0.03$. Taking $k_5 = (1.09 \pm 0.09) \times 10^{-12}$ cm^3 $molecule^{-1}$ s^{-1} from [Szabó 2008] and this work the following value was obtained:

$$k_7\ (302 \pm 4\ K) = (2.06 \pm 0.17) \times 10^{-12}\ cm^3\ molecule^{-1}\ s^{-1}$$

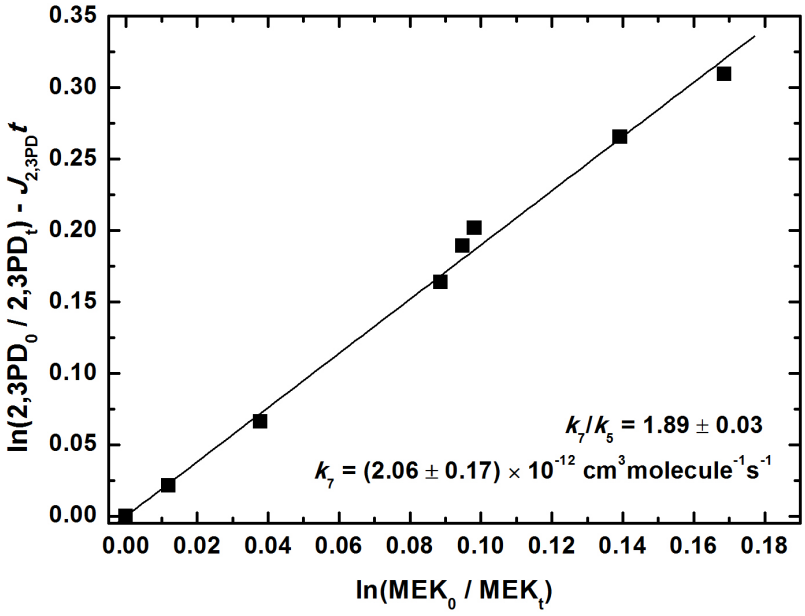

Figure 3.15: Plot used to determine rate constant ratio from measurements in the Pyrex reactor.

Relative - rate kinetic study (RR), (Douai)

Experiments were carried out in a 250 L, collapsible Teflon reactor in atmospheric pressure air, at T = 300 ± 2 K. Six fluorescent tubes emitting at 365 nm were used to produce OH radicals by the photooxidation of CH_3ONO. This reactor and the emission spectrum of lamp are presented in Section 2.2.2. Reference reactions were: OH + MEK (5) and OH + C_2H_5OH (EtOH) (24). The rate constant of OH + MEK reaction is: $k_5 = (1.09 \pm 0.09) \times 10^{-12}$ cm^3 molecule^{-1} s^{-1} at 297 ± 3 K [Szabó 2008] and for reaction OH + EtOH is $k_{24} = (3.38 \pm 0.30) \times 10^{-12}$ cm^3 molecule^{-1} s^{-1} at 298 K [Kovács 2006]. The selected value for this latter reaction agrees well with the IUPAC recommendation of $k_{24} = 3.2 \times 10^{-12}$ cm^3 molecule^{-1} s^{-1} with error given as $\Delta \log k = \pm 0.06$ (T = 298 K) [IUPAC 2009b]. The Teflon reactor was purged several times with synthetic air before each experiment to remove the residual gas mixtures and to clean the surface of the wall. After that, the Teflon-bag reactor was filled to half with synthetic air, and then 2,3PD and one of the reference compounds were injected and evaporated in the small glass vial (Section 2.2.2.) which was connected to the smog chamber. The next step was the introduction of synthetic air into the Teflon reactor. Finally, CH_3ONO was added

before the pressure in the reactor had reached 1000 mbar. The gas mixture was kept in the dark for at least 1 hour before the irradiation was started. The concentration depletion of the reactants was followed as a function of the reaction time by using a gas-chromatograph equipped with flame ionization detector; for details see Section 2.2.2. The GC analysis was started at 50 °C and followed by a programmed temperature heating up to 80 °C with a rate of 10 °C min^{-1}, then the temperature was increased to 200 °C with a rate of 15 °C min^{-1}.

The wall-loss of 2,3PD was checked the following way: 2,3PD was introduced into the reactor in 1000 mbar synthetic air and its concentration was monitored by GC-FID for 5 hours by regular sampling. The wall-loss was found around 1 %; no correction for this loss was made in the experiments. Table 3.9 presents the experimental conditions and kinetic results.

Table 3.9: Experimental conditions in the Teflon reactor and kinetic results for the reaction OH + 2,3PD (7).

reference reactant	**N° of exp.**	**$[2,3PD]_0$ [a]**	**$[ref]_0$ [a]**	**$(k_7 / k_{ref}) \pm 1\sigma$**	**$k_7 \pm 1\sigma$**
EtOH	2	2 -3	4.3	0.74 ± 0.02	2.50 ± 0.23
MEK	4	1.2 - 2	2.8 – 4.2	1.79 ± 0.05	1.95 ± 0.17

[a] In 10^{14} molecule cm^{-3}, [b] in 10^{-12} cm^3 $molecule^{-1}$ s^{-1}.

Figure 3.16 presents the plots used to determine the rate constant ratios from measurements with ethanol and methyl-ethyl-ketone as the reference compounds according to Equation 13. The measured 2,3PD concentration ratios were corrected with $J_{2,3PD}$, which is the photolysis rate constant of 2,3PD at 365 nm (see in Table 3.5): the correction was less than 15%. LSQ slopes of the straight lines of Figure 3.16 provide $k_7 / k_5 = 1.79 \pm 0.05$ and $k_7 / k_{24} = 0.74 \pm 0.02$ which are resolved to the following rate constant values:

MEK reference: k_7 (300 ± 2 K) = (1.95 ± 0.17) × 10^{-12} cm^3 $molecule^{-1}$ s^{-1}

EtOH reference: k_7 (300 ± 2 K) = (2.50 ± 0.23) × 10^{-12} cm^3 $molecule^{-1}$ s^{-1}

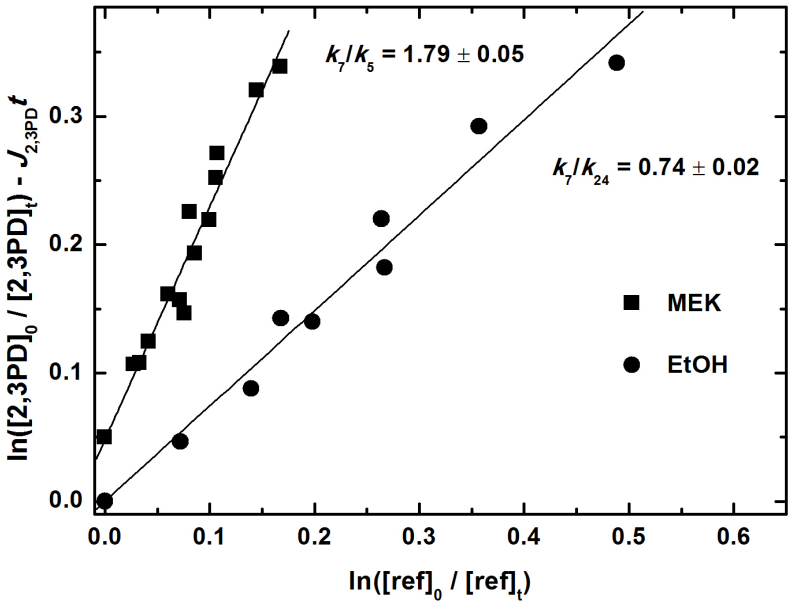

Figure 3.16: Plots used to determine rate constant ratios from the measurements in the Teflon-bag reactor. In the y-axis the data for MEK (squares) have been shifted by 0.05 for clarity.

Table 3.10 presents the summary of obtained rate constant values for reaction OH + 2,3PD (7). The error limits attached to k_7 values are 1σ statistical uncertainties in which the uncertainty of the reference reactions have been taken into account by using propagation of errors law. The average of the direct and relative kinetic studies is:

$$k_7 = (2.19 \pm 0.22) \times 10^{-12} \text{ cm}^3 \text{ molecule}^{-1} \text{ s}^{-1}.$$

Table 3.10: Summary of obtained rate constant values for the reaction OH + 2,3PD (7).

		Budapest	**Douai**	**Average**
$k_7 \pm 1\sigma$ [a]	RR	2.06 ± 0.17 [b]	1.95 ± 0.17 [b]	2.19 ± 0.22
		–	2.50 ± 0.23 [c]	
	DF-RF	2.25 ± 0.30	–	

[a] In 10^{-12} cm^3 molecule^{-1} s^{-1}.
[b] Reference reactant: MEK. [c] Reference reactant: EtOH.

It is noted that k_7 has been found invariant to the reaction pressure in a wide range between ~2 mbar and ~1000 mbar. The good agreement lends credence to the reliability of the results in particular that they were obtained from independent measurements in two laboratories using different experimental techniques.

3.3.6. Discussion of the photolysis and OH-kinetic results of 2,3PD

Photolysis quantum yield for 2,3PD

As presented in the previous sections, the photolysis quantum yield (QY) for 2,3-pentanedione was determined using 351 nm XeF laser and 254 nm, 312 nm, 365 nm fluorescence lamps at room temperature (T = 300 ± 2 K) in 1000 mbar air buffer gas with the results of $\Phi_{2,3PD}$(351 nm) = 0.11 ± 0.01, $\Phi_{2,3PD}^{eff}$(254 nm) = 0.29 ± 0.01 $\Phi_{2,3PD}^{eff}$(312 nm) = 0.41 ± 0.02 and $\Phi_{2,3PD}^{eff}$(365 nm) = 0.78 ± 0.05. The QYs at longer wavelengths are surprisingly high values and display significant disparity. They appear high in comparison, e.g., with the long-wavelength photolysis QYs of monoketones [Nádasdi 2010], and the 365 nm photolysis QY of the α-diketone biacetyl [Sheats and Noyes 1955], and show no discernible trend with the change of wavelength. On the other side, however high quantum yields have been reported for the photolysis of the α-ketoaldehyde, methyl-glyoxal, $CH_3C(O)C(O)OH$, even at around 400 nm wavelength [Chen 2000]. No obvious reason can be given to explain the inconsistency of the results, and clearly, further investigations are needed to determine accurate quantum yields. At the present stage of my research, the average value of $\Phi_{2,3PD} \approx 0.4$ is proposed over the wavelength range ~254–370 nm by noting the large uncertainty of this datum which probably represents an upper bound for the photochemical change of 2,3PD.

Rate constant for the OH + 2,3PD reaction

The recommended rate coefficient for the reaction of OH radicals with 2,3PD is the non-weighted average of the k_7 determinations:

$$k_7(300\ \mathrm{K}) = (2.19 \pm 0.22) \times 10^{-12}\ \mathrm{cm^3\ molecule^{-1}\ s^{-1}}.$$

To my knowledge, no prior rate constant has been reported for the OH + 2,3PD reaction. The only other α-diketone that has been a subject of OH-kinetic study is 2,3-butanedione ($CH_3C(O)C(O)CH_3$, or biacetyl). A rate constant value of $(2.3 \pm 0.2) \times 10^{-13}$ cm^3 $molecule^{-1}$ s^{-1} (T = 298 K) has been determined by Dagaut and co-workers for the OH + biacetyl reaction [Dagaut 1988b] in good agreement with a previous measurement by Darnall and co-workers [Darnall 1979]. The proposed rate constant for the OH + $CH_3C(O)C(O)CH_2CH_3$ (7) reaction is ~10-times higher, which can be rationalized, however, by the increased reactivity of the CH_2 group not present in the biacetyl molecule (see below).

A structural isomer of 2,3PD is 2,4-pentanedione (2,4PD), which is a β-diketone. Holloway and co-workers have carried out a detailed kinetic study of the reaction of OH with 2,4PD using both direct and relative kinetic methods [Holloway 2005]. The rate constant they have reported is $(8.78 \pm 0.58) \times 10^{-11}$ cm^3 $molecule^{-1}$ s^{-1} (T = 298 K) which is more than 40-times higher than the k_7 value I have determined for the OH + 2,3PD reaction. Holloway and co-workers have explained the high rate constant by that 2,4-pentanedione exists in the gas phase predominantly as the enol tautomer, $CH_3C(O)CH=C(OH)CH_3$, which undergoes fast addition reaction with the OH radical, while the keto-form ketones react via the slower hydrogen abstraction reactions. In contrast to 2,4PD, the vicinal diketone 2,3PD exists predominantly in the keto form wiht the enol form which is presented to a few percentages, at the most, in the gas phase at room temperature [Kung 1974], [Schwarzenbach 1947], [Soni 2008].

The reactivity properties of 2,3PD can be understood by the considerable knowledge that has been gathered throughout the years for the kinetics and mechanism of the reactions of OH radicals with the aliphatic mono-ketones, see e.g. [Le Calvé 1998], [Wallington1987], and also the review paper by Mellouki and co-workers [Mellouki 2003]. The C=O group slightly reduces the bond dissociation energy (BDE)

of a neighboring C–H bond [JPL 2006], [Espinosa-Garcia 2003], but it is strongly electron withdrawing, which overrides the BDE-reducing effect, and so hydrogen abstraction by the electrophilic OH radical becomes less facile at the *α*-position, [Mellouki 2003], [Kwok and Atkinson 1995]. On the other hand, a characteristic feature of the OH reactions of $C_n \geq 3$ ketones is the increased reactivity of the C–H bonds at the *β*-position [Wallington1987], [Mellouki 2003]. This latter effect is thought to be the decisive factor in determining the pronounced reactivity of 2,3PD toward OH, compared, for example, with propane, $CH_3CH_2CH_3$, which has got the same number and types of H atoms, but its rate coefficient is about half of that of the 2,3PD reaction (k (OH + propane) = 1.1×10^{-12} cm^3 $molecule^{-1}$ s^{-1}, T = 298 K [JPL 2006])).

An important development for understanding the reactivity of OH radicals with polar organic molecules, including carbonyls, has been the recognition of the important role that weakly bound ‘prereaction’ (or ‘prereactive’) complexes play in the molecular mechanisms of the reactions, as it has been reviewed [Smith 2002], [Hansen 2002], [Galano 2008] and discussed in detail, e.g., in [Henon 2003], [Alvarez-Idaboy 2004], [Carl 2007]. Specifically, the role of hydrogen bonded complexes in enhancing the reactivity of the *β*-C–H bond in the reactions of OH with aliphatic ketones has been assessed by Alvarez-Idaboy and co-workers by quantum chemical and theoretical reaction kinetics computations [Alvarez-Idaboy 2004]. They have shown that the *β*-prereaction complexes, C=O•••HO•••$H_\beta C_s$, significantly lower the reaction barrier via hydrogen-bond-like interactions in the transition state thus leading to increased rate coefficients.

3.4. Photolysis study of glycolaldehyde in the Teflon chamber

The study which is presented in the following sections was performed in Douai by using the Teflon environmental chamber and the analytical instruments available at this research site.

3.4.1. Literature survey on the atmospheric fate of glycolaldehyde

Glycolaldehyde, or hydroxyethanal (GA, $HOCH_2CHO$) is a type of a diose (2 carbon monosaccharide); it is a crystalline white powder at room temperature. GA is an important bio-ingredient because it can polymerize into higher forms of carbohydrates, such as ribose, and glucose.

Primary atmospheric source of glycolaldehyde is its direct emission from biomass fires. Secondary sources include the oxidation of several volatile organic compounds (VOCs), such as ethene, 2-methyl-3-buten-2-ol (MBO) and isoprene [Niki 1981], [Orlando 1999], [Ferronato 1998].

The atmospheric degradation of GA occurs via UV photolysis and OH-radical initiated oxidation. The photolysis is an important loss process in the atmosphere; it was investigated by Bacher, Magneron and Zhu and co-workers [Bacher 2001], [Magneron 2005], [Zhu and Zhu 2010].

Three photolysis channels are accessible at troposheric wavelengths (λ > 290 nm) as first proposed by Bacher and co-workers in their smog chamber studies [Bacher 2001]:

$$HOCH_2CHO + h\nu \rightarrow CH_2OH + HCO \quad (8a)$$

$$\rightarrow HOCH_2CO + H \quad (8b)$$

$$\rightarrow CH_3OH + CO \quad (8c)$$

Magneron and co-workers proposed a fourth photolysis channel which directly produces OH radicals [Magneron 2005]:

$$HOCH_2CHO + h\nu \rightarrow OH + CH_2CHO \quad (8d)$$

Table 4.1 presented in Appendix 4 summarizes the product studies of glycolaldehyde photolysis reported in the literature.

Beside photolysis, the reaction of GA with the OH-radicals is also an important process to initiate its depletion in the atmosphere. Reaction OH + glycolaldehyde has been studied by several research groups due to its atmospheric importance. The rate constant is of high value, as understood by the easily abstractable H atoms in the molecule; the IUPAC recommendation is k (298 K) = 0.8×10^{-11} cm^3 $molecule^{-1}$ s^{-1} [IUPAC 2007].

3.4.2. Results and discussion of the photolysis of glycolaldehyde

My objective was to determine photolysis rate constant, J_{GA}, for glycolaldehyde at λ = 312 nm and to estimate formaldehyde and methanol product yields experimentally.

As a first step, the GC and HPLC calibrations were carried out for GA and for the photolysis products, formaldehyde and methanol. The calibration of GA and HCHO was performed by HPLC using DNPH (dinitro-phenyl-hydrazine) cartridges; CH_3OH was analysed by GC-FID.

The wall-loss of GA was determined before the start of the photolysis experiments by allowing the mixture to stand in the dark for 3 hours. The dark reaction (wall loss) was found to represent less than 1 % contribution compared with the photolysis loss.

Three photolysis experiments were carried out in air at atmospheric pressure and at T = 300 ± 2 K using 8 lamps emitting at 312 nm; the initial concentration of GA was $(0.7 – 1.2) \times 10^{15}$ molecule cm^{-3}. Cyclohexane was used in one of the experiments as OH-scavenger: its initial concentration was 1.6×10^{15} molecule cm^{-3}. The photolysis of GA was started about 1 hour after injection in the Teflon-bag reactor.

The photolysis depletion of GA has been found to follow first order kinetics (Figure 3.18). As seen in Figure 3.18, the data determine the same straight line irrespective if the experiments were conducted in the presence or absence of the OH scavenger cyclohexane. The slope of the $\ln([GA]_0 / [GA]_t) – t$ straight line has provided:

$$J_{GA} (300K) = (1.48 \pm 0.05) \times 10^{-4} \text{ s}^{-1}$$

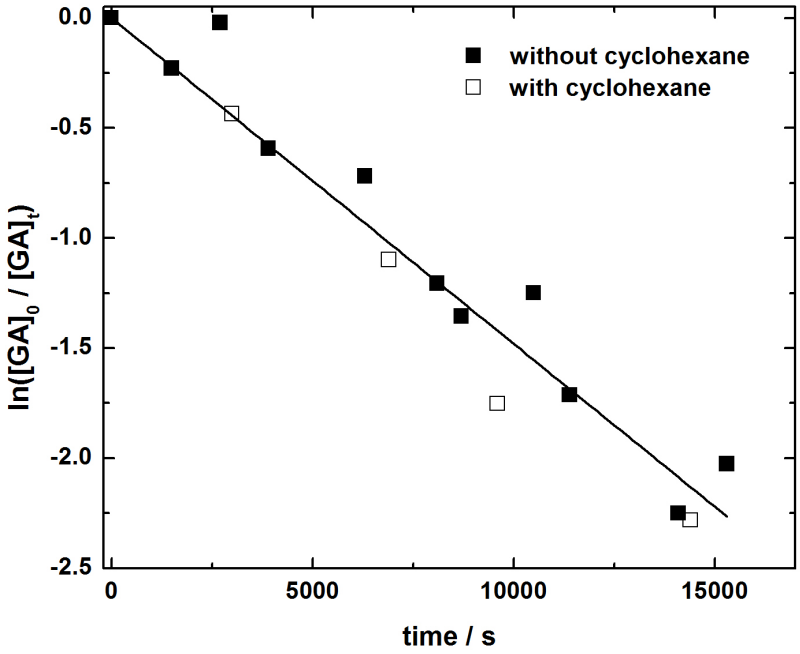

Figure 3.18: A semi-logarithmic plot used to determine the photolysis rate constant of GA at 312 nm.

The fact that no difference within experimental error has been observed for the measured J_{GA} in the presence and absence of cyclohexane may be due to that no sufficiently high scavenger concentration was used in the experiment.

In Figure 3.19 are shown the concentration-time profiles of GA and the photolysis products for the experiments carried out with (a) and without (b) cyclohexane. The observed photolysis products were formaldehyde and methanol. As presented in Figure 3.19, the formation of both HCHO and CH_3OH occurs antiparallel to the consumption of glycolaldehyde and their concentrations approach constant values at long reaction times. The concentration of formaldehyde was corrected for its photolysis rate since formaldehyde has fairly high absorption cross section at 312 nm (σ_{HCHO} = 1.19 × 10^{-20} cm^2 $molecule^{-1}$) and it is known to undergo photolysis at this wavelength [Meller 2000]. The photolysis rate of formaldehyde was measured in the following way: a solution containing 38% formaldehyde (solvent: 10 % CH_3OH in water) was vaporized in the glass vial (Figure 2.6) and then transferred to the Teflon-bag reactor (see Section 2.2.2.). After some dark sampling, the photolysis was performed for 90 minutes with 8 lamps emitting at 312 nm. The analysis was carried out using HPLC and DNPH cartridges (see Section 2.2.2). The photolysis rate constant,

J_{HCHO}, was obtained the usual way from the plot of $\ln([HCHO]_0 / [HCHO]_t)$ vs. time. The average of two experiments has provided $J_{HCHO} = (5.8 \pm 0.7) \times 10^{-5}$ s^{-1}. This means a large correction for measured HCHO yields in the photolysis experiments of GA that may be the reason of the significant disparity in the HCHO results.

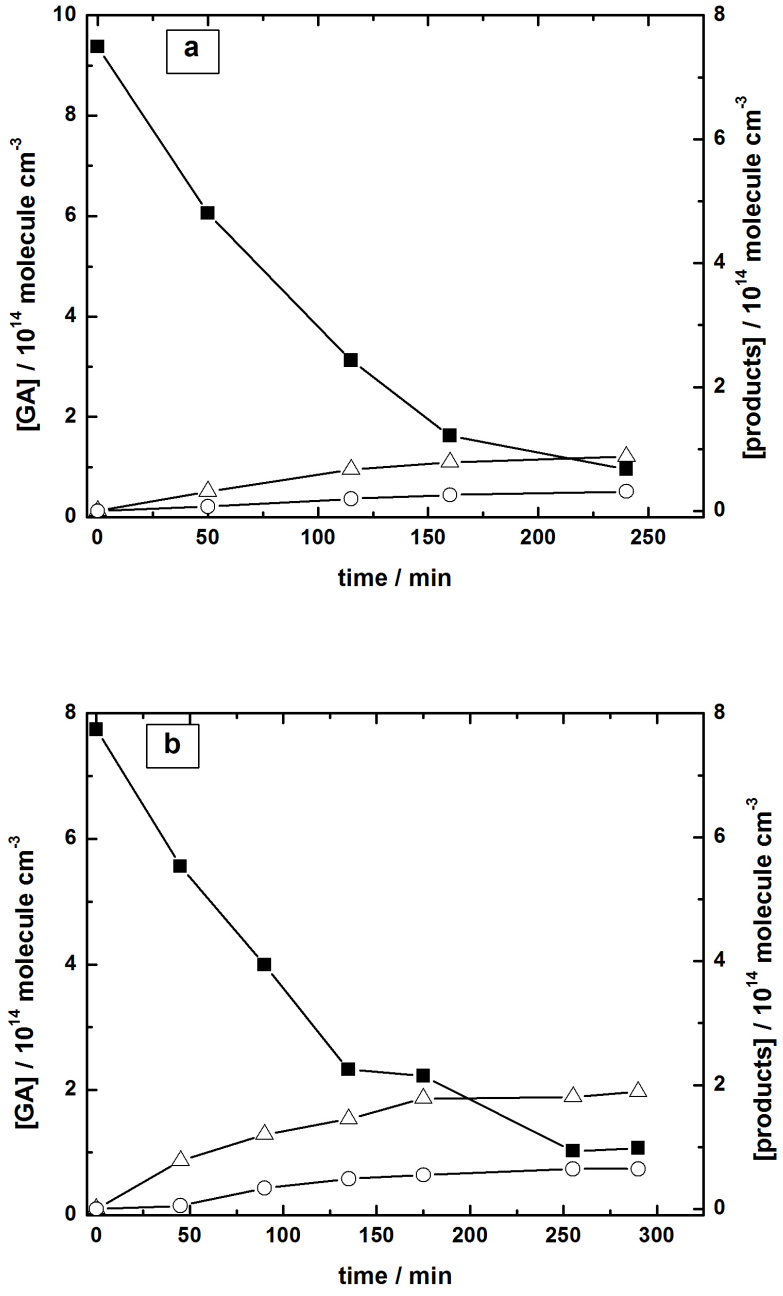

Figure 3.19: Glycolaldehyde consumption and product formation versus photolysis time: (a) with and (b) without cyclohexane (square, GA; triangle, HCHO; circle, CH_3OH).

The product yields, Γ_{HCHO} and Γ_{CH3OH} were obtained as the ratios of the measured maximal concentrations of HCHO (or CH_3OH) and the initial concentration of GA. Significant product yields were obtained, but with poor reproducibility and no perceptible dependence on the presence or absence of the OH-scavenger cyclohexane. In view of the large scatter of the data and that only three experiments were carried out, only approximate product yields can be given:

$$\Gamma_{HCHO} = 10.4 – 26.7\ \% \text{ and } \Gamma_{CH3OH} = 1.8 – 8.7\ \%$$

The yield of HCHO is relatively high which implies that the major photolysis channel leads to CH_2OH and HCO (8a) followed by the secondary oxidation of CH_2OH to HCHO [Bacher 2001]. The CH_3OH comes from the direct photolysis of glycolaldehyde (reaction 8c). The methanol yield is in the range reported in the literature, but the yields of formaldehyde are 2-3 times smaller compared with the results published recently [Zhu and Zhu 2010], (see also Table 4.1 in Appendix 4).

3.5. The reactivity of OH radicals with carbonyls

Assessment of reactivity by the Structure Activity Relationship (SAR) method

Due to the atmospheric importance of OH radicals, a great number of kinetic data are available for their reactions in the literature. The large data base permitted to formulate relations between the molecular parameters of organic compounds and their reactivity, and to develop methods with which experimentally not measured rate coefficient for OH radical reactions can be estimated. The most frequently used method was proposed by Atkinson and was developed further by Atkinson and Kwok, which is the "Structure Activity Relationship (SAR)" method [Atkinson 1985] [Kwok and Atkinson 1995]. This estimation schema is based on the observation that H abstraction from $–CH_3$, $–CH_2–$, >CH–, and –OH groups depend, beside the C-H strengths, also on the identity of the neighbouring groups (X, Y and Z):

$k(CH_3–X) = k_{CH3}\, F(X)$

$k(Y–CH_2–X) = k_{CH2}\, F(X)\, F(Y)$

$k(Y–CH–(X)\,–Z) = k_{CH}\, F(X)\, F(Y)\, F(Z)$

$k(OH–X) = k_{OH}\, F(X)$

where k_{CH3}, k_{CH2}, k_{CH}, k_{OH} are the generic rate constants of the H abstraction from $–CH_3$, $–CH_2–$, >CH–, and –OH groups in the case of a given standard neighbouring group that is connected to them. X, Y and Z are the substituent groups and the $F(X)$, $F(Y)$, and $F(Z)$ are the corresponding group factors. The standard substituent group chosen by Atkinson is the methyl group ($X = Y = Z = CH_3$); and its group factor is taken to be unity, by definition $F(CH_3) = 1.00$. The rate constant of a molecule for its OH radical reaction is given by the sum of the contributing H-abstraction group rate constants. Atkinson has recommended rate constant data at 298 K and carried out a non-linear least-squares analysis of the kinetic data available from the literature to derive $F(X)$ values for different substituent groups [Atkinson 1985], [Kwok and Atkinson 1995]. Kwok and Atkinson in their later work have re-investigated the Structure Activity Relationship methods using the available database [Kwok and Atkinson1995]; the k_{CH3},

k_{CH2}, k_{CH}, k_{OH} standard rate constants and the substituent factors have been tabulated by the authors. The estimated rate constant values of OH radical reactions of nearly 500 organic compounds were predicted within a factor of 2 of the experimental data for 90 % of the reported reactions.

On the relation between molecular structure and reactivity for OH radical reactions

All elementary reactions that I have studied are hydrogen abstraction reactions. Thus, the reactivity is expected to be influenced by the C-H bond dissociation energy of the H atom abstracted. The smaller dissociation energy is known to give rise to higher rate constants in the case of primary, secondary and tertiary C-H bonds for the reactions of hydrocarbon with OH [Berkowitz 1994] [Atkinson 1989].

Beside the thermochemistry, special inductive effects also influence the reactivity of OH radicals with organics. OH radicals are known to be electrophilic reactants: the electron-withdrawing substituents decrease the OH rate constant and electron-releasing ones increase the reactivity. Electron withdrawing substituents are for example the halogen atoms while electron-donating groups are for example the methyl- or *tert*-butyl-groups, etc.

In Table 3.13 are listed the room temperature rate constants that I have determined experimentally together with those estimated by the SAR method (details of the estimations are given in Appendix 5). A good agreement has been obtained for the rate constant of acetic acid and methyl-ethyl-ketone, but the 2,3-pentanedione rate constant is seen to be underestimated. This is because the currently available substituent factor, F(>CO) does not reflect the activating effect of a –C(O)C(O)– group [Szabó 2011a]. Conversely, the F(–C(O)C(O)–) factor can be calculated by the rate constant value that I have measured for the OH + 2,3PD reaction and using the group parameters given in [Kwok and Atkinson 1995].

k(2,3PD measured) = k_{prim} × F(–C(O)C(O)–) + k_{sec} × F(–C(O)C(O)–) × F(–CH_3) + k_{prim} × F(–CH_2C(O)–)

The estimation provides F(–C(O)C(O)–) = 1.55 which indicates a definite, but smaller activating effect than that of the –CH_2C(O)– group, F(–CH_2C(O)–) = 3.9 [Kwok and Atkinson 1995].

Estimation of k values for the deuterated acetic acid reactions is not feasible because there are no sufficient SAR parameters available. On the other hand, k_{CD3} can be calculated by making use of my experimental results to give the group rate constant of $k_{CD3} = 1.13 \times 10^{-13}$ cm^3 molecule^{-1} s^{-1}. Comparing with the literature group rate constant for the CH_3 group, $k_{CH3} = 1.36 \times 10^{-13}$ cm^3 molecule^{-1} s^{-1} [Kwok and Atkinson 1995], it can be concluded that deuterium substitution leads to a decrease of the group rate constant like in the case of deuterated alkanes [Atkinson 1985].

Table 3.13: Experimental rate constants for the studied OH reactions and comparison with the estimated rate constant values using the SAR method at 298 K.

organics (i)	k_i **(experimental) / cm^3 molecule^{-1} s^{-1}**	k_i **(calculated) / cm^3 molecule^{-1} s^{-1}**	$\frac{k_i \text{ (calculated)}}{k_i \text{ (experimental)}}$
$CH_3C(O)OH$ (1)	6.30×10^{-13}	6.47×10^{-13}	1.03
$CH_3C(O)OD$ (2)	1.50×10^{-13}	not calculated	-
$CD_3C(O)OH$ (3)	6.30×10^{-13}	$k_{CD3} = 1.13 \times 10^{-13}$	-
$CD_3C(O)OD$ (4)	0.90×10^{-13}	not calculated	-
$CH_3C(O)CH_2CH_3$ (5)	1.09×10^{-12}	0.97×10^{-12}	0.89
$CH_3C(O)C(O)CH_2CH_3$ (6)	2.19×10^{-12}	1.33×10^{-12}	0.61

As seen in the last column of Table 3.13, the rate constant for reaction OH + $CH_3C(O)OH$ could be estimated very well by using the SAR method, and the estimation works fairly well in the case of the OH + MEK reaction. On the other hand, the rate constant estimated by the standard substituent factors given in [Kwok and Atkinson 1995] supplies a significantly lower rate constant compared with that measured experimentally. As discussed above, the reason is simply that no proper substituent factors are currently available to estimate the rate constant of the reaction OH + 2,3PD (7).

Chapter 4: Atmospheric implications

In my Thesis, I have dealt with the OH kinetics and photochemistry of selected OVOCs. The results allow the estimation of their atmospheric lifetime. In general, the troposheric lifetime of organics is determined by their homogeneous reactions (mostly OH reactions), photodepletion in case the molecule absorbs in the actinic region (> 290 nm), and heterogeneous processes of wet and dry depositions.

Acetic acid and its deuterated isotopes:

In my work, I have measured room temperature rate constants for the reaction of OH radicals with acetic acid and a few rate constants for its deuterated counterparts. Table 4.1 shows the tropospheric lifetimes which have been calculated by the rate constants and $[OH]_{global} \approx 1 \times 10^6$ molecule cm^{-3} [Heard and Pilling 2003] using equation 14.

$$\tau_{OH}\,(i) \approx \frac{1}{k_i \times [OH]_{global}} \qquad \text{(Eq. 14)}$$

The OH reaction lifetime of acetic acid in the troposphere is 18 days which is in accordance of literature recommendations based on the room temperature rate constants [IUPAC 2009c]

Acetic acid does not photolyse in the atmosphere, but its most significant loss process is the wet deposition which results in ~ 2 days lifetime as proposed by Sanhueza and co-workers [Sanhueza 1996].

Table 4.1: Troposperic lifetimes of the studied OVOCs with the respect to their reaction with OH radicals.

organics (i)	**k_i (298 K) / cm^3 molecule^{-1} s^{-1}**	**τ_{OH} (i) / days**
$CH_3C(O)OH$ (1)	6.30×10^{-13}	18.4
$CH_3C(O)OD$ (2)	1.50×10^{-13}	77.2
$CD_3C(O)OH$ (3)	6.30×10^{-13}	18.4
$CD_3C(O)OD$ (4)	0.90×10^{-13}	128.6
$CH_3C(O)CH_2CH_3$ (5)	1.09×10^{-12}	10.6
$CH_3C(O)C(O)CH_2CH_3$ (7)	2.19×10^{-12}	5.3

Methyl-ethyl-ketone:

The reaction of OH + MEK (5) was investigated with the low pressure discharge flow technique and the rate constant of $k_5 = (1.09 \pm 0.09) \times 10^{-12}$ cm^3 molecule^{-1} s^{-1} was determined. The OH reaction lifetime of MEK is ~ 11 days (see Table 4.1), which has been estimated by the rate constant and taking an average global OH concentration of $[OH]_{global} \approx 1 \times 10^6$ molecule cm^{-3} similarly to acetic acid [Heard and Pilling 2003]. The other tropospheric sink of MEK is the photolysis. Nádasdi et al. showed in their study that the *T*- and *p*-dependent quantum yield of MEK and the *T*-dependent σ_{MEK} values imply that the photolysis rate of MEK is less important than the OH reaction up to a few kilometers in the troposphere [Nádasdi 2010].

2,3-pentanedione:

Since my work has provided the first kinetic and photochemical results on 2,3PD, I am going to discuss its atmospheric fate in more detail.

The absorption spectrum of 2,3-pentanedione extends to long wavelengths (Figure 3.6) where the solar flux increases rapidly in the troposphere, e.g., the flux is ~150 times higher at 400 nm than that at 300 nm on the Earth's surface. Also, as presented in Section 3.3.4, 2,3PD undergoes photochemical changes with quantum yields that are still fairly uncertain, but they are believed significant even at relatively

long wavelengths. These factors imply a likely short photolysis lifetime of 2,3PD, τ_{phot}(2,3PD), in the troposphere. τ_{phot}(2,3PD) has been estimated by making use of the measured photolysis rate constant ratio $J_{2,3PD}$ / J_{NO2} from my present work, (see also Table 4.2) and the reported global tropospheric photolysis rate constant (photolysis frequency) of NO_2, $J_{NO2,trop}$ [Wild 2000]:

$$J_{2,3PD,trop} = \frac{J_{2,3PD}}{J_{NO2}} \times J_{NO2,trop} \qquad \text{(Eq. 15)}$$

$$\tau_{phot}(2,3PD) = \frac{1}{J_{2,3PD,trop}} \qquad \text{(Eq.16)}$$

Table 4.2: Summary of photolysis rate constants measured in the Teflon-chamber experiments

organics (i)	**λ / nm** [a]	**J_i / $10^{-5}s^{-1}$**	**$J_{actinometry}$** [b]	**$\frac{J_i}{J_{actinometry}} \times 100$**
2,3-pentanedione	254 (5)	4.60 ± 0.09	8.68 ± 0.07 [d]	53.0 ± 1.00
	312 (6)	1.40 ± 0.03	0.78 ± 0.003 [c]	1.8 ± 0.04
	365 (6)	2.01 ± 0.04	0.69 ± 0.040 [c]	2.90 ± 0.20
glycolaldehyde	312 (8)	14.8 ± 0.5	1.04 ± 0.003	2.90 ± 0.20

[a] The number of lamps used are given in the parentheses.
[b] Photolysis rate constant measured for actinometry molecules.
[c] NO_2 actinometry, $J_{actinomerty}$ in 10^{-3} s^{-1}.
[d] Acetone actinometry, $J_{actinomerty}$ in 10^{-5} s^{-1}.

In this manner, τ_{phot}(2,3PD) = 3.9 hours have been estimated employing $J_{2,3PD}$ / J_{NO2} = 0.018 ($\lambda \approx$ 310–370 nm, $\Phi_{2,3PD} \approx 0.4$) from my measurements and taking the globally averaged tropospheric photolysis frequency of $J_{NO2,trop} \approx 4 \times 10^{-3}$ s^{-1} from [Wild 2000]. An alternative estimation procedure of using the measured quantum yields and absorption cross sections along with tabulated actinic fluxes [Finlayson-Pitts and Pitts 2000] provides < 1 hour for the atmospheric photolysis lifetime of 2,3PD during daytime at mid latitudes on the ground level.

Similarly to other unsaturated carbonyl molecules, OH-reaction can be important initiation step for the tropospheric degradation of 2,3PD beside photolysis. The value of k_7 determined at laboratory temperature can be used to estimate the tropospheric lifetime of 2,3PD with respect to its reaction with OH radicals, τ_{OH}(2,3PD). With an

average global OH concentration of $[OH]_{global}$ = 1 × 10^6 radicals cm^{-3} (24 h average) [Heard and Pilling 2003], the tropospheric lifetime of τ_{OH}(2,3PD) ≈ 5.3 days is estimated (Table 4.1).

The wet deposition, that is depletion by cloud and rain water, is expected to be only a slow process similarly to biacetyl and monoketones [Sander 2010], in view of the likely small Henry's law constant of 2,3PD.

In summary, the estimations show that photolysis is the dominant process to determine the loss of 2,3PD in the troposphere. While this conclusion is believed correct in qualitative terms, accurate lifetime can not be given as yet, mostly because of the uncertainty of the photolysis quantum yields. It is noted also that the simple assessment used here is based on the assumption that 2,3PD is uniformly mixed through the troposphere that is probably not the case in view of the short lifetime of this diketone and the average tropospheric transport time scale (1-2 months). The short lifetime indicates that 2,3PD will be removed rapidly close to its local sources in the atmosphere.

Glycolaldehyde:

The photolysis lifetime of glycolaldehyde, τ_{phot}(GA), can be estimated from the average of my measured photolysis rate constant relative to NO_2 photolysis frequency: J_{GA} / J_{NO2} = 0.138 (see Table 4.2) and taking $J_{NO2,trop} \approx 4 \times 10^{-3}$ s^{-1} from [Wild 2000] which is the globally averaged tropospheric photolysis frequency of NO_2.

$$J_{GA,trop} = \frac{J_{GA}}{J_{NO2}} \times J_{NO2,trop} \qquad \text{(Eq. 17)}$$

$$\tau_{phot}(GA) = \frac{1}{J_{GA,trop}} \qquad \text{(Eq.18)}$$

In this way, τ_{phot}(GA) ≈ 30 minutes is obtained for the photolytic lifetime of GA in the troposphere. This value is smaller than the photolysis lifetime of ~ 1 day reported by Magneron and co-workers [Magneron 2005]. The longer lifetime of τ_{phot}(GA) ≥ 17.6 h was also proposed in a most recent paper [Zhu and Zhu 2010]. One possibility to

explain the disparity is that the literature lifetimes refer to the ground level while my estimation gives a global average tropospheric lifetime for glycolaldehyde. As discussed in [Zhu and Zhu 2010], the OH-reaction of GA is of comparable significance with the photolysis under tropospheric conditions.

The Henry's law constant for glycolaldehyde is 4.1×10^4 M atm^{-1} at 298 K [Betteron 1988] which implies that wet deposition can also be considered as a potential way of depletion of glycolaldehyde in the atmosphere.

Chapter 5: Summary

Objectives of this work

The OH-kinetics and photochemistry of selected oxygenated volatile organic compounds (OVOCs) were studied in my PhD work. Selection of the model compounds and their reactions was based on their interest for basic research and also because of their importance for the chemistry of the atmosphere. The following reactions were studied:

OH + $CH_3C(O)OH$ (d_0-AA) → products	k_1	(1)
OH + $CH_3C(O)OD$ (d_1-AA) → products	k_2	(2)
OH + $CD_3C(O)OH$ (d_3-AA) → products	k_3	(3)
OH + $CD_3C(O)OD$ (d_4-AA) → products	k_4	(4)
OH + $CH_3C(O)CH_2CH_3$ (MEK)→ products	k_5	(5)
$CH_3C(O)C(O)CH_2CH_3$ (2,3PD) + $h\nu$ → products	$\sigma_{2,3PD}$, $J_{2,3PD}$, $\Phi_{2,3PD}$	(6)
OH + $CH_3C(O)C(O)CH_2CH_3$ (2,3PD) → products	k_7	(7)
$HOCH_2CHO$ (GA) + $h\nu$ → products	J_{GA}	(8)

Reaction rate constants, k_1-k_5, and k_7, photolysis quantum yield $\Phi_{2,3PD}$, and photolysis rate constants, $J_{2,3PD}$, J_{GA} were determined. Absorption cross sections of 2,3PD, $\sigma_{2,3PD}$, as a function of wavelength were also measured. Determination of rate constants for the OH reactions allowed to assess reactivity-molecule-structure relationships and to estimate the atmospheric lifetimes of the studied OVOCs with respect to their OH reactions. The determined photochemical parameters have provided insight into the photochemistry of carbonyl molecules in general, and allowed to estimate the photolysis atmospheric lifetimes of the studied photochemically active organics. Both the determined reaction kinetic and photochemical data can be used as input parameters for atmospheric modelling studies.

Experimental methods

I have applied several complementary experimental methods that are available in the Chemical Research Center, Budapest (CRC, Budapest) and at the Ecole des Mines de Douai (EMD, Douai). All experiments were performed at laboratory temperature ($T \approx 300$ K).

The relative rate (RR) method was applied to determine rate constant for reactions (1-4) as well as for reaction (7) at atmospheric pressure. In the application of the RR method, the rate constant of the studied reaction is compared with that of a reference reaction, the rate constant of which is accurately known. The experiments were carried out both in a ~ 250 L Teflon-bag reactor and a 10 L Pyrex bulb using the photooxidation of CH_3ONO as the source of OH radicals. Fluorescent tubes and Xe lamp were the light sources. The following reactions were used as reference: OH + CH_3OH, OH + CD_3OD, OH + MEK and OH + C_2H_5OH. Samples were withdrawn from the reactors at different reaction times and the concentration depletions of the organic substrates were determined by GC analysis using FID detection. Rate constant ratios were obtained that were put on the absolute scale by taking the rate constants of the reference reactions from the literature.

The direct discharge flow technique (DF-RF) was applied to determine the rate constants of the reactions OH + MEK (5) and OH + 2,3PD (7). OH radicals were monitored by resonance fluorescence (RF) detection. At employing the DF method, the reactions are carried out in a fast He flow (~ 10 m s^{-1}) at a few mbar overall pressure. The experiments were investigated under pseudo-first-order conditions, with large excess of the reactants over OH, by recording the RF signal of OH radicals in the presence and absence of the reactants. The OH radicals were produced by reacting H atoms with a slight excess of NO_2; H atoms were generated by microwave discharge dissociation of H_2.

The absorption spectrum of 2,3-pentanedione was measured using a home-built single-path UV / Vis spectrophotometer over the wavelength range of $\lambda = 210 – 450$ nm.

Photolysis quantum yields and photolysis frequencies of 2,3PD were determined at 254, 312 and 365 nm wavelengths in the Teflon-bag reactor using fluorescent lamps for irradiation. The photolysis frequencies of 2,3PD were made independent of the photon fluxes by using NO_2 and acetone actinometry and in this way effective quantum yields could be derived. Moreover, a XeF exciplex laser was used to determine the

photolysis quantum yield of 2,3PD at 351 nm. Both the laser photolysis and the continuous photolysis with the fluorescent lamps were carried out in atmospheric pressure air. The consumption of 2,3PD was determined as a function of reaction time using GC-FID; the rate of light absorption was determined by using a laser energy meter and chemical actinometry.

OH reaction kinetics of acetic acid and its deuterated isotopes

The reaction kinetics of OH + $CH_3C(O)OH$ (1) have been investigated in details in the past few years by several groups, and it has been discussed in a recent feature article [Carl 2007]. In contrast with this, only a few literature data are available on the OH + deuterated acetic acid reactions. Kinetic data on the reaction of OH with deuterated acetic acids are useful for a better understanding of the reaction mechanism of the basis reaction OH + $CH_3C(O)OH$ (1). The RR kinetic measurements were carried out in the collapsible Teflon-reactor in air at atmospheric pressure and T = 297 ± 3 K. The reference compounds were methanol for $CH_3C(O)OH$ (d_0-*AA*) and $CD_3C(O)OH$ (d_3-*AA*) and deuterated methanol for $CH_3C(O)OD$ (d_1-*AA*) and $CD_3C(O)OD$ (d_4-*AA*). The following rate constant values were obtained: k_1(OH + d_0-*AA*) = (6.3 ± 0.9), k_2(OH + d_1-*AA*) = (1.5 ± 0.3), k_3(OH + d_3-*AA*) = (6.3 ± 0.9) and k_4(OH + d_4-*AA*) = (0.90 ± 0.1) all given in 10^{-13} cm^3 $molecule^{-1}$ s^{-1}. The rate constant for the acetic acid + OH reaction agrees well with most of the literature data. To my knowledge, the rate constant for reaction OH + d_1-*AA* (2) represents the first kinetic determination [Szabó 2009]. The rate constants that I have determined for reactions (1) – (4), taken together, confirms the literature view [Butkovskaya 2004], [Carl 2007] that it is the acetic H-atom which is abstracted preferentially, in contrast that it has got higher bond dissociation energy than that of the C-H bond in the acetic acid molecule.

OH reaction kinetics of methyl-ethyl-ketone

The reaction OH + MEK (5) was studied by using the direct DF-RF method (T = 297 ± 3 K, p = 3.17 ± 0.08 mbar He). The following rate constant value is proposed: $k_5 = (1.09 \pm 0.09) \times 10^{-12}$ cm^3 $molecule^{-1}$ s^{-1}. The rate constant of this reaction has recently been evaluated by IUPAC and the recommended value is 1.1×10^{-12} cm^3

molecule^{-1} s^{-1} [IUPAC 2009a]. Important is that all previous determinations were performed with photolysis techniques, while I have applied the thermal DF-RF method [Szabó 2009]. The good agreement indicates that the rate constant of the OH + MEK (5) reaction has become well established, indeed, and so I have used this reaction and the determined k_5 value for the RR study of 2,3PD.

Photochemistry and OH reaction kinetics of 2,3-pentanedione

The most detailed investigations were done with 2,3-pentanedione and most of the results are reported the first time. 2,3PD belongs to the family of α-dicarbonyls, several of which are of great importance for the chemistry of the troposphere, e.g. glyoxal, methyl-glyoxal, and biacetyl.

Only little is known about the photochemistry of 2,3PD from the literature in contrast, e.g., with the aliphatic monoketones, acetone, MEK, etc. As a first step of the 2,3PD studies, the absorption cross sections were determined: the absorption spectrum of 2,3PD extends into the visible range and it is characterised by two broad absorption bands. Photolysis quantum yield (QY) of 2,3PD was determined in the Teflon-bag reactor at 254, 312 and 365 nm, and in a quartz cell using XeF exciplex laser at 351 nm (T = 300 ± 2 K, p = 1000 mbar air). The following QY values were obtained: $\Phi_{2,3PD}$(254 nm) = 0.29 ± 0.01, $\Phi_{2,3PD}$(312 nm) = 0.41 ± 0.02, $\Phi_{2,3PD}$(365 nm) = 0.78 ± 0.05, $\Phi_{2,3PD}$(351 nm) = 0.11 ± 0.005. The $\Phi_{2,3PD}$ results determined above 300 nm are surprisingly high values and display significant disparity. They appear high compared to the long-wavelengths photolysis QYs of monoketones but, on the other hand, the α-ketoaldehydes display high photolysis quantum yields even at long wavelengths. Further investigations are needed to explain this discrepancy. At the current stage of research, the average value of $\Phi_{2,3PD} \approx 0.4$ is proposed for the wavelength range ~310 – 370 nm.

To my knowledge, no prior rate constant has been reported for the reaction OH + 2,3PD (7). I have investigated this reaction by using both direct and relative rate techniques. The direct measurements were carried out in DF-RF apparatus (T = 300 ± 3 K, p = 2.49 ± 0.03 mbar He). The relative rate (RR) technique was applied in the experiments using the Teflon-bag and the Pyrex reactor in ~ 1000 mbar synthetic air at T = 300 ± 2 K and T = 302 ± 4 K, respectively. The reference compounds were methyl-ethyl-ketone and ethanol. The direct and RR methods have supplied rate constants in

good agreement with each other [Szabó 2011]. The recommended average value is k_7 (300 K) = (2.19 ± 0.22) × 10^{-12} cm^3 $molecule^{-1}$ s^{-1}. The rate constant has been found invariant to the reaction pressure in a wide range between ~2 mbar and ~1000 mbar. The determined k_7 implies significant enhanced reactivity compared, e.g., with the OH + propane and OH + 2,3-butanedione reactions known from the literature. The relatively high rate constant is attributed to the presence of the CH_2 group in β-position to one of the carbonyl groups in the 2,3PD molecule. In order to account for the activating effect of the vicinal carbonyl groups in a molecule, I have proposed the F(–C(O)C(O)–) = 1.55 value to be used in the group additivity estimations of OH reaction rate constants.

Photolysis study of glycolaldehyde

The experiments were carried out in the Teflon-bag reactor in air at atmospheric pressure and T = 300 ± 2 K using UV tubes emitting at 312 nm wavelength The photolysis rate constant (photolysis frequency) has been determined to be: J_{GA} = (1.48 ± 0.04) ×10^{-4} s^{-1}. Methanol and formaldehyde were detected as photooxidation products. The methanol yield is in agreement with the literature, but the yield of formaldehyde is 2-3 times smaller compared with literature results [Zhu and Zhu 2010]: Γ_{HCHO} = 10.4 – 26.7 % and Γ_{CH3OH} = 1.8 – 8.7 %.

Reactivity of OH radicals with carbonyls

All reactions that I have studied are hydrogen abstraction reactions. My results show that both thermochemical and inductive effects influence the reactivity of OH radicals toward carbonyls. The presence of a C=O group slightly reduces the C-H bond energy in the α-position. This effect is, however, overcompensated by the negative inductive effect of the carbonyl group that leads to a reduced reactivity. Such effects have already been taken into account in the group-additivity estimation procedure developed by Atkinson and co-workers [Kwok and Atkinson 1995]: the estimated rate constants agree well with my experimental determinations. Entirely new is the observation that the α-diketone 2,3PD shows an increased reactivity with OH that can be due to the formation of H-bonded complexes in the reaction [Szabó 2011].

Atmospheric implications

My experimental results provide information on the homogenous depletion processes of selected OVOCs, namely their OH reactions and photolysis.

In the case of acetic acid, the tropospheric lifetime is τ_{OH} (d_0-*AA*) = 18 days with respect to its OH reaction. Photolysis does not play a role, but the atmospheric fate of acetic acid is known to be determined essentially by wet deposition.

Concerning methyl-ethyl-ketone, τ_{OH} (MEK) is 11 days which is of comparable magnitude with its photolytic lifetime [Nádasdi 2010].

The rate constant I determined for the OH + 2,3PD reaction gives τ_{OH} (2,3PD) = 5.3 days OH reaction lifetime in the troposphere. Due to its significant absorption in the visible and the fairly large photolysis quantum yield, the photolytic lifetime of 2,3PD is very short even at the ground level. According to my estimation it is τ_{phot} (2,3PD) = 3.9 hours [Szabó 2011].

References

-a-

[Alvarez-Idaboy 2004] Alvarez-Idaboy J., Cruz-Torres A., Galano A., Ruiz-Santoyo M.; Structure – reactivity relationship in ketones + OH reactions: a quantum mechanical and TST approach, *J. Phys. Chem. A*, 108, 2740-2749, **2004**

[Andreae 1988] Andreae, M. O., Talbot R. W., Andreae T. W., Harriss R. C.; Formic and acetic acid over the Central Amazon Region, Brazil 1. Dry Season, *J. Geophys. Res.*, 93(D2), 1616-1624, **1988**

[Atkinson 1985] Atkinson R.; Kinetics and mechanism of the gas-phase reactions of the hydroxyl radical with organic compounds under atmospheric conditions, *Chem. Rev.*, 85(1), 69-201, **1985**

[Atkinson 1989] Atkinson R.; Kinetics and mechanisms of the gas-phase reactions of the hydroxyl radical with organic compounds, *J. Phys. Chem. Ref; Data*, Monograph 1, **1989**

[Atkinson 2000] Atkinson R.; Atmospheric chemistry of VOCs and NOx, *Atmos. Environ.*, 34, 2063-2101, **2000**

[Atkinson and Arey 2003] Atkinson R., Arey J.; Atmospheric degradation of volatile organic compounds, *Chem. Rev.*, 103, 4605-4638, **2003**

[Atkinson 2004] Atkinson R., Blauch D. L., Cox R. A., Crowley J. N., Hampson R. F., Hynes R. G., Jenkin M. E., Rossi M. J., Troe J.; Evaluated kinetic and photochemical data for atmospheric chemistry: Volume I – gas phase reaction of O_x, HO_x, NO_x and SO_x species, *Atmos. Chem. Phys.*, 4, 1461-1738, **2004**

[Atkinson 2006] Atkinson R., Blauch D. L., Cox R. A., Crowley J. N., Hampson R. F., Hynes R. G., Jenkin M. E., Rossi M. J., Troe J.; Evaluated kinetic and photochemical data for atmospheric chemistry: Volume II – gas phase reaction of organic species, *Atmos. Chem. Phys.*, 6, 3625-4005, **2006**

-b-

[Baasandorj 2009] Baasandorj M., Griffith S., Dusanter S., Stevens P. S.; Experimental and theoretical studies of the kinetics of the OH + hydroxyacetone reaction as a function of temperature, *J. Phys. Chem. A*, 113, 10495-10502, **2009**

[Bacher 2001] Bacher C., Tyndall G. S., Orlando J. J.; The atmospheric chemistry of glycolaldehyde, *J. Atm. Chem.*, 39, 171-189., **2001**

[Baeza-Romero 2007] Baeza-Romero M. T., Glowacki D. R., Blitz M. A., Heard D. E., Pilling M. J., Rickard A. R., Seakins P.; A combined experimental and theoretical study of the reaction between methylglyoxal and OH/OD radical: OH generation, *Phys. Chem. Chem. Phys.*, 9, 4114-4128, **2007**

[Baraldi 1999] Baraldi R., Rapparini F., Rossi F., Latella A., Ciccioli P.; Volatile organic compound emission from flowers of the most occuring and economically important species of fruit trees, *Phys. Chem. Earth (B)*, 24(6), 729-732, **1999**

[Berkowitz 1994] Berkowitz J., Ellison G. B., Gutman D.; Three methods to measure RH bond energies, *J. Phys. Chem.*, 98, 2744-2765, **1994**

[Bernard 2001] Bernard S. M., Samet j. M., Grambsch A., Elbi K. L., Romieu I.; The potential impact of climate variability and change on air pollution-related health effects in the United States, *Environ. Health Perspectives*, 109, 199-209, **2001**

[Betterton 1988] Betterton E. A., Hoffmann M. R.; Henry's law constant for some environmentally important aldehydes, *Environ. Sci. Technol.*, 22, 1415-1418, **1988**

[Bohn 2004] Bohn B., Rohrer F., Brauers T., Wahner A.; Actinometric measurements of NO_2 photolysis frequencies in the atmosphere simulation chamber SAPHIR, *Atmos. Chem. Phys. Discuss.*, 4, 8141-8170, **2004**

[Burdock 2005] Burdock G. A.; Fenaroli's handbook of flavour ingredients, 5^{th} edition, CRC, *Press: Boca Raton*, FL., **2005**

[Butkovskaya 2004] Butkovskaya N. I., Kukui A., Pouvesle N., Le Bras G.; Rate constant and mechanism of the reaction of OH radicals with acetic acid in the temperature range of 229-300 K, *J. Phys. Chem. A*, 108, 7021-7026, **2004**

[Butkovskaya 2006] Butkovskaya N; I., Pouvelse N., Kukui A., Le Bras G.; Mechanism of the OH-initiated oxidation of glycoladehyde over the temperature range 233-296 K, *J. Phys. Chem. A*, 110, 13492-13499., **2006**

-c-

[Carl 2007] Carl S. A., Vereecken L., Peeters J.; Kinetic parameters for gas-phase reactions: Experimental and theoretical challenges, *Phys. Chem. Chem. Phys.*, 9, 4071-4087, **2007**

[Carr 2008] Carr S. A., Baeza-Romero M. T., Blitz M. A., Price B. J. S., Seakins P. W.; Ketone photolysis in the presence of oxygen: A useful source of OH for flash photolysis kinetics experiments, *Int. J. Chem. Kin.*, 40(8), 504-514, **2008**

[Chen 2000] Chen Y., Wang W., Zhu L.; Wavelength-dependent photolysis of methylglyoxal in the 290 – 440 nm region, *J. Phys. Chem. A*; 104, 11126-11131, **2000**

[Chung 2002] Chung S. H., Seinfeld J. H.; Global distribution and climate forcing of carbonaceous aerosols, *J. Geophys. Res*., 107(D19), 4407-4440, **2002**

[Cox 1981] Cox R. A., Patrick K. F., Chant S. A.; Mechanism of atmospheric photooxidation of organic compounds. Reactions of alkoxy radicals in oxidation of n-butane and simple ketones, *Environ. Sci. Technol*., 15(5), 587-592, **1981**

[Crunaire 2006] Crunaire S., Tarmoul J., Fittschen C., Tomas A., Lemoine B., Coddeville P.; Use of cw-CRDS for studing the atmospheric oxidation of acetic acid in a simulation chamber, *Appl. Phys., B*, 85, 467-476, **2006**

-d-

[Dagaut 1988a] Dagaut P., Wallington T. J., Liu R., Kurylo M. J.; The gas phase reaction of hydroxyl radicals with a series of carboxylic acids over the temperature range 240-440 K, *Int. J. Chem. Kin.*, 20, 331-338, **1988**

[Dagaut 1988b] Dagaut P., Wallington T. J., Liu R., Kurylo M. J.; A kinetics investigation of the gas-phase reactions of OH radicals with cyclic ketones and diones: mechanistic insights, *J. Phys. Chem.*, 92, 4375-4377, **1988**

[Darnall 1979] Darnall K. R., Atkinson R., Pitts J. N. Jr.; Observation of biacetyl from the reaction of OH radicals with o-xylene. Evidence for ring cleavage, *J. Phys. Chem*., 83(15), 1943-1946, **1979**

[Dibb 2002] Dibb J. E., Arsenault M.; Shouldn't snowpacks be sources of monocarboxylic acids?, *Atmos. Environ.*, 36, 2513-2522, **2002**

-e-

[Edney 1986] Edney E. O., Kleindienst T. E., Corse E. W.; Room temperature rate constants for the reaction of OH with selected chlorinated and oxygenated hydrocarbons, *Int. J. Chem. Kin.*, 18(12), 1355-1371, **1986**

[Enders 1992] Enders G., Dlugi R., Steinbrecher R., Clement B., Daiber R., Eijk J.v., Gäb S., Haziza M., Helas G., Herrmann U., Kessel M., Kesselmeier J., Kotzias D., Kourtidis K., Kurth H.H., McMillen R.T., Roider G., Schürmann W., Teichmann U., Torres L.; Biosphere/atmosphere interactions: integrated research in a European coniferous forest ecosystem. *Atmos. Environ.*, 26,171-189, **1992**

[Espinosa-Garcia 2003] Espinosa-Garcia J., Marquez A., Dóbé S.; Theoretical enthalpy of formation of the acetonyl radical, *Chem. Phys. Lett*., 373, 350-356, **2003**

-f-

[Fehsenfeld 2006] Fehsenfeld F., Ancellet G., Bates T., Goldstein A., Hardesty R;, Honrath R., Law K., Lewis A., Leaitch R., McKeen S., Meagher J., Parrish D., Pszenny A., Russel P., Schlanger H., Seinfeld J., Talbot R., Zbinden R.; International consortium for atmospheric research on transport and transformation (ICARTT): North America to Europe – overview of the 2004 summer field study, *J. Geophys. Res.*, 111, D23S01, **2006**

[Ferronato 1998] Ferronato C., Orlando J. J., Tyndall G. S.; Rate and mechanism of the reactions of OH and Cl with 2-methyl-3-buten-2-ol, *J. Geophys. Research*, 103, 25579-25586, **1998**

[Finlayson-Pitts and Pitts 2000] Finlayson-Pitts J. B. and Pitts J. N. Jr; Chemistry of the Upper and Lower Atmosphere, Theory, Experiments, and Applications, *Academic Press*, San Diego, etc., **2000**

-g-

[Galano 2008] Galano A., Alvarez-Idaboy J. R.; Atmospheric reactions of oxygenated volatile organic compounds + OH radicals: role of hydrogen-bonded intermediates and transition states, *Advances in quantum chemistry, Applications of theoretical methods to atmospheric science*, 55, 245-274, **2008**

[Galbally 2007] Galbally I., Lawson S., Weeks I., Bentley S., Gillet R., Meyer M., Goldstein A.; Volatile organic compounds in marine air at Cape Grim, Australia, *Environ. Chem.*, 4(3), 178-182, **2007**

[Gierczak 1998] Gierczak T., Burkholder J. A., Bauerle S; Ravishankara A. R.; Photochemistry of acetone under tropospheric conditions, *Chemical Physics*, 231, 229-244, **1998**

-h-

[Hansen 2002] Hansen J. C., Francisco J. S.; Radical-molecule complexes: Changing our perspective on the molecular mechanisms of radical-molecule reactions and their impact on atmospheric chemistry, *Chem. Phys. Chem.* 3, 833-840, **2002**

[Harris 1982] Harris G. W., Carter W. P. L., Winer A. M., Pitts J. N. Jr., Platt U., Perner D.; Observation of nitrous acid in the Los Angeles atmosphere and implications for predictions of ozone-precursor relationships, *Envir. Sci. Technol.*, 16(7), 414-419, **1982**

[Heard and Pilling 2003] Heard D. E., Pilling M. J.; Measured of OH and HO_2 in the troposphere, *Chem. Rev.*, 103, 5161-5198, **2003**

[Henon 2003] Henon E., Canneaux S., Bohr F., Dóbé S.; Features of the potential energy surface for the reaction of OH radical with acetone, *Phys. Chem. Chem. Phys*., 5, 333-341, **2003**

[Holloway 2005] Holloway A-L., Treacy J., Sidebottom H., Mellouki A., Daële V., Le Bras G., Barnes I.; Rate coefficients for the reactions of OH radicals with the keto/enol tautomers of 2,4-pentanedione and 3-methyl-2,4-pentanedione, allyl alcohol and methyl vinyl ketone using the enols and methyl nitrite as photolytic sources of OH, *J. Photochem. and Photobiol. A: Chemistry*, 176, 183-190, **2005**

[Holmes 1973] Holmes J. R., O'Brien R. J., Crabtree J. H.; Measurement of ultraviolet radiation intensity in photochemical smog studies, *Envir. Sci. Technol.*, 7(6), 519-523, **1973**

[Horowitz 2001] Horowitz A.; Meller R., Moortgat G. K; The UV-Vis absorption cross sections of α-dicarbonyl compounds: pyruvic acid, biacetyl and glyoxal, *J. Photochem. Photobiol. A: Chemistry*, 146, 19-27, **2001**

[Howard 1979] Howard C. J.; Kinetic measurements using flow tubes, *J. Phys. Chem.*, 83, 3-9, **1979**

[Hoyermann 1975] Hoyermann K. H.: in: Physical Chemistry – An Advanced Treatise. Vol VI B. Kinetics of gas reactions, Chapter 12., Academic Press, New York, **1975**

[Huang 2009] Huang Y., Dransfield T. J., Miller J. D., Rojas R. D., Castillo X. G., Anderson J. G.; Experimental study of the kinetics of the reaction of acetic acid with hydroxyl radicals from 255-355 K, *J. Phys. Chem. A*, 113, 423-430, **2009**

[IARC 2010] IARC monographs on the evaluation of carcinogenic risks to humans. Complete list of agents evaluated and their classification. Web Version: http://monographs.iarc.fr/ENG/Classification/index.php, Vol 32, 33, 88, **2010**

[IUPAC 2007] (*HO + $HOCH_2CHO$ → products*), Atkinson R., Baulch D. L., Cox R. A., Crowley J. N., Hampson R. F., Hynes R. G., Jenkin M. E., Rossi M. J., Troe J.; Summary of evaluated kinetic and photochemical data for atmospheric chemistry, Web Version: http://www.iupackinetic.ch.cam.ac.uk. Data sheet HOx_VOC17, **2007**

[IUPAC 2009a] (*HO + $CH_3C(O)CH_2CH_3$ → products*), Ammann, M., Atkinson, R., Cox, R. A., Crowley, J., Jenkin, M. E., Hynes, R., Mellouki, A.; Rossi, M. J., Troe, J., Wallington, T; Summary of evaluated kinetic and photochemical data for atmospheric chemistry, Web Version: http://www.iupackinetic.ch.cam.ac.uk. Data sheet HOx_VOC20, **2009**

[IUPAC 2009b] (*HO + C_2H_5OH → products*), Ammann, M., Atkinson, R., Cox, R. A., Crowley, J., Jenkin, M. E., Hynes, R., Mellouki, A.; Rossi, M. J., Troe, J., Wallington, T; Summary of evaluated kinetic and photochemical data for atmospheric chemistry, Web Version: http://www.iupackinetic.ch.cam.ac.uk. Data sheet HOx_VOC24, **2009**

[IUPAC 2009c] (*HO + $CH_3C(O)OH$ → products*), Ammann, M., Atkinson, R., Cox, R. A., Crowley, J., Jenkin, M. E., Hynes, R., Mellouki, A.; Rossi, M. J., Troe, J., Wallington, T; Summary of evaluated kinetic and photochemical data for atmospheric chemistry, Web Version: http://www.iupackinetic.ch.cam.ac.uk. Data sheet HOx_VOC36, **2009**

-j-

[Jackson and Yarwood 1971] Jackson A. W. and Yarwood A. J.; Radiation and radiationless processes in 2,3-pentanedione; Phosphorescence lifetime in gas phase, *Canadian Journal of Chemistry*, 49, 987-993, **1971**

[Jackson and Yarwood 1972] Jackson A. W. and Yarwood A. J.; Fluorescence and phosphorescence of 2,3-pentanedione, *Canadian Journal of Chemistry*, 50, 1331-1337, **1972**

[Jagiella and Zabel 2008] Jagiella S., and Zabel F.; Thermal stability of carbonyl radicals. Part II. Reactions of methylglyoxyl and methylglyoxylperoxy radicals at 1 bar in the temperature range 275-311 K, *Phys. Chem. Chem. Phys.*, 10, 1799-1808, **2008**

[Jiménez 2005] Jiménez E., Ballesteros B. Martinez E., Albaladejo J.; Tropospheric reaction of OH with selected linear ketones: kinetic studies between 228 and 405 K, *Environ. Sci. Technol*., 39, 814-820, **2005**

[JPL 2006] Sander S. P., Friedl R. R., Golden D. M., Kurylo M. J., Moortgat G. K., Keller-Rudek H., Wine P. H., Ravishankara A. R., Kolb C. E., Molina M. J., Finlayson-Pitts B. J., Huie R. E., Orkin V. L.; Chemical kinetics and photochemical data for use in atmospheric studies, Evaluation number 15, *JPL Publication 06-2*, **2006**

-k-

[Karunanandan 2007] Karunanandan R., Hölscher D., Dillan T. J., Horowitz A., Crowley J. N., Vereecken L., Peeters J.; Reaction of HO with glycolaldehyde, $HOCH_2CHO$: rate coefficients (240-362 K) and mechanism, *J. Phys. Chem. A.*, 111, 897-908, **2007**

[Kawamura 1985] Kawamura K., Lai-Ling Ng., Kaplan I. R.; Determination of organic acids (C_1-C_{10}) in the atmosphere, motor exhausts, and engine oils, *Environ. Sci. Technol.*, 19, 1082-1086, **1985**

[Khamaganov 2006] Khamaganov V. G., Bui X. V., Carl S. A., Peeters J.; Absolute rate coefficient of the OH + $CH_3C(O)OH$ reaction at T=287-802 K. The two faces of pre-reactive H-bonding, *J. Phys. Chem. A*, 110 12852-12859, **2006**

[Kelly 1982] Kelly N. A.; Characterization of fluorocarbon-film-bags as smog chambers, *Environ. Sci. Technol*. 16(11), 763-770, **1982**

[Kercher 2005] Kercher J. P., Fogleman E. A., Koizumi H., Sztaray B., Baer T.; Heats of formation of the propionyl ion and radical and 2,3-pentanedione by threshold photoelectron photoion coincidence spectroscopy, *J. Phys. Chem. A*, 109, 939-946, **2005**

[Khwaja 2008] Khwaja H., Narang A.; Carbonyls and non-methane hydrocarbons at rural mountain site in northeastern United States, *Chemosphere*, 71, 2030-2043, **2008**

[Kovács 2006] Kovács G., Szász-Vadász T., Papadimitriou V. C., Dóbé S., Bérces T., Márta F.; Absolute rate constants for the reactions of OH radicals with CH_3CH_2OH, CF_2HCH_2OH and CF_3CH_2OH, *React. Kinet. Catal. Lett.*, 87(1), 129-138, **2006**

[Kovács 2007] Kovács G., Zádor J., Farkas E., Nádasdi R., Szilágyi I., Dóbé S., Bérces T., Márta F. Gy. Lendvay; Kinetic and mechanism of the reaction of CH_3CO and $CH_3C(O)CH_2$ radicals with O_2. Low-pressure discharge flow experiments and quantum chemical comutation, *Phys. Chem. Chem. Phys*. 9, 4142-4154, **2007**

[König 1995] König G., Brunda M., Puxbaum H., Hewitt N. C., Duckham S. C., Rudolf J.; Relative contribution of oxygenated hydrocarbons to the total biogenic VOC emissions of selected Mid-European agricultural and natural plant species, *Atmos. Environ*., 29(8), 861-874, **1995**

[Kung 1974] Kung T., J-F.; A new caramel compound from coffee, *Journal of Agricultural and Food Chemistry*, 22, 494-496, **1974**

[Kwok and Atkinson 1995] Kwok E. S. C., Atkinson R.; Estimation of hydroxyl radical reaction rate constants for gas-phase organic compounds using a structure-reactivity realationship: An update, *Atmos. Environ*., 29(14), 1685-1695, **1995**

-l-

[Lammel and Cape 1996] Lammel G. and Case J. N.; Nitrous acid and nitrite in the atmosphere, *Chem. Soc. Rev.*, 25, 361-369, **1996**

[Le Calvé 1998] Le Calvé S. Hitier D., Le Bras G., Mellouki A.; Kinetic studies of OH reaction with a series of ketones, *J. Phys. Chem. A*., 102, 4579-4584, **1998**

[Lonneman 1981] Lonneman W A., Bufalini J. J., Kuntz R. L., Meeks S. A.; Contamination from fluorocarbon films, *Environmental Science and Technology*, 15, 99-103, **1981**

-m-

[Magneron 2005] Magneron I., Mellouki A., Le Bras G.; Photolysis and OH initiated oxidation of glycolaldehyde under atmospheric conditions, *J. Phys. Chem. A*, 109, 4552-4561, **2005**

[Meller 2000] Meller R., Moortgat G. K.; Temperature dependence of the absorption cross sections of formaldehyde between 223 and 323 K in the wavelength range 225 - 375 nm, *J. Geophys. Res*., 105, 7089-7101, **2000**

[Mellouki 2003] Mellouki A., Le Bras G., Sidebottom H.; Kinetics and mechanisms of the oxidation of oxygenated organic compounds in the gas phase, *Chem. Rev*., 103, 5077-5096, **2003**

[Mészáros 1997] M észáros E.; Levegőkémia, *Veszprémi Egyetemi Könyvkiadó*, **1997**

[Moortgat 2010] Moortgat G. K., Meyrahn H., Warneck P.; Photolysis of acetaldehyde in air: CH_4, CO and CO_2 quantum yields, *J. Chem. Phys. Chem*., 11, 3896-3908, **2010**

-n-

[Nádasdi 2007] Nádasdi R., Szilágyi I., Demeter A., Dóbé S., Bérces T., Márta F.; Exciplex laser photolysis study of acetone with relevance to tropospheric chemistry, *Chem. Phys. Letters*, 440, 31-35, **2007**

[Nádasdi 2009] Nádasdi R. *Ph.D. Thesis*, Technical University, Budapest, **2009**

[Nádasdi 2010] Nádasdi R., Zügner G. L., Farkas M., Dóbé S., Maeda S., Morokuma K.; Photochemistry of methyl-ethyl-ketone: quantum yields and S_1/S_0 diradical mechanism of photodissociation, *Chem. Phys. Chem.*, 11, 3883-3895, **2010**

[Niki 1981] Niki H., Marker P. D., Savage C. M., Breintenbach L. P.; An FTIR study on mechanisms for the HO radical initiated oxidation of C_2H_4 in the presence of NO: detection of glycolaldehyde, *Chem. Phys. Letters*, 80, 499-503, **1981**

[Niki 1987] Niki H., Marker P. D., Savage C. M., Hurley M. D.; Fourier transform infrared study of the kinetics and mechanisms for the Cl-atom- and HO-radical-initiated-oxidation of glycolaldehyde, *J. Phys. Chem.*, 91, 2174-2178, **1987**

-o-

[Orlando 1999] Orlando J. J., Tyndall G. S., Fracheboud J. M., Estupinan E. G., Haberkorn S., Zimmer A.; The rate mechanism of the gas-phase oxidation of hydroxyacetone, *Atmos. Environ.*, 33, 1621-1629, **1999**

-p-

[Parker 2009] Parker A., Jain C., Schoemaecker C., Fittschen C.; Kinetics of the reaction of OH radicals with CH_3OH and CD_3OD studied by laser photolysis coupled to high repetition rate laser induced fluorescence, *React. Kinet., Catal., Lett*., 96, 291-297, **2009**

[Pearlyn 1977] Pearlyn D., Pereira D., Kathirgamanthan P.; An infinite optical path photoreactor and a filter for the isolation of light at 366 nm, *J. Nat. Sci. Coun. Sri Lanka*, 5, 41-58, **1977**

-q-

-r-

[Raber 1995] Raber W. H., Moortgat G. K.; Progress and problems in atmospheric chemistry, World Scientific Publishing Co.: Singapore, **1995**

-s-

[Sander 2010] Sander R.; Compilation of Henry's law constants for inorganic and organic species of potential importance in environmental chemistry, Web Version: http://www.mpch-mainz.mpg.de/~sander/res/henry.html, **2010**

[Sanhueza 1996] Sanhueza E., Figueora L., Santana M.; Atmospheric formic and acetic acids inVenezuela, *Atmos. Environ*., 30, 1861-1873, **1996**

[Schwarzenbach 1947] Schwarzenbach G., Wittwer Ch.; Die bromometrische Bestimmung des Enolgehaltes mit Hilfe der Strömungsapparatur, *Helvetica Chimica Acta*, 30, 656-658, **1947**

[Sheats and Noyes 1955] Sheats G. F. and Noyes W. A.; Photochemical studies. LI. The photochemistry of biacetyl at 3650 and 4358 Å and its relationship to fluorescence, *J. of the American Chemical Society*, 77, 1421-1426, **1955**

[Singh 2004] Singh H. B., Salas R. B., Chatfield R. B., Czech E., Fried A., Walega J., Evans M. J., Field B. D., Jacob D. J., Blake D., Heikes B., Talbot R., Sachse G., Crawford J. H., Avery M. A., Sandholm S., Fuelberg H.; Analysis of the atmospheric distribution, sources, ans sinks of oxygenated volatile organic chemicals based on measurements over the Pacific during TRACE-P, *J. Geophys. Res*. 109, D15S07, **2004**

[Singleton 1989] Singleton D. L., Parakevopoulos G., Irwin R. S.; Rates and mechanism of the reactions of hydroxyl radicals with acetic, deuterated acetic, and propionic acids in the gas phase, *J. Am. Chem. Soc*., 111, 5248-5251, **1989**

[Smith 2002] Smith I., Ravishankara A.; Role of hydrogen-bonded intermediates in the bimolecular reactions of the hydroxyl radical, *J. Phys. Chem. A*, 106, 4798-4808, **2002**

[Sommariva 2008] Sommariva R., de Gouw J. A., Trainer M., Atlas E., Goldan P. D., Kuster W. C., Waeneke C., Fehsenfeld F. C.; Emissions and photochemistry of oxygenated VOCs in urban plumes in the Northeastern United States, *Atmos. Chem. Phys. Disc.*, 8, 12371-12408, **2008**

[Soni 2008] Soni M., Ramjugernath D., Raal J. D.; Vapor-liquid equlibrium for binary systems of 2,3-pentanedione with biacetyl and acetone, *J. Chem. Eng. Data*, 53, 745-749, **2008**

[Szabó 2008] Szabó E., Zügner G. L., Szilágyi I., Dóbé S., Bérces T., Márta F.; Direct kinetic study of the reaction of OH radicals with methyl-ethyl-ketone, *React. Kinet. Catal. Lett.*, 95, 365-371, **2008**

[Szabó 2009] Szabó E., Tarmoul J., Tomas A., Fittschen C., Dóbé S., Coddeville P.; Kinetics of the OH-radical initiated reactions of acetic acid and its deuterated isomers, *React. Kinet. Catal. Lett.*, 96(2), 229-309, **2009**

[Szabó 2011a] Szabó E., Djehiche M., Riva M., Fittschen C., Coddeville P., Sarzyński D., Tomas A., Dóbé S.; Atmospheric chemistry of 2,3-pentanedione: photolysis and reactions with OH radicals and Cl atoms, *J. Phys. Chem. A*, **2011**

[Szabó 2011b] Szabó E., Zügner G. L., Farkas M., Szilágyi I., Dóbé S.; Direct kinetic study of the OH-radical initiated oxidation of pivalaldehyde, $(CH_3)_3CC(O)H$, in the gas phase, *Oxidation Communications*, (submitted: 09. 05. **2011**)

-t-

[Tadić 2001] Tadić J., Juranić I., Moortgat G.; Pressure dependence of the photooxidation of selected carbonyl compounds in air: *n*-butanal, *n*-pentanl, *J. Photochem. Photobiol. A: Chemistry*, 143, 169-179, **2001**

[Talbot 1990] Talbot, R. W., Andreae M. O., Berresheim H., Jacob D. J., Beecher K. M.; Sources and sinks of formic, acetic, and pyruvic acids over Central Amazonia 2. Wet Season, *J. Geophys. Res.*, 95(D10), 16799-16811, **1990**

[Talbot 1995] Talbot, R. W., Mosher B. W., Heikes B. G., Jacob D. J., Munger J. W., Daube B. C., Keene W. C., Maben J. R., Artz R. S.; Carboxylic acids in the rural continental atmosphere over the eastern United States during the Shenandoah Cloud and Photochemistry Experiment, *J. Geophys. Res.*, 100(D5), 9335-9343, **1995**

[Taylor 1980] Taylor W. D., Allston T. D., Moscato M. J., Fazekas G. B., Kozlowski R., Takacs, G. A.; Atmospheric photodissociation lifetimes for nitromethane, methyl nitrite, and methyl nitrate, *Int. J. Chem. Kinet.*,12, 231-240, **1980**

[Tuesday 1961] Tuesday C. S.; The atmospheric photooxidation of trans-2-butene and nitric oxide in chemical reactions in the lower and upper atmosphere, *Interscience*, New York, N. Y., 1-49, **1961**

[Turro and Lee 1969] Turro N. J. and Lee T. J.; Intramolecular photoreduction of alkyl α-diketones, *J. of the American Chemical Society*, 91, 5651-5652, **1969**

-u-

[Upadhyaya 2003] Upadhyaya H. P., Kumar A., Naik P.D.; Photodissociation dynamics of enolic-acetylacetone at 266, 248 and 193 nm: mechanism and nascent state product distribution of OH, *J. Chem. Phys*., 118(6), 2590-2598, **2003**

-v-

[Vimal 2006] Vimal D., Stevens P. S.; Experimental and theoretical studies of the kinetics of the reactions of OH radicals with acetic acid, acetic acid-d_3 and acetic acid-d_4 at low pressure, *J. Phys. Chem. A*, 110, 11509-11516, **2006**

-w-

[Wallington 1987] Wallington T. J., Kurylo M. J.; Flash photolysis resonance fluorescence investigation of the gas-phase reactions of OH radicals with a series of aliphatic ketones over the temperature range 240-440 K, *J. Phys. Chem.*, 91, 5050-5054, **1987**

[Wild 2000] Wild O., Zhu X., Prather J. M.; Fast-J: Accurate simulation of in- and below-cloud photolysis in tropospheric chemical models, *J. Atmos. Chem.*, 37, 245-282, **2000**

-x-

-y-

-z-

[Zetzsch and Stuhl 1982] Zetzsch C. and Stuhl F.; 2nd European Symposium on the Physico-chemical behaviour of atmospheric pollutants, Ed. Dordrecht, The Netherlands, **1982**

[Zhu and Zhu 2010] Zhu C. and Zhu L., Photolysis of glycolaldehyde in the 280-340 nm region, *J. Phys. Chem. A*, 114, 8384-8390, **2010**

[Zügner 2010] Zügner G. L., Szilágyi I, Zádor J., Szabó E., Dóbé S., Song X., Wang W.; OH yields for $C_2H_5CO + O_2$ at low pressure: experiment and theory, *Chem. Phys. Letters*, 495, 179-181, **2010**

[Zügner 2011] Zügner G. L., "Interaction between climate change and the chemistry of the atmosphere: kinetics studies of elementary chemical and photochemical reactions", PhD Thesis in preparation, Technical University, Budapest, **2011**

Acknowledgement

First of all, I wish to thank *Prof. Sándor Dóbé*, who has been a really great supervisor of my doctoral work at CRC Budapest, giving me help and advice in every respect.

I also thank *Dr. Christa Fittschen*, my thesis supervisor in France, for her support and scientific discussions. I would like to thank, moreover, *Dr. Alexandre Tomas*, my research advisor and the former and current directors *Prof. Jean-Claude Galloo* and *Prof. Patrice Coddeville* at Douai.

I would like to thank my fellow PhD students at Budapest, *Mária Farkas* and *Gábor L. Zügner* for their continuous help and friendship.

I gratefully acknowledge the financial support from the French Foreign Office and Region Nord – Pas de Calais in the framework of the ARCUS program and from the Hungarian Research Fund, OTKA (contract OMFB-00992/2009).

I am very grateful to my mum for the encouragement and love which gave me the possibility and ability to follow my dreams. I would like to thank to my two brothers *Attila* and *Dávid* and my sister *Zsuzsa* for their affectionate understanding.

Finally, I would like to thank *Jérémy Tarmoul*. You have shown love, encouragement and often patience, especially when I had critical times in my life.

Declaration

I, Emese Szabó undersigned, declare that this Thesis was prepared by myself and only the cited sources were used. Any part, which was literally or with identical content taken from other source has been unequivocally referred to.

Budapest, May 12, 2011.

……..…….

Emese Szabó

Appendix

Appendix 1: Rate constant determination using the relative - rate method

Relative-rate (RR) method with gas chromatographic analysis can be used to determine relative rate constants. The advantage of this method is that it is not necessary to know the absolute concentration of the measured chemical compounds. Generally, the OH radicals are produced in situ in the reaction mixture. This mixture contains also a reference compound (RC) and other compound (C), for which we wants to obtain the rate constant.

$$OH + RC \rightarrow H_2O + R \qquad (R1)$$

$$OH + C \rightarrow H_2O + C \qquad (R2)$$

The OH radical is produced by the photolysis of CH_3ONO or HONO. After switching on the photolysis lamps generation of OH radicals start. For example for the case of CH_3ONO the following reactions take place:

$$CH_3ONO + h\nu \rightarrow CH_3O + NO$$

$$CH_3O + O_2 \rightarrow HO_2 + HCHO$$

$$HO_2 + NO \rightarrow OH + NO_2$$

We do not need to know the concentration of OH radicals, since they cancel in the rate equations. Samples from the reaction mixture are analysed with GC at selected times to determine the concentration of $[RC]_t$ and $[C]_t$. The rate constants for reactions R1 and R2 can be given by the following way:

$$-\frac{d[RC]}{dt} = k_{R1}[OH][RC] \quad \text{and} \quad -\frac{d[C]}{dt} = k_{R2}[OH][C] \qquad \text{(Eq. A1)}$$

Integrating and combining the equations and considering the concentration of OH is constant, one obtaines:

$$\ln\frac{[C]_t}{[C]_0} = \frac{k_{R2}}{k_{R1}} \times \ln\frac{[RC_t]}{[RC]_0} \qquad \text{(Eq. A2)}$$

The plot of $\ln([C]_t / [C]_0)$ vs. $\ln([RC]_t / [RC]_0)$ should give a straight line and its slope gives the ratio of rate constants, k_{R2} / k_{R1}. Obviously,if k_{R1} is reliably known from measurements by other techniques, than k_{R2} can be obtained accurately.

Appendix 2: Table of absorption cross section of 2,3-pentanedione and Lambert-Beer plots at wavelengths used in the experiments

Table A2.1: Absorption cross section of 2,3-pentanedione

λ / nm	$\sigma_{2,3PD}$ / 10^{-20} cm^2 molecule^{-1}	± 2 stdev.		λ / nm	$\sigma_{2,3PD}$ / 10^{-20} cm^2 molecule^{-1}	± 2 stdev.
210	4.698	1.394		251	5.273	0.454
211	3.669	0.983		252	5.388	0.467
212	3.129	0.889		253	5.504	0.452
213	2.595	0.873		254	5.585	0.446
214	2.188	0.768		255	5.713	0.505
215	1.705	0.635		256	5.816	0.469
216	1.529	0.616		257	5.915	0.476
217	1.445	0.519		258	6.044	0.436
218	1.380	0.536		259	6.123	0.436
219	1.291	0.477		260	6.157	0.444
220	1.395	0.492		261	6.211	0.487
221	1.303	0.380		262	6.224	0.424
222	1.371	0.511		263	6.254	0.391
223	1.477	0.493		264	6.251	0.386
224	1.556	0.430		265	6.302	0.404
225	1.617	0.401		266	6.331	0.373
226	1.674	0.420		267	6.387	0.334
227	1.761	0.364		268	6.396	0.316
228	1.869	0.369		269	6.452	0.316
229	2.005	0.390		270	6.440	0.347
230	2.128	0.389		271	6.403	0.317
231	2.184	0.343		272	6.364	0.299
232	2.364	0.327		273	6.316	0.332
233	2.463	0.379		274	6.250	0.329
234	2.651	0.386		275	6.203	0.312
235	2.860	0.405		276	6.152	0.302
236	3.015	0.418		277	6.079	0.273
237	3.179	0.446		278	6.045	0.279
238	3.271	0.433		279	5.941	0.247
239	3.389	0.446		280	5.835	0.262
240	3.569	0.473		281	5.695	0.289
241	3.788	0.476		282	5.564	0.244
242	3.958	0.465		283	5.385	0.254
243	4.097	0.465		284	5.229	0.250
244	4.273	0.453		285	5.042	0.250
245	4.382	0.476		286	4.842	0.241
246	4.537	0.515		287	4.625	0.249
247	4.736	0.478		288	4.449	0.243
248	4.931	0.534		289	4.263	0.247
249	5.048	0.499		290	4.077	0.237
250	5.173	0.471		291	3.889	0.222

Table A2.1: (continued)

λ / nm	$\sigma_{2,3PD}$ / 10^{-20} cm^2 $molecule^{-1}$	± 2 stdev.		λ / nm	$\sigma_{2,3PD}$ / 10^{-20} cm^2 $molecule^{-1}$	± 2 stdev.
292	3.696	0.218		339	0.536	0.156
293	3.462	0.202		340	0.568	0.149
294	3.272	0.209		341	0.583	0.172
295	3.024	0.202		342	0.622	0.167
296	2.857	0.186		343	0.643	0.169
297	2.641	0.206		344	0.678	0.158
298	2.441	0.218		345	0.692	0.138
299	2.231	0.183		346	0.720	0.130
300	2.078	0.172		347	0.784	0.163
301	1.946	0.159		348	0.831	0.170
302	1.804	0.149		349	0.870	0.178
303	1.700	0.147		350	0.890	0.167
304	1.585	0.164		351	0.910	0.160
305	1.480	0.133		352	0.968	0.174
306	1.364	0.158		353	1.046	0.188
307	1.259	0.142		354	1.070	0.179
308	1.156	0.149		355	1.124	0.166
309	1.043	0.155		356	1.177	0.173
310	0.963	0.167		357	1.243	0.159
311	0.866	0.155		358	1.312	0.182
312	0.788	0.135		359	1.353	0.182
313	0.708	0.143		360	1.438	0.184
314	0.662	0.139		361	1.532	0.208
315	0.594	0.145		362	1.593	0.212
316	0.545	0.116		363	1.672	0.198
317	0.517	0.121		364	1.744	0.193
318	0.516	0.116		365	1.817	0.165
319	0.492	0.112		366	1.897	0.180
320	0.441	0.112		367	1.990	0.197
321	0.427	0.131		368	2.108	0.245
322	0.400	0.145		369	2.188	0.246
323	0.388	0.150		370	2.255	0.272
324	0.381	0.149		371	2.356	0.293
325	0.390	0.136		372	2.444	0.225
326	0.366	0.129		373	2.533	0.219
327	0.364	0.139		374	2.632	0.252
328	0.374	0.146		375	2.720	0.215
329	0.377	0.144		376	2.810	0.214
330	0.368	0.147		377	2.893	0.201
331	0.385	0.132		378	3.011	0.240
332	0.406	0.148		379	3.135	0.272
333	0.404	0.147		380	3.249	0.300
334	0.420	0.139		381	3.412	0.403
335	0.435	0.152		382	3.526	0.315
336	0.469	0.157		383	3.666	0.327
337	0.486	0.160		384	3.792	0.351
338	0.508	0.148		385	3.993	0.327

Table A2.1: (continued)

λ / nm	$\sigma_{2,3PD}$ / 10^{-20} cm^2 $molecule^{-1}$	± 2 stdev.	λ / nm	$\sigma_{2,3PD}$ / 10^{-20} cm^2 $molecule^{-1}$	± 2 stdev.
386	4.058	0.261	419	7.542	0.559
387	4.198	0.338	420	7.243	0.424
388	4.337	0.339	421	6.935	0.428
389	4.495	0.381	422	6.669	0.292
390	4.589	0.300	423	6.414	0.336
391	4.718	0.286	424	6.072	0.370
392	4.806	0.277	425	5.783	0.280
393	4.889	0.325	426	5.561	0.283
394	4.979	0.379	427	5.362	0.295
395	5.029	0.416	428	5.254	0.366
396	5.144	0.310	429	5.220	0.308
397	5.275	0.291	430	5.049	0.275
398	5.420	0.331	431	4.907	0.298
399	5.500	0.443	432	4.765	0.312
400	5.668	0.541	433	4.555	0.251
401	5.785	0.501	434	4.413	0.305
402	5.966	0.361	435	4.273	0.261
403	6.177	0.345	436	4.051	0.298
404	6.417	0.391	437	3.968	0.256
405	6.676	0.467	438	3.916	0.250
406	6.910	0.447	439	3.870	0.354
407	7.192	0.555	440	3.895	0.258
408	7.403	0.486	441	3.913	0.285
409	7.643	0.401	442	3.888	0.309
410	7.905	0.404	443	3.806	0.303
411	8.134	0.418	444	3.597	0.240
412	8.400	0.423	445	3.464	0.219
413	8.528	0.400	446	3.274	0.219
414	8.585	0.376	447	3.118	0.209
415	8.609	0.397	448	2.964	0.227
416	8.450	0.359	449	2.825	0.234
417	8.202	0.363	450	2.724	0.208
418	7.900	0.405			

Lambert-Beer plots:

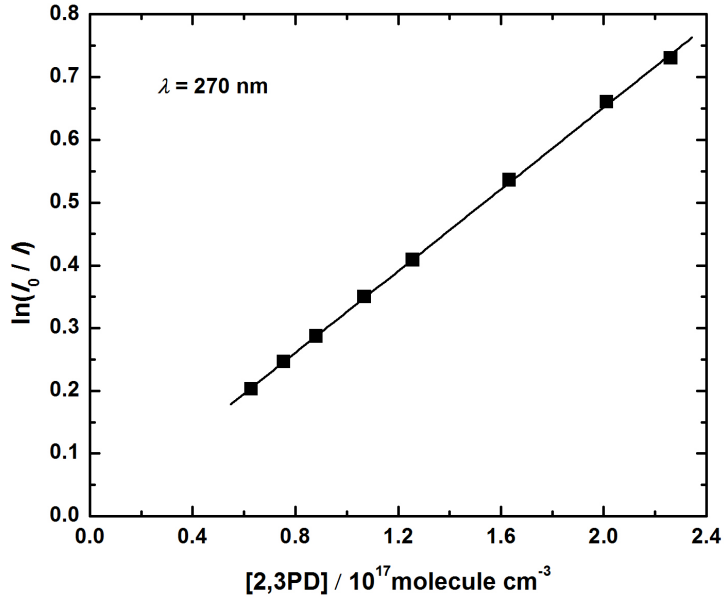

Figure A2.1: Lambert-Beer plot at the first maximum

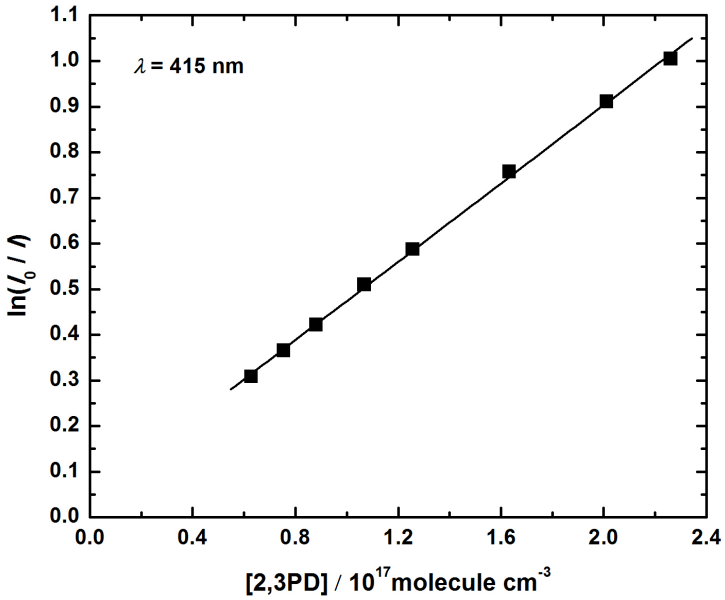

Figure A2.2: Lambert-Beer plot at the second maximum

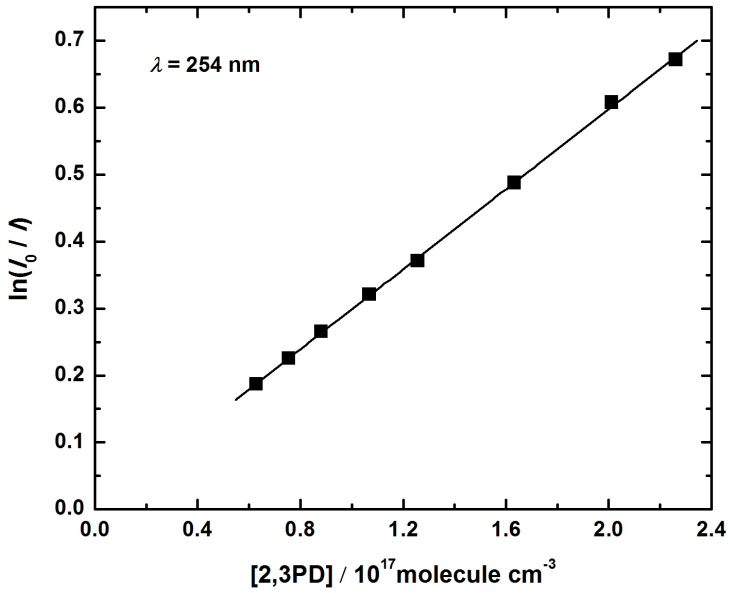

Figure A2.3: Lambert-Beer plot at 254 nm

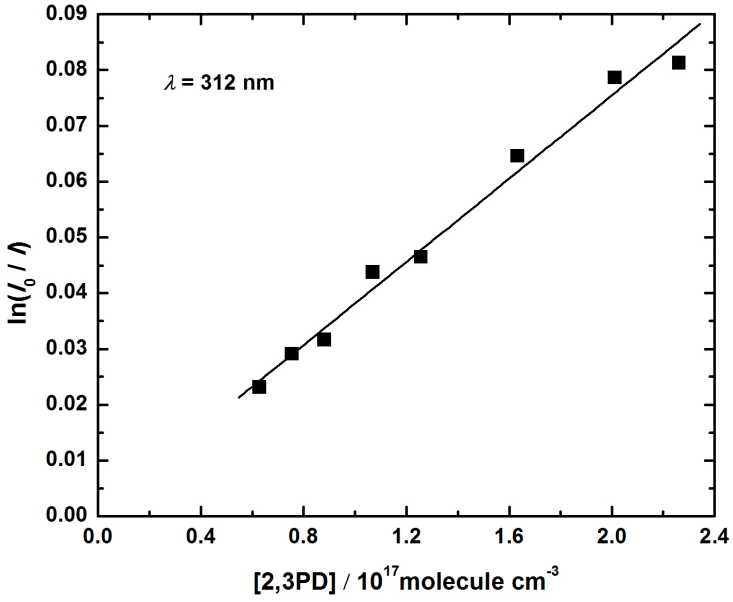

Figure A2.4: Lambert-Beer plot at 312 nm

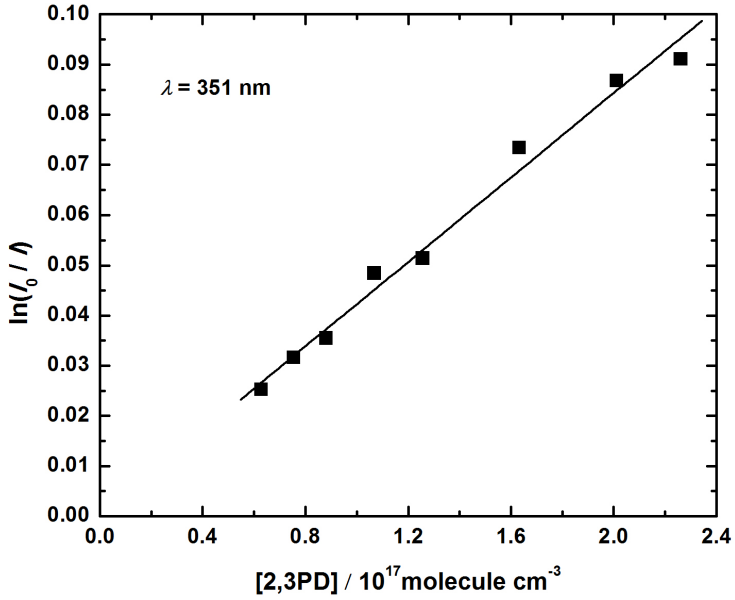

Figure A2.5: Lambert-Beer plot at 351 nm

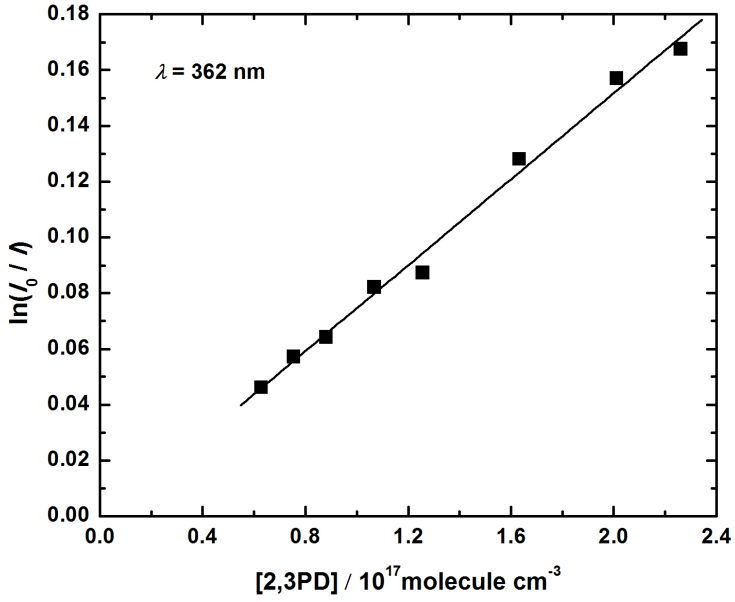

Figure A2.6: Lambert-Beer plot at 362 nm

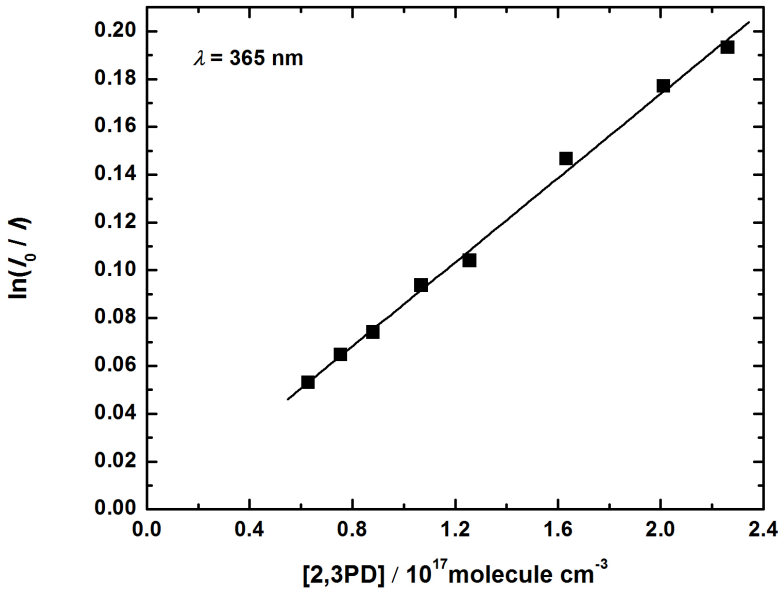

Figure A2.7: Lambert-Beer plot at 365 nm

Appendix 3: Semi-logarithmic plots used to determine the photolysis rate constants of 2,3PD at 254 nm and 312 nm

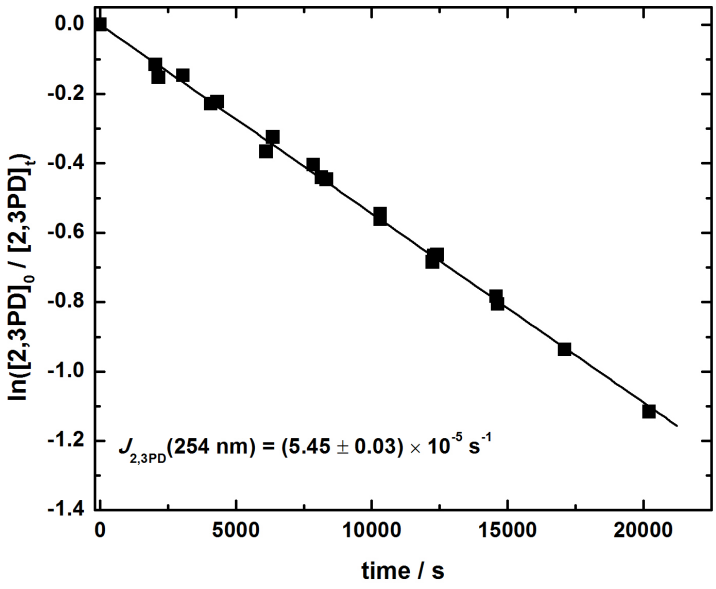

Figure A3.1: A semi-logarithmic plot used to determine the photolysis rate constant of 2,3PD at 254 nm without OH scavenger

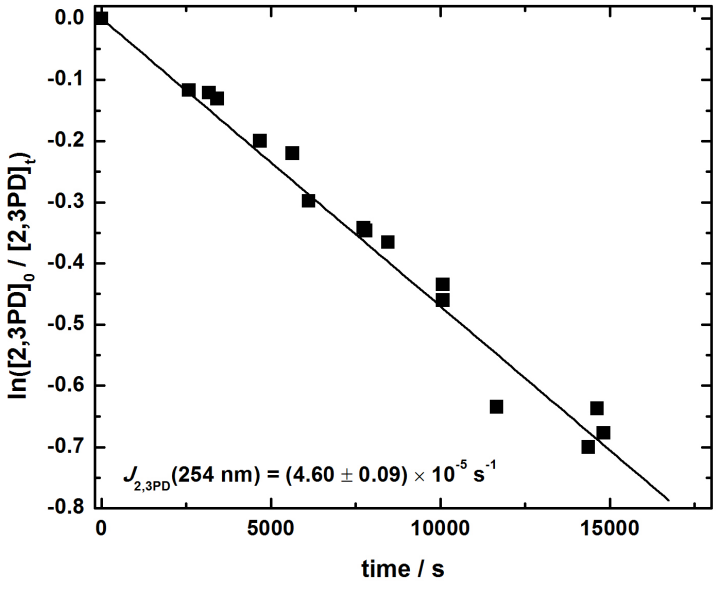

Figure A3.2: A semi-logarithmic plot used to determine the photolysis rate constant of 2,3PD at 254 nm with OH scavenger

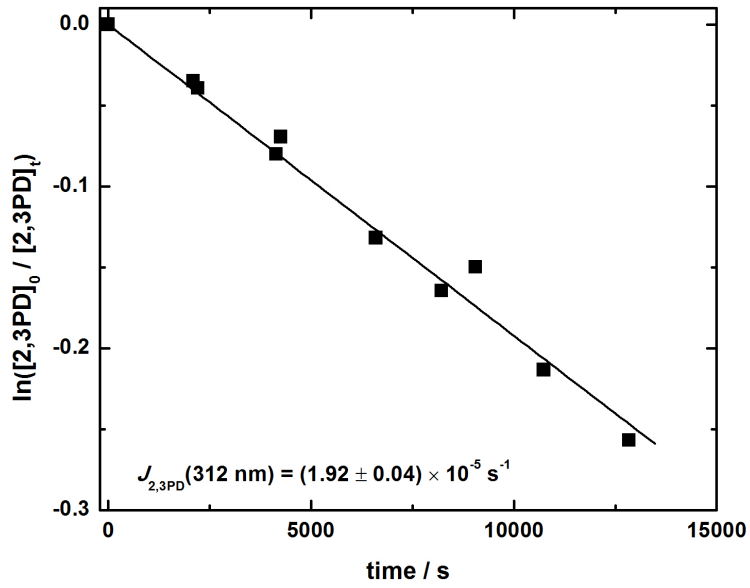

Figure A3.3: A semi-logarithmic plot used to determine the photolysis rate constant of 2,3PD at 312 nm without OH scavenger

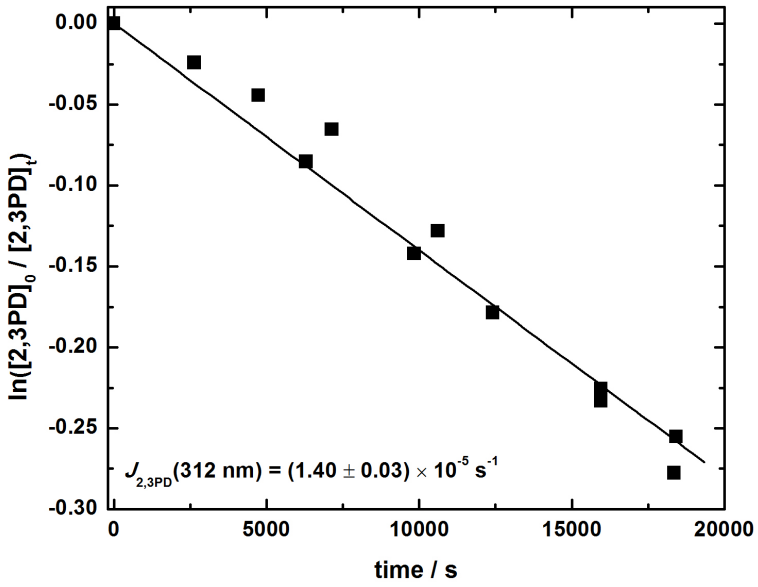

Figure A3.4: A semi-logarithmic plot used to determine the photolysis rate constant of 2,3PD at 312 nm with OH scavenger

Appendix 4: A literature survey for the photolysis reaction of glycolaldehyde

Table A4.1: Products yields of photolysis of glycolaldehyde reported in different studies

$[GA]_0$ / 10^{13} molecule cm^{-3}	HCHO (%)	CO (%)	HCOOH (%)	CH_3OH (%)	CO_2 (%)	Smog chamber	OH-scavenger or OH-tracer	Reference
4	41 ± 4	54 ± 6	7 ± 3	9 ± 2	31 ± 6	47L, stainless steel photolysis chamber, filtered xenon lamps (240 – 440 nm)	—	[Bacher 2001]
10 - 42	95 ± 19	61 ± 13	6 ± 1	4 ± 1	—	44.2L, quartz cell, TL12 sunlamps (275 – 380 nm)	none cyclohexane	[Magneron 2005]
7 - 74	81 ± 5	Same products as in the absence of cyclohexane Yields not determined due to IR bands overlapping					10-100 excess of cyclohexane	
0.6 - 1.8	54 ± 20	94 ± 20	7 ± 1	qualitatively detected	—	200 m^3, outdoor smog chamber, irradiation by solar light	di-*n*-butyl ether	
	not quantified	70	not quantified	—	—		cyclohexane	
100 - 1000	41 ± 5	60 ± 9	7 ± 2	7 ± 1	—	stainless steel cell (308 nm) low pressure	—	[Zhu and Zhu 2010]
	36 ± 5	55 ± 4	19 ± 3	4 ± 1	—	stainless steel cell, presence of O_2 (1-8 torr) (308 nm)	—	

Appendix 5: Estimation of rate constants by the SAR method (T = 298 K)

OH + $CH_3C(O)OH$:

$k(CH_3C(O)OH) = k_{prim} \times F(–C(O)OH) + k_{OH} \times F(CC(O)–) =$

$= (1.36 \times 0.74 + 1.4 \times 3.9) \times 10^{-13} = 6.47 \times 10^{-13}$ cm^3 $molecule^{-1}$ s^{-1}

OH + $CD_3C(O)OH$:

$k(CD_3C(O)OH) = 6.30 \times 10^{-13}$ cm^3 $molecule^{-1}$ s^{-1}

$k(CD_3C(O)OH) = k_{CD3} \times F(–C(O)OH) + k_{OH} \times F(CC(O)–)$

6.30×10^{-13} cm^3 $molecule^{-1}$ $s^{-1} = (k_{CD3} \times 0.74 + 1.4 \times 3.9) \times 10^{-13}$ cm^3 $molecule^{-1}$ s^{-1}

$k_{CD3} = 1.13$

OH + MEK:

$k(MEK) = k_{prim} \times F(>CO) + k_{sec} \times F(–CH_3) \times F(>CO) + k_{prim} F(–CH_2–)$

$k(MEK) = (1.36 \times 0.75 + 9.34 \times 1 \times 0.75 + 1.36 \times 1.23) \times 10^{-13} = 0.97 \times 10^{-12}$ cm^3 $molecule^{-1}$ s^{-1}

OH + 2,3PD:

$k(2,3PD) = k_{prim} \times F(>CO) + k_{sec} \times F(>CO) \times F(–CH_3) + k_{prim} \times F(–CH_2C(O)–)$

$k(2,3PD) = (1.36 \times 0.75 + 9.34 \times 0.75 \times 1.0 + 1.36 \times 3.9) \times 10^{-13} = 1.33 \times 10^{-12}$ cm^3 $molecule^{-1}$ s^{-1}

The $F(–C(O)C(O)–)$ can be derived by using our measured rate coefficient:

$k(2,3PD)$ measured $= k_{prim} \times F(–C(O)C(O)–) + k_{sec} \times F(–C(O)C(O)–) \times F(–CH_3) + k_{prim} \times F(–CH_2C(O)–)$

$21.9 \times 10^{-13} = (1.36 \times F(–C(O)C(O)–) + 9.34 \times F(–C(O)C(O)–) \times 1.0 + 1.36 \times 3.9) \times 10^{-13}$

$F(–C(O)C(O)–) = 1.55$

Scientific publications

Jointly published by
Akadémiai Kiadó, Budapest
and Springer, Dordrecht

React.Kinet.Catal.Lett.
Vol. 95, No. 2, 365–371 (2008)
10.1007/s11144-008-5404-5

RKCL5404

DIRECT KINETIC STUDY OF THE REACTION OF OH RADICALS WITH METHYL-ETHYL-KETONE

Emese Szabó, Gábor L. Zügner, István Szilágyi, Sándor Dóbé*, Tibor Bérces and Ferenc Márta**

Chemical Research Center,
Hungarian Academy of Sciences
Pusztaszeri út 59–67, H-1025 Budapest, Hungary

Received August 19, 2008, in revised form October 9, 2008, accepted October 15, 2008

Abstract

The low-pressure discharge flow technique with resonance fluorescence monitoring of OH has been applied to study the kinetics of the overall reaction:

$OH + CH_3C(O)CH_2CH_3 \rightarrow$ products (1)

The rate constant of $k_1 = (1.09 \pm 0.09(1\sigma)) \times 10^{-12}$ cm^3 molecule^{-1} s^{-1} has been determined at $T = 297 \pm 3$ K. This value agrees well with the IUPAC recommendation which is based on photolysis kinetic studies.

Keywords: Atmospheric chemistry, hydroxyl radical, butanone

INTRODUCTION

Methyl-ethyl-ketone ($CH_3C(O)CH_2CH_3$, butanone, MEK) occurs in significant concentration in the global troposphere [1] where it has both direct

* Corresponding author. E-mail: dobe@chemres.hu
** Deceased

0133-1736/2008/US$ 20.00.

anthropogenic and biogenic sources, and it is formed also via the atmospheric photo-oxidation of *n*-butane. MEK is removed from the atmosphere primarily by its reaction with OH radicals [2,3].

In this letter we present a room temperature experimental study aimed at determining the rate constant for the overall reaction (1) with the application of the thermal kinetic method of discharge flow and direct monitoring of OH. Several direct and relative-rate kinetic studies have been reported for this reaction, but all of them applied the photolysis method to produce the OH radicals [4].

$$OH + CH_3C(O)CH_2CH_3 \rightarrow \text{products} \qquad (1)$$

EXPERIMENTAL

The kinetics of the reaction between OH radicals and MEK were studied by using the low-pressure discharge flow method (DF). Direct monitoring of OH was achieved by $A^2\Sigma^+ - X^2\Pi$ (0,0) resonance fluorescence (RF) centered at around 309 nm. The flow reactor was made of Pyrex and had the dimensions of 40.3 mm internal diameter and 600 mm length. Its internal surface was coated with halocarbon wax to reduce the heterogeneous loss of OH radicals. A coaxially positioned moveable injector was used to vary the reaction time. OH radicals were produced in the injector via H + NO_2, H atoms were generated from H_2 in a microwave discharge. The DF-RF apparatus and experimental procedure have been described in detail previously [5,6].

Helium (Messer-Griesheim, 99.996%) was the main carrier gas, which was passed through liquid-nitrogen-cooled silica-gel traps before entering the flow system. $CH_3C(O)CH_2CH_3$ was obtained from Merck (>99.7% purity) and it was degassed by freeze-pump-thaw cycles prior to use. NO_2 (Messer-Griesheim, 98%) was purified by repeated low-temperature distillation. H_2 (Linde-Gas, 99.98%) was used premixed with helium and a few percent of argon. Ar was required to facilitate the dissociation of H_2 in the microwave discharge (the degree of dissociation was ~10%).

RESULTS AND DISCUSSION

The experiments were conducted at $T = 297 \pm 3$ K reaction temperature and $p = 3.17 \pm 0.08$ mbar pressure (the quoted uncertainties throughout the paper refer to one standard deviation precision, if not otherwise noted). The bimolecular rate constant for the overall reaction, k_1, was determined under pseudo-first-order conditions with $[CH_3C(O)CH_2CH_3] >> [OH]_0 \approx 4 \times 10^{11}$

molecule cm^{-3}. In the kinetic measurements, the magnitudes of the OH resonance fluorescence signals were recorded vs. the reaction distance (time). The reaction under study was isolated well from the interfering bimolecular reactions, but the consumption of OH was significant on the surface of the reactor; the heterogeneous loss of OH was found to obey first-order kinetics.

$$OH + wall \rightarrow products \qquad (w)$$

The experiments were carried out by applying the so-called "reactant-on reactant-off" measurement technique [7], which directly corrects for the wall-consumption of OH, provided the wall-activity is not very different in the presence and absence of $CH_3C(O)CH_2CH_3$ The experimental observables were evaluated according to the following equations:

$$-\ln (S_{on}/S_{off}) = k'_1 (\Delta z/\bar{v}) \qquad (I)$$
$$k'_1 = k_1 [CH_3C(O)CH_2CH_3] + const. \qquad (II)$$
$$-\ln S_{off} = k_w (\Delta z/\bar{v}) \qquad (III)$$

where S_{on} and S_{off} are the OH resonance-fluorescence signal strengths at a distance Δz from the detection site, with and without $CH_3C(O)CH_2CH_3$ flow, respectively, $\bar{v}$ is the linear gas velocity, k'_1 is the pseudo-first-order rate constant and k_w is the rate constant for the heterogeneous loss of OH. Plots according to equations (I) and (II) are presented in Figs 1 and 2, respectively. As seen, reasonably good straight lines were obtained for both the semi-logarithmic decay plots and the k_1' *vs*. $[CH_3C(O)CH_2CH_3]$ plots. Linear least-squares analysis was used to get k'_1 and k_1.

The ln S_{off} data plotted *vs*. the reaction distance, Eq. (III) displayed also straight lines (an example is shown in Fig. 1), the slopes of which provided k_w in the range of 18–62 s^{-1}. These "wall rate constants" are significantly larger than the typical values of 3–20 s^{-1} we have observed previously for the heterogeneous loss of OH radicals in DF reactors with inert wall coatings [5, 8-9]. No correlation could be established between k_w and the experimental conditions, e. g., MEK concentration, prolonged evacuation time, "aging" of the reactor surface, etc. Neither hysteresis ("remembering" effect due to the adsorption of MEK on the surface of the reactor) was observed for the OH signals, but the relatively large scatter of the data in Fig. 2 may indicate that some non-reproducible wall effect may have occurred in the experiments.

The experimental parameters and kinetic results have been summarized in Table 1. The following rate constant value is proposed from our current work for the reaction of OH radicals with methyl-ethyl-ketone (the error given is $\pm 1\sigma$ of the precision of the LSQ-fit):

$$k_1\,(297\ \mathrm{K}) = (1.09 \pm 0.09)\ \mathrm{x}\ 10^{-12}\ \mathrm{cm}^3\ \mathrm{molecule}^{-1}\ \mathrm{s}^{-1}$$

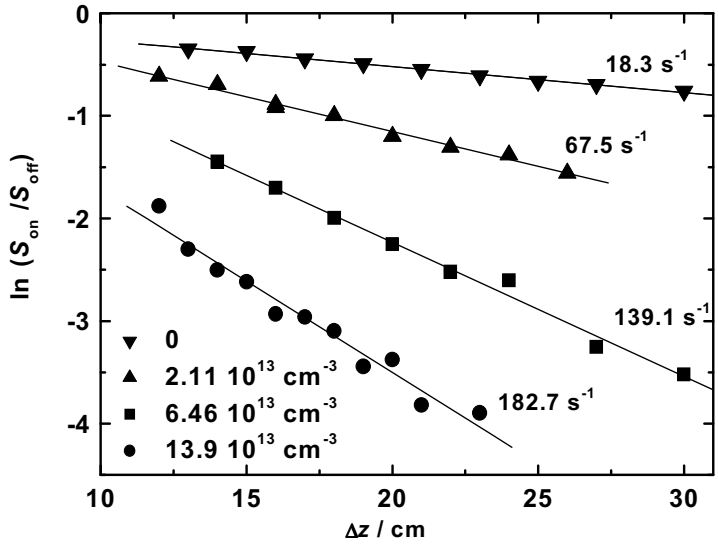

Fig. 1. Typical experimental OH decays presented in semi-logarithmic plot: the slopes of the straight lines give the pseudo-first-order rate constants for reaction (1)

In a very recent IUPAC data evaluation [4], the rate constants reported for the reaction between OH and methyl-ethyl-ketone have been critically evaluated. The analysis included 3 direct and 4 relative-rate kinetic studies which applied pulsed photolysis and stationary photolysis methods for the production of OH radicals in the experiments. The rate constant value of k_1 (298 K) = 1.2 (+0.5, –0.4) x 10^{-12} cm^3 $molecule^{-1}$ s^{-1} has been recommended [4] (the errors are the estimated maximal uncertainties, $\Delta \log k_1 = 0.15$, taken at the 95% confidence level). The IUPAC recommendation agrees well with our current k_1 value that we have determined at low pressure, using the thermal DF-RF technique. The agreement is even better with a more recent study: k_1 (298 K) = (1.04 ± 0.04) x 10^{-12} cm^3 $molecule^{-1}$ s^{-1} has been reported by Jiménez and co-workers who applied pulsed laser photolysis coupled with laser induced fluorescence detection of OH [10].

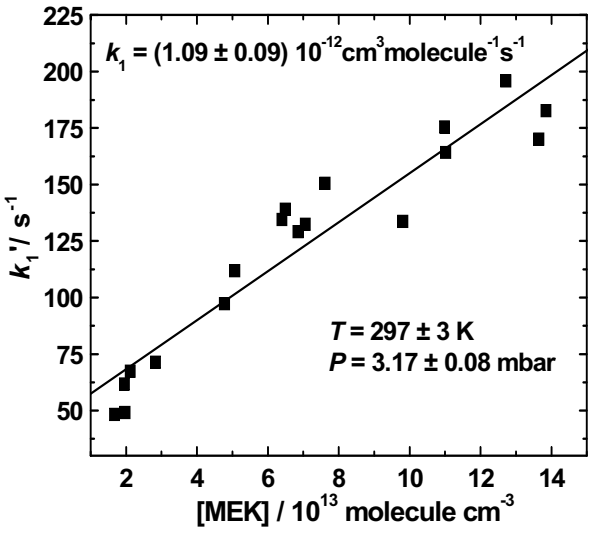

Fig. 2. Plot of pseudo-first-order rate constant versus the methyl-ethyl-ketone concentration: the slope of the straight line gives the bimolecular rate constant for reaction (1)

Table 1

Experimental conditions applied and kinetic results obtained for the reaction of OH radicals with $CH_3C(O)CH_2CH_3$ (T =297 ± 3 K, p = 3.17 ± 0.08 mbar, He buffer gas)

$\overline{v}$ (cm s^{-1})	[H$_2$][a]	[NO$_2$][a]	[MEK][b]	k'_1 (s^{-1})	No. of runs	($k_1 \pm 1\sigma$)[c]
1040-1127	0.81-5.18	0.98-6.95	1.67-13.85	48.3-195.8	18	1.09 ± 0.09

[a]In 10^{12} molecule cm^{-3}
[b]In 10^{13} molecule cm^{-3}
[c]In 10^{-12} cm^3 molecule^{-1} s^{-1}

In Table 2, the room temperature rate constants are compared that we have determined for the reaction series OH + $CH_3C(O)$–R (R = H, F, Cl, CH_3 and CH_3CH_2) in our laboratory. As seen by the presented data, the reactivity of OH is determined by both thermodynamic and inductive effects. OH reacts with MEK about 7-times faster and 16-times slower than with acetone and

acetaldehyde, respectively, reflecting the differences in the bond dissociation energies of the abstracted secondary-, primary- and aldehydic C–H bonds in the reactant molecules. Substitution by Cl- and F atoms reduces the reactivity strongly, in accordance with the known electrophylic character of OH in its elementary reactions.

Table 2

Comparison of room temperature rate constants for OH + $CH_3C(O)$–R (R = H, F, Cl, CH_3 and CH_3CH_2)

Reaction (i)	k_i (298 K) (cm^3 $molecule^{-1}$ s^{-1})	k_i/k_1	Reference
OH + $CH_3C(O)$–CH_2CH_3 (1)	1.1 x 10^{-12} [a]	1	This work
OH + $CH_3C(O)$–CH_3 (2)	1.7 x 10^{-13}	0.155	Vasvári *et al*. 2001 [8]
OH + $CH_3C(O)$–H (3)	1.7 x 10^{-11}	15.5	Dóbé *et al*. 1998 [5]
OH + $CH_3C(O)$–Cl (4)	1.7 x 10^{-14}	0.0155	Nádasdi *et al*. 2006 [9]
OH + $CH_3C(O)$–F (5)	7.4 x 10^{-15}	0.0067	Zügner *et al.* 2008 [11]

[a] T = 297 K

Reaction with OH radicals is the dominant depletion process for MEK at ground level in the atmosphere. Removal of MEK also takes place by photolysis, the significance of which increases with altitude. The high rate constant for the OH reaction, [2] and this work, as well as the recently reported significant decrease of the photodissociation quantum yield with decreasing temperature [2,3] imply that removal of methyl-ethyl-ketone by OH radicals remain important at all altitudes in the troposphere.

Acknowledgement. Our work has been supported by the EU Integrated Project SCOUT-O3 (contract GOCE-CT-2004-505390) and the Hungarian Scientific Research Fund OTKA (contract K68486).

REFERENCES

1. H.B. Singh, L.J. Salas, R.B. Chatfield, E. Czech, A. Fried, J. Walega, M.J. Evans, B.D. Field, D.J. Jacob, D. Blake, B. Heikes, R. Talbot, G. Sachse, J.H. Crawford, M.A. Avery, S. Sandholm, H. Fuelberg: *J. Geophys. Res.*, **109,** D15S07, (2004).
2. M.T. Baeza-Romero, M.A. Blitz, D.E. Heard, M.J. Pilling, B. Price, P.W. Seakins, L. Wang: *Faraday Discuss.,* **130,** 73 (2005).
3. R. Nádasdi, G.L. Zügner, M. Farkas, S. Dóbé, E. Szabó, A. Tomas, C. Fittschen: "Photolysis quantum yield and UV absorption spectrum for methyl-ethyl-ketone", *Z. Phys. Chem.,* (to be submitted, 2008).

4. *IUPAC Subcommittee on Gas Kinetic Data Evaluation – Data Sheet HOx_VOC20.* Website: http://www.iupac-kinetic.ch.cam.ac.uk/. Last evaluated 16th October 2007. Budapest, 2005.
5. S. Dóbé, L.A. Khachatryan, T. Bérces: *Ber. Bunsenges. Phys. Chem.,* **93**, 847 (1989).
6. E. Farkas: *Kinetic Studies of Selected Elementary Reactions of Acetone and the Acetonyl Radical of Relevance to Atmospheric Chemistry,* PhD Thesis (in Hungarian), Budapest, 2005.
7. K.H. Hoyermann: in: *Physical Chemistry – An Advanced Treatise.* Vol. VI B. *Kinetics of Gas Reactions,* Chapter 12., Academic Press, New York 1975.
8. G. Vasvári, I. Szilágyi, Á. Bencsura, S. Dóbé, T. Bérces, E. Henon, S. Canneaux, F. Bohr: *Phys. Chem. Chem. Phys.,* **3,** 551 (2001).
9. R. Nádasdi, I. Szilágyi, G. Kovács, S. Dóbé, T. Bérces, F. Márta: *React. Kinet. Catal. Lett.,* **89,** 193 (2006).
10. E. Jiménez, B. Ballesteros, E. Martinez, J. Albaladejo: *Environ. Sci. Technol.,* **39,** 814 (2005).
11. G.L. Zügner, M. Farkas, I. Szilágyi, S. Förgeteg, S. Dóbé, X. Song, B. Wang: "OH reaction rate constant and photolysis quantum yield for $CH_3C(O)F$: an experimental and theoretical study". Poster, presented at the 20th International Symposium on Gas Kinetics, Manchester, July 20-25, 2008, *Book of Abstracts,* p. 62.

Jointly published by
Akadémiai Kiadó, Budapest
and Springer, Dordrecht

React.Kinet.Catal.Lett.
Vol. 96, No. 2, 299–309 (2009)
10.1007/s11144-009-5511-y

RKCL5511

KINETICS OF THE •OH-RADICAL INITIATED REACTIONS OF ACETIC ACID AND ITS DEUTERATED ISOMERS

Emese Szabó[a,b,c,d], Jérémy Tarmoul[a,b,d], Alexandre Tomas[a,b,*], Christa Fittschen[a], Sándor Dóbé[c] and Patrice Coddeville[a,b]

[a] Université Lille Nord de France, F-59508 Douai, France
[b] École des Mines de Douai, Département Chimie-Environnement, BP 10838, F-59508 Douai, France
[c] Chemical Research Center, Hungarian Academy of Sciences, H-1525 Budapest, Hungary
[d] Laboratoire de Physico-Chimie des Processus de Combustion et de l'Atmosphère - CNRS UMR 8522, Université des Sciences et Technologies de Lille, F-59655 Villeneuve d'Ascq, France

Received January 05, 2009, in revised form January 20, 2009, accepted January 21, 2009

Abstract

Kinetics of the •OH-initiated reactions of acetic acid and its deuterated isomers have been investigated performing simulation chamber experiments at $T = 300 \pm 2$ K. The following rate constant values have been obtained ($\pm 1\sigma$, in cm^3 molecule^{-1} s^{-1}): $k_1(CH_3C(O)OH + {}^{\bullet}OH) = (6.3 \pm 0.9) \times 10^{-13}$, $k_2(CH_3C(O)OD + {}^{\bullet}OH) = (1.5 \pm 0.3) \times 10^{-13}$, $k_3(CD_3C(O)OH + {}^{\bullet}OH) = (6.3 \pm 0.9) \times 10^{-13}$, and $k_4(CD_3C(O)OD + {}^{\bullet}OH) = (0.90 \pm 0.1) \times 10^{-13}$. This study presents the first data on $k_2(CH_3C(O)OD + {}^{\bullet}OH)$. Glyoxylic acid has been detected among the products confirming the fate of the $^{\bullet}CH_2C(O)OH$ radical as suggested by recent theoretical studies.

Keywords: Acetic acid, KIE, OH kinetics, glyoxylic acid

INTRODUCTION

Acetic acid ($CH_3C(O)OH$) is one of the most abundant acid species in the atmosphere. As a ubiquitous compound, it has been detected both in the gaseous and condensed phases in the troposphere and up to the Upper Troposphere – Lower Stratosphere [1]. The reaction kinetics of the reaction between $CH_3C(O)OH$ and the •OH radical has been investigated in substantial detail in the past few years as it has been discussed in a recent feature article [2]. Below

* Corresponding author. E-mail: tomas@ensm-douai.fr

0133-1736/2009/US$ 20.00.

~ 500 K, the rate constant presents a slightly negative temperature dependence, while above ~ 600 K, it was found to display a very sharp increase with temperature [3,4]. With the aid of quantum chemical computations, this characteristic behaviour was attributed to the formation of a pre-reactive complex between $^{\bullet}OH$ and $CH_3C(O)OH$ stabilized at low temperature and to a change in the reaction mechanism when going to higher temperatures. Concerning the reaction mechanism, $^{\bullet}OH$ radicals are expected to react with $CH_3C(O)OH$ through two H-abstraction pathways:

$$CH_3C(O)OH + {}^{\bullet}OH \rightarrow CH_3C(O)O^{\bullet} + H_2O \quad (1a)$$

$$\rightarrow {}^{\bullet}CH_2C(O)OH + H_2O \quad (1b)$$

Contrary to what can be expected from bond dissociation energies, the dominant channel of reaction (1) has been found to be the acidic H-abstraction (channel (1a)), with a branching ratio k_{1a}/k_1 varying from 64% to 78% [4-6] around 300 K. Literature data on the $^{\bullet}OH$-initiated reactions of the deuterated acetic acids are very sparse [6-8], although such data would be useful for a better understanding of the reaction mechanism and in this way for assessing the impact of acetic acid on the chemistry of the atmosphere.

In this letter, we present new kinetic data on the reactions of $^{\bullet}OH$ radicals with acetic acid and its deuterated isomers $CD_3C(O)OH$, $CH_3C(O)OD$ and $CD_3C(O)OD$. The aim of the present study has been to propose rate constants for the four reactions under similar experimental conditions allowing direct comparison and an assessment of mechanistic features. The deuterated isotopes of acetic acid are expected to react with $^{\bullet}OH$ also via two types of hydrogen (deuterium) abstraction reactions:

$$CH_3C(O)OD + {}^{\bullet}OH \rightarrow CH_3C(O)O^{\bullet} + HDO \quad (2a)$$

$$\rightarrow {}^{\bullet}CH_2C(O)OD + H_2O \quad (2b)$$

$$CD_3C(O)OH + {}^{\bullet}OH \rightarrow CD_3C(O)O^{\bullet} + H_2O \quad (3a)$$

$$\rightarrow {}^{\bullet}CD_2C(O)OH + HDO \quad (3b)$$

$$CD_3C(O)OD + {}^{\bullet}OH \rightarrow CD_3C(O)O^{\bullet} + HDO \quad (4a)$$

$$\rightarrow {}^{\bullet}CD_2C(O)OD + HDO \quad (4b)$$

The rate constant of each reaction has been determined at laboratory temperature, with k_2 being determined for the first time, to our knowledge. In the following discussions, *AA* is used as a general abbreviation for all of the four acetic-acid isomers studied, while d_0*–AA*, d_1*–AA*, d_3*–AA,* and d_4*-AA* designate $CH_3C(O)OH$, $CH_3C(O)OD$, $CD_3C(O)OH$ and $CD_3C(O)OD$, respectively.

EXPERIMENTAL

All experiments were performed using a 250 L Teflon environmental chamber. Since the experimental set-up and procedure have been described in detail in previous studies [6, 9], only the main features are presented here.

The acetic acid reactant and the reference compound were introduced into a synthetic air flow and flushed into the reactor. Methyl nitrite (CH_3ONO), used as OH precursor, was synthesised following the classical procedure [10] and stored at – 30°C. It was introduced either in large quantities (up to 200 mL) at time zero, or in smaller portions (about 20 mL) every 30 min during the experiment. No difference could be observed in the results applying the two procedures. The primary gas components were allowed to mix in the chamber for about one hour before the reaction was initiated by turning on the lamps; the initial concentrations are listed in Table 1. Photolytic irradiation arising from 8 actinic lamps (300 nm < λ < 450 nm) initiated the reaction sequence by the photolysis of CH_3ONO:

$$CH_3ONO + h\nu \rightarrow CH_3O^{\bullet} + NO \quad (5)$$

$$CH_3O^{\bullet} + O_2 \rightarrow CH_2O + HO_2^{\bullet} \quad (6)$$

$$HO_2^{\bullet} + NO \rightarrow {}^{\bullet}OH + NO_2 \quad (7)$$

The acetic acid and the reference compound were regularly measured during the reaction with gas–chromatography (GC-FID) by sampling 20 mL gas aliquots from the photoreactor followed by flash injection through a thermodesorption system (Chrompack TCT).

The kinetics of the reactions were investigated using the relative rate method. In this method, the organic reactant (*OC*) is present in the reactor along with a reference compound (*ref*) which reacts with $^{\bullet}OH$ at a similar rate:

$$OC + {}^{\bullet}OH \rightarrow \text{products} \quad (k_{OC})$$

$$ref + {}^{\bullet}OH \rightarrow \text{products} \quad (k_{ref})$$

Table 1

Experimental conditions and results

Reaction (i)	Reactant	No. of Expts.	$[AA]_0$ (molecule cm^{-3})	$[ref]_0$ [a] (molecule cm^{-3})	$k_i/k_{ref} \pm 1\sigma$	$(k_i \pm 1\sigma \times 10^{13}$ (cm^3 $molecule^{-1}$ s^{-1})
(1)	$CH_3C(O)OH$	2	$(0.5–2) \times 10^{15}$	$(0.3–1.5) \times 10^{15}$	0.70±0.10	6.3±0.9
(2)	$CH_3C(O)OD$	3	$(0.5–2) \times 10^{15}$	$(0.5–2) \times 10^{15}$	0.46±0.08	1.5±0.3
(3)	$CD_3C(O)OH$	2	$(0.5–2) \times 10^{15}$	$(0.3–1.5) \times 10^{15}$	0.70±0.10	6.3±0.9
(4)	$CD_3C(O)OD$	4	$(0.5–2) \times 10^{15}$	$(0.5–2) \times 10^{15}$	0.28±0.04	0.90±0.10

[a] The reference compound, *ref*, is CH_3OH for reactions (1) and (2) and CD_3OD for reactions (2) and (4)

Assuming that the reactions with $^{\bullet}OH$ are the only consumption reactions for the target and the reference compounds, the following simple rate equation is obtained:

$$\ln \frac{[OC]_0}{[OC]_t} = \frac{k_{OC}}{k_{ref}} \times \ln \frac{[ref]_0}{[ref]_t} \qquad \text{(I)}$$

where $[ref]_0$ and $[OC]_0$ and $[ref]_t$ and $[OC]_t$ are the concentrations of the reference and target molecules at time 0 and time t, respectively. Therefore, a plot of $\ln([OC]_0/[OC]_t)$ *vs* $\ln([ref]_0/[ref]_t)$ should yield a straight line with a slope of k_{OC}/k_{ref}. In our experiments, *OC* corresponds, e. g., to acetic acid and *ref* to methanol.

Prior to the regular experiments, test runs were carried out in the absence of CH_3ONO: photolysis processes and wall losses were found negligible in the reaction system. Dimers of *AA* are expected to be formed in the gas phase through weak H- (or D-) bonds. Chao and Zwolinski [11], reviewing thermodynamic data for formic- and acetic acids, have proposed the following equilibrium constant, K_{eq}, for the dimerization reaction of $CH_3C(O)OH$:

$$K_{eq} = \frac{P_D}{P_M^2} = 7.1 \times 10^{-9} \exp\left(\frac{7705}{T}\right) \qquad \text{(II)}$$

where P_D and P_M are the partial pressures (in atm) of the dimer and the monomer at temperature T (in K), respectively, giving $K_{eq} = 1012.5$ atm^{-1} at 300 K. Re-arrangement of equation (II) and taking into account that the measured acetic acid concentration is $[AA]_{total} = 2 \times [AA]_{monomer} + [AA]_{dimer}$ yield the following equation:

$$[AA]_{monomer} = \frac{-1 + \sqrt{1 + 8 \times K_{eq} \times [AA]_{total}}}{4 \times K_{eq}} \qquad \text{(III)}$$

As it has been discussed by Singleton *et al.* [7], the dimer reacts with a much slower rate with OH radicals than the monomer does. In addition, considering the concentrations of *AA* used under the conditions of the present study (see Table 1), the dimer represented at the most 15% of the total AA concentration. In order to take into account the dimer formation, the initial monomer concentration $[AA]_{monomer,0}$, was calculated according to equation (III) from $[AA]_{total,0}$ while $[AA]_{monomer,t}$ was obtained from $[AA]_{monomer,t} = [AA]_{monomer,0} - ([AA]_{total,0} - [AA]_{total,t})$. That is, we have assumed that the dimer does not react with $^{\bullet}$OH. In the following considerations, $[AA]_{monomer,0}$ and $[AA]_{monomer,t}$ are designated simply as $[AA]_0$ and $[AA]_t$. For the deuterated acetic acid isomers, the same K_{eq} as used for acetic acid was assumed in the absence of other information.

Acetic acid (96%, Merck), acetic acid-d_1 (98% D, Acrôs Organics), acetic acid-d_3 (99.2% D, CDN Isotopes), acetic acid-d_4 (99.91% D, Euriso-top), methanol (99.9%, Merck) and methanol-d_4 (99.80% D, Euriso-top) were used as obtained.

RESULTS AND DISCUSSION

The kinetics of reactions (1) – (4) have been investigated at $T = (300 \pm 2)$ K and atmospheric pressure using the relative rate method as described in the experimental section. The reference compounds were *methanol* (for the kinetic study of $CH_3C(O)OH$ and $CD_3C(O)OH$) and *methanol-d_4* (for $CH_3C(O)OD$ and $CD_3C(O)OD$). The experimental conditions and results have been summarised in Table 1. Representative plots of $\ln([AA]_0/[AA]_t)$ *vs* $\ln([ref]_0/[ref]_t)$ are shown in Figs 1 and 2. The acetic acid isomers d_0–*AA* ($CH_3C(O)OH$) and d_3–*AA* ($CD_3C(O)OH$) present identical rate constant ratios: $k_1/k_{meth} = 0.70 \pm 0.10$ and $k_3/k_{meth} = 0.70 \pm 0.10$, while rate constant ratios for d_1–*AA* ($CH_3C(O)OD$) and d_4–*AA* ($CD_3C(O)OD$) differ by a factor of 1.6: $k_2/k_{meth\text{-}d4} = 0.46 \pm 0.08$ and $k_4/k_{meth\text{-}d4} = 0.28 \pm 0.04$. Using the recommended CH_3OH + OH rate constant, $k_{meth} = 9.0 \times 10^{-13}$ cm^3 molecule^{-1} s^{-1} [12], the respective rate constant ratios

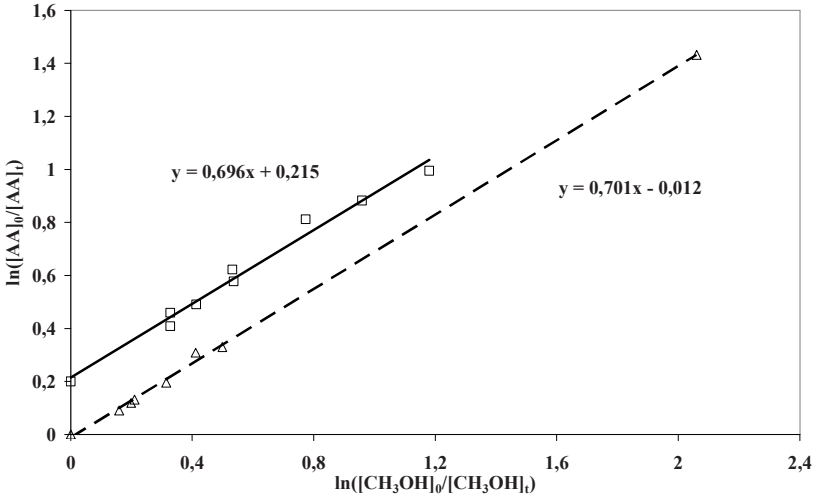

Fig. 1. Typical plots of $\ln([AA]_0/[AA]_t)$ *vs* $\ln([CH_3OH]_0/[CH_3OH]_t)$ for *AA* = $CH_3C(O)OH$ (squares) and $CD_3C(O)OH$ (triangles). The straight lines correspond to a linear regression on the experimental data. The $\ln([AA]_0/[AA]_t)$ data for $CH_3C(O)OH$ have been shifted by + 0.2 for clarity

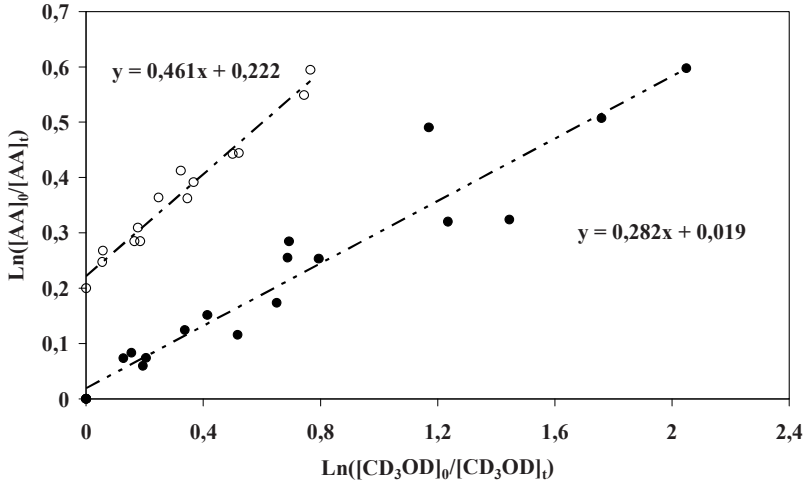

Fig. 2. Typical plots of $\ln([AA]_0/[AA]_t)$ *vs* $\ln([CD_3OD]_0/[CD_3OD]_t)$ for *AA* = $CH_3C(O)OD$ (circles) and $CD_3C(O)OD$ (full circles). The straight lines correspond to a linear regression on the experimental data. The $\ln([AA]_0/[AA]_t)$ data for $CH_3C(O)OD$ have been shifted by + 0.2 for clarity

translate to the absolute values of $k_1 = (6.3 \pm 0.9) \times 10^{-13}$ and $k_3 = (6.3 \pm 0.9) \times 10^{-13}$ cm^3 molecule^{-1} s^{-1}. For the CD_3OD + OH rate constant, we took the very recent determination of Parker *et al.* [13] (preceding paper): $k_{\text{meth-}d4} = 3.2 \times 10^{-13}$ cm^3 molecule^{-1} s^{-1} (which is in excellent agreement with Wallington *et al.* [14]: 3.23×10^{-13} cm^3 molecule^{-1} s^{-1}; the other measurement by McCaulley *et al.* [15]: 1.93×10^{-13} appears much lower). The resulting k_2 and k_4 rate constants are: $k_2 = (1.5 \pm 0.3) \times 10^{-13}$, and $k_4 = (0.90 \pm 0.1) \times 10^{-13}$ cm^3 molecule^{-1} s^{-1}. Quoted uncertainties (1σ) have been estimated by the statistical errors of the sampling procedure (~ 10%). They do not include the uncertainties in the reference rate constants, which are estimated to be about 15% for the methanol + OH reaction [12] and at least 30% for the methanol-d_4 + OH reaction.

Table 2

Comparison of room temperature rate constants for the reactions of •OH radicals with acetic acid and deutero acetic acids. The errors given are those reported by the authors

Reaction (i)	10^{13} x k_i (cm^3 molecule^{-1} s^{-1})	Reference
OH + $CH_3C(O)OH$ (1)	5.99 ± 0.39	[16]
	7.4 ± 0.3	[17]
	8.6 ± 0.3	[7]
	6.6 ± 0.4	[4]
	6.5 ± 0.3	[6]
	7.42 ± 0.06	[8]
	8.50 ± 0.45	[3]
	6.77 ± 0.14	[18]
	6.3 ± 0.9	This work
OH + $CD_3C(O)OH$ (2)	8.1 ± 0.2	[7]
	7.79 ± 0.08	[8]
	6.3 ± 0.9	This work
OH + $CH_3C(O)OD$ (3)	1.5 ± 0.3	This work
OH + $CD_3C(O)OD$ (4)	1.09 ± 0.09	[8]
	0.90 ± 0.1	This work

Table 2 gives a comparison of all the rate constant values that have been reported for reactions (1) – (4) in previous works [3, 4, 6-8, 16-18]. The rate constant for the acetic acid + OH reaction has been determined in several investigations. The present result is in good agreement with the previous studies, though it is in the lower range of the whole interval spanning from 5.99 to 8.6×10^{-13} cm^3 molecule^{-1} s^{-1}, as reported by Zetzsch and Stuhl [16] and Singleton *et al.* [7], respectively. However, we note that our rate constant agrees

very well with the very recent absolute determination of $k_1(295K) = (6.77 \pm 0.14) \times 10^{-13}$ cm^3 molecule^{-1} s^{-1} by Huang *et al.* [18] who performed highly sophisticated kinetic experiments. To the best of our knowledge, the rate constant we have measured for the d_1-*AA* + OH (2) reaction represents the first kinetic determination. Rate constants for the d_3-*AA* + OH (3) reaction have been reported in two papers [7, 8], with which our result agrees reasonably well: our value is on average about 25% smaller. In view that Singleton *et al.* [7] and Vimal and Stevens [8] applied direct kinetic methods under very different experimental conditions, the agreement is satisfactory. Concerning the d_4-*AA* + OH (4) reaction, the agreement with the only determination of k_4 available in the literature [8] is very good (Table 2), despite the fact that the authors used much higher acetic acid concentrations (up to 1840 ppmv) than we did in the present study (up to 81 ppm). It should be stressed that the uncertainty on $k_{\text{meth-d4}}$ is still significant (only three determinations). Application of CH_3OH as a reference for the $CD_3C(O)D$ reaction was unsuccessful because of the occurrence of significant isotope exchange reactions in the reaction system.

The difference in the reactivity between $CH_3C(O)OH$ and $CH_3C(O)OD$ on the one hand, and between $CD_3C(O)OH$ and $CD_3C(O)OD$ on the other hand confirms that reactions (1) and (3) proceed essentially through the abstraction of the H-atom from the carboxylic group. This mechanistic picture is reflected also by the observed kinetic isotope effect (KIE). KIE is defined here as the rate constant ratio of the OH reactions of two acetic acid isomer molecules, one of which contains H-atom(s) while the other one D-atom(s) in the same position. This can be calculated for reactions (2) to (4) from the experimental values of k_1 to k_4. KIE is found to be small for the hydrogen atoms in the methyl group, that is, $k_1/k_3 = 1.0$ and $k_2/k_4 = 1.6$, but large for the hydrogen atom in the carboxylic group: $k_1/k_2 = 5.2$ and $k_3/k_4 = 8.6$. Previous experimental studies on the kinetics of the reaction between $^{\bullet}$OH and acetic acid provide the possibility to calculate the ratios k_3/k_4 and k_1/k_3 for comparison. From the work by Singleton *et al.* [7], one obtains $k_1/k_3 = 1.1$ and from Vimal and Stevens [8] $k_1/k_3 = 0.95$ and $k_3/k_4 = 7.1$. These KIE values are consistent with the present findings and the proposed mechanism. The observed kinetic isotope effect can be qualitatively explained by the increase of the energy barrier of the abstraction channel due to the effect of zero-point energy lowering caused by D-substituents. A strong quantum tunnelling effect has also been invoked to play a role in the reaction mechanisms at the molecular level [8,19]. It is interesting to note that a similar KIE was observed in the formic acid + $^{\bullet}$OH reaction [20].

In the photooxidation reaction system, the $CH_3C(O)O^{\bullet}$ radical and its deuterated isomers undergo fast decomposition forming the methyl radical and CO_2 [2-4]. The further fate of the minor primary product $^{\bullet}CH_2C(O)OH$ (and its deuterated counterparts) has been examined in the present study by product analysis.

$$^{\bullet}CH_2C(O)OH + O_2 + M \rightarrow {}^{\bullet}O_2CH_2C(O)OH + M \quad (8)$$

$$^{\bullet}O_2CH_2C(O)OH + NO \rightarrow {}^{\bullet}OCH_2C(O)OH + NO_2 \quad (9)$$

$$^{\bullet}OCH_2C(O)OH + O_2 \rightarrow CH_2O + CO_2 + HO_2^{\bullet} \quad (10a)$$

$$\rightarrow HC(O)C(O)OH + HO_2^{\bullet} \quad (10b)$$

According to the assumed reaction mechanism (8)-(10), we have searched for glyoxylic acid (HC(O)C(O)OH) among the reaction products. For this purpose, gas samples were taken from the environmental chamber after 2 to 4 h of irradiation, by pumping about 50 L of the reaction mixture through an impinger containing a mixture of water and methanol (10% w/w) cooled down to ~ 3°C. The extraction solution was then analysed by ion chromatography (Dionex) with anion concentrator.

The ion chromatography analysis clearly showed the presence of glyoxylic acid (*GA*), as confirmed by injection of a standard solution and comparison of the retention times. Similarly, HC(O)C(O)OD was identified in the OH-initiated photooxidation of $CH_3C(O)OD$. These results suggest that the main fate of the $^{\bullet}OCH_2C(O)OH$ radical is its conversion to HC(O)C(O)OH through reaction with O_2 (reaction (10b)). This conclusion is supported also by the following considerations:

i) A heat of reaction about 51 – 83 kJ mol^{-1} can be estimated for the concurrent decomposition channel (10a) using reported heats of formation of the reactants and products [21-23] indicating that this channel cannot be important under ambient conditions.

ii) The fate of the similar $^{\bullet}OCH_2C(O)OCH_3$ alkoxy radical has been shown to be the reaction with O_2 rather than decomposition [24, 25].

Because of a lack of kinetic data on the reactivity of glyoxylic acid with $^{\bullet}OH$ radicals, it was not possible to determine the primary *GA* yield in the reaction system (*i.e.* to correct for consumption in the $^{\bullet}OH$ reaction). Calculation of the ratio of the concentration of *GA* formed and the concentration of *AA* reacted, both measured at the end of the experiment, provides the glyoxylic acid yields of 0.10 for reaction (1) and 0.15 for reaction (2). Taking into account the branching ratio of reaction (1) [4-6] and assuming channel (10a) to be negligible, *GA* yields of 0.22 to 0.36 are expected for the OH-initiated oxidation of $CH_3C(O)OH$. The lower experimental *GA* yields obtained in our study can be explained by considering first the *GA* wall losses and the consumption of *GA* by

$^{\bullet}OH$ and, second, the still possible occurrence of channel (10a)

Finally, we note that the non-negligible glyoxylic acid yield we have found in our experiments is in line with the recent theoretical study of Rosado-Reyes and Francisco [26] confirming their conclusion, that glyoxylic acid should be a significant organic by-product in the atmospheric oxidation of acetic acid.

Acknowledgements. This work is jointly supported by the Nord-Pas de Calais region in the frame of the IRENI research program, by the French Research Ministry and by the European Fund for Regional Economic Development (FEDER). E. Szabó thanks for financial support from the EU through project MEST-CT-2005-020659 and from the French Foreign Office and Région Nord – Pas de Calais with the framework of the ARCUS program. J. Tarmoul gratefully acknowledges the financial support from the Ecole des Mines de Douai and the CNRS.

REFERENCES

1. S. Preunkert, M. Legrand, B. Jourdain, I. Dombrowski-Etchevers: *J. Geophys. Res.*, **112**, 1 (2007).
2. S.A. Carl, L. Vereecken, J. Peeters: *Phys. Chem. Chem. Phys.*, **9**, 4071 (2007).
3. V.G. Khamaganov, X.V. Bui, S.A. Carl, J. Peeters: *J. Phys. Chem. A*, **110**, 12852 (2006).
4. N.I. Butkovskaya, A. Kukui, N. Pouvesle, G. Le Bras: *J. Phys. Chem. A*, **108**, 7021 (2004).
5. F. De Smedt, X.V. Bui, T.L. Nguyen, J. Peeters, L. Vereecken: *J. Phys. Chem. A*, **109**, 2401 (2005).
6. S. Crunaire, J. Tarmoul, C. Fittschen, A. Tomas, B. Lemoine, P. Coddeville: *Appl. Phys. B*, **85**, 467 (2006).
7. D.L. Singleton, G. Paraskevopoulos, R.S. Irwin: *J. Am. Chem. Soc.*, **111**, 5248 (1989).
8. D. Vimal, P.S. Stevens: *J. Phys. Chem. A*, **110**, 11509 (2006).
9. E. Turpin, A. Tomas, C. Fittschen, P. Devolder, J.-C. Galloo: *Env. Sci. Technol.*, **40**, 5956 (2006).
10. W.D. Taylor, T.D. Allston, M.J. Moscato, G.B. Fazekas, R. Kozlowski, G.A. Takacs: *Int. J. Chem. Kin.*, **12**, 231 (1980).
11. J. Chao, B.J. Zwolinski: *J. Phys. Chem. Ref. Data*, **7**, 363 (1978).
12. R. Atkinson, D.L. Baulch, R.A. Cox, J.N. Crowley, R.F. Hampson, R.G. Hynes, M.E. Jenkin, M.J. Rossi, J. Troe: *Atm. Chem. Phys.*, **6,** 3625 (2006).
13. A. Parker, C. Jain, C. Fittschen: *React. Kinet. Catal. Lett.*, preceding paper in this issue, (2009).
14. T.J. Wallington, P. Dagaut, M.J. Kurylo: *J. Phys. Chem.*, **92**, 5024 (1988).
15. J.A. McCaulley, N. Kelly, M.F. Golde, F. Kaufman: *J. Phys. Chem.*, **93**, 1014 (1989).
16. C. Zetzsch, F. Stuhl: 2nd European Symposium on the Physico-chemical Behavior of Atmospheric Pollutants, Ed. Dordrecht, The Netherlands (1982).
17. P. Dagaut, T.J. Wallington, R. Liu, M.J. Kurylo: *Int. J. Chem. Kin.*, **20**, 331 (1988).
18. Y. Huang, T.J. Dransfield, J.D. Miller, R.D. Rojas, X.G. Castillo, J.G. Anderson: *J. Phys. Chem. A*, **113**, 423 (2009).
19. W. Sun, M. Saeys: *J. Phys. Chem. A*, **112**, 6918 (2008).
20. D.L. Singleton, G. Paraskevopoulos, R.S. Irwin, G.S. Jolly, D.J. McKenney: *J. Am. Chem. Soc.*, **110**, 7786 (1988).

21. M.W. Chase, Jr.: *J. Phys. Chem. Ref. Data*, *Monograph*, **9**, 1 (1998).
22. H.-Y. He, W.-H. Fang: *J. Am. Chem. Soc.*, **125**, 16139 (2003).
23. G.S. Tyndall: *Personal communication*, (2005).
24. F. Cavalli, I. Barnes, K.H. Becker, T.J. Wallington: *J. Phys. Chem. A*, **104**, 11310 (2000).
25. G.S. Tyndall, A.S. Pimentel, J.J. Orlando: *J. Phys. Chem. A*, **108**, 6850 (2004).
26. C.M. Rosado-Reyes, J.S. Francisco: *J. Phys. Chem. A*, **110**, 4419 (2006).

Chemical Physics Letters 495 (2010) 179–181

Contents lists available at ScienceDirect

Chemical Physics Letters

journal homepage: www.elsevier.com/locate/cplett

OH yields for $C_2H_5CO + O_2$ at low pressure: Experiment and theory

Gábor L. Zügner [a], István Szilágyi [a], Judit Zádor [a,1], Emese Szabó [a], Sándor Dóbé [a,*], Xinli Song [b], Baoshan Wang [b,**]

[a] Chemical Research Center, Hungarian Academy of Sciences, Pusztaszeri út 59-67, H-1025 Budapest, Hungary
[b] College of Chemistry and Molecular Sciences, Wuhan University, Wuhan 430072, People's Republic of China

ARTICLE INFO

Article history:
Received 15 April 2010
In final form 29 June 2010
Available online 3 July 2010

ABSTRACT

Kinetics of OH formation for the reaction of C_2H_5CO radicals with O_2 have been studied using the low-pressure discharge flow technique coupled with resonance fluorescence monitoring of OH radicals at room temperature in He buffer gas. The OH yields are close to unity at the lowest pressures studied, but decrease rapidly with increasing pressure. The experimental OH yields are reproduced well using multichannel variational RRKM theory.

1. Introduction

One of the important recent findings in atmospheric chemistry is the recognition of the central role that carbonyl molecules play in the chemistry of the troposphere [1,2]. Atmospheric carbonyls include propanal, C_2H_5CHO, which has been found in surprisingly high concentrations in the free and upper troposphere [2]. Propanal reacts with OH radicals in the atmosphere to form propionyl radical, C_2H_5CO (1). Propionyl adds to O_2 (2a) and the formed propionyl-peroxyl radical, $C_2H_5C(O)O_2$, enters a series of reactions increasing the rate of NO to NO_2 conversion and in this way tropospheric ozone formation:

$$OH + C_2H_5CHO \rightarrow C_2H_5CO + HOH \quad (1)$$

$$C_2H_5CO + O_2 \rightarrow \text{products} \quad (2)$$

$$C_2H_5CO + O_2 + M \rightarrow C_2H_5C(O)O_2 + M \quad (2a)$$

$$C_2H_5CO + O_2 \rightarrow OH + \text{co-product} \quad (2b)$$

Despite its atmospheric importance, the kinetics of the reaction of C_2H_5CO with O_2 have been studied experimentally by one group only [3], and, apart from our own paper [4], no theoretical work has been published. Baeza-Romero et al. [3] applied pulsed-laser photolysis (PLP) to determine the rate constant for the overall reaction (2), k_2, and OH yields (branching ratios), $\Gamma_{2b} = k_{2b}/k_2$, at pressures between 70 and 530 mbar helium.

Here we report pressure dependent OH yields from discharge flow (DF)–OH resonance fluorescence (RF) experiments at room temperature, in the low pressure regime. The experimental data are compared with theoretical yields obtained from statistical rate theory computations.

2. Methods

2.1. Experimental

The DF–RF experimental method was very similar to what we applied previously to determine OH yields for the $CH_3CO + O_2$ reaction [5]. Briefly, a 60.0-cm-long, 4.01-cm-i.d. flow tube was used which was equipped with a moveable quartz injector. C_2H_5CO radicals were produced in the flow reactor by reacting OH radicals with excess propanal, while OH was obtained from $H + NO_2$ inside the moveable injector. Hydrogen atoms were generated by microwave-discharge dissociation of H_2. Helium was the carrier gas. OH radicals were detected by conventional $A \leftarrow X$ resonance fluorescence [6].

The experimental procedure involved monitoring of the concentration of OH radicals at different reaction times in the flow tube either in the presence or in the absence of O_2, i.e., for $OH + C_2H_5CHO + O_2$ or $OH + C_2H_5CHO$. Both propanal and O_2 were used in large excess over OH; the initial OH concentration was $[OH]_0 \approx 2 \times 10^{11}$ molecule cm^{-3}. The 'O_2 flow on' and 'O_2 flow off' runs, or vice versa, were conducted in a back-to-back manner.

Gases of the highest purity available from Messer-Griesheim were used in the experiments. Propanal ($\geqslant$99.5%, Fluka) was degassed by freeze–pump–thaw cycles prior to use.

2.2. Theory

Multichannel Rice–Rampsberger–Kassel–Marcus theory (MC-RRKM) [7] including variational transition state theory approach (VTST) [8] has been applied to estimate OH yields for the reaction

* Corresponding author.
** Corresponding author.
E-mail addresses: dobe@chemres.hu (S. Dóbé), baoshan@whu.edu.cn (B. Wang).
[1] Present address: Combustion Research Facility, Sandia National Laboratories, Livermore, CA 94551-0959, USA.

0009-2614/$ - see front matter © 2010 Elsevier B.V. All rights reserved.
doi:10.1016/j.cplett.2010.06.089

$C_2H_5CO + O_2$. Input parameters were taken from our recent high level ab initio molecular orbital study performed up to full coupled cluster theory with the complete basis set (FCC/CBS) [4]. The MC model requires the average energy transferred per collision, $\langle \Delta E \rangle$, which was chosen to fit the experimental OH yields. Details of the quantum chemical and rate theory calculations have been presented in [4,9].

3. Results and discussion

3.1. Experimental results for $OH + C_2H_5CHO + O_2$

A large increase in the OH signals was observed at a given reaction time when O_2 was added to the reaction system of OH with C_2H_5CHO. Since the initial OH concentration was the same, the reason was a slower depletion of OH in the presence of O_2 indicating the re-formation of OH radicals in the system. OH followed first-order kinetics for both $OH + C_2H_5CHO$ and $OH + C_2H_5CHO + O_2$ reaction systems (Fig. 1).

Under our experimental conditions only reactions (1), (2a), (2b) and the heterogeneous loss of OH took place. The underlying differential equation system can be solved analytically [5] providing Eq. (I) for the OH yield,

$$\Gamma_{2b} = \frac{\kappa_0 - \kappa^*}{\kappa_0 - k_{wOH}} \qquad (I)$$

where κ_0 is the OH decay constant with C_2H_5CHO, κ^* is the OH decay constant with $C_2H_5CHO + O_2$ and k_{wOH} is the heterogeneous ('wall') loss rate constant of OH.

Experiments were carried-out at room temperature, $T = 298 \pm 2$ K, in helium buffer gas, over the pressure range of 1.37–13.34 mbar. The experimental conditions and kinetic results are summarised in Table 1. The depletion of OH radicals on the wall of the reactor was determined in separate experiments to be small, $k_{wOH} = 5 \pm 2\ s^{-1}$. The errors given throughout the Letter refer to 2σ precision.

The OH yields presented in Table 1 show that OH formation is the dominant reaction channel for $C_2H_5CO + O_2$ at low pressures, but its significance decreases rapidly with increasing pressure: the OH yield is about 0.9 at ~1 mbar which decreases to about 0.3 at ~13 mbar pressure of helium (Fig. 3).

Table 1
Experimental OH yields, Γ_{2b}, for the reaction of C_2H_5CO radicals with O_2 ($T = 298 \pm 2$ K).

P(He) (mbar)	κ_0[a] (s^{-1})	[C_2H_5CHO] (10^{12} cm^{-3})	κ^*[b] (s^{-1})	Runs[c]	$\Gamma_{2b} \pm 2\sigma$
1.37	38–176	1.21–14.3	8–42	10	0.88 ± 0.12
2.00	90–129	5.55–10.60	9–33	6	0.86 ± 0.14
2.61	20–185	1.25–13.4	2–54	7	0.84 ± 0.12
3.59	14–155	0.50–6.99	8–63	7	0.68 ± 0.10
6.22	28–169	1.27–8.89	15–84	9	0.62 ± 0.12
8.15	27–57	0.43–5.33	16–43	11	0.53 ± 0.10
10.00	21–60	1.21–8.91	14–35	6	0.44 ± 0.07
13.34	32–112	8.34–12.8	23–77	6	0.33 ± 0.06

[a] OH decay constant in the absence of O_2.
[b] OH decay constant in the presence of O_2; the O_2 concentration was ~1×10^{15} molecule cm^{-3}.
[c] Number of back-to-back determinations of κ_0 and κ^*; data files of the individual experiments are available on request.

The κ_0 decay constants measured are in fact the usual pseudo-first-order rate constants for the reaction $OH + C_2H_5CHO$ (1), $\kappa_0 = k_1' = k_1[C_2H_5CHO] + const.$; a plot of the κ_0 values vs. the propanal concentration is presented in Fig. 2. The experimental data are seen to lie on a straight line with a very small intercept. A linear least squares slope has provided the rate constant value of $k_1(298\ K) = (1.85 \pm 0.12) \times 10^{-11}$ cm^3 $molecule^{-1}$ s^{-1} in excellent agreement with the recommended value of 1.9×10^{-11} cm^3 mol^{-1} s^{-1} [10].

3.2. Pressure dependence of the OH yield for $C_2H_5CO + O_2$

The observed pressure dependence of the OH yields (see Table 1 and Fig. 3) can be described by a chemical activation mechanism. When a propionyl radical combines with an oxygen molecule, a vibrationally excited $(C_2H_5C(O)O_2)^*$ radical is produced which may undergo further reactions, revert to reactants, or be stabilised by collisions:

$$C_2H_5CO + O_2 \rightarrow (C_2H_5C(O)O_2)^*$$
$$(C_2H_5C(O)O_2)^* \rightarrow C_2H_5CO + O_2$$
$$(C_2H_5C(O)O_2)^* + M \rightarrow C_2H_5C(O)O_2 + M$$
$$(C_2H_5C(O)O_2)^* \rightarrow OH + \text{co-product}$$

where M (=He) is the third-body collision partner. The pressure dependence of the OH yields shown in Fig. 3 implies that the

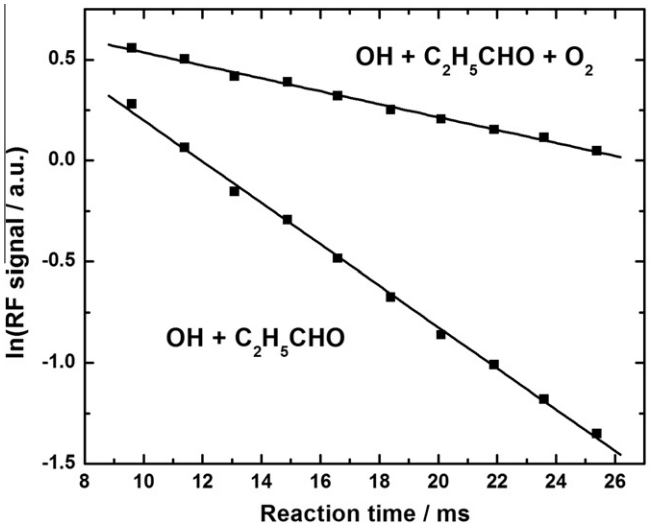

Fig. 1. Representative OH decay plots measured for $OH + C_2H_5CHO$ and $OH + C_2H_5CHO + O_2$ in back-to-back experiments ($P = 6.22$ mbar, $T = 300$ K; $[OH]_0 \approx 2.4 \times 10^{11}$, $[C_2H_5CHO] = 5.35 \times 10^{12}$ and $[O_2] = 1.03 \times 10^{15}$ molecule cm^{-3}).

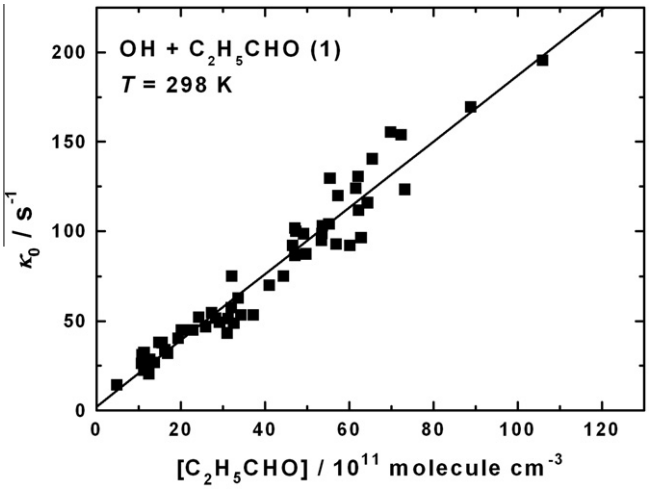

Fig. 2. Plot of the pseudo-first-order decay constant vs. the propanal concentration in the absence of O_2. The slope of the straight line provides the rate constant for the reaction $OH + C_2H_5CHO$ (1).

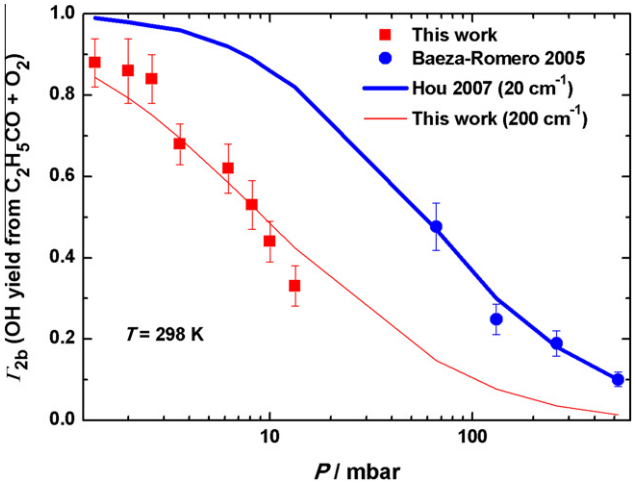

Fig. 3. Comparison of OH yields for the reaction $C_2H_5CO + O_2$ in He buffer gas. The symbols are experimental data: (●) [3]; (■), this work. The curves are theoretical results: thick line, $-\langle\Delta E\rangle = 20\ cm^{-1}$ [4]; thin line, $-\langle\Delta E\rangle = 200\ cm^{-1}$, this work.

propionyl-peroxyl radical is the dominant reaction product for the propionyl + O_2 reaction at pressures above about 10 mbar. We have presented molecular details of the above mechanism by high level quantum chemical computations in [4]. The OH-forming reaction route was shown to consist of consecutive steps and the cyclic α-lactone molecule was proposed as the main co-product to OH [4].

Baeza-Romero et al. [3] produced the propionyl radicals by pulsed exciplex laser photolysis of diethyl ketone (DEK) at 248 nm in He buffer gas, over the pressure range of 13–532 mbar at 295 and 213 K. The formation of OH in the presence of O_2 was monitored by off-resonance laser induced fluorescence and the kinetic traces measured were analysed in terms of a bi-exponential expression providing overall rate constant and OH yield for the $C_2H_5CO + O_2$ reaction.

The experimental OH yields we have determined are compared in Fig. 3 with those reported by Baeza-Romero et al. [3]. The Leeds group has found the OH yields to decrease with pressure, similarly to our findings, but in qualitative agreement only [3]. Although the investigations were performed in very different pressure ranges, it is obvious that significant disparity exists between the two data sets: the OH yields reported by Baeza-Romero et al. [3] are considerably greater and decrease more slowly with increasing pressure compared with our data.

No obvious reason can be given to explain the deviations between the results of the two studies. Baeza-Romero et al. have observed an overestimation of the OH yields at higher laser energies and high repetition frequencies which they have attributed to an additional OH source of the photolysis of $RC(O)O_2$ radicals [3]. This source of systematic errors has been reported to be eliminated by the authors in their regular experiments [3].

We estimate that the excess energy available to the products of the propionyl-source reaction (1) is ~137 kJ mol^{-1} in our experiments, while in the case of the 248 nm photodissociation of DEK it is ~150 kJ mol^{-1} [11]. A substantial portion of the available energy may channel into the internal degrees of freedom of the reaction products. In a very recent work at the University of Essen-Duisburg [12], the photodissociation of DEK has been studied at 248 nm. The CO quantum yield was found to decrease substantially with pressure (50–600 mbar air) indicating the occurrence of vibrationally excited $(C_2H_5CO)^*$ radicals in the photolysis system. The decomposition of 'hot' propionyl radicals may have led to an underestimation rather than overestimation of the OH yields in the experiments by Baeza-Romero et al. [3].

A similar disparity in the experimentally determined OH yields was seen for the analogous $CH_3CO + O_2$ reaction [5,13–16]. In our prior study [5], we established significantly smaller OH yields using the DF method compared with the PLP results of Blitz et al. [13]. While our reported data are in-line with those determined by others [14,15], the Leeds group has recently confirmed their results by applying the 248 nm photolysis of CH_3COOH [16].

Fig. 3 presents the FCC/MC-RRKM OH yields that we computed by taking $-\langle\Delta E\rangle = 200\ cm^{-1}$ as the average energy transferred per collision (thick line). This is seen to reproduce well our experimental OH yields. That is, the OH fraction of $C_2H_5CO + O_2$ is close to unity at around 1 mbar of He and decreases rapidly with increasing pressure. The theory reveals the OH yields to be entirely negligible under atmospheric conditions. In contrast, $-\langle\Delta E\rangle = 20\ cm^{-1}$ was found in our previous theoretical work [4] to reproduce well the significantly different OH yields reported by Baeza-Romero et al. [3] (Fig. 3, thick line). Unfortunately, currently there are no 'first principle' methods available to estimate collisional energy transfer parameters which would help decide between the conflicting experimental data.

Similar differences were observed by Maranzana et al. [17] who solved the time dependent master equation for $CH_3CO + O_2$ to simulate the formation of OH radicals in the reaction. The 'low' value of $\alpha_{He} = 180\ cm^{-1}$ has been returned for the energy transfer parameter by fitting the experimental data of Blitz et al. [13], while the best agreement with the experiments of Kovács et al. [5] and Talukdar et al. [15] has been found with the 'high' value of $\alpha_{He} = 520\ cm^{-1}$.

Clearly, further measurements and theoretical investigations of the OH yields for both reactions $C_2H_5CO + O_2$ and $CH_3CO + O_2$ are required to resolve persisting discrepancies in the literature.

Acknowledgements

This work has been supported by the European FP6 Project SCOUT-O3 and the Hungarian Research Fund OTKA (contract K68486).

References

[1] D.J. Lary, D.E. Shallcross, J. Geophys. Res. Atmos. 105 (2000) 19771.
[2] H.B. Singh et al., J. Geophys. Res. Atmos. 109 (2004) D15S07.
[3] M.T. Baeza-Romero, M.A. Blitz, D.E. Heard, M.J. Pilling, B. Price, P.W. Seakins, Chem. Phys. Lett. 408 (2005) 232.
[4] H. Hou, B. Wang, J. Chem. Phys. 127 (2007) 54306.
[5] G. Kovács et al., Phys. Chem. Chem. Phys. 9 (2007) 4142.
[6] S. Dóbé, L.A. Khachatryan, T. Bérces, Ber. Bunsenges. Phys. Chem. 93 (1989) 847.
[7] M. Berman, M.C. Lin, J. Phys. Chem. 87 (1983) 3933.
[8] A. Fernandez-Ramos, J.A. Miller, S.J. Klippenstein, D.G. Truhlar, Chem. Rev. 106 (2006) 4518.
[9] H. Hou, A. Li, H. Hu, Y. Li, H. Li, B. Wang, J. Chem. Phys. 122 (2005) 224304.
[10] M. Ammann et al., IUPAC Subcommittee on Gas Kinetic Data Evaluation, 2010. <http://www.iupac-kinetic.ch.cam.ac.uk/>.
[11] D. Harrop, A.J. Head, G.B. Lewis, J. Chem. Thermodyn. 2 (1970) 203.
[12] T. Ufer, Ph.D. Thesis, Universität Duisburg-Essen, 2008.
[13] M.A. Blitz, D.E. Heard, M.J. Pilling, Chem. Phys. Lett. 365 (2002) 374.
[14] G.S. Tyndall, J.J. Orlando, T.J. Wallington, M.D. Hurley, Int. J. Chem. Kinet. 29 (1997) 655.
[15] R.K. Talukdar, M.E. Davis, L. Zhu, A.R. Ravishankara, J.B. Burkholder, in: P. Dagaut, A. Mellouki (Eds.), Proceedings of the 19th International Symposium on Gas Kinetics, LCSR-CNRS, Orleans, 2006, p. 95.
[16] S. Carr, M.T. Baeza-Romero, M.A. Blitz, M.J. Pilling, D.E. Heard, P.W. Seakins, Chem. Phys. Lett. 445 (2007) 108.
[17] A. Maranzana, J.R. Barker, G. Tonachini, Phys. Chem. Chem. Phys. 9 (2007) 4129.

THE JOURNAL OF PHYSICAL CHEMISTRY A

ARTICLE

pubs.acs.org/JPCA

Atmospheric Chemistry of 2,3-Pentanedione: Photolysis and Reaction with OH Radicals

Emese Szabó,[†,‡,§,∥] Mokhtar Djehiche,[†,‡] Matthieu Riva,[†,‡] Christa Fittschen,[†,∥] Patrice Coddeville,[†,‡] Dariusz Sarzyński,[⊥] Alexandre Tomas,[*,†,‡] and Sándor Dóbé[*,§]

[†]Université de Lille Nord de France, F-59000, Lille, France

[‡]Ecole des Mines de Douai, Département Chimie et Environnement, 941 rue Charles Bourseul, 59500 Douai, France

[§]Institute of Materials and Environmental Chemistry, Chemical Research Center of the Hungarian Academy of Sciences, Pusztaszeri út 59-67, H-1025 Budapest, Hungary

[∥]PhysicoChimie des Processus de Combustion et de l'Atmosphère PC2A, UMR CNRS 8522, University of Lille 1, 59650 Villeneuve d'Ascq, France

[⊥]Department of Physical Chemistry, Wroclaw Medical University, 50-140 Wroclaw, pl. Nankiera 1, Poland

Supporting Information

ABSTRACT: The kinetics of the overall reaction between OH radicals and 2,3-pentanedione (1) were studied using both direct and relative kinetic methods at laboratory temperature. The low pressure fast discharge flow experiments coupled with resonance fluorescence detection of OH provided the direct rate coefficient of $(2.25 \pm 0.44) \times 10^{-12}$ cm^3 molecule^{-1} s^{-1}. The relative-rate experiments were carried out both in a collapsible Teflon chamber and a Pyrex reactor in two laboratories using different reference reactions to provide the rate coefficients of 1.95 ± 0.27, 1.95 ± 0.34, and 2.06 ± 0.34, all given in 10^{-12} cm^3 molecule^{-1} s^{-1}. The recommended value is the nonweighted average of the four determinations: k_1 (300 K) = $(2.09 \pm 0.38) \times 10^{-12}$ cm^3 molecule^{-1} s^{-1}, given with 2σ accuracy. Absorption cross sections for 2,3-pentanedione were determined: the spectrum is characterized by two wide absorption bands between 220 and 450 nm. Pulsed laser photolysis at 351 nm was used and the depletion of 2,3-pentanedione (2) was measured by GC to determine the photolysis quantum yield of $\Phi_2 = 0.11 \pm 0.02(2\sigma)$ at 300 K and 1000 mbar synthetic air. An upper limit was estimated for the effective quantum yield of 2,3-pentanedione applying fluorescent lamps with peak wavelength of 312 nm. Relationships between molecular structure and OH reactivity, as well as the atmospheric fate of 2,3-pentanedione, have been discussed.

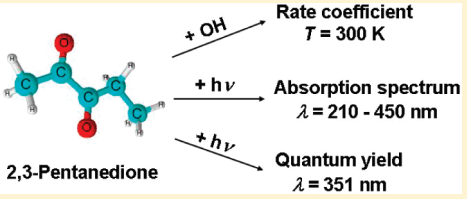

1. INTRODUCTION

2,3-Pentanedione ($CH_3C(O)C(O)CH_2CH_3$, 2,3PD) is a constituent of natural fragrances and synthetic flavoring agents, a selective polar solvent, and a starting material for the manufacture of dyes and pharmaceuticals.[1] It is volatile enough to escape into the atmosphere where it is expected to react primarily with OH radicals and to undergo photolysis. 2,3PD belongs to the family of α-dicarbonyls, several of which are of great importance for the chemistry of the troposphere, including glyoxal, C(O)(H)C(O)(H), methyl-glyoxal, $CH_3C(O)C(O)H$, and biacetyl, $CH_3C(O)C(O)CH_3$. While these latter oxygenates have been the subjects of numerous reaction kinetic and photochemical studies, see, for example, refs 2−4 and refs 5−7, respectively, no such studies have been reported for 2,3PD in the homogeneous gas phase.

We have performed reaction kinetic and photochemical investigations of 2,3-pentanedione. The objectives of the present study were to improve our understanding of the effect of vicinal carbonyl groups on the reactivity with OH radicals and to asses the atmospheric fate of the potentially important volatile organic compound (OVOC), 2,3PD. In this paper we present rate coefficients for the overall reaction of 2,3PD with OH radicals, k_1, absorption cross sections as a function of wavelength, $\sigma_{2,3PD}(\lambda)$, photolysis rate coefficients, J_2, and quantum yield, Φ_2, at selected wavelengths, all of them determined at laboratory temperature ($T \approx 300$ K).

$$OH + CH_3C(O)C(O)CH_2CH_3 \rightarrow \text{products} \quad k_1 \qquad (1)$$

$$CH_3C(O)C(O)CH_2CH_3 + h\nu \rightarrow \text{products} \quad \Phi_2 \text{ and } J_2 \qquad (2)$$

Experiments were carried out both in the Chemical Research Center, Budapest (CRC, Budapest), and the École des Mines de Douai (EMD, Douai) by employing the complementary experimental techniques that are available at the two research sites.

Received: April 30, 2011
Revised: July 21, 2011
Published: July 25, 2011

Thus, kinetic experiments were carried out using the direct discharge flow method and using also relative-rate techniques to obtain rate coefficient for reaction (1). Photolysis experiments were performed employing both a pulsed laser at 351 nm and a continuous broadband irradiation source at 312 nm. The kinetic and photochemical data we present are believed to be the first determinations in the literature and, apart from the work of Jackson and Yarwood,[8] no absorption spectrum for 2,3PD has been reported.

2. EXPERIMENTAL SECTION

Discharge Flow Technique. Absolute rate coefficient for the reaction OH + $CH_3C(O)C(O)CH_2CH_3$ (1) was determined in Budapest by using the low pressure fast discharge flow technique (DF) coupled with resonance fluorescence detection (RF).[9,10]

The flow-tube reactor was constructed of Pyrex and had an inner diameter of 4.0 cm and an overall length of 60 cm. The internal surface of the reactor was coated with a thin film of halocarbon wax to reduce heterogeneous loss of OH radicals. The reactor was equipped coaxially with a movable injector; helium was the carrier gas. OH radicals were produced inside the injector by reacting H atoms with a slight excess of NO_2: H + $NO_2 \rightarrow$ OH + NO; H atoms were generated by microwave discharge of trace H_2 in helium flow. 2,3-Pentanedione was used, premixed in helium, from blackened bulb reservoirs and the concentration of the mixture was checked by GC or UV−vis absorption before use.

The OH(A−X) excitation radiation was produced by a microwave powered resonance lamp operated with flowing Ar/H_2O at low pressure. The RF radiation emerging from the detection cell was passed through an interference filter centered at 307 nm and detected by a photomultiplier. The minimum detectable OH concentration was approximately 2×10^9 molecules cm^{-3}.

Relative-Rate Experiments Using a Pyrex Reactor. Kinetic experiments were performed in a 10 L Pyrex bulb, PR, to determine relative rate coefficient for reaction (1) in Budapest (RR-PR experiments). OH radicals were produced by the photooxidation of CH_3ONO in synthetic air. The photolytic light source was a modified movie projector operated with a 3 kW Xe arc. The irradiating light was passed through a heat reflecting mirror and three liquid filters of 12 cm optical path each in the following order: water, an aqueous solution of chrome alum, and an aqueous solution of methylene blue.[11] The transmitted light had a bell-shaped intensity profile with a maximum at λ_{max} = 362 nm and a full width at half-maximum of w = 28 nm.

The reaction mixtures contained $(5.6 - 6.0) \times 10^{15}$ molecules cm^{-3} 2,3PD, $(7.9 - 8.5) \times 10^{15}$ molecules cm^{-3} MEK (methyl ethyl ketone, reference reactant), 1.0×10^{15} molecules cm^{-3} c-C_4F_8 (GC standard), $\sim 4 \times 10^{16}$ molecules cm^{-3} methyl nitrite, and synthetic air made up to 1050 mbar overall pressure. The reaction temperature was measured inside the reactor using a retractable thermocouple. It was found constant and slightly above the ambient temperature (T = 302 ± 4 K). Samples for analysis were withdrawn by a gastight syringe through a septum connected to a thin glass tube which reached in the middle of the bulb. Concentrations were determined by isothermal GC and flame ionization detection (FID). The GC parameters are given in Table SI-2 in the Supporting Information.

Relative-Rate and Photochemical Experiments Using a Collapsible Teflon Reactor. A collapsible Teflon reactor, TR, was used at Douai[12] to determine relative rate coefficients for reaction 1, as well as to obtain photolysis rate coefficients for 2,3PD, J_2. The reactor had a volume of ∼250 L. Two types of fluorescent tubes were used for irradiation: Vilbert-Lourmat T-20 M (20 W) with peak intensity at λ_{max} = 312 nm and w = 11 nm, as well Philips TL-K (40 W) with λ_{max} = 365 nm and w = 34 nm.

Most of the reactants were volatile liquids (2,3PD, MEK, etc.), measured amounts of which were injected in a small evacuated glass vessel first, and were then flushed into the Teflon-bag reactor one by one with a stream of purified air. In the final step, the reactor was filled to its full volume with air (or N_2 in the case of NO_2 photolysis). Concentration depletion of the organics was measured at regular intervals using online GC-FID analysis (Table SI-2 in the Supporting Information).

The following were the initial concentrations: OH-reaction (RR-TR experiments), $[2,3PD]_0 = (1.2 - 3.0) \times 10^{14}$ molecules cm^{-3}, $[ethanol]_0 = 4.3 \times 10^{14}$ molecules cm^{-3} (reference reactant), $[MEK]_0 = (2.8 - 4.2) \times 10^{14}$ molecules cm^{-3} (reference reactant), and $[CH_3ONO]_0 \approx 1 \times 10^{16}$ molecules cm^{-3} (OH radical source); continuous photolysis (CP-TR experiments): $[2,3PD]_0 = (2.5 - 6.5) \times 10^{14}$ molecules cm^{-3}.

In the NO_2 actinometry measurements, the photolysis rate coefficient, J_{NO_2}, was determined at 312 nm by monitoring the consumption of NO_2 during the irradiation of dilute NO_2/N_2 mixtures; the initial concentration was $[NO_2]_0 \approx 8 \times 10^{13}$ molecules cm^{-3}. A calibrated commercial NO_x analyzer was used for the concentration measurements, which was operated continuously by sampling a small flow of the irradiated gas mixture from the Teflon bag.

Measurements of Absorption Cross Sections. The UV−vis absorption spectrum of 2,3PD was determined in Budapest employing a home-built gas spectrophotometer.[14] Briefly, the light beam of a D_2 lamp was passed through a 50.2 cm absorption cell thermostatted to T = 298 ± 1 K, dispersed by a 0.25 m monochromator, and detected by a photomultiplier interfaced to a lock-in amplifier and PC. The spectral resolution was ∼0.4 nm. The light intensity was strongly reduced by using neutral filters to minimize potential photolysis of the analyzed samples.

Laser Photolysis Technique. Pulsed laser photolysis (PLP) at 351 nm was used to determine photolysis quantum yield for 2,3PD, Φ_2(351 nm) in Budapest. The concentration depletion was determined after a measured number of laser shots using GC analysis.[13,14]

An exciplex laser provided the pulsed laser light; the laser was operated at 5 Hz. Photolysis was performed in a 11.6 (optical path) × 3.6 cm (internal diameter) cylindrical quartz cell (PLP-QR experiments). A septum joint was attached to the cell for GC sampling (Table SI-2). The laser energy was measured using a calibrated laser energy meter; the energy was typically ∼20 mJ $pulse^{-1}$. The photolysis was carried out in synthetic air with mixtures containing 6.3×10^{15} molecules cm^{-3} 2,3-pentanedione and 1.5×10^{15} molecules cm^{-3} c-C_4F_8.

Chemicals. 2,3PD was purchased from Merck and Sigma-Aldrich with the nominal purities of ≥98 and 97%, respectively. The samples were purified by multiple trap-to-trap distillations in vacuum (6×), retaining ∼2/3 middle fraction at each step. Purity of the distilled 2,3PD was 98.5% in the liquid phase and ≥99.5% in the gas phase. MEK (Sigma-Aldrich, >99.7%), c-C_4F_8 (PCR Inc., 99%), methanol (Merck, 99.9%) and ethanol (Merck, 99.9%) were degassed by several freeze−pump−thaw cycles prior to use. Most of the gases were used as obtained: H_2 (99.95%, Messer-Griesheim), He (99.996%, Messer-Griesheim), synthetic air (Messer Hungaria, ≥ 99.5%), zero-grade air (Claind

Type AZ 2000 generator). NO_2 (Messer-Griesheim, 98%) was purified by repeated trap-to-trap distillations in vacuum from slurries kept at low temperatures. Methyl nitrite, CH_3ONO, was prepared from methanol with nitrous acid[15] and was purified by trap-to-trap distillations.

Errors. Unless otherwise stated, the quoted uncertainties are two standard deviations throughout the paper and represent precision only. The errors are typically those that have returned from regression analyses and have always been propagated for the derived quantities.

3.1. KINETIC RESULTS AND DISCUSSION

3.1.1. DF-RF Determination of k_1. The experiments were conducted at $T = 300 \pm 3$ K reaction temperature and $P = 2.49 \pm 0.06$ mbar He pressure. The standard pseudo-first-order kinetic method was employed to determine absolute rate coefficient for OH + $CH_3C(O)C(O)CH_2CH_3$ (1) with a large excess of [2,3PD] over the hydroxyl radical concentration of $[OH]_0 \approx 3 \times 10^{11}$ molecules cm^{-3}. The experiments were performed by recording the OH resonance fluorescence signal strengths versus the varied reaction distance, z, with, S^{OH}_{on}, and without, S^{OH}_{off}, of the reactant 2,3-pentanedione flow. Under the plug-flow condition of the low-pressure DF technique, the reaction time equals $z \times v_{lin}^{-1}$, where v_{lin} is the average linear flow velocity in the flow tube. The bimolecular reaction between OH and 2,3PD was kinetically isolated from the interfering reactions in the homogeneous gas phase, but the consumption of OH was significant on the surface of the reactor, which was found to obey first-order kinetics with an effective "wall rate coefficient" of k_w.

Therefore, assuming pseudo-first-order kinetics and with the provision that the wall activity for OH was not very different in the presence and absence of 2,3PD, the experimental observables were evaluated by the eqs I–III:

$$-\ln \frac{S^{OH}_{on}}{S^{OH}_{off}} = k_1' \frac{z}{v_{lin}} \quad \text{(I)}$$

$$k_1' = k_1[2,3PD] + \text{const} \quad \text{(II)}$$

$$-\ln S^{OH}_{off} = k_w \frac{z}{v_{lin}} \quad \text{(III)}$$

The measured hydroxyl decays, when plotted according to eq I, displayed straight lines, indicating the validity of first-order kinetics. The slopes provided the pseudo-first-order rate coefficient, k_1', by linear least-squares analysis (LSQ). Sample decay plots are shown in the inset of Figure 1. The main panel of this figure shows a plot of k_1' versus [2,3PD] (eq II); the bimolecular rate coefficient, k_1, was obtained as LSQ slope. The plotted ln S^{OH}_{off} versus z data gave also straight lines, the slopes of which supplied k_w (eq III).

Large heterogeneous effects were observed in the first experiments portrayed by very high OH consumption on the surface of the reactor and a smaller than expected signal magnitudes in the experiments that were carried out in close succession to each other. Such effects are indicative of the adsorption of 2,3PD on the walls of the reactor and an enhanced heterogeneous reaction with the OH radicals. Similar behavior was reported by Stevens and co-workers for discharge flow reactions of OH with different polar reactants including carbonyls (see, e.g., ref 16 and references therein). These authors have reported the heterogeneous

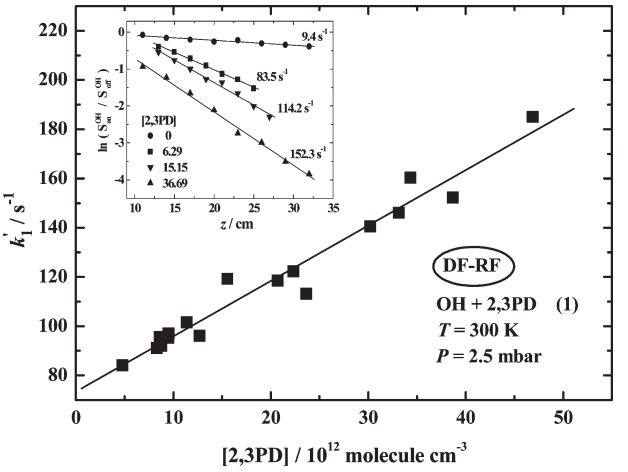

Figure 1. Plots used to determine k_1. The figure in the inset shows representative OH-decays vs the reaction distance, where S^{OH}_{on} and S^{OH}_{off} are the OH signal strengths with and without 2,3PD flow, respectively, and the 2,3PD concentrations are given in 10^{12} molecules cm^{-3}.

effects to be minimized by the addition of O_2. However, this option was not feasible in our current experiments because a substantial reformation of OH was observed when oxygen flow was added to the reaction system that might have caused an underestimation of the rate coefficients in the measurements. Long evacuation time and conditioning of the walls of the flow tube with OH radicals were used prior to each experiment. In this way, reasonable reproducibility was achieved, but the bimolecular rate coefficient plot showed a significant intercept (Figure 1), and the $k_w = 7–47$ s^{-1} values were somewhat larger than the usual wall consumption of OH ($\sim 3–20$ s^{-1}) that we observed previously in DF experiments with inert wall coatings.

The experimental conditions and kinetic results are summarized in Table 1. We have not corrected the measured rate coefficient for viscous flow and axial diffusion in the present work. Instead, an 8% contribution was included in the error margins to account for such effects and other potential systematic errors by experience with previous reaction systems. Thus, the following rate coefficient is proposed by the DF-RF study for the reaction of OH radicals with 2,3-pentanedione: $k_1(300\ K) = (2.25 \pm 0.44) \times 10^{-12}$ cm^3 molecule^{-1} s^{-1} given with an overall uncertainty at the 2σ level.

3.1.2. Relative-Rate Kinetic Studies. Relative rate coefficients for the reaction of OH with 2,3-pentanedione were determined by comparing the rate of loss of the substrate to that of a reference compound the rate coefficient for which is accurately known. 2,3PD was found to photolyze slowly at the wavelengths used to produce OH, however, no loss of the reference compounds at the time scale of the kinetic experiments was observed by test irradiations conducted in the absence of 2,3PD and the OH-source CH_3ONO.

$$\text{OH} + \text{2,3-pentanedione} \rightarrow \text{products}, \quad k_1 \quad (1)$$

$$\text{OH} + \text{reference} \rightarrow \text{products}, \quad k_{ref} \quad (\text{ref})$$

$$\text{2,3-pentanedione} + h\nu \rightarrow \text{products}, \quad J_2 \quad (2)$$

$\lambda_{max} = 362$ and 365 nm.

Table 1. Summary of Experimental Conditions and Results for the Reaction OH + 2,3PD (1) Using the DF-RF Method (T = 300 ± 3 K, P = 2.49 ± 0.06 mbar He Buffer Gas)[a]

ν_{lin} (cm s^{-1})	$[OH]_0$ (10^{11} molecules cm^{-3})	[2,3PD] (10^{12} molecules cm^{-3})	k_w (s^{-1})	k_1' (s^{-1})	No. of expts	k_1 (10^{-12} cm^3 molecule^{-1} s^{-1})[a]
874−1055	2−10	4.79−46.9	7−47	84−185	17	2.25 ± 0.24

[a] The errors represent 2σ statistical uncertainties.

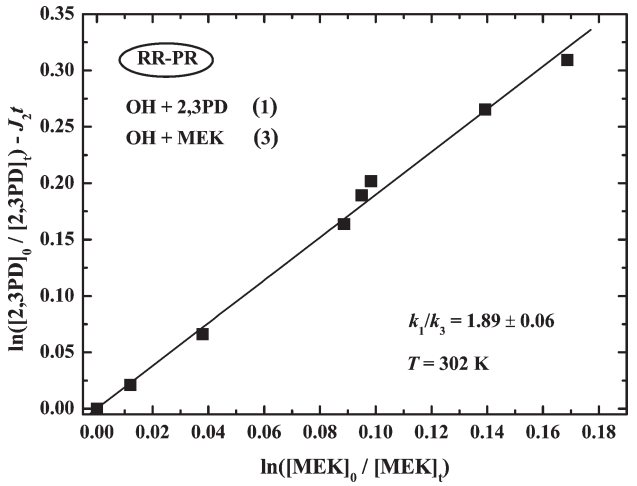

Figure 2. Plot used to determine rate coefficient ratio for the reaction of OH radicals with 2,3PD obtained from measurements using the Pyrex reactor and MEK as the reference reactant.

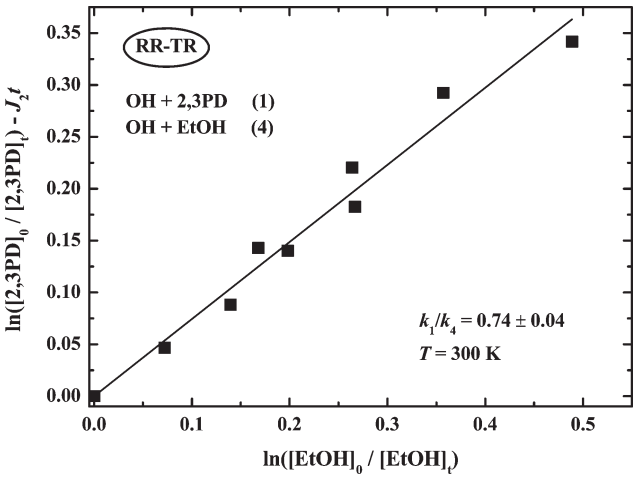

Figure 3. Plot used to determine rate coefficient ratio for the reaction of OH radicals with 2,3PD obtained from measurements using the Teflon bag reactor and EtOH as the reference reactant.

Provided that 2,3PD and the reference compounds are lost only by reactions with OH, neither 2,3PD, nor the reference compounds are reformed in the systems and that the photolysis of 2,3PD is slow compared to the studied chemical reactions, the following expression is obtained

$$\ln\{[2,3\mathrm{PD}]_0/[2,3\mathrm{PD}]_t\} - J_2 \times t = (k_1/k_{\mathrm{ref}}) \times \ln\{[\mathrm{ref}]_0/[\mathrm{ref}]_t\} \quad \text{(IV)}$$

where $[2,3PD]_0$, $[2,3PD]_t$, $[ref]_0$, and $[ref]_t$ are the concentrations of the 2,3PD and reference at time zero and t, J_2 is the photolysis rate coefficient determined from separate experiments, t is the reaction time, k_1 and k_{ref} are the rate coefficients for the 2,3PD reaction and the reference reaction, respectively. Thus, plots of the left-hand side of eq IV versus ln $\{[ref]_0/[ref]_t\}$ should be linear with zero intercept and slope equal to k_1/k_{ref}.

OH radicals were produced by the photolysis of methyl nitrite in air

$$\mathrm{CH_3ONO} + h\nu \rightarrow \mathrm{CH_3O} + \mathrm{NO} \quad (\lambda_{\max} = 362 \text{ and } 365 \text{ nm})$$

$$\mathrm{CH_3O} + \mathrm{O_2} \rightarrow \mathrm{HO_2} + \mathrm{HCHO}$$

$$\mathrm{HO_2} + \mathrm{NO} \rightarrow \mathrm{OH} + \mathrm{NO_2}$$

RR-PR Determination of k_1. Relative-rate kinetic experiments were carried out in synthetic air, at T = 302 ± 4 K reaction temperature and 1050 mbar overall pressure, using the Pyrex reactor. The reaction with methyl ethyl ketone, OH + MEK (3), served as reference. The measured concentration ratios plotted according to eq IV are presented in Figure 2. The photolysis rate coefficient needed for the data evaluation was determined by measuring the photodepletion of 2,3PD in the absence of CH_3ONO and MEK but, otherwise, under the same experimental conditions. Single exponential time dependence was observed providing $J_2(362 \text{ nm}) = (1.99 \pm 0.32) \times 10^{-5}$ s^{-1} as the decay constant. This photolysis rate has resulted in a maximum correction of ~9% of the OH-reaction in eq IV. Linear least-squares analysis of the data plotted in Figure 2 have supplied $k_1/k_3 = 1.89 \pm 0.06$. The rate coefficient ratio has been put to an absolute scale by taking $k_3 = (1.09 \pm 0.18) \times 10^{-12}$ cm^3 molecule^{-1} s^{-1} from ref 17 to give $k_1 = (2.06 \pm 0.34) \times 10^{-12}$ cm^3 molecule^{-1} s^{-1}. (The rate coefficient value we use for the reference reaction agrees within 10% with those recommended by the IUPAC and JPL data evaluations.[18,19])

RR-TR Determination of k_1. Two reference reactions, OH + MEK (3) and OH + C_2H_5OH (EtOH; 4), were used in the relative-rate experiments that were performed in the Teflon-bag reactor. The reaction conditions were: T = 300 ± 2 K and P = 1000 mbar overall pressure synthetic air. Similar to the Pyrex-reactor experiments, photolysis loss of 2,3PD had to be taken into account in deriving the rate coefficient ratios. The photolysis rate coefficient has been determined to be $J_2(365 \text{ nm}) = (2.01 \pm 0.08) \times 10^{-5}$ s^{-1}; the correction for photolysis was less than 15%. A plot according to eq IV is presented in Figure 3 displaying results with the application of the EtOH reference reaction. An LSQ slope of the straight line of Figure 3 provides $k_1/k_4 = 0.74 \pm 0.04$, which is resolved to the absolute rate coefficient of $k_1 = (1.95 \pm 0.27) \times 10^{-12}$ cm^3 molecule^{-1} s^{-1} by taking $k_4 = (3.2 \pm 0.4) \times 10^{-12}$ cm^3 molecule^{-1} s^{-1} from ref 18.

Well-obeyed straight line with zero intercept similar to those shown in Figures 2 and 3 was obtained also with the application

of the methyl ethyl ketone reference reaction[17] in the Teflon-reactor experiments supplying $k_1/k_3 = 1.79 \pm 0.11$ and $k_1 = (1.95 \pm 0.34) \times 10^{-12}$ cm^3 molecule^{-1} s^{-1}. The relative-rate plot obtained with the OH + MEK (3) reference reaction is presented as Figure SI-2 in the Supporting Information.

3.1.3. Reactivity of 2,3-Pentanedione with OH. The absolute and relative-rate kinetic studies have provided rate coefficients for reaction (1) in good agreement with each other: DF-RF, 2.25 ± 0.44; RR-PR, 2.06 ± 0.34; RR-TR, 1.95 ± 0.27 and 1.95 ± 0.34, all given in 10^{-12} cm^3 molecule^{-1} s^{-1}. Note also that k_1 has been found invariant to the reaction pressure in a wide range between ~2 and ~1000 mbar. The good agreement lends credence to the reliability of the results in particular that they were obtained from independent measurements in two laboratories using different experimental techniques. The recommended rate coefficient for the reaction of OH radicals with 2,3PD is the nonweighted average of the k_1 determinations:

$$k_1(300\ \mathrm{K}) = (2.09 \pm 0.38) \times 10^{-12}\ \mathrm{cm^3\ molecule^{-1}\ s^{-1}}$$

given with an overall accuracy proposed to be valid at the 95% confidence level.

To our knowledge, no prior rate coefficient has been reported for reaction (1). The only other α-diketone that has been a subject of OH-kinetic study is 2,3-butanedione ($CH_3C(O)C(O)CH_3$, or biacetyl). A rate coefficient of $(2.3 \pm 0.2) \times 10^{-13}$ cm^3 molecule^{-1} s^{-1} (T = 298 K) has been determined by Dagaut et al.[4] for the OH + biacetyl reaction in good agreement with a previous measurement by Darnall et al.[20] The rate coefficient we propose from our current work for the OH + $CH_3C(O)C(O)CH_2CH_3$ (1) reaction is ~10 times higher, which can be rationalized, however, by the increased reactivity of the CH_2 group not present in the biacetyl molecule (see below).

A structural isomer of 2,3PD is 2,4-pentanedione (2,4PD), which is a β-diketone. Holloway and co-workers have carried out a detailed kinetic study of the reaction of OH with 2,4PD using both direct and relative kinetic methods.[21] The rate coefficient they have reported is $(8.78 \pm 0.58) \times 10^{-11}$ cm^3 molecule^{-1} s^{-1} (T = 298 K), which is more than 40 times higher than the k_1 value we have determined for the OH + $CH_3C(O)C(O)CH_2CH_3$ (1) reaction. Holloway et al.[21] have explained the high rate coefficient by that 2,4-pentanedione exists in the gas phase predominantly as the enol tautomer, $CH_3C(O)CH{=}C(OH)CH_3$, which undergoes fast addition reaction with the OH radical, while the keto-form ketones react via the slower hydrogen abstraction reaction. In contrast to 2,4PD, the vicinal diketone 2,3PD exists predominantly in the keto form with the enol form being present to a few percentages, at the most, in the gas phase at room temperature.[22,23]

The reactivity properties of 2,3PD can be understood by the considerable knowledge that has been gathered throughout the years for the kinetics and mechanism of the reactions of OH radicals with the aliphatic monoketones, see, for example, refs 24 and 25 and also the review paper by Mellouki et al.[26] The C=O group slightly reduces the bond dissociation energy (BDE) of a neighboring C−H bond,[19] but it is strongly electron withdrawing, which overrides the BDE-reducing effect, and so hydrogen abstraction by the electrophilic OH radical becomes less facile at the α-position.[26,27] On the other hand, a characteristic feature of the OH reactions of $C_n \geq 3$ ketones is the increased reactivity of the C−H bonds at the β-position.[25,26] This latter effect is thought to be the decisive factor in determining the pronounced reactivity of 2,3PD toward OH, compared, for example, with propane, $CH_3CH_2CH_3$, which has the same number and types of H atoms, but its rate coefficient is about half of that of the 2,3PD reaction (k(OH + propane) = 1.1×10^{-12} cm^3 molecule^{-1} s^{-1}, T = 298 K[19]).

An important development for understanding the reactivity of OH radicals with polar organic molecules, including carbonyls, has been the recognition of the important role that weakly bound 'prereaction' (or 'prereactive') complexes play in the molecular mechanisms of the reactions, as it has been reviewed[28−30] and discussed in detail, for example, in refs 31 and 32. Specifically, the role of hydrogen bonded complexes in enhancing the reactivity of the β-C−H bond in the reactions of OH with aliphatic ketones has been assessed by Alvarez-Idaboy and co-workers by quantum chemical and theoretical reaction kinetics computations.[32] They have shown that the β-prereaction complexes, C=O···HO··$\cdot$H$_\beta$C$_s$, significantly lower the reaction barrier via hydrogen-bond-like interactions in the transition state thus leading to increased rate coefficients.

One of the most frequently used methods to estimate OH reaction rate coefficients for gas-phase organic compounds has been Atkinson's structure−reactivity (SAR) approach,[27] which was found to work very well for the OH + aliphatic ketones reactions.[24] According to the SAR procedure, the total rate coefficient for the reaction OH + $CH_3C(O)C(O)CH_2CH_3$ (1) can be estimated as the sum of the following group rate coefficients (T = 298 K):

$$k_1 = k_{\mathrm{prim}}F(>\mathrm{CO}) + k_{\mathrm{sec}}F(>\mathrm{CO})F(-\mathrm{CH_3}) + k_{\mathrm{prim}}F(-\mathrm{CH_2C(O)}-) \quad \text{(V)}$$

where k_{prim} and k_{sec} are the rate coefficients per CH_3- and $-CH_2-$ groups and Fs are the substituent factors. Taking the tabulated generic rate coefficients k_{prim}, k_{sec} and the substituent factors from ref 27 one obtains $k_1 = 1.33 \times 10^{-12}$ cm^3 molecule^{-1} s^{-1}, which is an ~50% underestimate of the experimental value. We believe the reason is simply that the substituent factors currently available do not reflect the activating effect of a −C(O)C(O)− moiety on the β-C−H bond. Conversely, a $F(-C(O)C(O)-)$ factor can be derived by using our measured rate coefficient and the group reactivity parameters given in ref 27.

$$k_1(\mathrm{meas}) = k_{\mathrm{prim}}F(-\mathrm{C(O)C(O)}-) + k_{\mathrm{sec}}F(-\mathrm{C(O)C(O)}-)F(-\mathrm{CH_3}) + k_{\mathrm{prim}}F(-\mathrm{CH_2C(O)}-) \quad \text{(VI)}$$

This estimation provides $F(-C(O)C(O)-) = 1.55$, which indicates a definite, but smaller, activating effect than that of the $-CH_2C(O)-$ group, $F(-CH_2C(O)-) = 3.9$.[27]

3.2. PHOTOCHEMICAL RESULTS AND DISCUSSION

3.2.1. UV−Vis Absorption Spectrum of 2,3-Pentanedione. The absorption spectrum for 2,3PD was determined over the wavelength range of λ = 210−450 nm, at room temperature (T = 298 ± 1 K). The wavelength-dependent cross sections, $\sigma_{2,3\mathrm{PD}}(\lambda)$, were obtained from absorption measurements applying the Beer−Lambert law:

$$\ln\{(I_0)/(I)\} = \sigma_{2,3\mathrm{PD}}(\lambda)\ell[2,3\mathrm{PD}] \quad \text{(VII)}$$

where ℓ (= 50.2 cm) is the optical path length, and I_0 and I are the

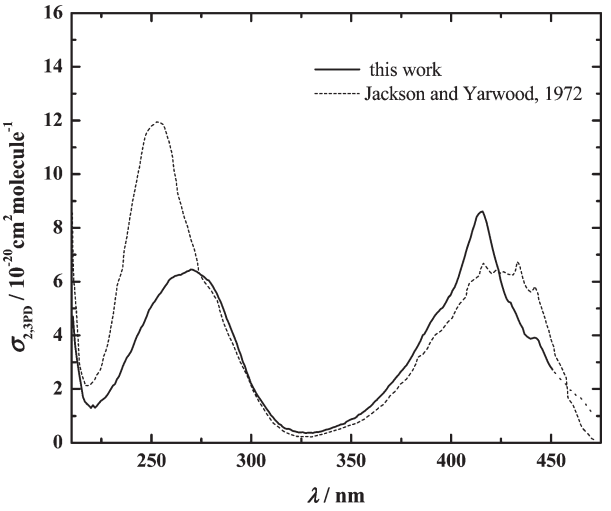

Figure 4. Absorption spectrum of 2,3-pentanedione in the gas phase at laboratory temperature: (—), this work; (····), Jackson and Yarwood.[8].

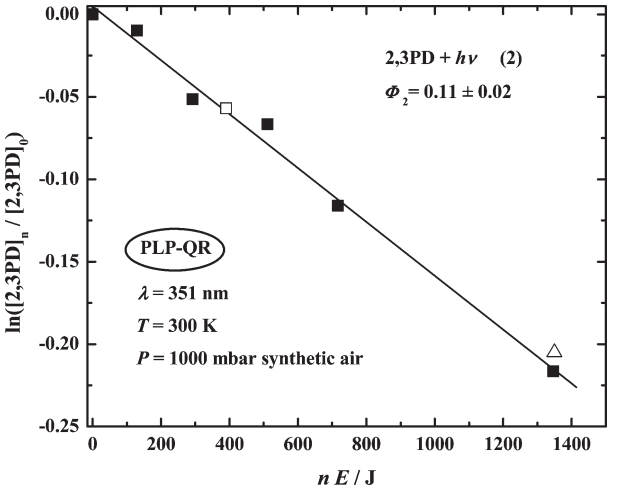

Figure 5. Depletion of 2,3PD concentration in pulsed laser photolysis experiments: n is the number of laser shots and E is the energy per pulse. The slope is proportional to the Φ_2(351 nm) photolysis quantum yield. The open symbols designate experiments performed with reaction mixtures containing 1-pentene as an OH scavenger.

transmitted light intensities in the absence and presence of 2,3PD, respectively. The spectrum is shown in Figure 4 and the corresponding absorption cross sections, $\sigma_{2,3PD}(\lambda)$, are tabulated in 1 nm intervals in the Supporting Information (Table SI-1) where representative Beer−Lambert (BL) plots are also presented (Figure SI-1).

As a first step, survey spectra were taken using the 2,3PD, as obtained from the supplier (nominally ≥98% purity sample). One of the characteristic features of the spectrum determined was a strong absorption band at ∼250 nm, which had a shoulder at ∼270 nm. The 250 nm peak disappeared, however, when the spectrum was recorded with the purified sample and a lower-intensity unstructured band emerged with a maximum at 270 nm. The short-wavelength feature of the spectrum appeared again when the 2,3PD/He mixture applied for the analysis was prepared and stored in a bulb, which was used previously for storing other organics in gas mixtures, indicating the potential chemical transformation of 2,3PD on contaminated surfaces. Therefore, new, carefully cleaned glass parts were installed, and the absorption spectra were taken with the purified 2,3PD samples from mixtures stored for 1, 2, and 15 days, and recording of the spectra was done under static and flow-through conditions as well. The measurements have provided absorption cross sections in good agreement and so their average is proposed as the final result. This spectrum is presented in Figure 4.

As seen in Figure 4, 2,3PD has two broad absorption bands in the spectral range above ∼220 nm: one in the UV and the other one in the visible with maximum at 270 and 415 nm, respectively. There is some indication for a vibrational structure of the second band, which may have been blurred, however, by the relatively low resolution (∼0.4 nm) of our spectrometer. We have observed weak absorption extended to even longer wavelengths in the visible region but do not report the spectrum above 450 nm because of the large scatter and significant intercept of the BL-plots. The absorption spectrum of 2,3PD is similar to that of biacetyl in terms of the band positions, absorption cross sections and band widths.[33]

The only absorption spectrum that is available for 2,3PD from the literature has been reported by Jackson and Yarwood,[8] which is presented also in Figure 4. The UV-portion of the spectrum reported by these authors, a large peak at 253 nm with a shoulder at 280 nm, shows close resemblance to that we observed with the 2,3PD sample when used without purification. As discussed, the strong short-wavelength band was absent in the spectrum that we obtained with the purified 2,3PD. The absorption band lying at longer wavelengths shows significant disparity as well (Figure 4). We note that we have obtained the same spectrum with the purified sample and without purification above ∼350 nm. Clearly, this is not yet a proof for that our spectrum should be preferred at longer wavelengths as well.

3.2.2. Pulsed Laser Photolysis Results. The 351 nm PLP-QR experiments were performed at laboratory temperature (T = 300 ± 2 K) in synthetic air at 1000 mbar total pressure to determine the photolysis quantum yield, Φ_2(351 nm). The concentration of 2,3PD was measured before photolysis, [2,3PD]$_0$, and after n laser shots, [2,3PD]$_n$, by GC analysis. Fresh gas mixtures were prepared for each irradiation. The experimental observables were evaluated according to eq VIII:[13,14]

$$\ln([2,3\mathrm{PD}]_n/[2,3\mathrm{PD}]_0) = -C \times \Phi_2(351\ \mathrm{nm}) \times (n \times E) \quad \text{(VIII)}$$

$$\text{with} \quad C = f_w(351\ \mathrm{nm}) \times E_{Ph}(351\ \mathrm{nm})^{-1} \times \sigma_{2,3PD}(351\ \mathrm{nm}) \times \ell \times V^{-1}$$

where E is the laser energy (mJ) per pulse, f_w(351 nm) is the transmission of the entrance window (the measured value was 0.930 for one window), E_{Ph}(351 nm) is the energy of one photon (mJ photon^{-1}), ℓ (= 11.6 cm) is the optical path length, and V is the total volume of the cell (cm^3). Φ_2(351 nm) was obtained by plotting ln([2,3PD]$_n$/[2,3PD]$_0$) against ($n \times E$) and making use of the absorption cross section measured in the present work and the known parameters in eq VIII. A plot of ln([2,3PD]$_n$/[2,3PD]$_0$) versus ($n \times E$) is presented in Figure 5.

The reaction mixture contained 1-pentene in two experiments to trap the OH radicals potentially formed in the photo-oxidation system. Open symbols in Figure 5 represent the data obtained in the presence of OH-scavenger. The concentration of 1-pentene was 9.11 × 10^{14} and 8.9 × 10^{15} molecules cm^{-3} at low and high

dx.doi.org/10.1021/jp205595c |J. Phys. Chem. A 2011, 115, 9160–9168

2,3PD depletion, respectively. The result is seen invariant to the absence or presence of the OH scavenger 1-pentene that is believed to be a strong indication for the reliability of the quantum yield determined in the PLP-QR experiments. Linear least-squares analysis of all data in Figure 5 has provided $\Phi_2(351\ \text{nm}) = 0.11 \pm 0.01$, where the error given represents 2σ statistical uncertainty. Systematic errors were assessed for the parameters used in eq VIII, for example, it is ±4% for the energy measurement judged by NO_2 actinometry. Root mean squares combination of the statistical and systematic errors gives ±20%, which is the proposed overall uncertainty at the 2σ (95% confidence) level. That is, the recommended quantum yield from our present study is:

$$\Phi_2(351\ \text{nm}) = 0.11 \pm 0.02$$

The "real" accuracy of the measurements can be considerable poorer than that given above due to the small absorption cross section of the 2,3PD molecule at the 351 nm photolysis wavelength.

3.2.3. Broadband Photolysis Results. Continuous photolysis of 2,3PD was carried out in the collapsible Teflon reactor in air buffer gas using fluorescent UV lamps with maximum emissions at 312 nm ($T = 300 \pm 2$ K, $P = 1000$ mbar, CP-TR experiments). The photolysis rate coefficient ("photolysis frequency"), J_2(312 nm), was determined by monitoring the loss of the photolyte via online GC analysis. Experiments were performed with and without adding 1-pentene to the irradiated gas mixtures. 1-Pentene served to trap the OH radicals that potentially formed in the reaction systems. The depletion of 2,3PD concentration has been found to follow first-order kinetics as shown in Figure 6,

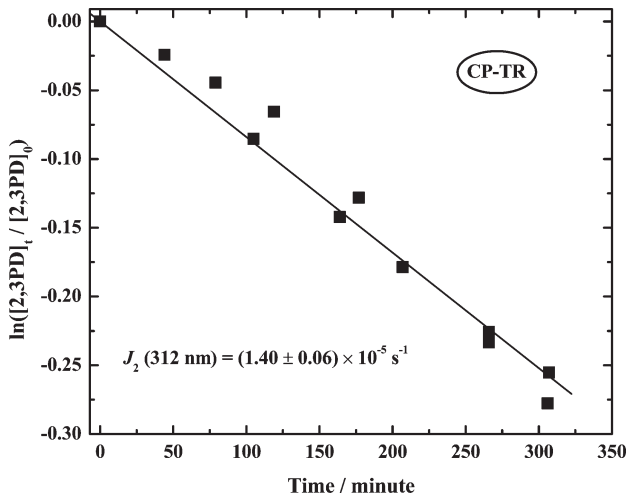

Figure 6. Depletion of 2,3PD concentration in the broadband photolysis experiments performed in the Teflon-film reactor at 312 nm. The reaction mixtures contained 1-pentene as an OH scavenger. The slope of the straight line gives the J_2 photolysis rate coefficient.

where the $\ln([2,3PD]_t/[2,3PD]_0)$ data are plotted against the reaction time, t, from two series of photolysis experiments. The J_2 values have been obtained by linear regression as the slope of the straight lines and are listed in the second column of Table 2.

The photolysis rate coefficient determined for 2,3PD is higher by ~30% in the absence of OH-scavenger. The OH radicals that caused the additional consumption of 2,3PD were probably formed via secondary reactions involving peroxy-radical chemistry in the photo-oxidation systems. The formation of OH by the primary photodissociation of 2,3PD can not be excluded either, but no products were determined in our current photolysis study to assess the primary and secondary photochemical processes. The photolysis rate coefficient determined in the presence of the OH scavenger is discussed next.

J_2 has been normalized to the photon flux by using NO_2 actinometry (note that the emission spectrum of the fluorescent lamps and the absorption spectra of 2,3PD and NO_2[19] overlap in a substantial wavelength range). A dilute mixture of NO_2 in atmospheric pressure N_2 buffer gas was photolyzed in the Teflon reactor under the very same irradiation conditions than those of the 2,3PD photolysis experiments and the concentration depletion of NO_2 was measured as a function of the photolysis time up to 15−20% conversion. A plot of $\ln[NO]_2$ versus t yielded a straight line, the slope of which was equated to J_{NO_2} after minor correction for secondary reactions as proposed by Holmes et al.[34,35] The determined J_{NO_2} photolysis frequencies along with the ratios J_2/J_{NO_2} are given in Table 2.

The J_2/J_{NO_2} values in Table 2 have been utilized to estimate an "integral" or "effective" quantum yield,[36,37] Φ_2^{eff}, for the photolysis of 2,3PD with the broad-band fluorescent lamp with $\lambda_{max} = 312$ nm and $w = 12$ nm maximal emission wavelength and a full width at half maxima, respectively. The following expression was used:

$$\Phi_2^{\text{eff}} = \frac{J_2}{J_{NO_2}} \times \left\{ \frac{0.5\sigma_{NO_2}(\lambda_{max} - 0.5w) + \sigma_{NO_2}\lambda_{max} + 0.5\sigma_{NO_2}(\lambda_{max} + 0.5w)}{0.5\sigma_{2,3PD}(\lambda_{max} - 0.5w) + \sigma_{2,3PD}\lambda_{max} + 0.5\sigma_{2,3PD}(\lambda_{max} + 0.5w)} \right\} \times \Phi_{NO_2} \quad \text{(IX)}$$

In eq IX, Φ_{NO_2} is the quantum yield for nitrogen dioxide photolysis, which was taken unity[19,37] over the whole wavelength range studied; the absorption cross sections of NO_2, $\sigma_{NO_2}(\lambda)$, were taken from ref 19 for the calculations and the $\sigma_{2,3PD}(\lambda)$ values from the present work (Table SI-1 in the Supporting Infrmation). The estimated effective quantum yield is $\Phi_2^{\text{eff}}(312\ \text{nm}) = 0.41 \pm 0.05$. Trial calculations have shown only small change of the effective quantum yields when more overlap between the emission spectrum of the lamp and the absorption spectra of NO_2 and 2,3PD were taken into account.

As discussed, there was a strong, albeit indirect, indication for the formation of OH radicals in the broadband photolysis study performed at 312 nm causing a potential overestimation of the

Table 2. Photolysis Rate Coefficients and Effective Quantum Yields Determined in the Collapsible Teflon Reactor at 312 nm Using Broadband Fluorescent Lamps ($T = 300 \pm 2$ K, $P = 1000$ mbar Air)

OH scavenger	J_2[a] (10^{-5} s^{-1})	J_{NO_2}[a] (10^{-3} s^{-1})	$100 \times (J_2/J_{NO_2})$	Φ_2^{eff}[b]
no scavenger	1.92 ± 0.08 (2)	0.78 ± 0.01 (9)	1.80 ± 0.12[d]	0.41 ± 0.05[d]
1-pentene[c]	1.40 ± 0.06 (3)			

[a] The number of experiments are given in the parentheses; 6 × 20 W lamps were used in the experiments. [b] Effective quantum yield (see text). [c] OH-scavenger: $[1\text{-pentene}]_0 = 9.1 \times 10^{14}$ molecules cm^{-3}. [d] Using J_2 values determined in the presence of OH scavenger.

dx.doi.org/10.1021/jp205595c | J. Phys. Chem. A 2011, 115, 9160–9168

quantum yields. In contrast, no such problem was observed in the PLP experiments at 351 nm. No obvious reason can be given to explain the diverse behavior. We just note that more photolysis channels are accessible at the lower wavelength studied (see next section) that may have led to different secondary photooxidation processes. The concentration of 1-pentene was not varied in the CP experiments, but it was assumed to be sufficiently high to scavenge all OH formed in the system. Thus, the determined quantum yield is proposed to be only an upper limit, that is, $\Phi_2^{eff}(312\ nm) \leq 0.41$.

3.2.4. Photochemistry of 2,3PD. We have determined photolysis quantum yields for 2,3-pentanedione using 351 nm XeF laser and 312 nm fluorescence lamps at room temperature ($T = 300 \pm 2$ K) in 1000 mbar air buffer gas with the results of $\Phi_2(351\ nm) = 0.11 \pm 0.02$ and $\Phi_2^{eff}(312\ nm) \leq 0.41$. These are high values for the studied wavelengths and pressure. They appear high in comparison, for example, with the long-wavelength photolysis quantum yields of monoketones[14] and the 365 nm quantum yield of the α-diketone biacetyl.[38] On the other side, however, high quantum yields have been reported for the photolysis of the α-ketoaldehyde, methylglyoxal, $CH_3C(O)C(O)H$, even at around 400 nm photolysis wavelength, although determined at lower pressures.[6] Clearly, further investigations are needed to determine accurate photolysis quantum yields for 2,3PD. Among the quantum yields determined, we give preference to that obtained by the laser photolysis method.

Consumption yields were measured and no photolysis products were determined in our current work. Thermochemistry and the scarce information available from the literature suggest channels 2a−2d to be primary photolysis channels for 2,3PD at the relatively low excitation energies of the investigations:

$$CH_3C(O)C(O)CH_2CH_3 + h\nu$$

$$\rightarrow CH_3CO + CH_3CH_2CO \quad \Delta_{2a}H^\circ_{298} = 302\ kJ\ mol^{-1}\ [19,39],\ \lambda_{threshold} = 395\ nm \qquad (2a)$$

$$\rightarrow CH_3CO + CH_3CH_2 + CO \quad \Delta_{2b}H^\circ_{298} = 344\ kJ\ mol^{-1}\ [19,39],\ \lambda_{threshold} = 346\ nm \qquad (2b)$$

$$\rightarrow CH_3C(O)C(O) + CH_3CH_2 \quad \Delta_{2c}H^\circ_{298} = 354\ kJ\ mol^{-1}\ [19,39,40],\ \lambda_{threshold} = 336\ nm \qquad (2c)$$

$$\Delta_{2d}H^\circ_{298} < 274\ kJ\ mol^{-1},\ \lambda_{threshold} > 435\ nm\ [41] \qquad (2d)$$

The applied photolysis wavelengths of 312 and 351 nm correspond to the excitation energies of 382 and 340 kJ mol^{-1}, respectively. Three different C−C photodissociation routes are energetically accessible at 312 nm excitation, channels 2a−2c, while at 351 nm, only the formation of $CH_3CO + CH_3CH_2CO$, channel 2a, is feasible at ambient temperatures. The free radical product $CH_3C(O)C(O)$ formed via channel 2c may undergo decomposition depending on its excess energy[3,40] to form CH_3CO and CO. The photoisomerization reaction 2d may take place at both excitation wavelengths studied: this channel has been proposed by Turro and Lee in a classical liquid-phase photochemical study[41] (see below). (The reaction enthalpies for the different photolysis channels have been obtained by taking the recently published standard enthalpy of formation of $\Delta_f H^\circ_{298}(2,3PD) = -343.7 \pm 2.5$ kJ mol^{-1} from ref 39 and the other enthalpy data from refs 19,39, and 40.)

Little is known about the photochemistry of 2,3PD from the literature. Turro and Lee[41] have studied the photochemistry of 2,3PD in solution at 435 nm. They have shown that photolysis of 2,3PD forms 1-hydroxy-1-methyl-2-cyclobutanone via an intramolecular photoreduction process, eq 2d, with a quantum yield of ∼0.06.[41] Jackson and Yarwood[42] have investigated the fluorescence and phosphorescence of 2,3PD in the gas phase at 365, 405, and 436 nm. They have derived a rate coefficient expression by the temperature dependent quenching of the phosphorescence of 2,3PD[42] consistent with the eq 2d photoisomerization process.[41] In an unpublished photo-oxidation study, performed at 254 nm in the Teflon reactor in our own laboratory, the build-up of acetaldehyde, CH_3CHO, was observed concomitant with the consumption of 2,3PD,[35] indicating the occurrence of photodissociation channels 2a−2c.

3.3. ATMOSPHERIC IMPLICATIONS

The absorption spectrum of 2,3-pentanedione extends to long wavelengths (Figure 4) where the solar flux increases rapidly in the troposphere, for example, the flux is ∼150 times higher at 400 nm than that at 300 nm at the Earth's surface. Also, as presented in sections 3.2.2−3.2.4, 2,3PD undergoes photochemical changes with quantum yields that are still fairly uncertain, but they are believed significant even at relatively long wavelengths. These factors imply a likely short photolysis lifetime of 2,3PD, τ_{phot}, in the troposphere.

As discussed, we prefer the quantum yield determined with the monochromatic laser light, $\Phi_2(351\ nm) = 0.11 \pm 0.02$. We estimate τ_{phot}[43] by assuming Φ_2 to be 0.1 over the whole wavelength range of 290−450 nm and utilizing the measured absorption cross sections along with tabulated actinic fluxes taken from ref 43. This estimation has provided the photolysis lifetime of less than one hour for 2,3PD during daytime at mid latitudes on the ground level. The same qualitative result is obtained assuming 0.06 for the photolysis quantum yield[41] due to the significant absorption of 2,3PD and the high solar flux in the longer wavelength region.

Similar to other carbonyl molecules, OH-reaction can be an important initiation step for the tropospheric degradation of 2,3PD beside photolysis. The k_1 value determined at laboratory temperature can be used to estimate the tropospheric lifetime of 2,3PD with respect to its reaction with OH radicals, τ_{OH}. With an average global OH concentration of $[OH]_{global} = 1 \times 10^6$ radicals cm^{-3} (24 h average),[44] the tropospheric lifetime of $\tau_{OH} \approx 1/[k_1(300\ K) \times [OH]_{global}] = 5.3$ days is estimated.

In summary, our estimations show that photolysis is likely the dominant process to control the loss of 2,3PD in the troposphere. While this conclusion is believed correct in qualitative terms, accurate lifetime can not be given as yet, mostly because of the uncertainty of the photolysis quantum yields. It is noted also that the simple assessment used here is based on the assumption that 2,3PD is uniformly mixed through the troposphere that is probably not the case in view of the short lifetime of this OVOC and the average tropospheric transport time scale (1−2 months). The short lifetime indicates that 2,3PD will be removed rapidly close to its local sources in the atmosphere.

■ ASSOCIATED CONTENT

Supporting Information. Absorption cross sections for 2,3-pentanedione tabulated in 1 nm intervals along with representative Beer−Lambert plots; GC conditions; relative-rate plot to obtain $k_1(OH + 2,3PD)/k_3(OH + MEK)$. This material is available free of charge via the Internet at http://pubs.acs.org.

AUTHOR INFORMATION

Corresponding Author
*E-mail: dobe@chemres.hu; alexandre.tomas@mines-douai.fr.

ACKNOWLEDGMENT

This work has been supported in part by the Hungarian Research Fund OTKA (Contract OMFB-00992/2009). E.Sz. gratefully acknowledges the financial support from the French Foreign Office and Région Nord—Pas de Calais in the framework of the ARCUS program. The authors are indebted to the reviewers for their comments and helpful suggestions.

REFERENCES

(1) Burdock, G. A. *Fenarolli's Handbook of Flavor Ingredients*, 5th ed.; CRC Press: Boca Raton, FL, 2005.
(2) Feierabend, K. J.; Zhu, L.; Talukdar, R. K.; Burkholder, J. B. *J. Phys. Chem. A* **2008**, *112*, 73.
(3) Baeza-Romero, M. T.; Glowacki, D. R.; Blitz, M. A.; Heard, D. E.; Pilling, M. J.; Rickard, A.; Seakins, P. W. *Phys. Chem. Chem. Phys.* **2007**, *9*, 4114.
(4) Dagaut, P.; Wallington, T. J.; Liu, R.; Kurylo, M. J. *J. Phys. Chem.* **1988**, *92*, 4375.
(5) Feierabend, K. J.; Flad, J. E.; Brown, S. S.; Burkholder, J. B. *J. Phys. Chem. A* **2009**, *113*, 7784.
(6) Chen, Y.; Wang, W.; Zhu, L. *J. Phys. Chem. A* **2000**, *104*, 11126.
(7) Klotz, B.; Graedler, F.; Sorensen, S.; Barnes, I.; Becker, K. H. *Int. J. Chem. Kinet.* **2001**, *33*, 9.
(8) Jackson, A. W.; Yarwood, A. J. *Can. J. Chem.* **1972**, *50*, 1331.
(9) Imrik, K.; Farkas, E.; Vasvári, G.; Szilágyi, I.; Sarzyński, D.; Dóbé, S.; Bérces, T.; Márta, F. *Phys. Chem. Chem. Phys.* **2004**, *6*, 3958.
(10) Dóbé, S.; Khachatryan, L.; Bérces, T. *Ber. Bunsen-Ges. Phys. Chem.* **1989**, *93*, 847.
(11) Pearlyn, D.; Pereira, D.; Kathirgamanthan, P. *J. Nat. Sci. Counc. Sri Lanka* **1977**, *5*, 41.
(12) Crunaire, S.; Tarmoul, J.; Fittschen, C.; Tomas, A.; Lemoine, B.; Coddeville, P. *Appl. Phys. B: Lasers Opt.* **2006**, *85*, 467.
(13) Gierczak, T.; Burkholder, J. B.; Talukdar, R. K.; Mellouki, A.; Barone, S. B.; Ravishankara, A. R. *J. Photochem. Photobiol., A* **1997**, *110*, 1.
(14) Nádasdi, R.; Zügner, G. L.; Farkas, M.; Dóbé, S.; Maeda, S.; Morokuma, K. *ChemPhysChem* **2010**, *11*, 3883.
(15) Ohbayashi, K.; Akimoto, H.; Tanaka, I. *J. Phys. Chem.* **1977**, *81*, 798.
(16) Baasandorj, M.; Griffith, S.; Dusanter, S.; Stevens, P. S. *J. Phys. Chem. A* **2009**, *113*, 10495.
(17) Szabó, E.; Zügner, G. L.; Szilágyi, I.; Dóbé, S.; Bérces, T.; Márta, F. *React. Kinet. Catal. Lett.* **2008**, *95*, 365.
(18) Atkinson, R.; Baulch, D. L.; Cox, R. A.; Crowley, J. N.; Hampson, R. F.; Hynes, R. G.; Jenkin, M. E.; Rossi, M. J.; Troe, J. *Atmos. Chem. Phys.* **2006**, *6*, 3625.IUPAC Subcommittee for Gas Kinetic Data Evaluation, http://www.iupac-kinetic.ch.cam.ac.uk.
(19) Sander, S. P.; Finlayson-Pitts, B. J.; Friedl, R. R.; Golden, D. M.; Huie, R. E.; Keller-Rudek, H.; Kolb, C. E.; Kurylo, M. J.; Molina, M. J.; Moortgat, G. K.; Orkin, V. L.; Ravishankara, A. R.; Wine, P. H. *Evaluation Number 15*, Jet Propulsion Laboratory: Pasadena, 2006.
(20) Darnall, K.; Atkinson, R.; Pitts, J. N. *J. Phys. Chem.* **1979**, *83*, 1943.
(21) Holloway, A.; Treacy, J.; Sidebottom, H.; Mellouki, A.; Daele, V.; Le Bras, G.; Barnes, I. *J. Photochem. Photobiol., A* **2005**, *176*, 183.
(22) Kung, J. F. T. *J. Agric. Food Chem.* **1974**, *22*, 494.
(23) Schwarzenback, G.; Wittwer, C. *Helv. Chim. Acta* **1947**, *30*, 656.
(24) Le Calvé, S.; Hitier, D.; Le Bras, G.; Mellouki, A. *J. Phys. Chem. A* **1998**, *102*, 4579.
(25) Wallington, T. J.; Kurylo, M. J. *J. Phys. Chem.* **1987**, *91*, 5050.
(26) Mellouki, A.; Le Bras, G.; Sidebottom, H. *Chem. Reviews* **2003**, *103*, 5077.
(27) Kwok, E.; Atkinson, R. *Atmos. Environ.* **1995**, *29*, 1685.
(28) Smith, I. W. M.; Ravishankara, A. R. *J. Phys. Chem. A* **2002**, *106*, 4798.
(29) Hansen, J.; Francisco, J. *ChemPhysChem* **2002**, *3*, 833.
(30) Galano, A.; Alvarez-Idaboy, J. R. *Applications of Theoretical Methods to Atmospheric Science. Adv. Quantum Chem.* **2008**, *55*, 245.
(31) Henon, E.; Canneaux, S.; Bohr, F.; Dóbé, S. *Phys. Chem. Chem. Phys.* **2003**, *5*, 333.
(32) Alvarez-Idaboy, J. R.; Cruz-Torres, A.; Galano, A.; Ruiz-Santoyo, Ma. E. *J. Phys. Chem. A* **2004**, *108*, 2740.
(33) Horowitz, A.; Meller, R.; Moortgat, G. K. *J. Photochem. Photobiol., A* **2001**, *146*, 19.
(34) Holmes, J. R.; O'Brien, R. J.; Crabtree, J. H.; Hecht, T. A.; Seinfeld, J. H. *Environ. Sci. Technol.* **1973**, *7*, 519.
(35) Szabó, E. Atmospheric kinetics and photochemistry of oxygenated volatile organic compounds. *Ph.D. Thesis*, University of Lille and University of Szeged, 2011 (submitted).
(36) Tadić, J.; Juranić, I.; Moortgat, G. K. *J. Photochem. Photobiol., A* **2001**, *143*, 169.
(37) Raber, W. H.; Moortgat, G. K. *Progress and Problems in Atmospheric Chemistry*; World Scientific Publishing Co.: Singapore, 1995.
(38) Sheats, G. F.; Noyes, W. A. *J. Am. Chem. Soc.* **1955**, *77*, 1421.
(39) Kercher, J.; Fogleman, E.; Koizumi, H.; Sztáray, B.; Baer, T. *J. Phys. Chem. A* **2005**, *109*, 939.
(40) Jagiella, S.; Zabel, F. *Phys. Chem. Chem. Phys.* **2008**, *10*, 1799.
(41) Turro, N. J.; Lee, T.-J. *J. Am. Chem. Soc.* **1969**, *91*, 5651.
(42) Jackson, A. W.; Yarwood, A. J. *Can. J. Chem.* **1971**, *49*, 987.
(43) Finlayson-Pitts, B. J.; Pitts, J. N., Jr *Chemistry of the Upper and Lower Atmosphere: Theory, Experiments, and Applications*; Academic Press: San Diego, 2000.
(44) Heard, D. E.; Pilling, M. J. *Chem. Rev.* **2003**, *103*, 5163.

Oxidation Communications, submitted, May 9, 2011

DIRECT KINETIC STUDY OF THE OH-RADICAL INITIATED OXIDATION OF PIVALALDEHYDE, $(CH_3)_3CC(O)H$, IN THE GAS PHASE

E. SZABÓ, G. L. ZÜGNER, M. FARKAS, I. SZILÁGYI, S. DÓBÉ*

Institute of Materials and Environmental Chemistry, Chemical Research Center of the Hungarian Academy of Sciences, Pusztaszeri út 59-67, H-1025 Budapest, Hungary

E-mail: dobe@chemres.hu

ABSTRACT

The low-pressure fast discharge flow method was used to study the kinetics of the oxidation reaction system OH + $(CH_3)_3CC(O)H$ + O_2 at room temperature. OH radicals were monitored by resonance florescence detection; helium was the carrier gas. The rate constant for the overall reaction between OH radicals and pivalaldehyde, $(CH_3)_3CC(O)H$, (1) was determined to be $k_1(298\ K) = (2.65 \pm 0.34) \times 10^{-12}$ cm^3 molecule^{-1} s^{-1}, given with 2σ statistical uncertainty. The OH yields of $\Gamma_{OH} = 0.26 \pm 0.10$ and $\Gamma_{OH} = 0.15 \pm 0.06$ were measured for the pivaloyl radical, $(CH_3)_3CC(O)$, + O_2 reaction at P = 1.81 and 3.46 mbar reaction pressures, respectively. Comparison with literature and the atmospheric implications have been discussed.

Keywords: atmospheric kinetics, pivalaldehyde, OH reaction rate constant, OH product yield.

* For correspondence.

INTRODUCTION

Aldehydes, among them pivalaldehyde (PVA), 2,2-dimethyl-propanal ($(CH_3)_3CC(O)H$), are important trace constituents of the atmosphere. They are emitted from both biogenic and anthropogenic sources, and are reaction intermediates formed in the atmospheric degradation of most atmospheric organics[1]. The oxidative degradation of aldehydes contributes significantly to the HO_x and O_3 budget of the troposphere and they are precursors for peroxyacylnitrates, which are components of urban smog and efficient reservoirs of NO_x [2]. Similarly to other aldehydes, a major atmospheric loss process of pivalaldehyde is the reaction with OH radicals (1). The reaction takes place predominantly via the abstraction of the aldehydic H atom[3-4] leading to the pivaloyl (PVL), 2,2-dimethyl-propionyl ($(CH_3)_3CC(O)$), radical. PVL reacts exclusively with O_2 in the atmosphere and is known to form the pivaloyl-peroxyl radical, $(CH_3)_3CC(O)O_2$ (2a) [3]. By analogy with the acetyl (CH_3CO) + O_2 [5-6] and propionyl (C_2H_5CO)+ O_2 [7-8] reactions, OH formation is also an expected reaction channel in the reaction of PVL radicals with O_2 (2b).

$$OH + (CH_3)_3CC(O)H \rightarrow (CH_3)_3CC(O) + H_2O \quad (1)$$

$$(CH_3)_3CC(O) + O_2 \rightarrow \text{products} \quad (2)$$

$$(CH_3)_3CC(O) + O_2 + M \rightarrow (CH_3)_3CC(O)O_2 + M \quad (2a)$$

$$(CH_3)_3CC(O) + O_2 \rightarrow OH + \text{other products} \quad (2b)$$

Objective of our study was to determine rate constant for the overall reaction between OH radicals and pivalaldehyde, k_1, and to determine OH yields (branching ratios), $\Gamma_{OH} = k_{2b}/k_2$, at room temperature and a few mbar pressure of helium.

EXPERIMENTAL

The low-pressure fast discharge flow method (DF) was applied to investigate the oxidation kinetics of pivalaldehyde initiated by OH radicals. OH was detected directly by $A^2\Sigma(v=0)\leftarrow X^2\Pi(v=0)$ resonance fluorescence (RF) using a microwave-powered resonance lamp for excitation. Details of the kinetic apparatus and RF detection have been presented previously [9-10].

The 60.0-cm-long, 4.01-cm-i.d. flow tube reactor was constructed of Pyrex and was coaxially equipped with a moveable quartz injector. The inner surface of the reactor was coated with a thin layer of halocarbon wax to reduce heterogeneous wall effects. OH radicals were reacted with $(CH_3)_3CC(O)H$ in the flow reactor in the presence and absence of O_2. OH was produced in the reaction of H atoms with a slight excess of NO_2 inside the moveable injector: $H + NO_2 \rightarrow OH + NO$. Hydrogen atoms were obtained by microwave-discharge dissociation of H_2, in large excess of He flow. Helium was the main carrier gas which was regulated by calibrated mass flow controllers. The smaller flows of reactants and radical-source molecules were regulated by needle valves and determined from the pressure rise over time in known volumes. The reaction pressure was measured with a calibrated capacitance manometer. The flow tube was connected downstream to a detection block where the induced resonance fluorescence of OH was viewed through an interference filter centred at 307 nm and detected by a photomultiplier. The multiplier output was fed into a purpose-built data acquisition PC-board for signal averaging and further analysis. The detection limit for OH was ~2×10^9 molecule cm^{-3} (at $S/N = 1$ signal-to-noise ratio).

The experimental procedure involved monitoring of the concentration of OH radicals at different positions of the moveable injector (at varied reaction times) in the presence and absence of O_2, i.e., for $OH + (CH_3)_3CC(O)H$ and $OH + (CH_3)_3CC(O)H + O_2$. Both

pivaldehyde and O_2 were used in large excess over OH and they entered the reactor upstream through side arms. The initial OH concentration was $[OH]_0 \approx 3 \times 10^{11}$ molecule cm^{-3}, along with $[(CH_3)_3CC(O)H] \approx 4 \times 10^{12}$ and $[O_2] \approx 1 \times 10^{15}$ molecule cm^{-3}. The "O_2 flow on" and "O_2 flow off" runs, or vice versa, were conducted in a back-to-back manner. The linear flow velocity was $v_{lin} \approx 15$ m s^{-1} allowing kinetic measurements to be performed on the ms time scale.

Table 1. Materials used in the experiments

Name	Supplier	Purity (%)	Notes
He	Messer-Griesheim	99.996	*a*
H_2	Messer Griesheim	99.995	*b*
Ar	Linde	99.9990	*b*
O_2	Messer Griesheim	99.995	
NO_2	Messer Griesheim	98	*c*
$(CH_3)_3CC(O)H$	Aldrich	> 97	*d*

a As a carrier gas, it was passed through liquid-nitrogen-cooled silica-gel traps before entering the flow system. *b* Used as 5% H_2 + 10% Ar mixture in He. *c* Purified by low-temperature trap-to-trap distillation in vacuum and used as 1% mixture in He. *d* Degassed by freeze-pump-thaw cycles prior to use. It was metered in the flow tube either directly or premixed in 10–15% with He.

RESULTS

The experiments were carried-out at room temperature, $T = 298 \pm 3$ K, and $P = 1.82$ and 3.46 mbar pressures of He.

OH signals were found to decrease with increasing reaction time both in the absence and presence of O_2, but the depletion was slower and the OH signals were bigger when oxygen was added to the system indicating the reformation of OH via reaction (2b). OH obeyed first-order kinetics for both OH + PVA and OH + PVA + O_2. Figure 1 presents

representative OH kinetic plots, where the decay curves drawn are non-linear least-squares (LSQ) fits to the experimental data.

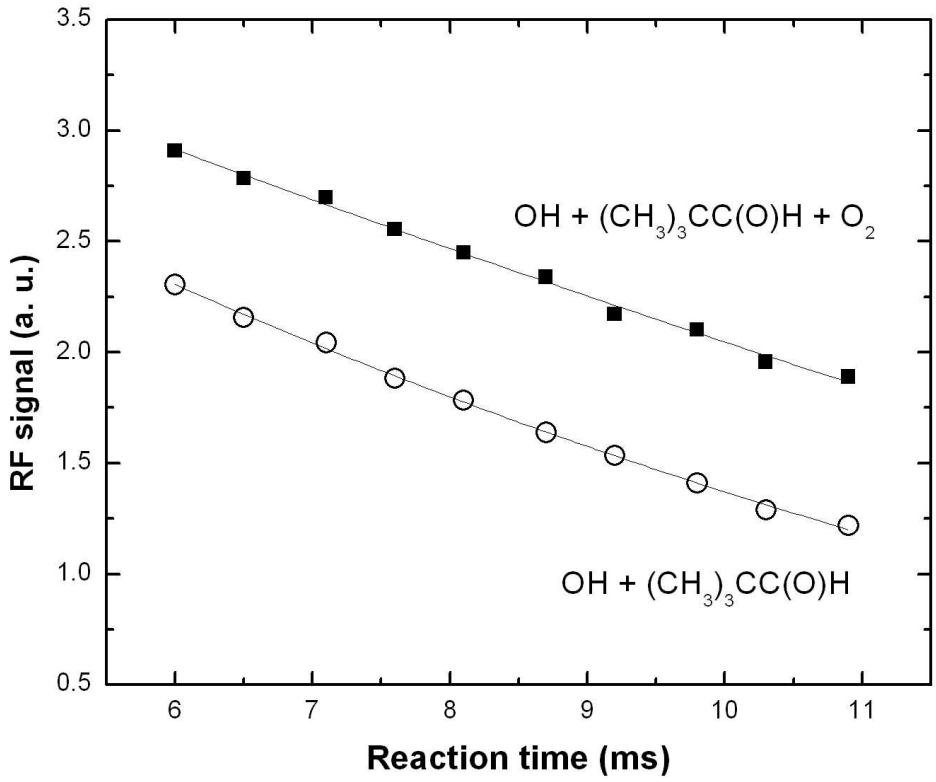

Figure 1. Typical OH decay plots determined for OH + $(CH_3)_3CC(O)H$ and OH + $(CH_3)_3CC(O)H + O_2$ in back-to-back experiments (P = 1.82 mbar, T = 299 K, $[OH]_0 \approx 3.4 \times 10^{11}$, [PVA] = 3.6×10^{12} and $[O_2] = 1.9 \times 10^{15}$ molecule cm^{-3}).

The decay constant measured in the absence of O_2 is the pseudo-first-order rate constant for the reaction OH + PVA (1), $k_1' = k_1$ [PVA] + *const*; a plot of the k_1' values vs. the pivalaldehyde concentration is shown in Figure 2. Data plotted include all k_1' from both the 1.82 and 3.46 mbar experiments and show no discernible pressure dependence. The experimental data have defined a reasonable good straight line with a small intercept. A linear LSQ analysis has provided the rate constant value of

$$k_1(298\ \mathrm{K}) = (2.65 \pm 0.34) \times 10^{-12}\ \mathrm{cm^3\ molecule^{-1}\ s^{-1}}.$$

(The errors above and throughout this Communication designate 2σ statistical uncertainty.)

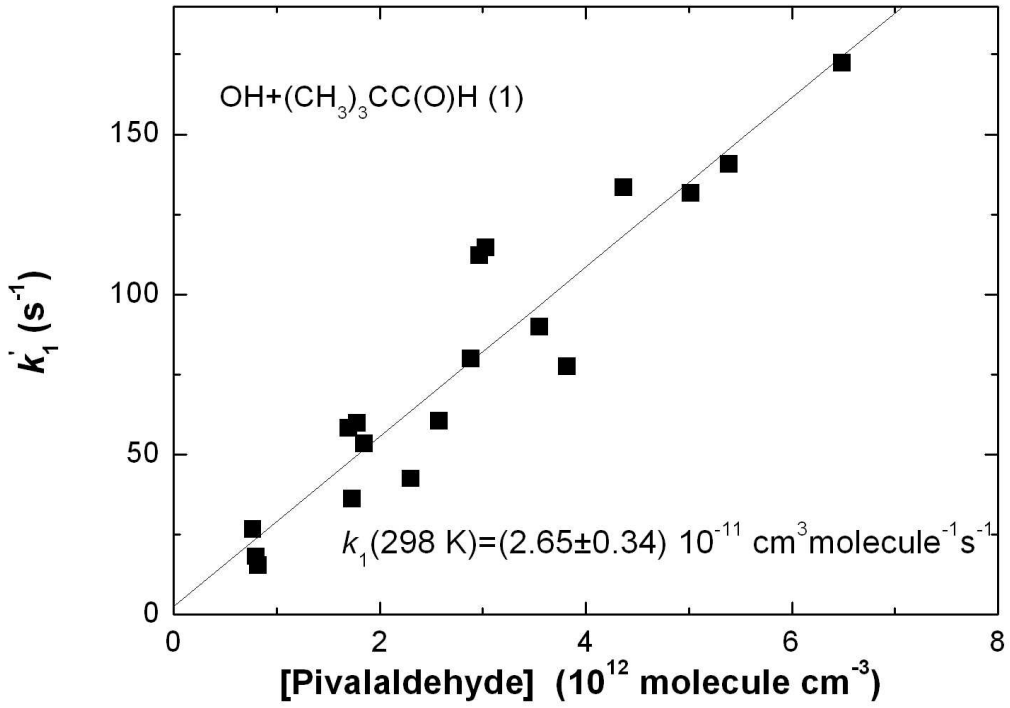

Figure 2. Plot of the pseudo-first-order decay constant vs. the pivalaldehyde concentration in the absence of O_2. The slope of the straight line provides the rate constant for the reaction OH + $(CH_3)_3CC(O)H$ (1).

Under our experimental conditions only reactions (1), (2a), (2b) and the heterogeneous loss of OH took place, OH + wall → products (w). As we have shown in a previous publication[5], the system of differential equations of reactions (1)–(w) can be solved analytically, providing Eq. (I) for the OH yield:

$$\Gamma_{OH} = (k_1' - k^*) / (k_1' - k_w) \qquad \text{(I)}$$

where k_1' is, the OH decay constant with $(CH_3)_3CC(O)H$ (see also above), k^* is the OH decay constant with $(CH_3)_3CC(O)H + O_2$ and k_w is the 'wall' rate constant of OH. The depletion of OH radicals on the wall of the reactor was determined in separate experiments to be $k_w = 8 \pm 3\ s^{-1}$.

The experimental conditions and kinetic results are summarised in Table 2. The OH yield has been found significant at the low pressures of the investigations; the more accurate result was obtained at 1.81 mbar where the OH reformation was more significant and the reproducibility was better: $\Gamma_{OH}(1.81\ mbar) = 0.26 \pm 0.10$.

Table 2. Experimental conditions and kinetic results for the OH-initiated oxidation of pivalaldehyde ($T = 298 \pm 3$ K)

P(He) (mbar)	[PVA] (10^{12} cm^{-3})	k'_1 [a] (s^{-1})	k^* [b] (s^{-1})	$\Gamma_{OH} \pm 2\sigma$ [c]	Runs [d]
1.81	0.77–4.37	22.8–223.3	18.1–192.1	0.26 ± 0.10	13
3.46	1.70–6.49	63.6–177.6	58.2–172.2	0.15 ± 0.06	5

[a] OH decay constant in the absence of O_2. [b] OH decay constant in the presence of O_2; the O_2 concentration was ~2×10^{15} molecule cm^{-3}. [c] OH yield (branching ratio), $\Gamma_{OH} = k_{2b}/k_2$. [d] Number of back-to-back determinations of k'_1 and k^*.

DISCUSSION

The rate constant we have determined for the overall reaction between OH radicals and pivalaldehyde, $k_1(300\ \mathrm{K}) = (2.65 \pm 0.34) \times 10^{-11}$ cm^3 molecule^{-1} s^{-1}, agrees well with most of the data reported in the literature. As for instance, in a recent study by D'Anna et al. [4] the rate constant value of $k_1(298\ \mathrm{K}) = (2.86 \pm 0.13) \times 10^{-11}$ cm^3 molecule^{-1} s^{-1} has been determined by relative-rate kinetic experiments (for further references see also the paper of these authors). In an early work from our own laboratory, a significantly higher rate constant was determined for reaction (1) using also the DF-RF method [9]. The reason of the disparity is not known; the only apparent difference is a somewhat higher, but still not unusually high, wall consumption of OH ($k_w = 20$ s^{-1}) in the previous experiments [9].

Le Crâne and co-workers[3] have carried out a detailed laboratory study on the atmospheric chemistry of pivalaldehyde using flash photolysis – UV absorption and continuous photolysis – FTIR absorption methods in 930 mbar synthetic air at 296 K. Pivaloyl (PVL), $(CH_3)_3CC(O)$, radicals were produced by reacting pivalaldehyde with Cl atoms. The authors have shown that the atmospheric fate of PVL radicals is the addition to O_2 to give pivalylperoxyl radical, $(CH_3)_3CC(O)O_2$, (reaction (2a)) with a yield of >0.98. The OH yields of 0.26 and 0.15 we have determined do not contradict with the results of Le Crâne et al., since we have performed the experiments at much lower pressures. In two of our recent studies, OH formation was shown to be the dominating reaction product for the $CH_3CO + O_2$ [5] and $C_2H_5CO+O_2$ [7] reactions in the low pressure regime of the DF technique. At ~1 mbar pressure of He, the OH yields were found close to unity, but they decreased quickly with increasing pressure as understood by the efficient competition between the pressure dependent O_2-addition and the pressure independent OH-elimination [5,7]. In our current study, we have observed also significant, although smaller OH yields for the reaction $(CH_3)_3CC(O) + O_2$.

Some pressure dependence is also evident by the presented data, but measurements were done only at two pressures and no OH yields could be determined above ~4 mbar because of the small OH signals at higher pressures. The OH yields are compared in Table 3.

Table 3. Comparison of OH yields (Γ_{OH}) for the acyl + O_2 reactions in the low pressure regime (T = 300 K).

Reaction	P(He) (mbar)	Γ_{OH}	Reference
$(CH_3)_3CC(O) + O_2$	1.81	0.26 ± 0.10	This work
$CH_3CO + O_2$	2.00	0.86	Kovács et. al [5]
$C_2H_5CO + O_2$	2.00	0.86 ± 0.14	Zügner et al. [7]
$(CH_3)_3CC(O) + O_2$	3.46	0.15 ± 0.06	This work
$CH_3CO + O_2$	3.50	0.57	Kovács et. al [5]
$C_2H_5CO + O_2$	3.59	0.68 ± 0.10	Zügner et al. [7]

The OH yields presented in Table 3 are seen to be close to each other for the $CH_3CO + O_2$ and $C_2H_5CO + O_2$ reactions, while they are more than 3-times smaller for the $(CH_3)_3CC(O) + O_2$ reaction at comparable pressures. One possible explanation for the apparent small OH yields is that the pivaloyl radical is much less stable thermally compared with its acetyl and propionyl counterparts [3,11] and so the decomposition reaction of PVL, $(CH_3)_3CC(O) + M \rightarrow (CH_3)_3C + CO + M$, could compete efficiently with its reaction with the oxygen molecule. In this case, estimation of Γ_{OH} is no longer viable by using the simple Eq. (I).

The high rate constant we have determined for reaction (1) implies a short tropospheric lifetime of pivalaldehyde. Taking an average global OH concentration of $[OH]_{global} = 1 \times 10^6$ molecule cm^{-3} [12], one obtains $\tau_{OH} \approx 1/(k_1(298\ K) \times [OH]_{global}) = 11$ hours estimate for the lifetime of PVA in the troposphere with respect to its reaction with OH radicals. Photolysis may be of comparable importance for the atmospheric removal of PVA,

but no photochemical study of pivalaldehyde has been reported in the gas phase. Based on our current experimental findings, and analogies with the acetyl and propionyl radical reactions with O_2 [5,7], the OH yield for the PVA + O_2 reaction must be very small in atmospheric pressure air. Thus, the atmospheric photooxidation of pivalaldehyde is likely to occur via the OH initiation step, followed by the formation of the peroxyl radical $(CH_3)_3CC(O)O_2$ which undergoes subsequent reactions with NO, NO_2 and other peroxyl radicals.

ACKNOWLEDGEMENTS

This work has been supported by the European Atmospheric Chemistry Project SCOUT-O3 (contract GOCE-CT2004-505390) and the Hungarian Research Fund (contract OMFB-00992/2009).

REFERENCES

1. A. MELLOUKI, G. LE BRAS, H. SIDEBOTTOM: Kinetics and mechanisms of the oxidation of oxygenated organic compounds in the gas phase. Chemical Reviews, **103,** 5077 (2003).

2. B. J. FINLAYSON-PITTS, J. N. PITTS: Chemistry of the upper and lower Atmosphere. Theory, Experiments, and Applications. Academic Press, San Diego, San Francisco, New York, etc., 2003.

3. J. P. LE CRÂNE, E. VILLENAVE, M. D. HURLEY, T. J. WALLINGTON, S. NISHIDA, K. TAKAHASHI, Y. MATSUMI: Atmospheric chemistry of pivalaldehyde and isobutyraldehyde: Kinetics and mechanisms of reactions with Cl atoms, fate of $(CH_3)_3CC(O)$ and $(CH_3)_2CHC(O)$ radicals, and self-reaction kinetics of $(CH_3)_3CC(O)O_2$ and $(CH_3)_2CHC(O)O_2$ radicals. Journal of Physical Chemistry A, **108,** 795 (2004).

4. B. D'ANNA, W. ANDRESEN, Z. GEFEN, C. NIELSEN: Kinetic study of OH and NO_3 radical reactions with 14 aliphatic aldehydes. Physical Chemistry Chemical Physics, **3,** 3057 (2001).

5. G. KOVÁCS, J. ZÁDOR, E. FARKAS, R. NÁDASDI, I. SZILÁGYI, S. DÓBÉ, T. BÉRCES, F. MÁRTA, G. LENDVAY: Kinetics and mechanism of the reactions of CH3CO and CH3C(O)CH2 radicals with O-2. Low-pressure discharge flow experiments and quantum chemical computations. Physical Chemistry Chemical Physics, **9**, 4142 (2007).

6. M. A. BLITZ, D. E. HEARD, M. J. PILLING: OH formation from CH_3CO+O_2: A convenient experimental marker for the acetyl radical. Chemical Physics Letters, **365**, 374 (2002).

7. G. L. ZÜGNER, I. SZILÁGYI, J. ZÁDOR, E. SZABÓ, S. DÓBÉ, X. L. SONG, B. S. WANG: OH yields for $C_2H_5CO + O_2$ at low pressure: Experiment and theory. Chemical Physics Letters, **495**, 179 (2010).

8. M. T. BAEZA-ROMERO, M. A. BLITZ, D. E. HEARD, M. J. PILLING, B. PRICE, P. W. SEAKINS: OH formation from the $C_2H_5CO+O_2$ reaction: An experimental marker for the propionyl radical. Chemical Physics Letter, **408,** 232 (2005).

9. S. DÓBÉ, L. KHACHATRYAN, T. BÉRCES: Kinetics of reactions of hydroxyl radicals with a series of aliphatic aldehydes. Ber. Bunsenges. Phys. Chem., **93,** 847 (1989).

10. K. IMRIK, E. FARKAS, G. VASVÁRI, I. SZILÁGYI, D. SARZYŃSKI, T. BÉRCES, F. MÁRTA: Laser spectrometry and kinetics of selected elementary reactions of the acetonyl radical. Phys. Chem. Chem. Phys., **6,** 3958 (2004).

11. S. JAGIELLA, H. G. LIBUDA, F. ZABEL: Thermal stability of carbonyl radicals. Part I. Straight-chain and branched C-4 and C-5 acyl radicals. Phys. Chem. Chem. Phys., **2,** 1175 (2000).

12. D. E. HEARD, M. J. PILLING: Measurement of OH and HO_2 in the troposphere. Chemical Reviews, **103,** 5163 (2003).